frontiers | Research Topics

Head and neck squamous cell carcinoma: navigating the dawn of personalized medicine

Edited by
Ye Guo, Luis Abel Quiñones and
Fujun Han

Published in
Frontiers in Pharmacology
Frontiers in Oncology

ISSN 1664-8714
ISBN 978-2-8325-6963-4
DOI 10.3389/978-2-8325-6963-4

Generative AI statement
Any alternative text (Alt text) provided alongside figures in the articles in this ebook has been generated by Frontiers with the support of artificial intelligence and reasonable efforts have been made to ensure accuracy, including review by the authors wherever possible. If you identify any issues, please contact us.

About Frontiers

Frontiers is more than just an open access publisher of scholarly articles: it is a pioneering approach to the world of academia, radically improving the way scholarly research is managed. The grand vision of Frontiers is a world where all people have an equal opportunity to seek, share and generate knowledge. Frontiers provides immediate and permanent online open access to all its publications, but this alone is not enough to realize our grand goals.

Frontiers journal series

The Frontiers journal series is a multi-tier and interdisciplinary set of open-access, online journals, promising a paradigm shift from the current review, selection and dissemination processes in academic publishing. All Frontiers journals are driven by researchers for researchers; therefore, they constitute a service to the scholarly community. At the same time, the *Frontiers journal series* operates on a revolutionary invention, the tiered publishing system, initially addressing specific communities of scholars, and gradually climbing up to broader public understanding, thus serving the interests of the lay society, too.

Dedication to quality

Each Frontiers article is a landmark of the highest quality, thanks to genuinely collaborative interactions between authors and review editors, who include some of the world's best academicians. Research must be certified by peers before entering a stream of knowledge that may eventually reach the public - and shape society; therefore, Frontiers only applies the most rigorous and unbiased reviews. Frontiers revolutionizes research publishing by freely delivering the most outstanding research, evaluated with no bias from both the academic and social point of view. By applying the most advanced information technologies, Frontiers is catapulting scholarly publishing into a new generation.

What are Frontiers Research Topics?

Frontiers Research Topics are very popular trademarks of the *Frontiers journals series*: they are collections of at least ten articles, all centered on a particular subject. With their unique mix of varied contributions from Original Research to Review Articles, Frontiers Research Topics unify the most influential researchers, the latest key findings and historical advances in a hot research area.

Find out more on how to host your own Frontiers Research Topic or contribute to one as an author by contacting the Frontiers editorial office: frontiersin.org/about/contact

Head and neck squamous cell carcinoma: navigating the dawn of personalized medicine

Topic editors
Ye Guo — Tongji University, China
Luis Abel Quiñones — University of Chile, Chile
Fujun Han — The First Hospital of Jilin University, China

Citation
Guo, Y., Quiñones, L. A., Han, F., eds. (2025). *Head and neck squamous cell carcinoma: navigating the dawn of personalized medicine*.
Lausanne: Frontiers Media SA. doi: 10.3389/978-2-8325-6963-4

Table of contents

frontiers | Frontiers in Oncology

TYPE Editorial
PUBLISHED 24 September 2025
DOI 10.3389/fonc.2025.1684617

OPEN ACCESS

EDITED AND REVIEWED BY
Sharon R. Pine,
University of Colorado Anschutz Medical Campus, United States

*CORRESPONDENCE
Luis Abel Quiñones
lquinone@uchile.cl

RECEIVED 12 August 2025
ACCEPTED 09 September 2025
PUBLISHED 24 September 2025

CITATION
Quiñones LA, Guo Y and Han F (2025) Editorial: Head and neck squamous cell carcinoma: navigating the dawn of personalized medicine.
Front. Oncol. 15:1684617.
doi: 10.3389/fonc.2025.1684617

Editorial: Head and neck squamous cell carcinoma: navigating the dawn of personalized medicine

Luis Abel Quiñones[1,2,3,4]*, Ye Guo[5] and Fujun Han[6]

[1]Laboratory of Chemical Carcinogenesis and Pharmacogenetics (CQF), Department of Basic and Clinical Oncology, Faculty of Medicine, University of Chile, Santiago, Chile, [2]Department of Pharmaceutical Sciences and Technology, Faculty of Chemical and Pharmaceutical Sciences, University of Chile, Santiago, Chile, [3]Latin American Network for Implementation and Validation of Clinical Pharmacogenomics Guidelines (RELIVAF), Santiago, Chile, [4]Center for Cancer Prevention and Control (CECAN), Santiago, Chile, [5]Department of Oncology, Shanghai East Hospital, School of Medicine, Tongji University, Shanghai, China, [6]Cancer Centre, First Hospital of Jilin University, Changchun, China

KEYWORDS

biomarker, head and neck neoplasms, precision therapy, artificial intelligence, personalized cancer therapy

Editorial on the Research Topic
Head and neck squamous cell carcinoma: navigating the dawn of personalized medicine

Head and neck cancers (HNC), including squamous cell carcinoma (HNSCC) and rare subtypes, constitute a highly heterogeneous group of malignancies characterized by complex molecular profiles and wide variability in clinical outcomes (1–3). Recent advances in precision medicine, biomarker discovery, computational modelling, and pharmacovigilance have enabled significant progress in early diagnosis, therapeutic stratification, and the development of individualized treatment approaches. This Research Topic compiles nine articles that span a diverse array of contributions, from molecular biology and machine learning to clinical pharmacogenetics and adverse drug reaction monitoring, all aimed at improving outcomes for patients with head and neck malignancies.

In the context of tumor immunity, Lin et al. identified the Integrin Subunit Alpha L (ITGAL) as a pan-cancer biomarker associated with magnesium-mediated CD8+ T cell activation and immune infiltration in HNSCC, suggesting its potential as both a prognostic indicator and immunotherapy target. In parallel, Wang et al. reported that high cGAS-STING pathway activation enhances the efficacy of neoadjuvant chemo-immunotherapy in HNSCC, correlating with increased T cell infiltration and cytotoxic activity. Moreover, Zhou et al. characterized a four-gene signature linked to propionate metabolism in HNSCC, offering insights into immune evasion mechanisms and potential prognosis, and possible therapeutic targets.

Regarding therapy resistance, Chaudhary et al. identified *ACTL6A* and *ERCC1* as key chemoresistance genes in cisplatin-treated HNC, combining qPCR, bioinformatic modelling, and meta-analysis to propose drug repurposing strategies. Complementarily, He et al. demonstrated that aloe-emodin downregulates lncRNA D63785, thereby inhibiting the PI3K/Akt/mTOR axis in nasopharyngeal carcinoma, suggesting a novel pharmacological approach.

In the realm of prognostic modelling and treatment stratification, Liu et al. developed a ubiquitin-related gene signature for laryngeal cancer, linking it signatures to immune microenvironment modulation and treatment sensitivity. Similarly, Zhang et al. applied deep learning algorithms to personalize treatment in locally advanced HNSCC, enhancing survival prediction with performance comparable or superior to current clinical guidelines.

Addressing treatment safety, Gao et al. conducted an interesting pharmacovigilance study using WHO-VigiAccess (4), characterizing adverse drug reactions associated with five anti-HNSCC agents emphasizing the need for personalized safety monitoring.

Finally, Fan et al. reported a rare case of laryngeal sarcomatous carcinoma, reviewing molecular markers with potential therapeutic implications for aggressive HNC subtypes (5).

Together, these contributions highlight the multifaceted progress being made in head and neck oncology, with implications for biomarker-driven precision medicine, AI-supported clinical decision-making, and safety profiling. These advances are essential to improving both survival and quality of life for patients facing these challenging cancers.

Author contributions

LQ: Conceptualization, Validation, Writing – original draft, Writing – review & editing. FH: Writing – review & editing. YG: Writing – review & editing.

Conflict of interest

The authors declare that the research was conducted in the absence of any commercial or financial relationships that could be construed as a potential conflict of interest.

The author(s) declared that they were an editorial board member of Frontiers, at the time of submission. This had no impact on the peer review process and the final decision.

Generative AI statement

The author(s) declare that no Generative AI was used in the creation of this manuscript.

Any alternative text (alt text) provided alongside figures in this article has been generated by Frontiers with the support of artificial intelligence and reasonable efforts have been made to ensure accuracy, including review by the authors wherever possible. If you identify any issues, please contact us.

Publisher's note

References

1. Johnson DE, Burtness B, Leemans CR, Lui VWY, Bauman JE, Grandis JR. Head and neck squamous cell carcinoma. *Nat Rev Dis Primers*. (2020) 6:92. doi: 10.1038/s41572-020-00224-3. *Erratum in*: Nat Rev Dis Primers. 2023 Jan 19;9(1):4. doi: 10.1038/s41572-023-00418-5.

2. Vakili S, Behrooz AB, Whichelo R, Fernandes A, Emwas AH, Jaremko M, et al. Progress in precision medicine for head and neck cancer. *Cancers (Basel)*. (2024) 16:3716. doi: 10.3390/cancers16213716

3. Saini KS, Somara S, Ko HC, Thatai P, Quintana A, Wallen ZD, et al. Biomarkers in head and neck squamous cell carcinoma: unraveling the path to precision immunotherapy. *Front Oncol*. (2024) 14:1473706. doi: 10.3389/fonc.2024.1473706

4. WHO-Vigiaccess (2015). Available online at: https://www.vigiaccess.org/?utm_source=chatgpt.com (Accessed august 7th).

5. Liu Y, Zhang N, Wen Y, Wen J. Head and neck cancer: pathogenesis and targeted therapy. *MedComm (2020)*. (2024) 5:e702. doi: 10.1002/mco2.702

frontiers | Frontiers in Pharmacology

TYPE Original Research
PUBLISHED 13 November 2024
DOI 10.3389/fphar.2024.1464830

OPEN ACCESS

EDITED BY
Fujun Han,
The First Hospital of Jilin University, China

REVIEWED BY
Ruo Wang,
Shanghai Jiao Tong University, China
Mercy Rophina,
New York University, United States

*CORRESPONDENCE
Sufang Qiu,
sufangqiu@fjmu.edu.cn
Yunbin Ye,
yeyb@fjzlhospital.com

†These authors have contributed equally to this work and share first authorship

RECEIVED 15 July 2024
ACCEPTED 29 October 2024
PUBLISHED 13 November 2024

CITATION
Lin F, Yang H, Huang Z, Li Y, Ding Q, Ye Y and Qiu S (2024) Magnesium-related gene ITGAL: a key immunotherapy predictor and prognostic biomarker in pan-cancer.
Front. Pharmacol. 15:1464830.
doi: 10.3389/fphar.2024.1464830

Magnesium-related gene ITGAL: a key immunotherapy predictor and prognostic biomarker in pan-cancer

Fengjie Lin[1†], Hanxuan Yang[1†], Zongwei Huang[1], Ying Li[1], Qin Ding[1], Yunbin Ye[2,3]* and Sufang Qiu[1]*

[1]Department of Radiation Oncology, Clinical Oncology School of Fujian Medical University, Fujian Cancer Hospital, Fujian, China, [2]Laboratory of Immuno-Oncology, Fujian Cancer Hospital and Fujian Medical University Cancer, Hospital, Fuzhou, China, [3]Fujian Key Laboratory of Translational Cancer Medicine, Fuzhou, China

Background: Integrin subunit alpha L (ITGAL) is crucial for activating $CD8^+$ T cells through magnesium-mediated immune synapse formation and specific cytotoxicity. ITGAL might exert an important function in the growth and transformation of cancer.

Methods: Our study comprehensively analyzed ITGAL expression across various cancers, validated by Immunochemistry (IHC) in the laboratory. ITGAL showed prognostic significance in pan-cancer patients, correlated with clinical features, and associated with specific signaling pathways. We also observed a relationship between ITGAL and immune cell infiltration. In HNSCC, ITGAL demonstrated prognostic value and potential implications for immunotherapy response and novel drug targets.

Results: ITGAL expression linked to tumor prognosis across 27 cancers. Elevated ITGAL correlated with good prognosis in CESC, LUAD, SARC, HNSCC, and SKCM. ITGAL involved in immune regulation pathways and showed positive correlation with immune cell infiltration. ITGAL associated with $CD8^+$ T cell infiltration. And high ITGAL expression in $CD8^+$ T cells and NK cells. In HNSCC, ITGAL linked to favorable prognosis and sensitivity to immunotherapy. Predicted potential drugs for HNSCC.

Conclusion: ITGAL is remarkably associated with CD8+T cells and crucial in the tumor immune microenvironment of pan-cancer. Furthermore, our findings may provide a targeted anti-tumor strategy for ITGAL by influencing the tumor immune microenvironment.

KEYWORDS

ITGAL, pan-cacner, immunothearpy, magnesium-related, HNSCC

Introduction

Integrin alpha L chain encoded by integrin subunit alpha L (ITGAL) is critically involved in intercellular adhesion between leukocytes by binding to intercellular adhesion molecules 1–3 (ICAMs 1–3) (Corbi et al., 1988; Hickman et al., 2022). Moreover, previous studies have demonstrated that the LFA-1 (Lymphocyte Function-associated Antigen 1) encoded by ITGAL is crucial in the inflammatory response (Whitcup et al., 1999), which

includes cytotoxic T cell dependent killing, antibody mediated killing by granulocytes, monocytes and leukocyte-endothelial cell interaction. It also promotes the cytotoxicity of natural killer (NK) cells (Barber et al., 2004).

LFA-1 encoded by ITGAL has recently been found to be involved in $CD8^+$ T cell activation. To acquire active conformation, magnesium is required by LFA-1 on CD8+T cells. As a result calcium flux, metabolic reprogramming, signal transduction, immune synapse formation, and specific cytotoxicity are enhanced (Lotscher et al., 2022).

ITGAL belongs to the integrin family, and the integrin family plays a critical role in the control of angiogenesis and lymphangiogenesis, fundamental processes crucial for the advancement and spread of tumors. The exploration of integrins as therapeutic targets shows significant potential in the realm of cancer treatment (Avraamides et al., 2008). In T cell-mediated immunity, integrins are pivotal in governing lymphocyte recirculation, activating T cells, and delineating distinct subsets of T cells and antigen-presenting cells (Pribila et al., 2004). Integrins are also pivotal in the processes of tumour stemness, metastasis, and drug tolerance. A comprehensive understanding of their regulatory mechanisms holds the promise of unveiling innovative therapeutic strategies aimed at enhancing tumor responsiveness to treatments while mitigating metastatic characteristics (Seguin et al., 2015). Existing studies have shown that ITGAL can affect the prognosis and survival of tumors such as melanoma and gastric cancer through tumor immunity (Zhang et al., 2022; Deng et al., 2023). Furthermore, ITGAL is associated with poor prognosis in ovarian cancer (Wu A. et al., 2020), while it also suggests better prognosis and inhibits tumor proliferation in NSCLC (Wang et al., 2023). The above studies reflect the heterogeneity of the impact of ITGAL on different cancers, and there are no studies on pan-cancer analysis of ITGAL, which triggered our interest in doing pan-cancer analysis of ITGAL.

The objective of this research is to evaluate the correlation between ITGAL expression and prognosis in various cancer types, as well as the impact on the immune microenvironment. At the same time, we hope to propose a targeted anti-tumor strategy for ITGAL by regulating the tumor immune microenvironment (TME) and find corresponding anti-cancer drugs.

Methodology

Immunochemistry (IHC)

A semiquantitative integration method was utilized to evaluate the intensity of IHC staining in eight different types of cancer tissues and adjacent normal tissues. Images of the stained tissues were captured using a microscope (3DHISTECH, Hungary) at ×20 magnification. Protein expression levels were quantified using the histochemistry score (H-score), calculated with the following formula: H-score = (proportion of cells exhibiting low intensity × 1) + (proportion of cells exhibiting middle intensity × 2) + (proportion of cells exhibiting high intensity × 3).

Database

The TCGA database was utilized to retrieve the RNA-seq data of tumor and paired-healthy tissues (https://portal.gdc.cancer.gov/). Data from UCSC's XENA database were acquired from the TCGA and GTEx for unpaired analyses (https://xenabrowser.net/datapages/). TCGA-HNSC collection (https://portal.gdc.cancer.gov/projects/TCGA-HNSC) was accessed for gathering clinical information on head and neck squamous cell carcinoma (HNSCC).

Exploring the relationship between ITGAL and clinical features

To analyze the data, a univariate COX regression model was built using the "survival" package in R. The predictive significance of ITAGL was assessed using four clinical endpoints: OS (overall survival), DSS (disease-specific survival), DFS (disease-free interval), and PFS (progression-free interval). In the evaluation of prognostic markers, we conducted an analysis that involved calculating hazard ratios (HR), 95% confidence intervals, and p-values. To determine the statistical significance in this study, we utilized a significance level of $p < 0.05$. This threshold helped us identify associations that were unlikely to occur by chance and confirmed the statistical significance of our findings. To examine the association between the clinical stage and the expression of ITGAL, we performed correlation analysis utilizing the R packages "limma" and "ggpubr."

Immune infiltration analysis

We used the "limma" package in R to assess the expression levels of these genes as well as examining their correlation coefficients using the Pearson statistical method. Afterwards, we employed the "ESTIMATE" package to compute the StromalScore, ImmuneScore, and ESTIMATE scores for a dataset consisting of 10,180 tumor samples across 44 different tumor types. To analyze the statistical correlation between gene expression and immune infiltration scores in each tumor, we utilized the "psych" package in R. This analysis revealed significant associations between gene expression and immune infiltration scores. To further validate these findings, immune cell infiltration data for 33 different types of cancer were retrieved from the TIMER 2.0 database (http://timer.cistrome.org) for comparison (Li et al., 2020). The visualization of the results was accomplished using the R packages "reshape2" and "RColorBrewer."

Biomarker Exploration of Solid Tumors

The survival prognosis of associated genes could be assessed through Biomarker Exploration of Solid Tumors (BEST) (http://www.rookieutopia.com) by mapping the survival curve utilizing pan-cancer samples, including GBM (CGGA325, CGGA693), LGG (CGGA301, CGGA325, CGGA693, and TCGA), CESC (TCGA), LUAD [GSE72094 (Schabath et al., 2016), GSE41271 (Sato et al., 2013; Riquelme et al., 2014; Girard et al., 2016; Parra et al., 2016), and GSE26939 (Wilkerson et al., 2012)], HNSCC [GSE65858 (Wichmann et al., 2015)], SKCM (GSE53118 (Mann et al., 2013;

Barter et al., 2014), GSE54467 (Jayawardana et al., 2015), GSE1900113 (Farshidfar et al., 2022), and TCGA), SARC [GSE21257 (Buddingh et al., 2011) and TCGA]. The ITGAL's prognostic value in pan-cancer in terms of overall survival (OS) and post-progression survival (PPS) was assessed utilizing this database. The log-rank p-value and the hazard ratio (HR) with 95% confidence intervals were also estimated. $p < 0.05$ was taken as statistically significant.

Enrichment analysis and analysis of genomic heterogeneity as well as stemness

The biological roles of ITGAL in tumors were determined through Gene set enrichment analysis (GSEA). We downloaded the gene ontology (GO) from the official GSEA website (https://www.gsea-msigdb.org/gsea/downloads.jsp). R-packages "clusterProfiler"were employed for functional analysis.

Single-cell sequencing analysis

A single-cell RNA-sequencing (scRNA-seq) data of BLCA [GSE145281_aPDL1 (Yuen et al., 2020)], CRC [GSE136394 (Lu et al., 2019), GSE139555 (Wu T. D. et al., 2020; Banta et al., 2022), and GSE146771 10X (Zhang et al., 2020)], HNSCC [GSE103322 (Puram et al., 2017), and GSE139324 (Cillo et al., 2020; Ruffin et al., 2021)], and SKCM [GSE72056 (Tirosh et al., 2016), GSE115978_aPD1 (Jerby-Arnon et al., 2018), and GSE120575_aPD1aCTLA4 (Sade-Feldman et al., 2018)] were studied based on the Tumor Immune Single Cell Hub (TISCH) database (Sun et al., 2021). The immune cells were annotated into five clusters: NK cells, B cells, CD8+T cells, monocyte or macrophage (Mono/Macro), and conventional CD4 T cells (CD4Tconv).

Drug targeted therapy and Candidate drug prediction and analysis of genomic heterogeneity as well as stemness

A gene-specific targeted therapy analysis was conducted through the BEST website, focusing on the impact of the key gene (ITGAL) on immune modulation therapy in the Cho (2020) and Hwang (2020) cohorts. Additionally, a drug prediction analysis was carried out to explore potential targeted therapy options for Head and Neck Squamous Cell Carcinoma (HNSCC), utilizing datasets such as GSE117973, E_MTAB_8588, TCGAHNSC, GSE75538, and GSE65858. We obtained and analyzed the MSI scores, TMB scores, and RNA-seq data for a specific tumor from the sangerbox3.0 platform. (Shen et al., 2022).

Result

Expression of ITGAL in pan-cancer

Through the integration and exploration of the TCGA and GTEx databases, we acquired the expression levels of ITGAL across multiple cancer types, providing evidence that ITGAL is overexpressed in 18 different tumors such as GBM, GBMLGG, LGG, BRCA, CESC, ESCA, STES, KIRP, KIPAN, STAD, HNSCC, KIRC, LIHC, SKCM, OV, PAAD, TGCT, LAML (Figure 1; Table 1). We also observed significant downregulation of ITGAL expression in 11 tumors, such as LUAD, PRAD, LUSC, WT, BLCA, THCA, READ, UCS, ALL, ACC, KICH (Figure 1; Table 1).

Immunochemistry (IHC)

In order to verification the different expression of ITGAL in tumor and peritumoral tissues. We observed variations in the levels of ITGAL expression between seven types of cancer and their corresponding paracancerous tissues (Thyroid carcinoma, Prostate adenocarcinoma, Lung squamous cell carcinoma, Lung adenocarcinoma, Cervical squamous cell carcinoma and endocervical adenocarcinoma, Ovarian serous cystadenocarcinoma, Bladder Urothelial Carcinoma) (Figures 2A–H). The conclusions reached were the same as the previous analysis and showed that the expression of ITGAL in prostate cancer, thyroid cancer, bladder cancer, lung squamous cell carcinoma, and lung adenocarcinoma are highly expressed in adjacent cancer tissues, on the other hand, ovarian cancer, renal clear cell carcinoma, and cervical cancer are highly expressed in cancer tissues Table 2.

Survival analysis

By conducting survival analysis in four domains—Overall Survival (OS), Disease-Specific Survival (DSS), Progression-Free Survival (PFS), and Disease-Free Survival (DFS)—we discovered the prognostic significance of ITGAL across various cancer types. Applying Cox regression model analysis, we found a correlation between elevated ITGAL expression and a higher likelihood of decreased overall survival (OS) in patients diagnosed with five specific types of tumors: GBMLGG, LGG, KIPAN, UVM, and LAML (as demonstrated in Figure 3A). Conversely, ITGAL acted as a protective factor in six cancer types, namely CESC, LUAD, LARC, HNSCC, SKCM-P, SKCM, and SKCM-M. Additional investigation revealed a notable correlation between the expression of ITGAL and Disease-Specific Survival (DSS) across various carcinoma categories, such as GBMLGG, LGG, KIPAN, UVM, BRCA, CESC, LUAD, HNSCC, SKCM-P, SKCM, and SKCM-M as depicted in Figure 3B. Furthermore, a Univariate Cox regression model was employed to investigate the correlation between ITGAL expression and Progression-Free Survival (PFS) in various cancer types. In nine types of tumors, namely UVM, UCEC, BRCA, CESC, HNSCC, SKCM, SKCM-M, ACC, and CHOL, the study found a significant correlation between the expression of ITGAL and a positive prognosis (as shown in Figure 3C). Additionally, high expression of ITGAL was indicative of lower Disease-Free Survival (DFS) specifically in the case of BRCA (as depicted in Figure 3D).

The association between ITGAL and pathological grades

After conducting a more comprehensive analysis of ITGAL expression levels across different pathological grades in the

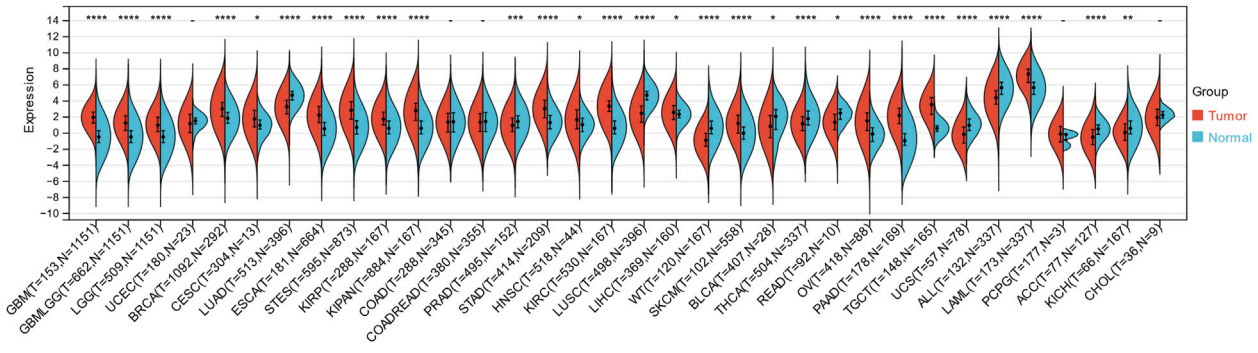

FIGURE 1
The expression of ITGAL in pan-cancer and healthy tissues (TCGA + GTEx). (-, $p \geq 0.05$; *, $p < 0.05$; **, $p < 0.01$; ***, $p < 0.001$; ****, $p < 0.0001$).

context of pan-cancer, we observed a notable discrepancy in seven tumor types in Figure 4. In this study, we employed R software to compute the expression variations of genes within each tumor across samples with different clinical stages. To assess the significance of the differences between the two groups, we conducted a statistical analysis using the unpaired Student's t-test and analysis of variance (ANOVA). Difference test for multiple groups of samples in clinical stage analysis, we observed significant differences in seven types of tumors such as STES (Stage I = 76, II = 201, III = 230, IV = 57) (p = 2.4e-3), KIPAN (Stage I = 464, II = 107, III = 189, IV = 103) (p = 9.5e-4), STAD (Stage I = 58, II = 121, III = 169, IV = 41) (p = 3.3e-3), THYM (Stage I = 36, II = 61, III = 14, IV = 6) (p = 2.3e-4), THCA (Stage I = 283, II = 52, III = 112, IV = 55) (p = 6.5e-3), SKCM (Stage II = 66, III = 26, IV = 3) (p = 0.02), CHOL (Stage I = 19, II = 9, IV = 7) (p = 0.02). And we also found differences in eight types of tumors such as GBMLGG (G2 = 247, G3 = 260) (p = 6.2e-7), LGG (G2 = 247,G3 = 260) (p = 6.2e-7), STES (G1 = 30,G2 = 222,G3 = 294) (p = 4.0e-11), KIPAN (G1 = 14, G2 = 228, G3 = 206, G4 = 74) (p = 0.02), STAD (G1 = 12,G2 = 148,G3 = 245) (p = 1.2e-9), HNSCC(G1 = 61,G2 = 304,G3 = 124,G4 = 7) (p = 6.1e-4), KIRC (G1 = 14,G2 = 228,G3 = 206,G4 = 74) (p = 0.02), AAD (G1 = 31,G2 = 95,G3 = 48) (p = 0.04) in Difference test for multiple groups of samples in stage pathological analysis.

ITGAL exhibits a strong association with immune infiltration and immune checkpoint

The study focused on investigating the role of ITGAL in the TME, its relationship with immune infiltration in different cancer types. Specifically, the researchers analyzed the correlation between ITGAL and three distinct immune scores. The results of this analysis are showcased in Figures 5A–R, which highlight the six most notable correlations between ITGAL and the diverse immune scores in specific cancer types. According to the ImmuneScore revealed that the expression of ITGAL in SKCM, SKCM-M, PAAD, TGCT, SKCM-P and UVM was positively correlated with immune infiltration (Figures 5A–F). According to the EstimateScore, the analysis suggests that the expression of ITGAL is correlated with increased levels of immune infiltration in several tumor types, including KIPAN, SKCM-M, SKCM, PAAD, SKCM-P, and UVM (Figures 5G–L). This trend was also suggested by the StromalScore, ITGAL expression in GBMLGG, LGG, KIPAN, PAAD, UVM and ACC was significantly positive correlated with immune infiltration (Figures 5M–R). Despite numerical variations in the three scores, there was a consistent overall trend indicating that ITGAL plays a significant regulatory role in the tumor microenvironment to some extent in malignant conditions. In our study, we undertook a thorough analysis to investigate the potential correlation between ITGAL expression and 60 genes related the immune checkpoint pathway in diverse cancer types. The findings, depicted in Figure 5S, revealed significant correlations between ITGAL and a wide range of immunosuppressive/immunostimulatory genes present in pan-cancer. Specifically, ITGAL exhibited strong positive correlations with most immune checkpoint pathway genes. These results indicate that ITGAL is closely associated with immune checkpoint genes and predominantly facilitates the infiltration of immune cells.

ITGAL-related GSEA

The GSEA algorithm analysis was carried out in pan-cancer to elucidate the underlying physiological processes that might be mediated by ITGAL and subsequently, six tumors with similar results were selected (Supplementary Figure S1). It was found that ITGAL participated in pan-cancer immune regulation-related pathways, particularly in leukocyte-mediated cytotoxicity, lymphocyte-mediated immunity, adaptive immune response, cytokine signaling in the immune system, and antigen processing and presentation. It was highlighted by these findings that ITGAL is crucially involved in tumor immunity.

Immune infiltration analysis

According to the data, five cancer types with high ITGAL expression predicted good prognosis (TCGA-CESC [N=273, p<0.05], TCGA-LUAD [N=490, p<0.05], TCGA-SARC [N=254, p<0.05], TCGA-HNSC [N=509, p<0.05], and TCGA-SKCM [N=444, p<0.05]), while two cancer types with high ITGAL expression predicted poor prognosis (TCGA-LGG [N=504, p<0.05] and TCGA-GBM [N=152, p<0.05]) (Figure 6). The immune cells such

TABLE 1 Differential expression of ITGAL in cancer and adjacent normal tissues.

Tumor type	Tumor (Mean ± SD)	Normal (Mean ± SD)	p-value	Regulation status
GBM	1.95 ± 1.09	−0.38 ± 1.29	2.40E-61	Overexpression
GBMLGG	1.29 ± 1.30	−0.38 ± 1.29	3.70E-117	Overexpression
LGG	1.10 ± 1.30	−0.38 ± 1.29	8.90E-84	Overexpression
BRCA	2.91 ± 1.36	1.78 ± 1.13	6.20E-40	Overexpression
CESC	1.73 ± 1.54	0.92 ± 1.22	0.05	Overexpression
ESCA	2.20 ± 1.53	0.55 ± 1.27	3.70E-35	Overexpression
STES	2.77 ± 1.54	0.76 ± 1.31	9.20E-109	Overexpression
KIRP	1.81 ± 1.28	0.74 ± 1.38	3.40E-16	Overexpression
KIPAN	2.57 ± 1.61	0.74 ± 1.38	1.80E-37	Overexpression
STAD	3.02 ± 1.48	1.43 ± 1.23	1.10E-33	Overexpression
HNSC	1.60 ± 1.68	1.06 ± 1.14	0.01	Overexpression
KIRC	3.30 ± 1.25	0.74 ± 1.38	7.30E-58	Overexpression
LIHC	2.53 ± 1.24	2.34 ± 0.74	0.01	Overexpression
SKCM	1.22 ± 1.73	−0.02 ± 1.16	4.30E-12	Overexpression
OV	1.37 ± 1.68	−0.11 ± 1.22	1.50E-15	Overexpression
PAAD	2.08 ± 1.53	−0.67 ± 1.40	1.10E-38	Overexpression
TGCT	3.38 ± 1.42	0.62 ± 0.66	2.80E-45	Overexpression
LAML	7.06 ± 1.26	5.57 ± 1.24	2.10E-30	Overexpression
LUAD	3.17 ± 1.22	4.68 ± 0.77	6.00E-75	Downregulation
PRAD	1.00 ± 1.27	1.46 ± 1.22	1.30E-04	Downregulation
LUSC	2.33 ± 1.41	4.68 ± 0.77	1.70E-111	Downregulation
WT	−0.92 ± 1.26	0.74 ± 1.38	2.90E-21	Downregulation
BLCA	0.87 ± 1.84	1.66 ± 1.87	0.01	Downregulation
THCA	1.24 ± 1.39	1.95 ± 1.39	5.60E-12	Downregulation
READ	1.27 ± 1.39	2.36 ± 1.04	0.02	Downregulation
UCS	−0.10 ± 1.53	1.13 ± 0.98	1.80E-07	Downregulation
ALL	4.26 ± 1.53	5.57 ± 1.24	2.30E-17	Downregulation
ACC	−0.51 ± 1.52	0.44 ± 0.84	2.70E-07	Downregulation
KICH	0.06 ± 1.34	0.74 ± 1.38	2.60E-03	Downregulation

as CD8+T cells and activated CD4 memory cells had high infiltration in cancers where higher expression levels of ITGAL indicated good prognosis, while low $CD8^+$ T cells' infiltration was observed in two cancer types where high ITGAL expression was linked to poor prognosis. In all cancer types, NK cells exhibited low levels of infiltration. CD4 memory T cells showed high infiltration in LGG and LAML. M1 showed high invasion in all seven cancer types. Contralaterally, M2 showed high invasion in two cancer types with low ITGAL expression, indicating a good prognosis. Regulatory T cells (T-regs) invaded five cancer types with a p-value of 0.05 or higher. In seven cancer types among the species, the activated dendritic cells showed low invasion in most cancers but high invasion in LGG.

ITGAL can be utilized as a biomarker for the detection of head and neck squamous cell carcinoma

The studies revealed a substantial upregulation of ITGAL in HNSCC. Survival analysis further demonstrated a significant correlation between the expression level of ITGAL and the overall survival (OS) of HNSCC patients. Additionally, this correlation remained significant when examining the association between ITGAL and RNAss (RNA based Stemness Scores). Consequently, our subsequent investigation delved into the potential biological functions of ITGAL specifically within the context of HNSCC. In order to improve prognostic

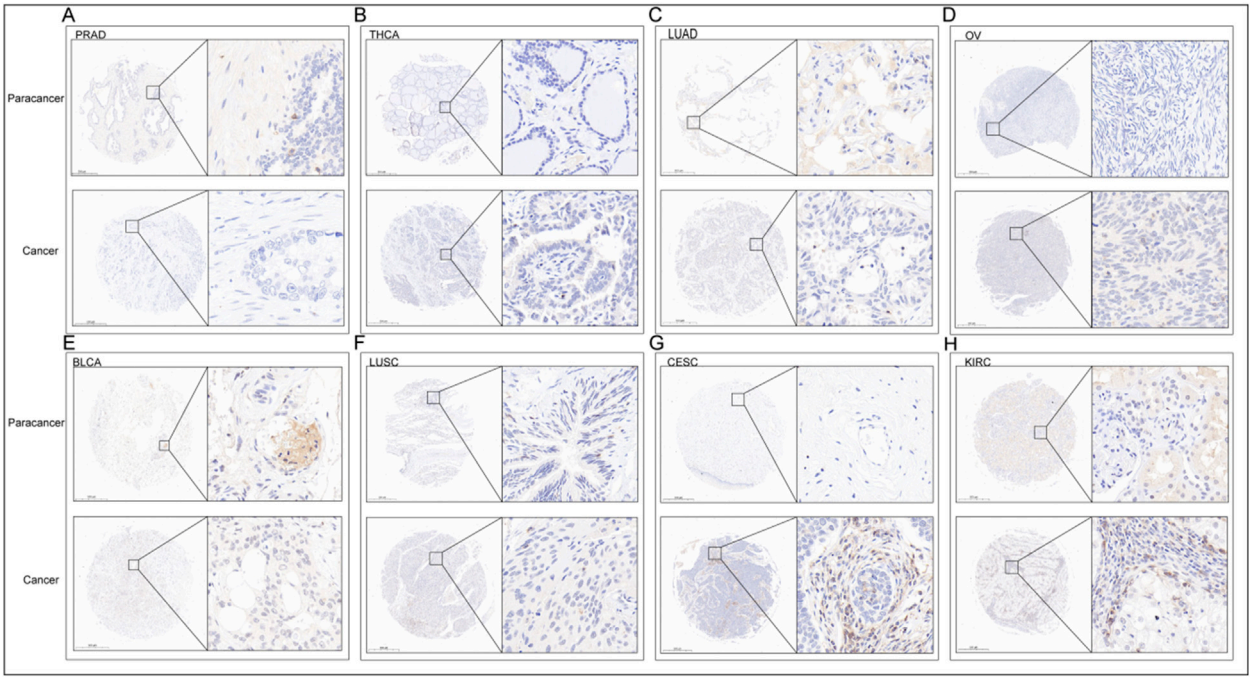

FIGURE 2
IHC of PRAD **(A)**, THCA **(B)**, LUAD **(C)**, OV **(D)**, BLCA **(E)**, LUSC **(F)**, CESC **(G)**, KIRC **(H)**. The upper row is the paracancerous tissue, and the lower row is the cancer tissue in each unit.

TABLE 2 Numerical values related to ICH experimental results.

Cancer type	Tissue type	Positive cells, %	Positive cells density, number/mm^2	Mean density	H-score	IRS
PRAD	paracancerous tissues	0.99%	17	1.9798	2.65	0
	cancerous tissues	3.12%	292	1.0625	6.77	0
THCA	paracancerous tissues	7.22%	117	1.2745	19.42	3
	cancerous tissues	5.00%	183	1.9055	13.71	0
LUAD	paracancerous tissues	21.97%	110	0.5126	39.06	2
	cancerous tissues	6.81%	148	1.0810	16.29	2
OV	paracancerous tissues	0.82%	34	2.5953	2.30	0
	cancerous tissues	7.63%	369	0.6443	12.51	2
BLCA	paracancerous tissues	50.49%	201	0.8031	114.85	6
	cancerous tissues	21.70%	434	0.7575	35.27	2
LUSC	paracancerous tissues	14.47%	252	1.0096	36.73	3
	cancerous tissues	13.51%	362	0.7841	30.46	2
CESC	paracancerous tissues	10.77%	112	2.8235	30.67	3
	cancerous tissues	21.34%	1,017	0.7500	47.63	2
KIRC	paracancerous tissues	29.80%	567	0.4881	54.88	4
	cancerous tissues	43.31%	998	0.6414	83.56	4

assessment for patients in clinical settings, we developed a nomogram that integrates the expression of ITGAL and the pathological stage. This nomogram provides a more accurate tool for predicting patient outcomes in HNSCC and can aid in clinical decision-making. The nomogram depicted in Figure 7A functions as a valuable instrument in clinical practice for

10.3389/fphar.2024.1464830

FIGURE 3
Univariate COX regression analysis was performed to assess the association between ITGAL and O), PFS, DFS, DSS. **(A)** Correlation between ITGAL expression and OS; **(B)**, DSS; **(C)**, PFS; **(D)**, DFS. OS, overall survival; DSS, disease-specific survival; DFS, disease-free survival; PFS, progression-free survival.

foreseeing patient outcomes. Additionally, calibration curves were employed to evaluate the accuracy of the current model in forecasting the prognosis of patients with HNSCC at 1-year, 3-year, and 5-year intervals. The results, depicted in Figure 7B, demonstrate a favorable performance in the assessment of patient prognosis.

To gain deeper insights into the potential ways in which ITGAL affects patient prognosis, we conducted an analysis to determine the relationship between gene expression and pathway scores. Our findings indicate a significant correlation between ITGAL expression and various factors including cell motility, B cell activation, T cell activation, lymphocyte-mediated immunity,

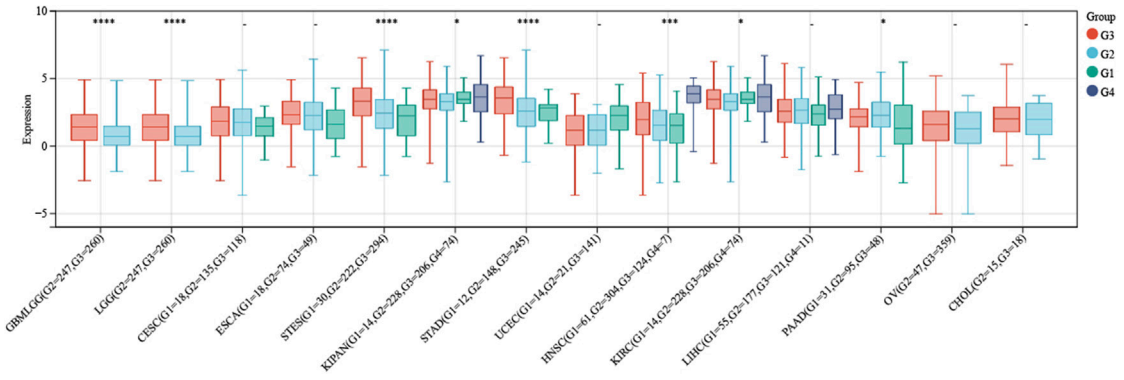

FIGURE 4
Expression levels of ITGAL at distinct pathological grade in pan-cancer.

leukocyte-mediated immunity, leukocyte proliferation, cellular community, transport and catabolism, as well as carbohydrate metabolism in HNSCC (Figures 8A, B). Drawing from the GSEA results, we put forth the hypothesis that the influence on the malignant growth of HNSCC could potentially be accomplished by modulating signaling communication via the TGF-b pathway (Figure 8A).

Link of the HNSCC signature with the TME

It has been suggested by several reports that TME is associated with the efficacy of immunotherapy (Ock et al., 2016; Varn et al., 2017; Bagaev et al., 2021). Bagaev et al. (2021), classified HNSCC immune microenvironment into four types: immune-depleted (D), fibrotic (F), immune-enriched (IE), and non-fibrotic and immune-enriched/fibrotic (IE/F) (Figure 9). His findings revealed that ITGAL expression was closely related to the, IE subtype, which is linked to a good prognosis.

Single-cell analysis

Considering the contribution of TME to tumor onset and progression and its prognostic effect, HNSCC (GSE103322 and GSE139324) were analyzed in TISCH to assess the expression of ITGAL in TME-linked cells. The GSE103322 and GSE139324 datasets of HNSCC were analyzed and classified into 11 types of cells. CD8 T exhausted cells were the most abundant in the GSE103322 dataset. As indicated by Figure 10, the infiltration degree of ITGAL in TME-linked cells was higher in CD8+T, CD8 T exhausted, and CD4 conventional cells, which is in line with the findings presented in Figure 8B. In the GSE139324 dataset, the most abundant immune cells were CD4 conventional cells. The infiltration degree of ITGAL in TME-linked cells was higher in CD8+T, CD8 T exhausted, monocytes/macrophages, and B cells (Figure 11), which is in line with the findings in Figure 8B. It is suggested by these findings that ITGAL is closely linked to the TME in HNSCC.

Pan-cancer analysis of ITGAL expression in correlation with the tumour purity, TMB, MSI, as well as stemness

In order to determine the suitability of immune checkpoint therapy, the correlation between ITGAL expression and TMB (Tumor Mutational Burden) as well as MSI (Microsatellite Instability) was investigated and compared across various cancer types. It was observed that TMB and MSI play a crucial role in this determination. Across various cancer types, the expression of ITGAL showed predominantly positive correlations with both TMB and MSI. Specifically, in COAD, COADREAD, UCEC, READ, OV, there was a significant positive association observed between the manifestation of ITGAL and TMB scores (Figure 12D). On the other hand, in patients with GBMLGG, BRCA, KIRP, KIPAN, HNSCC, OV, TGCT, DLBC, the expression of ITGAL displayed a closer and negative correlation with MSI. (Figure 12C). The effectiveness of immune checkpoint inhibitor (ICI) treatment can be influenced by tumor purity. During our analysis of 35 tumors, we identified a noteworthy negative correlation between the ITGAL expression and tumor purity. The observation made in our analysis indicates that there is a consistent association between higher levels of ITGAL expression and decreased tumor purity across all the tumor types that were examined (Figure 12A). Furthermore, the stemness score, which is associated with drug resistance and continuous tumor cell proliferation, was also evaluated in relation to ITGAL expression. In our study, we conducted a Pearson correlation analysis to investigate the relationship between ITGAL expression and RNAss across various tumors. The findings, depicted in Figure 12D, demonstrated significant correlations between ITGAL and tumor stemness scores in 32 tumor samples. Among these, 31 tumors exhibited a significant negative correlation. Notably, LGG ($R = -0.55$), KIPAN ($R = -0.53$), GBMLGG ($R = -0.52$), COAD ($R = -0.47$), READ ($R = -0.46$), PAAD ($R = -0.45$), and ACC ($R = -0.40$) were among the cancer types with the most significant correlations (Figure 12B). However, it is worth mentioning that THYM displayed a significant positive correlation in this relationship ($R = 0.40$).

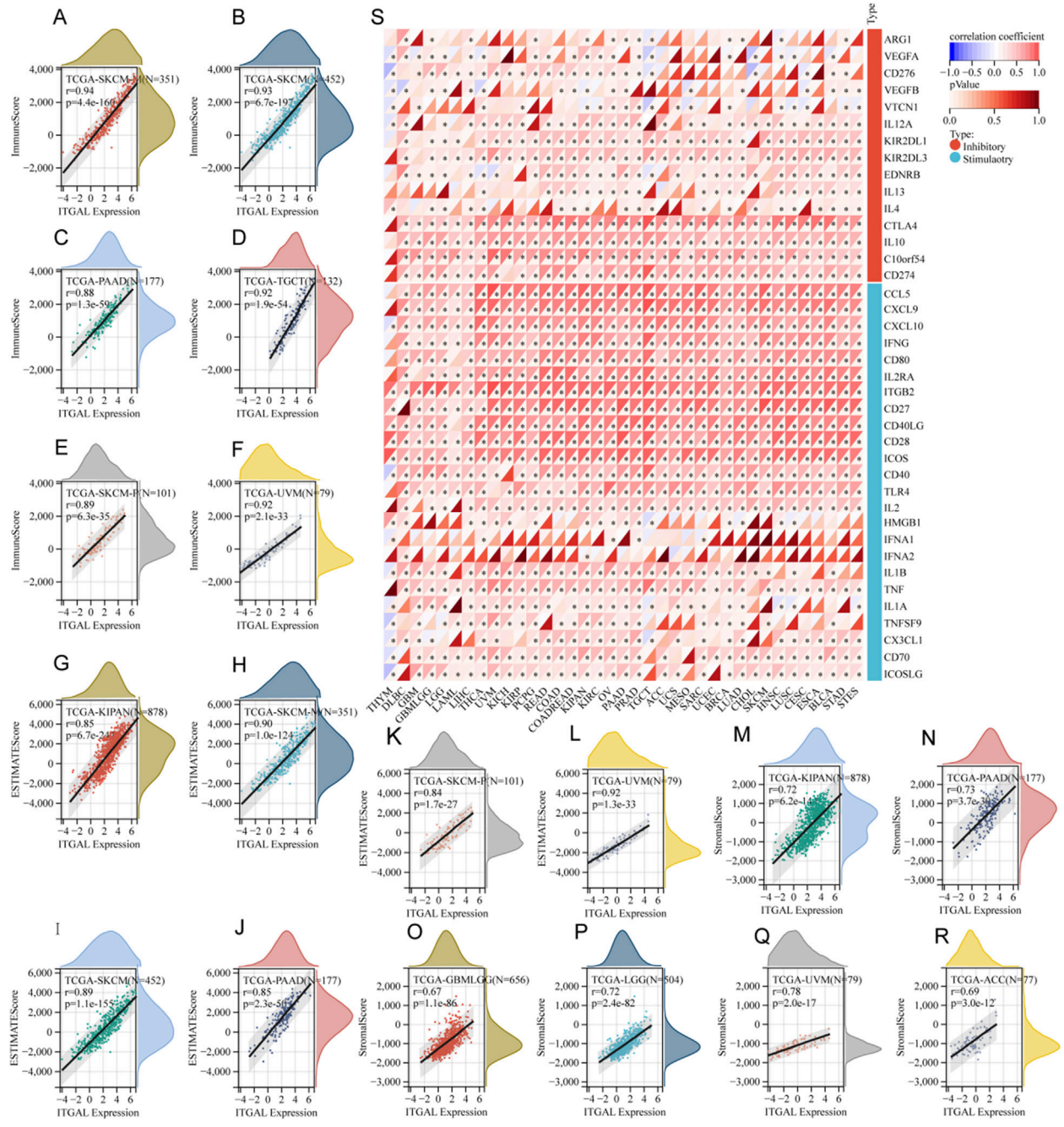

FIGURE 5
The relationship between ITGAL expression and immune infiltration as well as immune checkpoints. **(A–F)** Correlation of ITGAL expression with ImmuneScore; **(S)** Correlation of ITGAL expression with immune checkpoint-related genes; **(G–L)** Correlation of ITGAL expression with EstimateScore; **(M–R)** Correlation of ITGAL expression with StromalScore.

Immunotherapy response analysis

We studied the drug treatment of HNSCC. In the Cho cohort 2020, it was discovered that the efficacy of Anti-PD-1/PD-L1 on HNSCC was closely related to the ITGAL expression. Those with high ITGAL expression were more efficient than the Anti-PD-1/PD-L1 (Figure 13A), and the probability was as high as 96.4% (Figure 13B). As depicted in Figure 13C, it could be seen that the PFS of those with high ITGAL expression was remarkably higher in comparison to the low expression group, confirming the role of ITGAL in the efficacy of Anti-PD-1/PD-L1. As per the cohort of Hwang 2020, we also found that the efficacy of Anti-PD-1 monotherapy on HNSCC was closely related to the ITGAL expression, and those with high ITGAL expression were more likely to respond to Anti-PD-1 (Figure 13D), and the probability was as high as 76.9% (Figure 13E). As shown in Figure 13F, the PFS of the ITGAL high-expression group was considerably higher in contrast with the low-expression group, confirming the role of ITGAL in the efficacy of Anti-PD-1. These findings revealed that the expression of

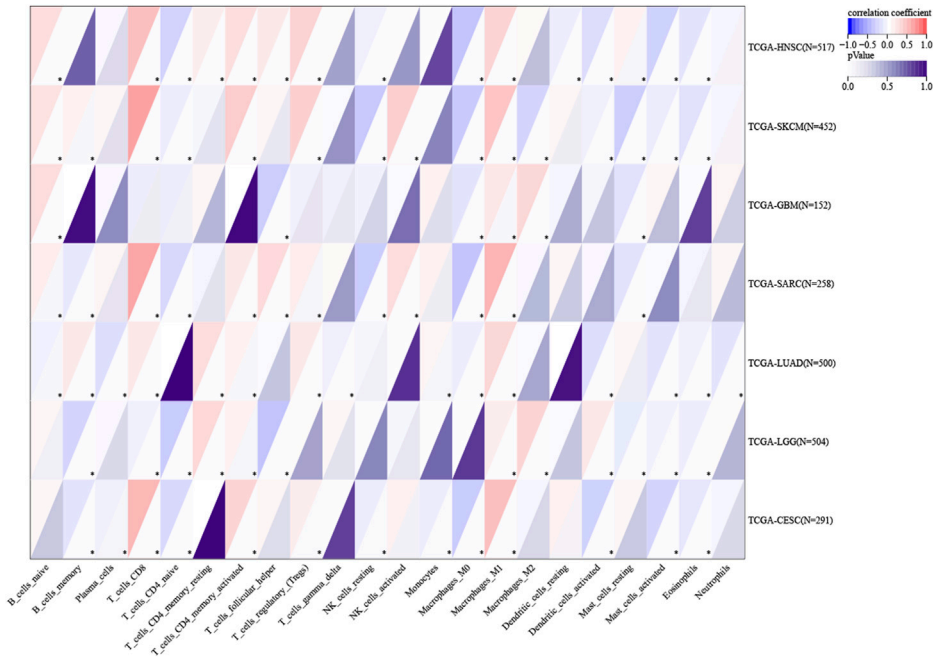

FIGURE 6
Association of ITGAL with the tumor microenvironment. Red highlights a positive correlation, and blue highlights a negative correlation; the darker the color, the stronger the association. (*p < 0.05, **p < 0.01, ***p < 0.001, ****p < 0.0001).

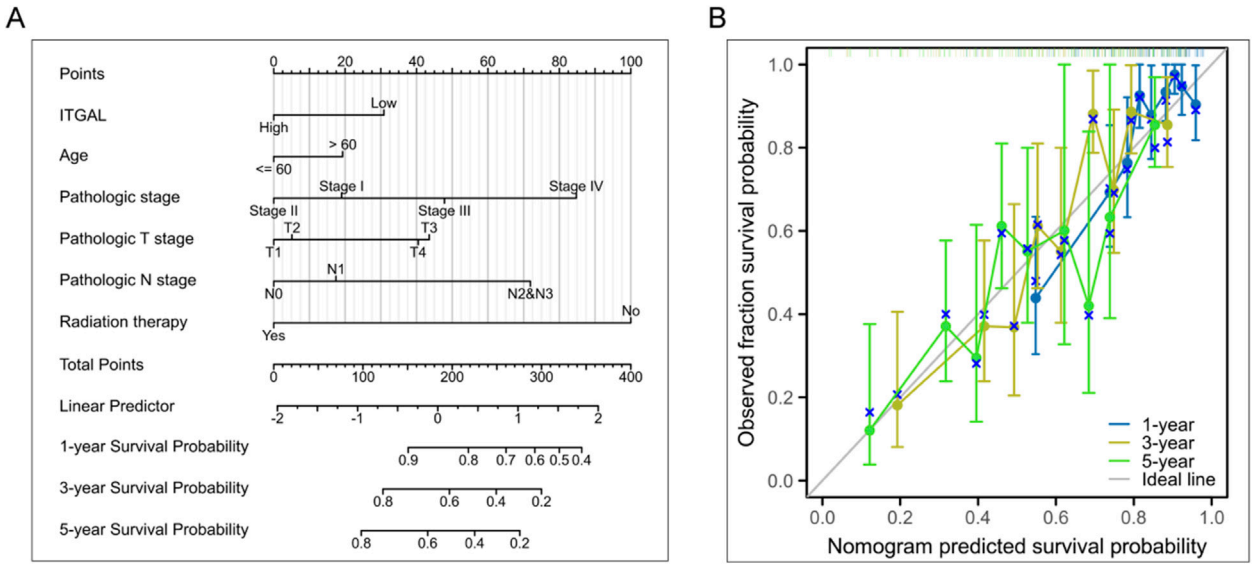

FIGURE 7
Investigation of the clinical significance of ITGAL in HNSCC. **(A)** Development of a nomogram utilizing ITGAL expression and pathological staging. **(B)** Prognostic standard curve of nomogram.

ITGAL may be associated with the efficacy of Anti-PD-1/PD-L1 and Anti-PD-1 on HNSCC.

In order to conduct a more thorough examination of potential drugs that could effectively target the overexpression of ITGAL, we conducted a comparison of the estimated IC50 levels for lots chemotherapy drugs or inhibitors in "GDSC1" database. Figure 14 displays a selection of representative drugs. We found that several drugs are potential for treating patients with ITGAL high. Expression, such as MK-2206_1053, PF-4708671_1129, NG-25 260, VX-702_1028, AKT inhibitor VIll_228, Linifanib_277, Ara-G 427, PIK-93303 and so on.In order to conduct a more thorough examination of potential drugs that could effectively target the overexpression of ITGAL, we conducted a

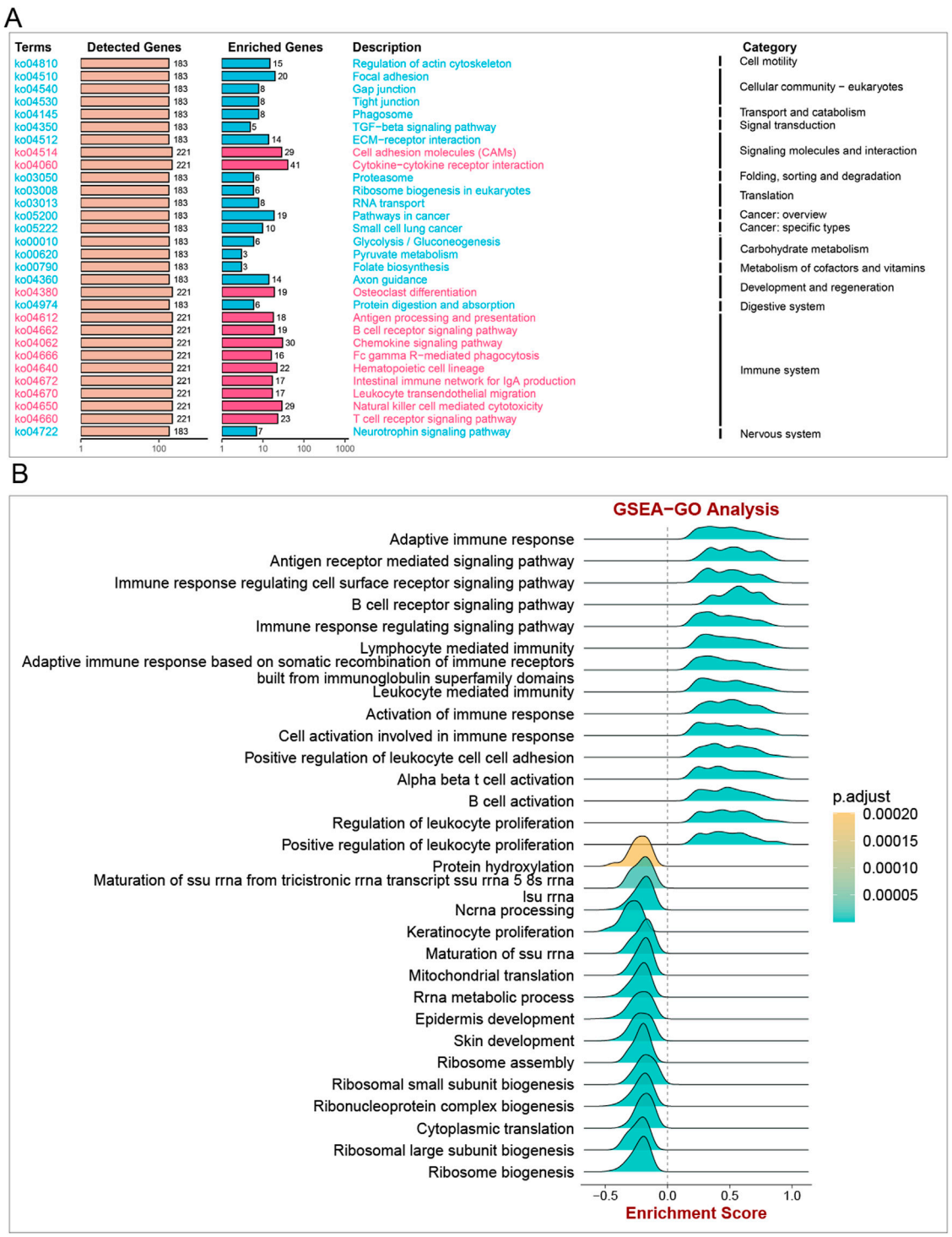

FIGURE 8
Enrichment analysis of ITGAL in HNSCC. **(A)** GSEA-KEGG analysis, **(B)** GSEA-GO analysis.

comparison of the estimated IC50 levels for lots chemotherapy drugs or inhibitors in "GDSC1" database. Figure 13 displays a selection of representative drugs. We found that several drugs are potential for treating patients with ITGAL high Expression, such as MK-2206_1053, PF-4708671_1129, NG-25 260, VX-702_1028, AKT inhibitor VIll_228, Linifanib_277, Ara-G 427, PIK-93303 and so on.

Discussion

Integrin alpha L chain encoded by ITGAL plays a crucial role in intercellular adhesion between leukocytes by binding to intercellular adhesion molecules 1–3 (ICAMs 1–3) (Corbi et al., 1988; Hickman et al., 2022). Furthermore, prior research suggests that LFA-1

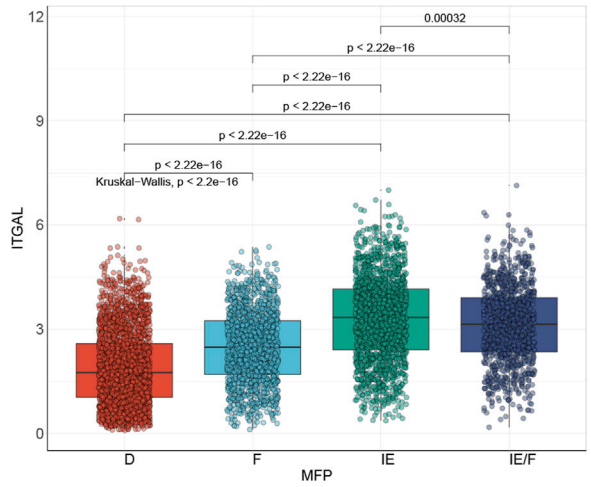

FIGURE 9
The association of ITGAL expression with tumor microenvironment subtype.

encoded by ITGAL is closely associated with inflammatory responses, which are reduced significantly via the mechanism of blocking LFA-1 (Whitcup et al., 1999). These activities involve the interaction between leukocytes and endothelial cells, the killing of target cells by cytotoxic T-cells, and the killing of target cells through the assistance of antibodies by granulocytes and monocytes. It also promotes the cytotoxicity of natural killer cells (Barber et al., 2004).

We discovered that the expression of ITGAL in cancer tissues and paracancerous tissues is different in most cancer types, except UCEC, COAD, COADREAD, PCPG, CHOL. We conducted COX regression analysis and KM survival curves, which provided some confirmation that ITGAL has the potential to be a dependable biomarker. Upon comparing these results with those of the survival analysis, we discovered a significant association between ITGAL and four prognostic factors, namely OS, DSS, DFS, and PFS, across eight types of tumors, including GBMLGG, LGG, KIPAN, UVM, CESC, LUAD, HNSCC, SKCM. The potential of ITGAL as a biomarker is substantiated by its differential expression levels across distinct pathological stages within the same tumor. Increased expression of ITGAL is notably observed in the higher stages, further highlighting its significance as a potential biomarker. Immune cells and fibroblasts can exhibit both tumor-promoting and tumor-inhibiting effects within the microenvironment of a tumor. (Dudas, 2015), Improved understanding of the biological mechanisms that govern the tumor microenvironment (TME) could lead to more effective and targeted immunotherapies for various types of difficult-to-treat cancers, making it a valuable and potent tool in the fight against these diseases. At present, there are single-cancer immunoassay for ITGAL, but there is still a lack of an immunoassay for pan-cancer. Initially, we evaluated three immune scores, namely StromalScore, ImmuneScore, and EstimateScore, to determine their correlation with ITGAL in pan-cancer. Our findings indicated a strong positive correlation between ITGAL and these immune scores, indicating that ITGAL expression significantly contributes to the enhancement of immunity, which may be the reason why some cancers have a better prognosis, such as HNSCC, LUAD and SKCM. However, there are still many cancers with poor prognosis, including LGG, BGMLGG, KIPAN and UVM. Amanda's study showed that ITGAL promotes Cx3cr1 expression, cx3cl1-mediated migration and Ccl5 expression in microglia, thereby promoting microglial infiltration and tumor formation (De Andrade Costa et al., 2021). Based on this study, we speculate that in KIPAN and UVM, ITGAL also increases the migration and invasion ability of cancer cells by affecting certain regulatory genes. The regulatory mechanism needs to be further studied and verified through experiments. In addition to that, we conducted a comprehensive analysis to determine the relationship between ITGAL and the infiltration of various immune cells. The results strongly suggest a notable association between the expression of ITGAL and multiple types of immune cells. Specifically, ITGAL expression positively influenced the infiltration of $CD8^+$ T cells, Macrophages_M1 cells, and B cells, while inhibiting the infiltration of Macrophages_M2 cells. Prior research has demonstrated that the infiltration of $CD8^+$ T cells can have a positive impact on the prognosis of patients (Liu et al., 2017), and high tumor stromal density of M2-like macrophages was associated with worse cancer-specific survival, which partly explains the improvement of prognosis

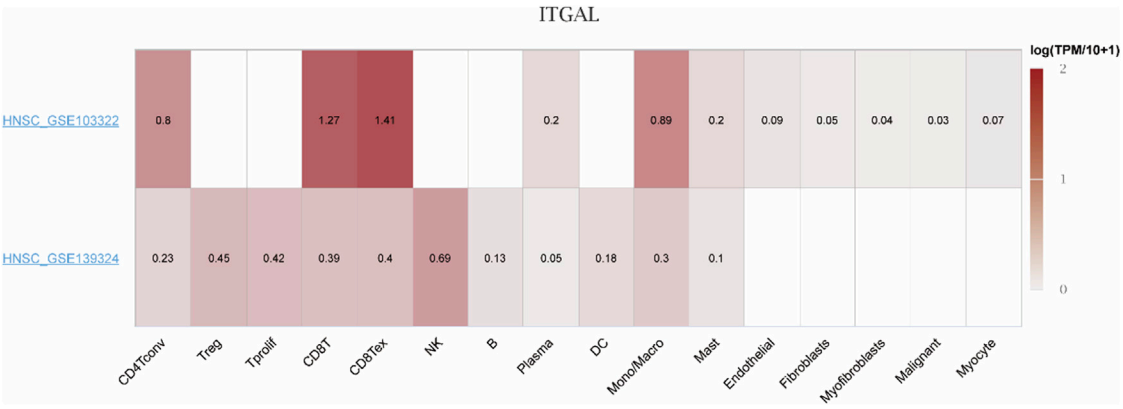

FIGURE 10
Correlation analysis between the expressions of ITGAL in HNSCC tissues and the TME, employing TISCH. Red indicates a positive correlation; the darker the color, the stronger the correlation.

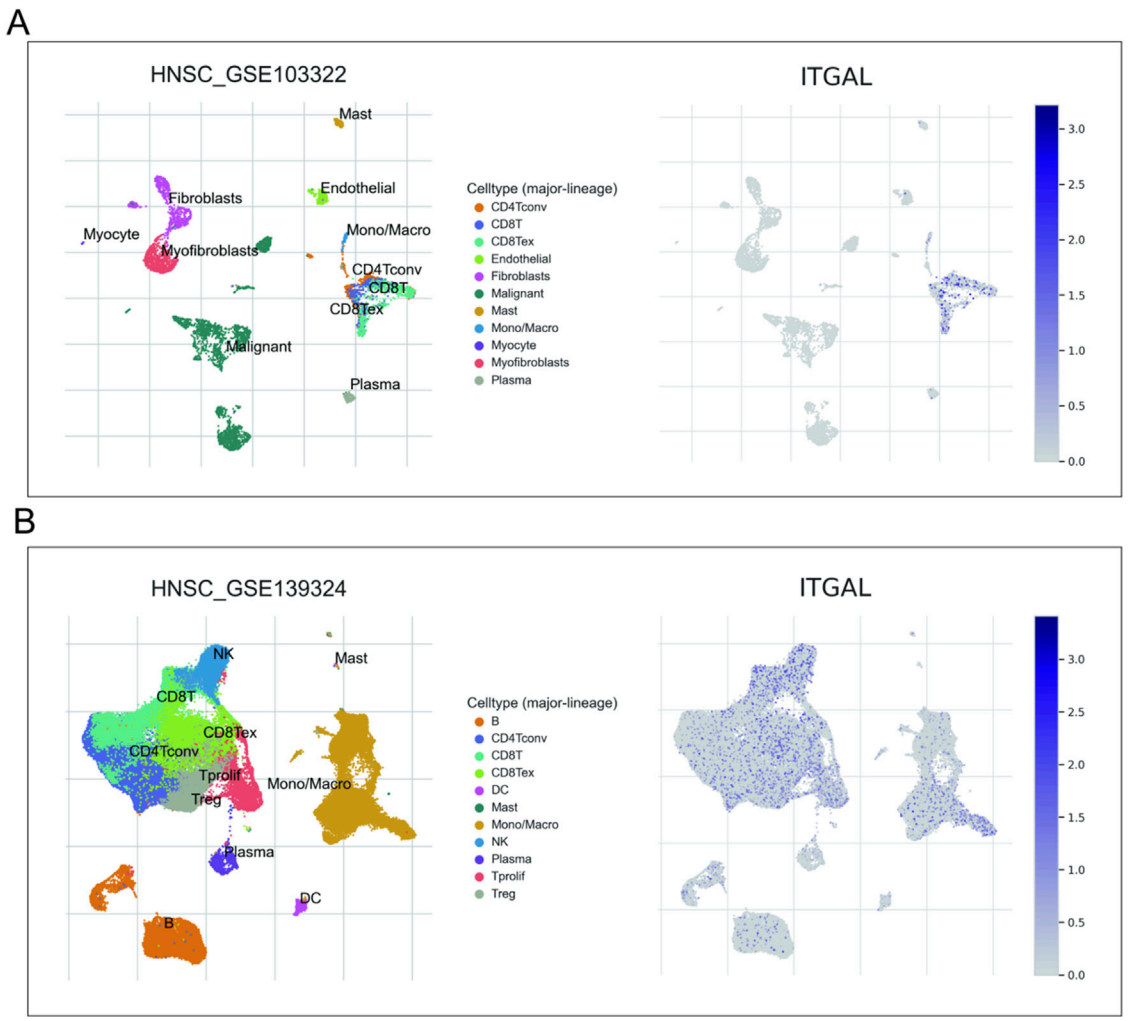

FIGURE 11
Correlation analysis between the expression of ITGAL in cancer tissues [GSE103322 **(A)** and GSE139324 **(B)**] and the TME utilizing TISCH.

of CESC, LUAD, HNSCC, SKCM with high expression of ITGAL. Moreover, the correlation linking ITGAL to immunomodulatory genes, including MHC, chemokines, and genes related to chemokine receptors, provides additional evidence of its association with tumor immunity. This association is bolstered by the observation that increasing ITGAL expression leads to a noticeable increase in MHC-1 expression. This is also one of the reasons why CESC, LUAD, HNSCC, SKCM have good prognosis when ITGAL is highly expressed.

The absence of immune cells within the tumor microenvironment has been linked to unfavorable outcomes in most cancer cases. This exclusion of immune cells is commonly observed alongside the presence of a stem cell-like characteristic, referred to as "stemness," in tumors. The activation of a stemness program seems to hinder the body's immune responses against the tumor through various mechanisms, such as the tumor cells themselves silencing endogenous retrovirus expression, suppressing type I interferon signaling, and increasing the expression of immunosuppressive checkpoints (Miranda et al., 2019). The study investigated the relationship between DNAss and ITGAL in different types of cancer, specifically LGG, UVM, LUAD, SKCM, and HNSCC. The findings revealed a positive correlation between ITGAL and DNAss in LGG and UVM, whereas a negative correlation was observed in LUAD, SKCM, and HNSCC. These results align with the prognostic outcomes, indicating that ITGAL potentially affects DNAss.

Head and neck squamous cell carcinoma ranks as the sixth most common cancer globally and holds the highest incidence in South Asia. This type of cancer accounts for approximately 890,000 newly reported cases and around 450,000 reported deaths worldwide (Kamal et al., 2023). We performed a focused analysis of the performance of ITGAL in HNSCC. And our analysis indeed revealed that ITGAL could serve as an independent prognostic factor for patients with HNSCC. And through online analysis, we looked for the possible action pathway of ITGAL, TGF-βsignaling pathway. The classification of HNSCC according to the effect of ITGAL on the immune microenvironment also shows that ITGAL can affect the prognosis of head and neck cancer through the immune microenvironment.

We used "IOBR" to analyze the infiltration degree of Immune cells in ITGAL. The results showed that high expression of ITGAL was positively correlated with the infiltration of CD8+T and Macrophages_

10.3389/fphar.2024.1464830

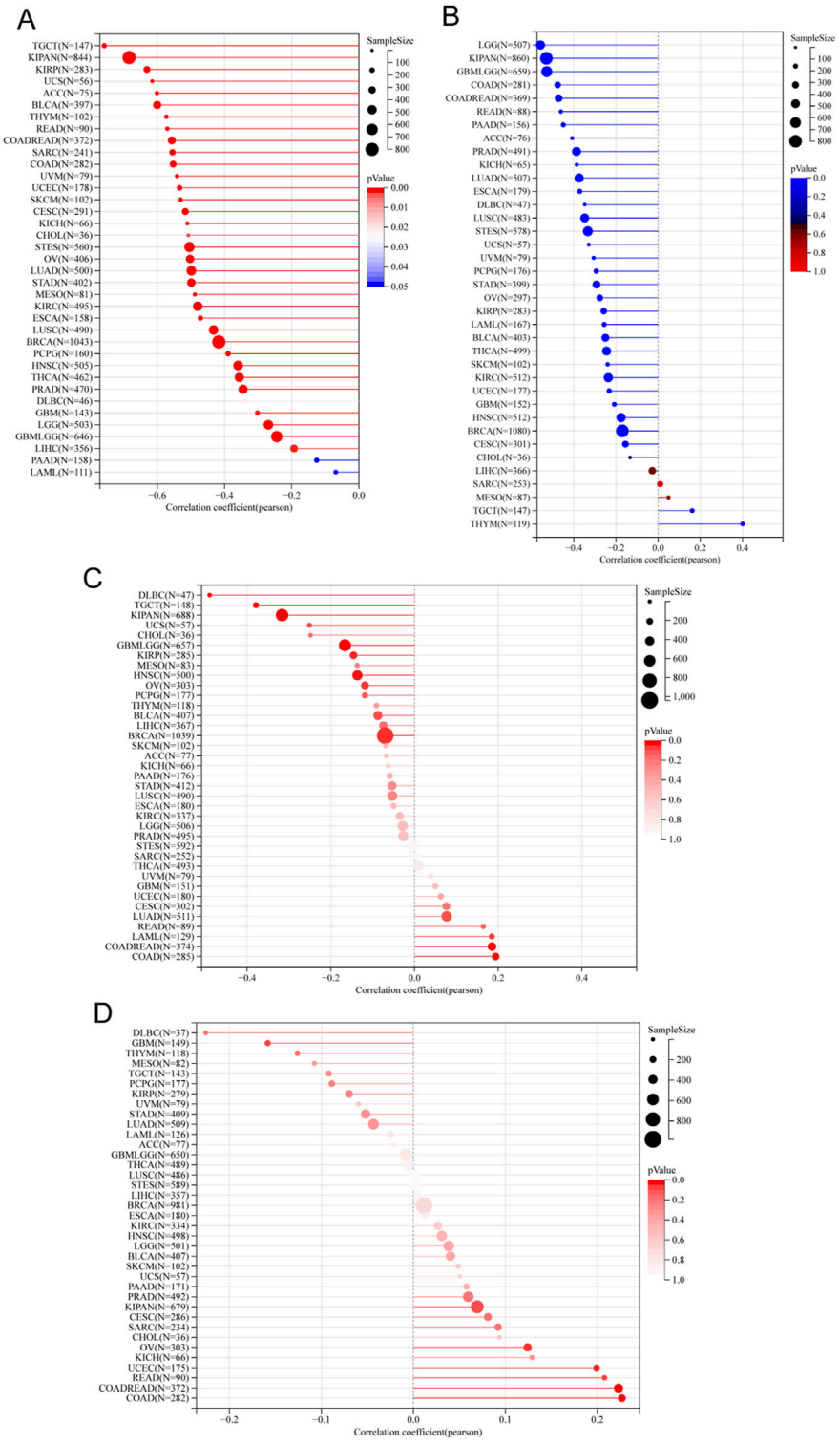

FIGURE 12
Correlation analysis of the association between ITGAL expression and tumour purity **(A)**, RNAss **(B)**, MSI **(C)** and TMB **(D)**.

M1 and the signature scores of CD8 T cells, T cell inflamed GEP, exhausted CD8, co-stimulation T, and inflamed T cells were remarkably higher. This increase indicated that ITGAL is closely related to T-cell immunity. Our findings suggested that ITGAL is critically involved in tumor immunity. To obtain a deeper understanding of the TME in HNSCC, we conducted a comprehensive analysis of cell types, annotating them at the single-cell level. We discovered that ITGAL was positively correlated with CD8+T, CD4+T, NK, and monocyte/macrophage infiltration in HNSCC, which can enhance immune killing against tumors.

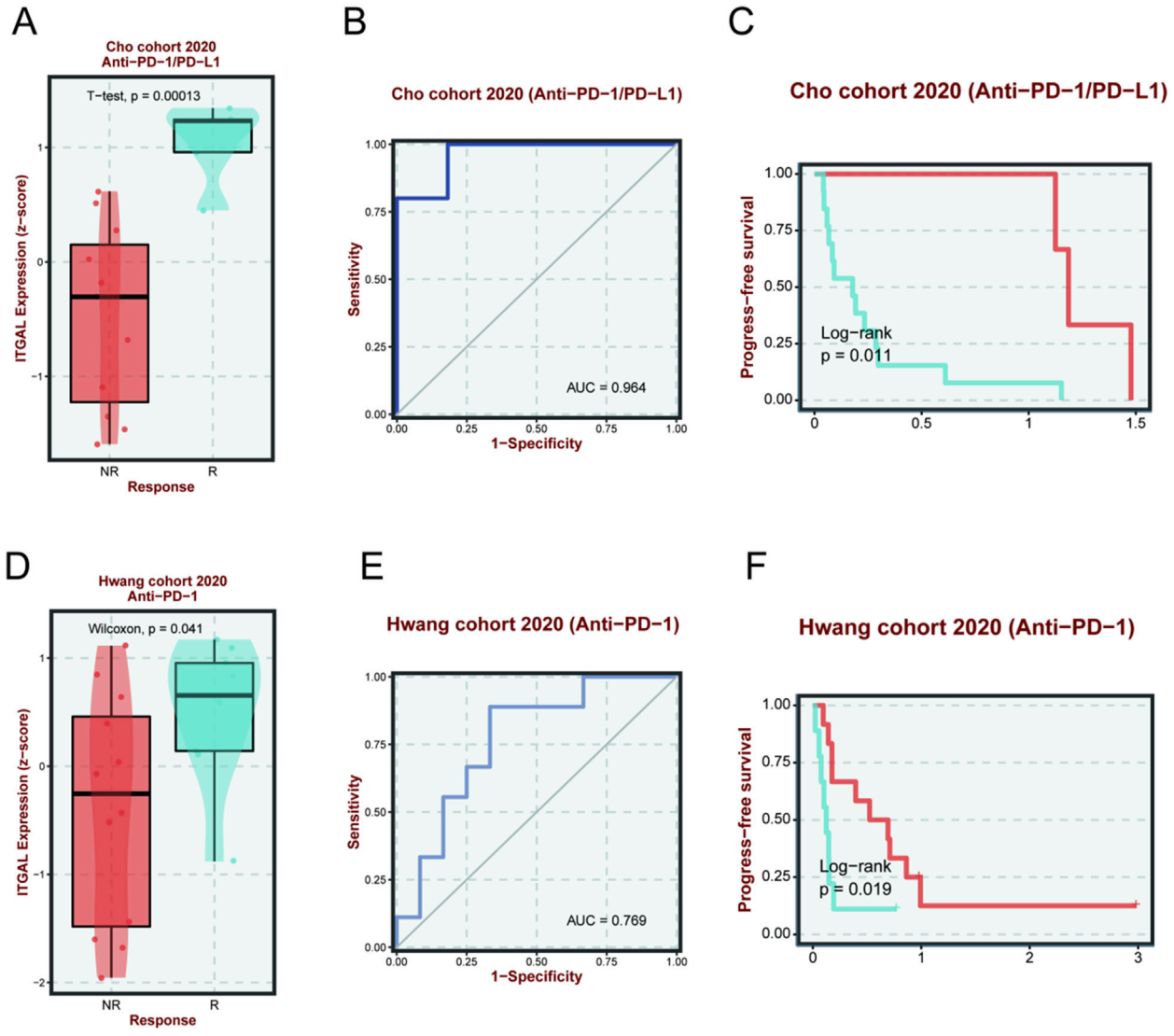

FIGURE 13
The relationship between ITGAL expression and immunotherapy sensitivity and prognosis of Cho cohort 2020 (Anti-PD-1/PD-L1) **(A–C)** and Hwang cohort 2020 (Anti-PD-1) **(D–F)**. The red line indicates a high expression of ITGAL, and the blue line indicates a lower expression of ITGAL.

Importantly, our research findings suggested that the efficacy of Anti-PD-1/PD-L1 and Anti-PD-1 on HNSCC was closely linked to the ITGAL expression; and those with high ITGAL expression were more likely efficient in Anti-PD-1/PD-L1. This finding may provide a targeted anti-tumor strategy for ITGAL to treat HNSCC. We further analyzed the effect of ITGAL on drug IC50, and found that with the increase of ITGAL expression, the IC50 of various drugs decreased, reflecting that ITGAL plays a positive role in the treatment of HNSCC.

Our findings may provide a targeted anti-tumor strategy for ITGAL by influencing the tumor immune microenvironment to treat HNSCC. Our study, however, has certain limitations. In this research, most of the data were retrieved from online databases, which are constantly updated and expanded; this may have influenced our research outcomes. Furthermore, we have not added information about complications. Third, whether immune cell infiltration correlates with the OS of patients was not determined in this research. This may provide an interesting research direction for further studies. While the present study has shed some light on the role of ITGAL in the realm of immunotherapy from a broad standpoint, it emphasizes the need for additional experimental investigations. The current findings provide strong indications for the importance of conducting further research in this area.

Conclusion

In briefly, ITGAL acts as a pan-oncogene and displays distinct expression patterns in different types of cancer. These patterns provide valuable insights into patient prognosis and survival across various malignancies. It serves as a valuable therapeutic and prognostic indicator for diverse malignancies, particularly in HNSCC. Additionally, ITGAL displays noteworthy associations

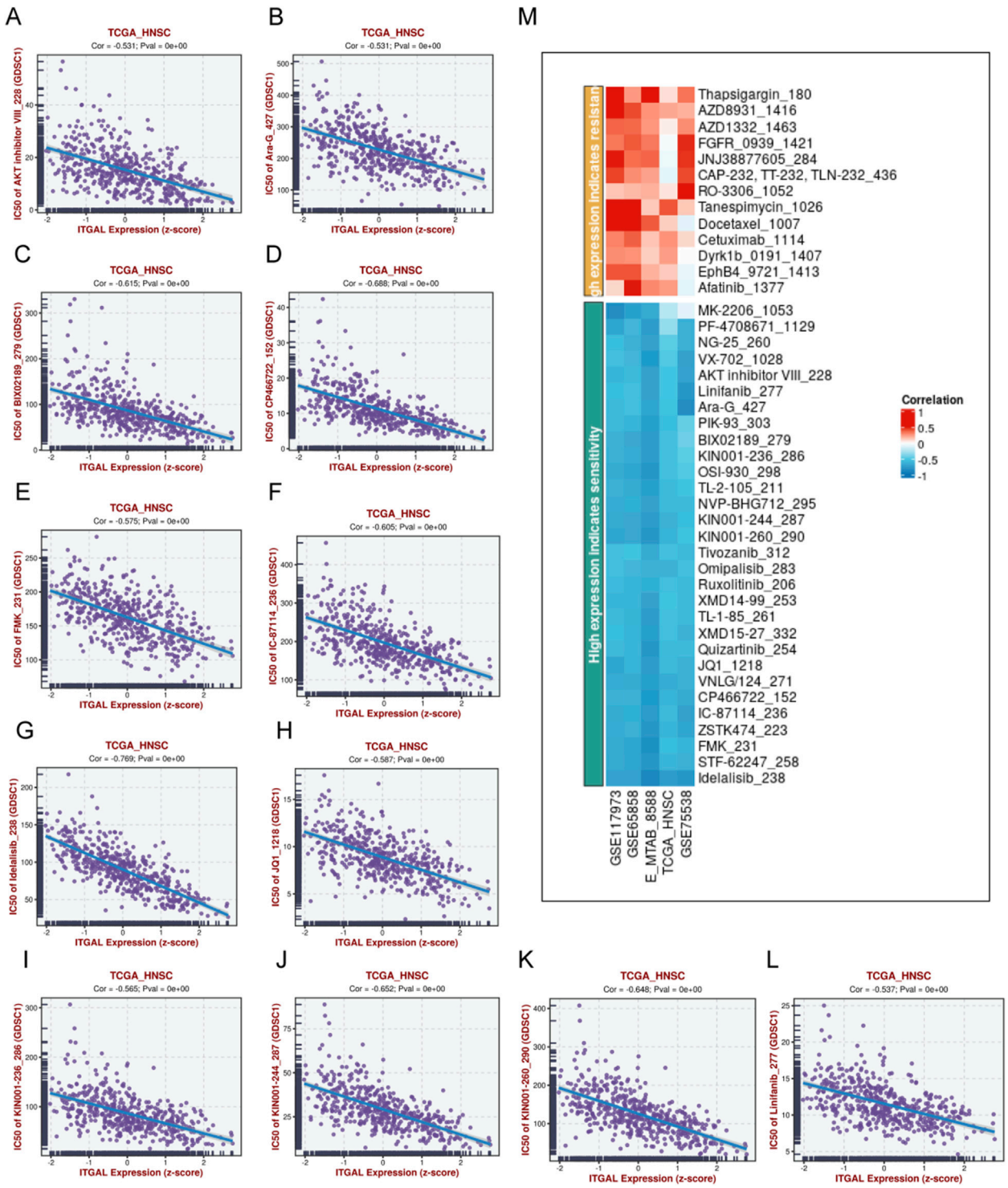

FIGURE 14
Potential drugs prediction of HNSCC. **(A)** IC50 of AKT inhibitor VIII_228, Ara-G_427 **(B)**, BIX02189279 **(C)**, CP466722_152 **(D)**, FMK_231 **(E)**, IC-87114_236 **(F)**, Idelalisib_238 **(G)**, JQ1_1218 **(H)**, KIN001-236_286 **(I)**, KIN001-244_287 **(J)**, KIN001-260_290 **(K)**, Linifanib_277 **(L)**,heatmap of the relationship between drugs sensitivity and ITGAL expression **(M)**.

with infiltration of immune cell and immune checkpoint related genes, indicating its potential as a promising target in tumor immunotherapy. The findings from our research present a potential strategy to target ITGAL for anti-tumor purposes, with a specific focus on modulating the immune microenvironment of the tumor.

Data availability statement

The datasets presented in this study can be found in online repositories. The names of the repository/repositories and accession number(s) can be found in the article/Supplementary Material.

Author contributions

FL: Supervision, Writing–review and editing. HY: Data curation, Formal Analysis, Investigation, Writing–original draft, Writing–review and editing. ZH: Formal Analysis, Supervision, Writing–review and editing. YL: Supervision, Validation, Writing–review and editing. QD: Supervision, Writing–review and editing. YY: Supervision, Writing–review and editing. SQ: Funding acquisition, Supervision, Writing–review and editing.

Funding

The author(s) declare that financial support was received for the research, authorship, and/or publication of this article. This work was supported by the grants of Science and Technology Program of Fujian Province, China (2018Y2003); Fujian Provincial Clinical Research Center for Cancer Radiotherapy and Immunotherapy (2020Y2012); The National Clinical Key Specialty Construction Program (2021); Fujian Clinical Research Center for Radiation and Therapy of Digestive, Respiratory and Genitourinary Malignancies (2021Y2014);National Natural Science Foundation of China (82072986); Major Scientific Research Program for Young and Middle-aged Health Professionals of Fujian Province, China (Grant No.2021ZQNZD010); Science and Technology Pilot Program of Fujian Province, China (2021Y0053); Wu Jieping Medical Foundation (320.6750.2021-01-27); Joint Funds for the Innovation of Science and Technology, Fujian province (2021Y9196); and High-level Talent Training Program of Fujian Cancer Hospital (2022YNG07);Innovative Medicine Subject of Fujian Provincial Health Commission, China (2021CXA029); Natural Science Foundation of Fujian province (2023J01121763); Fujian Provincial Health Technology Project (Grant number: 2023CXA036); Natural Science Foundation of Fujian province (2024J011086).

Acknowledgments

The authors are grateful to the Biomarker Exploration of Solid Tumors (BEST) (http://www.rookieutopia.com) for providing analysis help.

Conflict of interest

The authors declare that the research was conducted in the absence of any commercial or financial relationships that could be construed as a potential conflict of interest.

Publisher's note

Supplementary material

The Supplementary Material for this article can be found online at: https://www.frontiersin.org/articles/10.3389/fphar.2024.1464830/full#supplementary-material

SUPPLEMENTARY FIGURE S1
GSEA of ITGAL in TCGA pan-cancer. The 15 leading significant pathways indicated by ITGAL GSEA results across the mentioned tumor types. Text in the same color represents the same signaling pathway in different cancers. **(A-F)**.

References

Avraamides, C. J., Garmy-Susini, B., and Varner, J. A. (2008). Integrins in angiogenesis and lymphangiogenesis. *Nat. Rev. Cancer* 8 (8), 604–617. doi:10.1038/nrc2353

Bagaev, A., Kotlov, N., Nomie, K., Svekolkin, V., Gafurov, A., Isaeva, O., et al. (2021). Conserved pan-cancer microenvironment subtypes predict response to immunotherapy. *Cancer Cell* 39 (6), 845–865.e7. doi:10.1016/j.ccell.2021.04.014

Banta, K. L., Xu, X., Chitre, A. S., Au-Yeung, A., Takahashi, C., O'Gorman, W. E., et al. (2022). Mechanistic convergence of the TIGIT and PD-1 inhibitory pathways necessitates co-blockade to optimize anti-tumor CD8(+) T cell responses. *Immunity* 55 (3), 512–526 e9. doi:10.1016/j.immuni.2022.02.005

Barber, D. F., Faure, M., and Long, E. O. (2004). LFA-1 contributes an early signal for NK cell cytotoxicity. *J. Immunol.* 173 (6), 3653–3659. doi:10.4049/jimmunol.173.6.3653

Barter, R. L., Schramm, S. J., Mann, G. J., and Yang, Y. H. (2014). Network-based biomarkers enhance classical approaches to prognostic gene expression signatures. *BMC Syst. Biol.* 8 (Suppl. 4), S5. doi:10.1186/1752-0509-8-S4-S5

Buddingh, E. P., Kuijjer, M. L., Duim, R. A. J., Bürger, H., Agelopoulos, K., Myklebost, O., et al. (2011). Tumor-Infiltrating macrophages are associated with metastasis suppression in high-grade osteosarcoma: a rationale for treatment with macrophage activating agents. *Clin. Cancer Res.* 17 (8), 2110–2119. doi:10.1158/1078-0432.CCR-10-2047

Cillo, A. R., Kürten, C. H. L., Tabib, T., Qi, Z., Onkar, S., Wang, T., et al. (2020). Immune landscape of viral- and carcinogen-driven head and neck cancer. *Immunity* 52 (1), 183–199. doi:10.1016/j.immuni.2019.11.014

Corbi, A. L., Larson, R. S., Kishimoto, T. K., Springer, T. A., and Morton, C. C. (1988). Chromosomal location of the genes encoding the leukocyte adhesion receptors LFA-1, Mac-1 and p150,95. Identification of a gene cluster involved in cell adhesion. *J. Exp. Med.* 167 (5), 1597–1607. doi:10.1084/jem.167.5.1597

De Andrade Costa, A., Chatterjee, J., Cobb, O., Sanapala, S., Scheaffer, S., Guo, X., et al. (2021). RNA sequence analysis reveals ITGAL/CD11A as a stromal regulator of murine low-grade glioma growth. *Neuro-Oncology* 24 (1), 14–26. doi:10.1093/neuonc/noab130

Deng, T., Wang, C., Gao, C., Zhang, Q., and Guo, J. (2023). ITGAL as a prognostic biomarker correlated with immune infiltrates in melanoma. *Front. Oncol.* 13, 1181537. doi:10.3389/fonc.2023.1181537

Dudas, J. (2015). Supportive and rejective functions of tumor stroma on tumor cell growth, survival, and invasivity: the cancer evolution. *Front. Oncol.* 5, 44. doi:10.3389/fonc.2015.00044

Farshidfar, F., Rhrissorrakrai, K., Levovitz, C., Peng, C., Knight, J., Bacchiocchi, A., et al. (2022). Integrative molecular and clinical profiling of acral melanoma links focal amplification of 22q11.21 to metastasis. *Nat. Commun.* 13 (1), 898. doi:10.1038/s41467-022-28566-4

Girard, L., Rodriguez-Canales, J., Behrens, C., Thompson, D. M., Botros, I. W., Tang, H., et al. (2016). An expression signature as an aid to the histologic classification of non-small cell lung cancer. *Clin. Cancer Res.* 22 (19), 4880–4889. doi:10.1158/1078-0432.CCR-15-2900

Hickman, A., Koetsier, J., Kurtanich, T., Nielsen, M. C., Winn, G., Wang, Y., et al. (2022). LFA-1 activation enriches tumor-specific T cells in a cold tumor model and synergizes with CTLA-4 blockade. *J. Clin. Invest.* 132 (13), e154152. doi:10.1172/JCI154152

Jayawardana, K., Schramm, S. J., Haydu, L., Thompson, J. F., Scolyer, R. A., Mann, G. J., et al. (2015). Determination of prognosis in metastatic melanoma through integration of clinico-pathologic, mutation, mRNA, microRNA, and protein information. *Int. J. Cancer* 136 (4), 863–874. doi:10.1002/ijc.29047

Jerby-Arnon, L., Shah, P., Cuoco, M. S., Rodman, C., Su, M. J., Melms, J. C., et al. (2018). A cancer cell program promotes T cell exclusion and resistance to checkpoint blockade. *Cell* 175 (4), 984–997. doi:10.1016/j.cell.2018.09.006

Kamal, M. V., Damerla, R. R., Dikhit, P. S., and Kumar, N. A. (2023). Prostaglandin-endoperoxide synthase 2 (PTGS2) gene expression and its association with genes regulating the VEGF signaling pathway in head and neck squamous cell carcinoma. *J. Oral Biol. Craniofacial Res.* 13 (5), 567–574. doi:10.1016/j.jobcr.2023.07.002

Li, T., Fu, J., Zeng, Z., Cohen, D., Li, J., Chen, Q., et al. (2020). TIMER2.0 for analysis of tumor-infiltrating immune cells. *Nucleic Acids Res.* 48 (W1), W509–W514. doi:10.1093/nar/gkaa407

Liu, Z., Hao, X., Zhang, Y., Zhang, J., Carey, C. D., Falo, L. D., et al. (2017). Intratumoral delivery of tumor antigen-loaded DC and tumor-primed CD4+ T cells combined with agonist α-GITR mAb promotes durable CD8+ T-cell-dependent antitumor immunity. *OncoImmunology* 6 (6), e1315487. doi:10.1080/2162402X.2017.1315487

Lotscher, J., Martí I Líndez, A. A., Kirchhammer, N., Cribioli, E., Giordano Attianese, G. M. P., Trefny, M. P., et al. (2022). Magnesium sensing via LFA-1 regulates CD8(+) T cell effector function. *Cell* 185 (4), 585–602 e29. doi:10.1016/j.cell.2021.12.039

Lu, Y. C., Jia, L., Zheng, Z., Robbins, P. F., and Rosenberg, S. A. (2019). Single-cell transcriptome analysis reveals gene signatures associated with T-cell persistence following adoptive cell therapy. *Cancer Immunol. Res.* 7 (11), 1824–1836. doi:10.1158/2326-6066.CIR-19-0299

Mann, G. J., Pupo, G. M., Campain, A. E., Carter, C. D., Schramm, S. J., Pianova, S., et al. (2013). BRAF mutation, NRAS mutation, and the absence of an immune-related expressed gene profile predict poor outcome in patients with stage III melanoma. *J. Investigative Dermatology* 133 (2), 509–517. doi:10.1038/jid.2012.283

Miranda, A., Hamilton, P. T., Zhang, A. W., Pattnaik, S., Becht, E., Mezheyeuski, A., et al. (2019). Cancer stemness, intratumoral heterogeneity, and immune response across cancers. *Proc. Natl. Acad. Sci.* 116 (18), 9020–9029. doi:10.1073/pnas.1818210116

Ock, C.-Y., Keam, B., Kim, S., Lee, J. S., Kim, M., Kim, T. M., et al. (2016). Pan-cancer immunogenomic perspective on the tumor microenvironment based on PD-L1 and CD8 T-cell infiltration. *Clin. Cancer Res.* 22 (9), 2261–2270. doi:10.1158/1078-0432.CCR-15-2834

Parra, E. R., Behrens, C., Rodriguez-Canales, J., Lin, H., Mino, B., Blando, J., et al. (2016). Image analysis-based assessment of PD-L1 and tumor-associated immune cells density supports distinct intratumoral microenvironment groups in non-small cell lung carcinoma patients. *Clin. Cancer Res.* 22 (24), 6278–6289. doi:10.1158/1078-0432.CCR-15-2443

Pribila, J. T., Quale, A. C., Mueller, K. L., and Shimizu, Y. (2004). Integrins and T Cell–Mediated immunity. *Annu. Rev. Immunol.* 22 (22), 157–180. doi:10.1146/annurev.immunol.22.012703.104649

Puram, S. V., Tirosh, I., Parikh, A. S., Patel, A. P., Yizhak, K., Gillespie, S., et al. (2017). Single-cell transcriptomic analysis of primary and metastatic tumor ecosystems in head and neck cancer. *Cell* 171 (7), 1611–1624. doi:10.1016/j.cell.2017.10.044

Riquelme, E., Suraokar, M., Behrens, C., Lin, H. Y., Girard, L., Nilsson, M. B., et al. (2014). VEGF/VEGFR-2 upregulates EZH2 expression in lung adenocarcinoma cells and EZH2 depletion enhances the response to platinum-based and VEGFR-2-targeted therapy. *Clin. Cancer Res.* 20 (14), 3849–3861. doi:10.1158/1078-0432.CCR-13-1916

Ruffin, A. T., Cillo, A. R., Tabib, T., Liu, A., Onkar, S., Kunning, S. R., et al. (2021). B cell signatures and tertiary lymphoid structures contribute to outcome in head and neck squamous cell carcinoma. *Nat. Commun.* 12 (1), 3349. doi:10.1038/s41467-021-23355-x

Sade-Feldman, M., Yizhak, K., Bjorgaard, S. L., Ray, J. P., de Boer, C. G., Jenkins, R. W., et al. (2018). Defining T cell States associated with response to checkpoint immunotherapy in melanoma. *Cell* 175 (4), 998–1013 e20. doi:10.1016/j.cell.2018.10.038

Sato, M., Larsen, J. E., Lee, W., Sun, H., Shames, D. S., Dalvi, M. P., et al. (2013). Human lung epithelial cells progressed to malignancy through specific oncogenic manipulations. *Mol. Cancer Res.* 11 (6), 638–650. doi:10.1158/1541-7786.MCR-12-0634-T

Schabath, M. B., Welsh, E. A., Fulp, W. J., Chen, L., Teer, J. K., Thompson, Z. J., et al. (2016). Differential association of STK11 and TP53 with KRAS mutation-associated gene expression, proliferation and immune surveillance in lung adenocarcinoma. *Oncogene* 35 (24), 3209–3216. doi:10.1038/onc.2015.375

Seguin, L., Desgrosellier, J. S., Weis, S. M., and Cheresh, D. A. (2015). Integrins and cancer: regulators of cancer stemness, metastasis, and drug resistance. *Trends Cell Biol.* 25 (4), 234–240. doi:10.1016/j.tcb.2014.12.006

Shen, W., Song, Z., Zhong, X., Huang, M., Shen, D., Gao, P., et al. (2022). Sangerbox: a comprehensive, interaction-friendly clinical bioinformatics analysis platform. *iMeta* 1 (3), e36. doi:10.1002/imt2.36

Sun, D., Wang, J., Han, Y., Dong, X., Ge, J., Zheng, R., et al. (2021). TISCH: a comprehensive web resource enabling interactive single-cell transcriptome visualization of tumor microenvironment. *Nucleic Acids Res.* 49 (D1), D1420–D1430. doi:10.1093/nar/gkaa1020

Tirosh, I., Izar, B., Prakadan, S. M., Wadsworth, M. H., Treacy, D., Trombetta, J. J., et al. (2016). Dissecting the multicellular ecosystem of metastatic melanoma by single-cell RNA-seq. *Science* 352 (6282), 189–196. doi:10.1126/science.aad0501

Varn, F. S., Wang, Y., Mullins, D. W., Fiering, S., and Cheng, C. (2017). Systematic pan-cancer analysis reveals immune cell interactions in the tumor microenvironment. *Cancer Res.* 77 (6), 1271–1282. doi:10.1158/0008-5472.CAN-16-2490

Wang, Q., Xiao, G., Jiang, X., and Li, C. (2023). lncRNA PCBP1-AS1 mediated downregulation of ITGAL as a prognostic biomarker in lung adenocarcinoma. *Aging (Albany NY)* 15 (10), 4510–4523. doi:10.18632/aging.204756

Whitcup, S. M., Chan, C. C., Kozhich, A. T., and Magone, M. T. (1999). Blocking ICAM-1 (CD54) and LFA-1 (CD11a) inhibits experimental allergic conjunctivitis. *Clin. Immunol.* 93 (2), 107–113. doi:10.1006/clim.1999.4775

Wichmann, G., Rosolowski, M., Krohn, K., Kreuz, M., Boehm, A., Reiche, A., et al. (2015). The role of HPV RNA transcription, immune response-related gene expression and disruptive TP53 mutations in diagnostic and prognostic profiling of head and neck cancer. *Int. J. Cancer* 137 (12), 2846–2857. doi:10.1002/ijc.29649

Wilkerson, M. D., Yin, X., Walter, V., Zhao, N., Cabanski, C. R., Hayward, M. C., et al. (2012). Differential pathogenesis of lung adenocarcinoma subtypes involving sequence mutations, copy number, chromosomal instability, and methylation. *PLoS One* 7 (5), e36530. doi:10.1371/journal.pone.0036530

Wu, A., Zhang, S., Liu, J., Huang, Y., Deng, W., Shu, G., et al. (2020a). Integrated analysis of prognostic and immune associated integrin family in ovarian cancer. *Front. Genet.* 11, 705. doi:10.3389/fgene.2020.00705

Wu, T. D., Madireddi, S., de Almeida, P. E., Banchereau, R., Chen, Y. J. J., Chitre, A. S., et al. (2020b). Peripheral T cell expansion predicts tumour infiltration and clinical response. *Nature* 579 (7798), 274–278. doi:10.1038/s41586-020-2056-8

Yuen, K. C., Liu, L. F., Gupta, V., Madireddi, S., Keerthivasan, S., Li, C., et al. (2020). High systemic and tumor-associated IL-8 correlates with reduced clinical benefit of PD-L1 blockade. *Nat. Med.* 26 (5), 693–698. doi:10.1038/s41591-020-0860-1

Zhang, J., Wang, H., Yuan, C., Wu, J., Xu, J., Chen, S., et al. (2022). ITGAL as a prognostic biomarker correlated with immune infiltrates in gastric cancer. *Front. Cell Dev. Biol.* 10, 808212. doi:10.3389/fcell.2022.808212

Zhang, L., Li, Z., Skrzypczynska, K. M., Fang, Q., Zhang, W., O'Brien, S. A., et al. (2020). Single-cell analyses inform mechanisms of myeloid-targeted therapies in Colon cancer. *Cell* 181 (2), 442–459. doi:10.1016/j.cell.2020.03.048

Glossary

CESC	Cervical squamous cell carcinoma and endocervical adenocarcinoma
LUAD	Lung adenocarcinoma
SARC	Sarcoma
HNSCC	Head and Neck cell carcinoma
SKCM	Skin Cutaneous Melanoma
GBM	Glioblastoma multiforme
LGG	Brain Lower Grade Glioma
BLCA	Bladder Urothelial Carcinoma
CRC	Colon adenocarcinoma/Rectum adenocarcinoma Esophageal carcinoma
GBMLGG	Glioma
BRCA	Breast invasive carcinoma
ESCA	Esophageal carcinoma
STES	Stomach and Esophageal carcinoma
KIRP	Kidney renal papillary cell carcinoma
KIPAN	Pan-kidney cohort
STAD	Stomach adenocarcinoma
KIRC	Kidney renal clear cell carcinoma
LIHC	Liver hepatocellular carcinoma
OV	Ovarian serous cystadenocarcinoma
PAAD	Pancreatic adenocarcinoma
TGCT	Testicular Germ Cell Tumors
LAML	Acute Myeloid Leukemia
PRAD	Prostate adenocarcinoma
LUSC	Lung squamous cell carcinoma
WT	High-Risk Wilms Tumor
THCA	Thyroid carcinoma
READ	Rectum adenocarcinoma
UCS	Uterine Carcinosarcoma
ALL	Acute Lymphoblastic Leukemia
ACC	Adrenocortical carcinoma
KICH	Kidney Chromophobe
NSCLC	Non-small-cell lung cancer
CHOL	Cholangiocarcinoma

frontiers | Frontiers in Medicine

TYPE Original Research
PUBLISHED 06 January 2025
DOI 10.3389/fmed.2024.1478842

OPEN ACCESS

EDITED BY
Fujun Han,
The First Hospital of Jilin University, China

REVIEWED BY
Renjie He,
University of Texas MD Anderson Cancer Center, United States
Haitao Zhu,
Peking University, China

*CORRESPONDENCE
Zisheng Ai
azs1966@126.com
Jiansheng Su
sjs@tongji.edu.cn

†These authors have contributed equally to this work and share first authorship
‡These authors have contributed equally to this work

RECEIVED 11 August 2024
ACCEPTED 28 November 2024
PUBLISHED 06 January 2025

CITATION
Zhang L, Zhu E, Shi J, Wu X, Cao S, Huang S, Ai Z and Su J (2025) Individualized treatment recommendations for patients with locally advanced head and neck squamous cell carcinoma utilizing deep learning.
Front. Med. 11:1478842.
doi: 10.3389/fmed.2024.1478842

Individualized treatment recommendations for patients with locally advanced head and neck squamous cell carcinoma utilizing deep learning

Linmei Zhang [1†], Enzhao Zhu [2†], Jiaying Shi[1], Xiao Wu[3], Shaokang Cao[4], Sining Huang[5], Zisheng Ai[6*‡] and Jiansheng Su[1*‡]

[1]Shanghai Engineering Research Center of Tooth Restoration and Regeneration, Tongji Research Institute of Stomatology, Department of Prosthodontics, Shanghai Tongji Stomatological Hospital, Dental School, Tongji University, Shanghai, China, [2]School of Medicine, Tongji University, Shanghai, China, [3]Shanghai Engineering Research Center of Tooth Restoration and Regeneration, Tongji Research Institute of Stomatology, Department of Periodontics, Shanghai Tongji Stomatological Hospital, Dental School, Tongji University, Shanghai, China, [4]Shanghai Engineering Research Center of Tooth Restoration and Regeneration, Tongji Research Institute of Stomatology, Department of Oral and Maxillofacial Surgery, Shanghai Tongji Stomatological Hospital, Dental School, Tongji University, Shanghai, China, [5]Shanghai Engineering Research Center of Tooth Restoration and Regeneration, Tongji Research Institute of Stomatology, Department of Oral Implantology, Shanghai Tongji Stomatological Hospital, Dental School, Tongji University, Shanghai, China, [6]Department of Medical Statistics, School of Medicine, Tongji University, Shanghai, China

Background: The conventional treatment for locally advanced head and neck squamous cell carcinoma (LA-HNSCC) is surgery; however, the efficacy of definitive chemoradiotherapy (CRT) remains controversial.

Objective: This study aimed to evaluate the ability of deep learning (DL) models to identify patients with LA-HNSCC who can achieve organ preservation through definitive CRT and provide individualized adjuvant treatment recommendations for patients who are better suited for surgery.

Methods: Five models were developed for treatment recommendations. Their performance was assessed by comparing the difference in overall survival rates between patients whose actual treatments aligned with the model recommendations and those whose treatments did not. Inverse probability treatment weighting (IPTW) was employed to reduce bias. The effect of the characteristics on treatment plan selection was quantified through causal inference.

Results: A total of 7,376 patients with LA-HNSCC were enrolled. Balanced Individual Treatment Effect for Survival data (BITES) demonstrated superior performance in both the CRT recommendation (IPTW-adjusted hazard ratio (HR): 0.84, 95% confidence interval (CI), 0.72–0.98) and the adjuvant therapy recommendation (IPTW-adjusted HR: 0.77, 95% CI, 0.61–0.85), outperforming other models and the National Comprehensive Cancer Network guidelines (IPTW-adjusted HR: 0.87, 95% CI, 0.73–0.96).

Conclusion: BITES can identify the most suitable treatment option for an individual patient from the three most common treatment options. DL models facilitate the establishment of a valid and reliable treatment recommendation system supported by quantitative evidence.

KEYWORDS

head and neck squamous cell carcinoma, chemoradiotherapy, deep learning, causal inference, precise medicine

Introduction

Head and neck squamous cell carcinoma (HNSCC) is one of the most prevalent cancers worldwide (1), often diagnosed at an advanced stage due to the lack of effective early screening strategies (2).

Conventional treatment typically involves surgery followed by radiotherapy (RT) (3). While adjuvant chemoradiotherapy (CRT) has been shown to enhance progression-free survival by sensitizing tumors to RT under certain conditions (4), its use is controversial due to potential toxicity and complications (5).

Furthermore, the trauma and dysfunction associated with surgery have prompted interest in definitive CRT for organ preservation (6). Studies have indicated that CRT may improve outcomes in patients with non-T4 disease and high nodal burden compared to surgery, which, conversely, may benefit T4 patients (7). The response of patients to the same treatment is influenced by many underlying clinical features (8), suggesting significant treatment heterogeneity.

Given the challenges and costs associated with conducting randomized clinical trials, there is a growing demand for innovative survival analysis methods to address this heterogeneity (8). Deep learning (DL) has proven to be more accurate than traditional statistical analysis (9) and has demonstrated the potential to provide individualized recommendations based on calculated risk (10).

This study aimed to assess DL's capability to provide individualized treatment recommendations, identifying patients who might benefit from organ preservation through CRT and tailoring adjuvant treatment for those better suited for surgical interventions.

Methods

Study design and data source

This was a population-based retrospective cohort study designed to provide personalized treatment recommendations for locally advanced HNSCC (LA-HNSCC) patients using DL models. The evaluation of the treatment options was categorized into two phases, with phase one individualizing treatment recommendations between CRT and surgery plus CRT/RT and phase two individualizing treatment recommendations between surgery plus CRT and surgery plus RT.

The population for this study was sourced from the Surveillance, Epidemiology, and End Results (SEER) 18 database, which represents approximately 27.8% of the U.S. population (11). This study followed the Strengthening the Reporting of Observational Studies in Epidemiology guidelines (12).

Study population and eligibility criteria

Patients with HNSCC originating from four anatomical sites (such as the oral cavity, sinonasal cavity, pharynx, and larynx), diagnosed as stage III to IVa from 1 January 2004 to 31 December 2015, and treated with definitive CRT or radical resection plus postoperative RT/CRT were included in this study. Nasopharyngeal and salivary gland carcinomas were not included due to differences in pathology and treatment.

Ethnicity (13), sex (13), marital status (14), age (15), histological grade (16), laterality (17), primary tumor site (18), TNM stage (3), tumor size (3), number of lymph nodes (19), number of positive lymph nodes (20), and lymph node surgery (21) were included as variables affecting efficacy because they are known to play critical roles in predicting prognosis and guiding treatment decisions in HNSCC. OS was used to measure the efficacy of each treatment regimen.

Clinical cases were excluded if they met the following criteria: (1) unknown or ambiguous demographic information; (2) unknown histologic grades or tumor type; (3) unknown tumor location or size; (4) unknown TNM stage; (5) unknown treatment modality; (6) stage I, II, or IVb; (7) unknown laterality; (8) incomplete follow-up; (9) multiple malignancies; and (10) metastatic tumors. The cohort selection is illustrated in Figure 1A.

TNM stage was determined in accordance with the 7th American Joint Committee on Cancer staging manual. Patients who were alive as of 31st December 2020 were censored. Therefore, the follow-up period ranged from 5 to 16 years.

Algorithms

The individual treatment effect (ITE) reflects the difference in survival outcomes between two potential intervention scenarios. The T-learner is a common type of model used for inferring the ITE, which adopts two models to estimate the ITE as $ITE = \mu_1(x) - \mu_0(x)$, where μ_0 and μ_1 denote the models trained on the corresponding treatment groups (22). The T-learner excludes

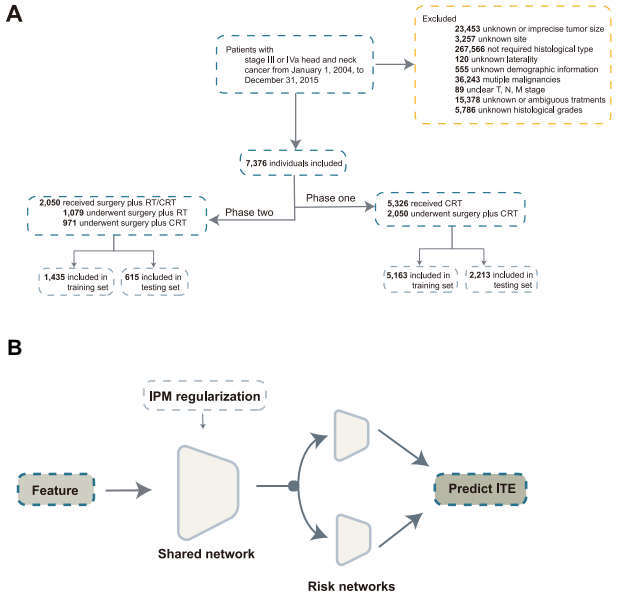

FIGURE 1
Inclusion process and model architecture. **(A)** Inclusion process; **(B)** architecture of the balanced individual treatment effect for survival data. RT, radiation; CRT, chemoradiation; IPM, integral probability metrics; ITE, individual treatment effect.

some confounding artifacts; however, it can still be affected by inconsistent predictive performance of models (23) and biased treatment allocation (24).

With the development of DL, more methods have been proposed to estimate the unbiased ITE. Balanced Individual Treatment Effect for Survival data (BITES) (24) addresses this issue through representation-based causal inference. BITES has a shared network and two risk networks. In the shared network, integral probability metrics are used to maximize the p-Wasserstein distance of different treatment arms. The risk networks calculate the ITE in the form of a T-learner. The architecture of BITES is illustrated in Figure 1B.

Cox Mixtures with Heterogeneous Effects (CMHE) (25) uses a latent variable approach to model heterogeneous treatment effects by assuming that an individual can belong to one of the latent clusters with distinct response characteristics.

Calculation of the individual treatment effect

For censored data, the models output log hazard ratios; however, these cannot be used directly because the baseline hazards of different treatment groups also reflect crucial prognostic information.

Here, we defined the potential outcome with a good clinical interpretation as the area under the individual survival curve for an individual within a specific period (5 years), called the restricted survival time (RST). The formula was described as $ITE_{RST}(X;t) = \sum_{x\in\mathcal{X}}\left[\int_0^t \hat{S}_1(t \mid x)dt - \int_0^t \hat{S}_0(t \mid x)dt\right]$, where t indicated the preset time horizon and $\hat{S}_0(t \mid x)$ and $\hat{S}_1(t \mid x)$ were the predicted survival distributions for an individual under different treatments. It can be simply interpreted as the additional amount of time a patient survived within 5 years when receiving treatment 1 compared with receiving treatment 0.

Model development, validation, and treatment recommendation

We trained and compared five models, including BITES, CMHE, DeepSurv (26), the Cox proportional hazards (CPH) model, and random survival forest (RSF). These models, divided into deep learning models (BITES, CMHE, and DeepSurv) and traditional machine learning models (CPH and RSF), all employed the same ITE calculation method. The deep learning models were chosen for their ability to capture complex non-linear relationships, while the traditional models were used as benchmarks for performance comparison.

All patients were randomly allocated to a training set comprising 70% of the samples used for training the models and a testing set comprising 30% of the samples to evaluate the model performance and recommendation effect. During the training period, we used five-fold cross-validation to tune the model hyperparameters. Each time, the model was trained on four-fifths of the training set and validated on the remaining one-fifth. The training process was automatically terminated if the validation loss did not decrease after 1,000 iterations. Hyperparameter tuning was conducted using grid search to explore the predefined ranges of key parameters. These parameters included learning rate, mini-batch size, the percentage of dropout, number of layers, number of nodes in the multilayer perceptron, strength of the regularization method, number of trees, and tree depth, depending on the model. The optimal hyperparameters were selected based on the validation loss.

To evaluate the models' treatment recommendation effect, the patients were divided into the recommended (Consis.) and anti-recommended (Inconsis.) groups, based on whether the actual treatment they received was consistent with the model recommendations. We calculated several indicators between the Consis. and Inconsis. groups to quantify the survival advantages of the following models' recommendations: multivariate hazard ratio (HR), 5-year absolute risk reduction (ARR), and the difference in restricted mean survival time (DRMST) over five years. Considering the potential imbalance of the baseline features between the Consis. and Inconsis. groups, inverse probability treatment weighting (IPTW) was used to reduce selection bias.

Model interpretation

The model interpretation was twofold: (1) the importance of the features for the overall output and (2) the impact of the features on the treatment recommendations.

SHapley Additive exPlanations (SHAP) is a widely used local interpretation method from game theory that explains the extent to which each variable affects the model output with respect to the

10.3389/fmed.2024.1478842

TABLE 1 Patients.

	Concurrent chemoradiation ($n = 5,326$)	Surgery and postoperative radiation ($n = 1,079$)	Surgery and postoperative chemoradiation ($n = 971$)
Age, median (IQR), y	60.0 (53.0–67.0)	61.0 (54.0–70.0)	59.0 (53.0–60.0)
Tumor size, median (IQR), mm	32.0 (24.0–44.0)	35.0 (25.0–45.0)	38.0 (27.0–50.0)
Married	2,911 (54.7)	540 (50.1)	494 (50.9)
Ethnicity–White	4,496 (84.4)	859 (79.6)	770 (79.3)
Male	4,410 (82.8)	787 (72.9)	742 (76.4)
Grade			
I	333 (6.3)	111 (10.3)	86 (8.9)
II	2,565 (48.2)	670 (62.1)	532 (54.8)
III	2,380 (44.7)	295 (27.3)	350 (36.0)
IV	48 (0.9)	3 (0.3)	3 (0.3)
Laterality			
Left	960 (18.0)	84 (7.8)	92 (9.5)
Right	1,031 (19.4)	95 (8.8)	90 (9.3)
Not paired	3,335 (62.6)	90 (83.4)	789 (81.3)
Oral cavity			
Lip	1 (0.0)	17 (1.6)	6 (0.6)
Base of tongue	1,832 (34.4)	48 (4.4)	76 (7.8)
Other parts of tongue	230 (4.3)	105 (9.7)	132 (13.6)
Gum	23 (0.4)	144 (13.3)	95 (9.8)
Palate	115 (2.2)	32 (3.0)	30 (3.1)
Floor of mouth	82 (1.5)	166 (15.4)	135 (13.9)
Mouth	81 (1.5)	131 (12.1)	132 (13.6)
Pharynx			
Tonsil	1,432 (26.7)	7 (0.6)	14 (1.4)
Oropharynx	106 (2.0)	1 (0.1)	1 (0.1)
Pyriform	270 (5.1)	3 (0.3)	0 (0.0)
Hypopharynx	207 (3.9)	3 (0.3)	6 (0.6)
Paranasal sinus	30 (0.6)	17 (1.6)	12 (1.2)
Larynx	926 (17.4)	405 (37.5)	332 (34.2)
Stage			
III	1,501 (28.2)	289 (26.8)	153 (15.8)
IVa	3,825 (71.8)	790 (73.2)	818 (84.2)
T stage			
T1	706 (13.3)	77 (7.1)	69 (7.1)
T1NOS	4 (0.1)	1 (0.1)	0 (0.0)
T1a	2 (0.0)	0 (0.0)	0 (0.0)
T1b	1 (0.0)	1 (0.1)	0 (0.0)
T2	2,071 (38.9)	163 (15.1)	165 (17.0)
T3	1,422 (26.7)	262 (24.3)	194 (20.0)
T4a	1,120 (21.0)	575 (53.3)	543 (55.9)

(Continued)

TABLE 1 (Continued)

	Concurrent chemoradiation ($n = 5,326$)	Surgery and postoperative radiation ($n = 1,079$)	Surgery and postoperative chemoradiation ($n = 971$)
N stage			
N0	669 (12.6)	451 (41.8)	195 (20.1)
N1	1,320 (24.8)	257 (23.8)	205 (21.1)
N2NOS	112 (2.1)	7 (0.6)	8 (0.8)
N2a	398 (7.5)	32 (3.0)	38 (3.9)
N2b	1,685 (31.6)	232 (21.5)	331 (34.1)
N2c	1,142 (21.4)	100 (9.3)	194 (20.0)
Follow-up, median (IQR), month	64.0 (17.0–107.0)	41.0 (14.0–89.0)	33.0 (13.0–84.0)

baseline average. In this study, we employed SurvSHAP(t) (27), a time-dependent SHAP analysis, to explain the output of the best model.

We calculated the probability that a patient with a certain characteristic is recommended for a specific treatment minus the probability that a patient without that characteristic is recommended for the same treatment. This difference is called the probability difference (PD), which is similar to the calculation of risk difference. Based on the PD, the impact of features on treatment recommendations can be quantified. We also used IPTW to exclude the influence of other characteristics, thereby obtaining the independent impact.

Statistical analysis

The models were built using Python 3.8 with the packages Pytorch 2.0 and Scikit-survival 0.19.0. Statistical analyses were performed using R 4.1.38. Continuous variables were expressed as medians and interquartile ranges (IQRs), and categorical variables were expressed as numbers and percentages (%). The log-rank test was used to compare the Kaplan–Meier (KM) curves.

Results

Patients

A total of 7,376 patients with locally advanced HNSCC were enrolled, with a median follow-up of 58 (IQR: 16–102) months, including 3,613 (49.0%) patients with oral cavity cancer, 2,041 (27.7%) patients with pharyngeal cancer, 59 (0.8%) patients with sinonasal cavity cancer, and 1,663 (22.5%) patients with laryngeal cancer. Of these, 5,326 patients were treated with CRT and 2,050 patients were treated with surgery. Adjuvant RT was administered to 1,079 of the patients who underwent surgery, and adjuvant CRT was administered to an additional 971 patients. The overall mortality rate was 61.6% [95% confidence interval (CI): 60.5%−62.8%]. The detailed baseline demographic and clinical characteristics of the included patients are presented in Table 1.

Performance

All evaluations of the model were performed on the testing set, which included 2,213 patients for the phase one and 651 patients for phase two recommendations. The detailed model performance is presented in Table 2.

The integrated Brier score (IBS) was used to measure the discrimination of the models. The CPH model was observed to have the best discrimination in both phase one (IBS in the CRT group (IBS^a): 0.17, 95% CI, 0.16–0.18; IBS in the surgery plus RT/CRT group (IBS^b): 0.17, 95% CI, 0.16–0.18) and phase two recommendations (IBS in the surgery plus RT group (IBS^c): 0.17, 95% CI, 0.15–0.18; IBS in the surgery plus CRT group (IBS^d): 0.18, 95% CI, 0.16–0.21), followed by the RSF model (IBS^a: 0.17, 95% CI, 0.17–0.18; IBS^b: 0.18, 95% CI, 0.16–0.19; IBS^c: 0.17, 95% CI, 0.16–0.19; IBS^d: 0.18, 95% CI, 0.17–0.20).

The metric of interest lies in how much survival advantage can be gained by following model recommendations. IPTW was used to adjust for tumor size, tumor locations, laterality, TNM stages, demographic features, and actual treatments. We set the metrics that determined the performance of the model to those corrected with IPTW, as they were largely unaffected by other factors as well as the actual treatment proportions.

In the phase one recommendation, BITES performed the best (HR: 0.92, 95% CI, 0.81–1.04; IPTW-adjusted HR (HR^e): 0.84, 95% CI, 0.72–0.98; DRMST: 6.71, 95% CI, 4.75–8.67; IPTW-adjusted DRMST ($DRMST^e$): 10.40, 95% CI, 8.33–12.75; ARR: 16.90, 95% CI, 12.50–21.20; IPTW-adjusted ARR (ARR^e): 14.80, 95% CI, 10.60–19.10). The NCCN Clinical Practice Guidelines in Oncology (NCCN Guidelines) were also compared with the models. The patients whose actual treatment was consistent with the NCCN guidelines were compared with those whose treatment was inconsistent. As the NCCN has no prioritized treatment guidelines for pharyngeal cancers, these patients were excluded from this calculation. No significant differences were observed in the results of the NCCN guideline recommendations (HR^e: 0.87, 95% CI, 0.73–0.96; $DRMST^e$: −4.37, 95% CI, −6.40-−2.12; ARR^e: −8.34, 95% CI, −13.00-−3.65).

For the phase two recommendation, the BITES model was noteworthy (HR: 0.87, 95% CI, 0.72–1.06; HR^e: 0.77,

TABLE 2 Performance.

Model	HR	IPTW-adjusted HR	5-year DRMST (month)	IPTW-adjusted 5−year DRMST (month)	5-year ARR (%)	IPTW-adjusted 5-year ARR (%)	IBSa	IBSb
Chemoradiation vs. surgery plus radiation/chemoradiation								
BITES	0.92 (0.81–1.04)	**0.84 (0.72–0.98)**	6.71 (4.75–8.67)	**10.40 (8.33–12.75)**	**16.90 (12.50–21.20)**	**14.80 (10.60–19.10)**	0.21 (0.21–0.22)	0.19 (0.18–0.20)
CMHE	0.77 (0.67–0.89)	Reference	−0.23 (−2.16–1.71)	4.25 (2.20–6.36)	−2.71 (−7.04–1.63)	−1.78 (−5.98–2.42)	0.20 (0.19–0.20)	0.22 (0.22–0.23)
DeepSurv	0.77 (0.67–0.89)	Reference	−0.23 (−2.16–1.71)	Reference	−2.64 (−6.97–1.69)	−1.79 (−5.99–2.42)	0.37 (0.35–0.39)	0.29 (0.27–0.32)
RSF	0.82 (0.73–0.92)	0.85 (0.75–0.96)	**7.37 (5.48–9.25)**	9.70 (7.65–12.49)	13.90 (9.78–18.10)	10.20 (6.11–14.30)	0.17 (0.17–0.18)	0.18 (0.16–0.19)
CPH	**0.76 (0.67–0.86)**	0.98 (0.78–1.24)	3.74 (1.88–5.61)	4.84 (2.72–6.25)	7.52 (3.34–11.70)	6.93 (2.89–11.00)	**0.17 (0.16–0.18)**	**0.17 (0.16–0.18)**
NCCN	0.88 (0.73–1.06)	0.87 (0.73–0.96)	−4.12 (−6.31–−1.92)	−4.37 (−6.40–−2.12)	−9.29 (−14.20–−4.43)	−8.34 (−13.00–−3.65)	..	..
Model	**HR**	**IPTW–adjusted HR**	**5–year DRMST (month)**	**IPTW–adjusted 5–year DRMST (month)**	**5–year ARR (%)**	**IPTW–adjusted 5–year ARR (%)**	**IBSc**	**IBSd**
Surgery plus radiation vs. surgery plus chemoradiation								
BITES	0.87 (0.72–1.06)	**0.77 (0.61–0.85)**	**4.59 (1.18–8.01)**	**4.65 (1.32–7.73)**	**11.10 (3.58–18.60)**	**10.50 (3.16–17.90)**	0.22 (0.21–0.23)	0.20 (0.18–0.22)
CMHE	**0.82 (0.66–1.03)**	0.83 (0.65–1.07)	3.56 (0.14–6.98)	3.55 (0.29–7.36)	4.60 (−2.96–12.20)	4.66 (−2.75–12.10)	0.23 (0.22–0.23)	0.22 (0.21–0.23)
DeepSurv	0.93 (0.76–1.15)	0.94 (0.76–1.17)	−1.26 (−4.69–2.18)	−1.22 (−4.80–2.02)	−1.51 (−9.09–6.07)	−1.31 (−8.75–6.14)	0.33 (0.30–0.37)	0.45 (0.40–0.48)
RSF	0.86 (0.71–1.04)	0.90 (0.73–1.10)	2.55 (−0.91–6.00)	2.59 (−0.73–5.94)	6.88 (−7.23–14.50)	6.37 (−1.10–13.80)	0.17 (0.16–0.19)	0.18 (0.17–0.20)
CPH	0.84 (0.67–1.05)	0.79 (0.61–1.02)	3.66 (0.13–7.18)	3.61 (0.04–7.22)	7.93 (0.19–15.70)	7.39 (−0.23–15.00)	**0.17 (0.15–0.18)**	**0.18 (0.16–0.21)**

IPTW, inverse probability weighting; HR, multivariate hazards ratio; DRMST, the difference in restricted mean survival time; ARR, absolute risk reduction; IBSa, integrated Brier score in chemoradiation group; IBSb, integrated Brier score in surgery plus radiation/chemoradiation group; IBSc, integrated Brier score in surgery plus radiation group; IBSd, integrated Brier score in surgery plus chemoradiation group; BITES, Balanced Individual Treatment Effect for Survival data; CMHE, Cox Mixtures with Heterogeneous Effects; CPH, Cox proportional hazards model; RSF, random survival forest; NCCN, National comprehensive cancer network guideline; Reference, statistical model did not fit.

The bold font indicates that the model performed best in this metric.

According to the NCCN guidelines, surgery is recommended for patients with the following location characteristics and TNM stages: oral cavity cancer patients with T3 and N0, T1-3 and N 1-3, or T4a and N0-3; laryngeal cancer patients with T4a and N-3; ethmoid sinus patients with T3–4a; and maxillary sinus patients with T3–4 and N0 or T1–4a and N+.

95% CI, 0.61–0.85; DRMST: 4.59, 95% CI, 1.18–8.01; DRMST^{e}: 4.65, 95% CI, 1.32–7.73; ARR: 11.10, 95% CI, 3.58–18.60; ARR^{e}: 10.50, 95% CI, 3.16–17.90), outperforming all other models.

We present the KM curves of the Consis. vs. Inconsis. groups for the phase one and phase two recommendations in Figures 2A, B, respectively. Better OS in the Consis. group was observed for both phase one (P of the log-rank test < 0.001; P of the IPTW-adjusted log-rank test < 0.001) and phase two (P of the log-rank test < 0.001; P of the IPTW-adjusted log-rank test < 0.001) recommendations.

Whether the protective effect of BITES was due to an imbalance in the treatment proportions in the two groups was also of interest. Thus, we treated surgery plus RT/CRT as a mediator and adjusted for all baseline features to calculate the natural direct effect (NDE) and natural indirect effect, which are presented in Figure 3A. Similarly, surgery plus CRT was treated as a mediator in the evaluation of the phase two recommendation (Figure 3B). The NDE measured the direct effect of BITES recommendation on mortality reduction, excluding the effect of the actual treatment. These values are presented as the slope of a linear regression. Both phase one (NDE: −0.03, 95% CI, −0.04–−0.02) and phase two (NDE: −0.07, 95% CI, −0.08–−0.06) recommendations had a direct effect on overall mortality reduction.

We also assessed the protective effect of BITES on various causes of death, as presented in Supplementary Table S1. As competing risks were considered, when a particular cause of death was tested, other deaths were treated as competing risks. The HR^{e} with the competing risks was calculated using a marginal structural cause-specific Cox proportional hazards model (MSM) (28). For the phase one recommendation, the patients who followed the

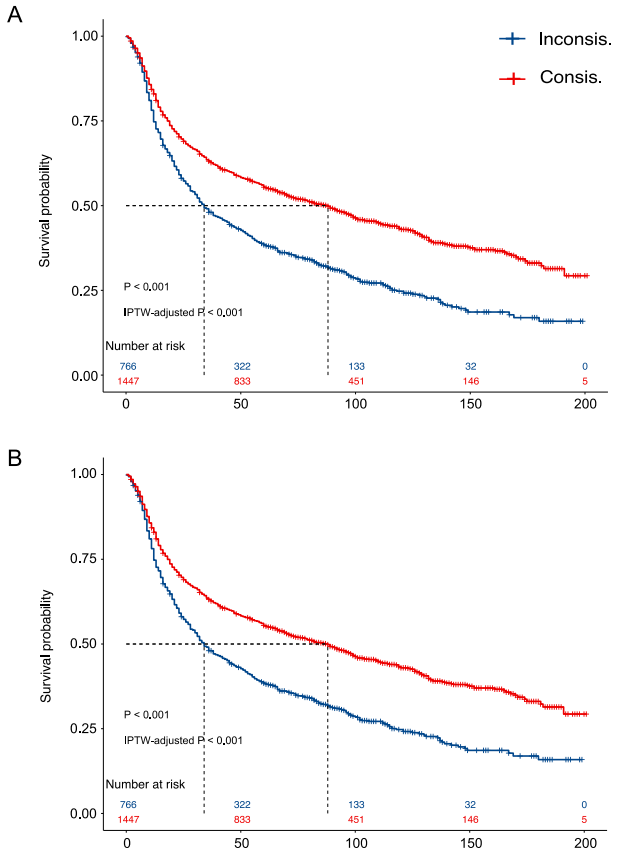

FIGURE 2
The Kaplan–Meier curves of the Consis. Group vs. the Inconsis. **(A)** The Kaplan–Meier curves of the phase one recommendation; **(B)** The Kaplan–Meier curves of the phase two recommendation. P, the *p*-value of the log-rank test; IPTW, inverse probability treatment weighting.

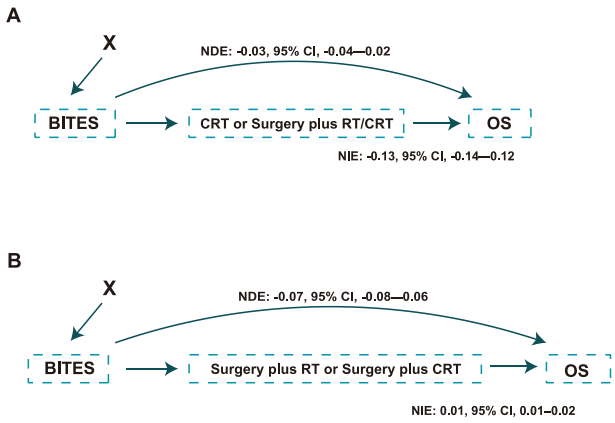

FIGURE 3
Causal path of the protection effect of the model recommendation. **(A)** Causal path of the protection effect in the phase one recommendation; **(B)** Causal path of the protection effect in the phase two recommendation. NDE, natural direct effect; NIE, natural indirect effect; BITES, Balanced Individual Treatment Effect for Survival data; OS, overall survival; RT, radiation; CRT, chemoradiation.

model recommendation had a lower death rate from HNSCC (HR^e: 0.84, 95% CI, 0.69–0.94), cardiovascular diseases (HR^e: 0.66, 95% CI, 0.45–0.96), and adverse effects (HR^e: 0.68, 95% CI, 0.38–0.92). The phase two recommendation reduced deaths caused by HNSCC (HR^e: 0.86, 95% CI, 0.66–0.93).

Treatment heterogeneity

Treatment heterogeneity can be captured by the presence of varied average treatment effects (ATEs) across different subgroups, indicating that patients with different characteristics respond heterogeneously to the same treatment. The patients were divided into the surgery recommended (SR) and surgery not recommended (SNR) groups based on the ITE that BITES predicted in the phase one recommendation. Similarly, the surgery plus CRT recommended (SCR) and surgery plus RT recommended (SRR) groups were established. The HR and HR^e were calculated to visualize the ATE in the overall patients and those subgroups. IPTW was used to adjust for tumor size, tumor locations, laterality, TNM stages, and demographic features. These results are presented in Figures 4A, B for the phase one and phase two recommendations, respectively.

In CRT vs. surgery plus RT/CRT, the ATE reflected the protective effect of surgery compared with CRT. Surgery demonstrated a very weak and statistically insignificant protective effect in all patients (HR^e: 0.87, 95% CI, 0.70–1.08). However, it showed a protective effect in the SR group (HR^e: 0.60, 95% CI, 0.45–0.97) and a risky effect in the SNR group (HR^e: 1.57, 95% CI, 1.38–1.77).

The ATE of surgery plus CRT compared with surgery plus RT was not statistically significant in all patients (HR^e: 0.87, 95% CI, 0.71–1.07). It became favorable in the SCR group (HR^e: 0.71, 95% CI, 0.51–0.98) and not favorable in the SRR group (HR^e: 1.13, 95% CI, 1.08–1.14).

Therapeutic insights and model interpretation

Here, the PD and IPTW-adjusted PD (PD^e) were used to quantify the impact of tumor location, age, and TNM stage on treatment selection. Figures 5A, B represent the probability differences for the phase one recommendation, while Figures 5C, D show similar results for the phase two recommendation. The PD represented the probability that a patient with the characteristic was recommended for surgery and surgery plus CRT minus the probability in the absence of the characteristic in phase one and phase two, respectively, whereas the IPTW correction provided a more unbiased result.

For the phase one recommendation, a higher likelihood of being recommended to receive surgery was found in the patients with tumors in the tonsil (PD^e: 40.60%, 95% CI: 38.30%−42.90%), lip (PD^e: 5.78%, 95% CI: 1.65%−9.90%), gum (PD^e: 25.60%, 95% CI: 15.10%−36.10%), oropharynx (PD^e: 9.57%,

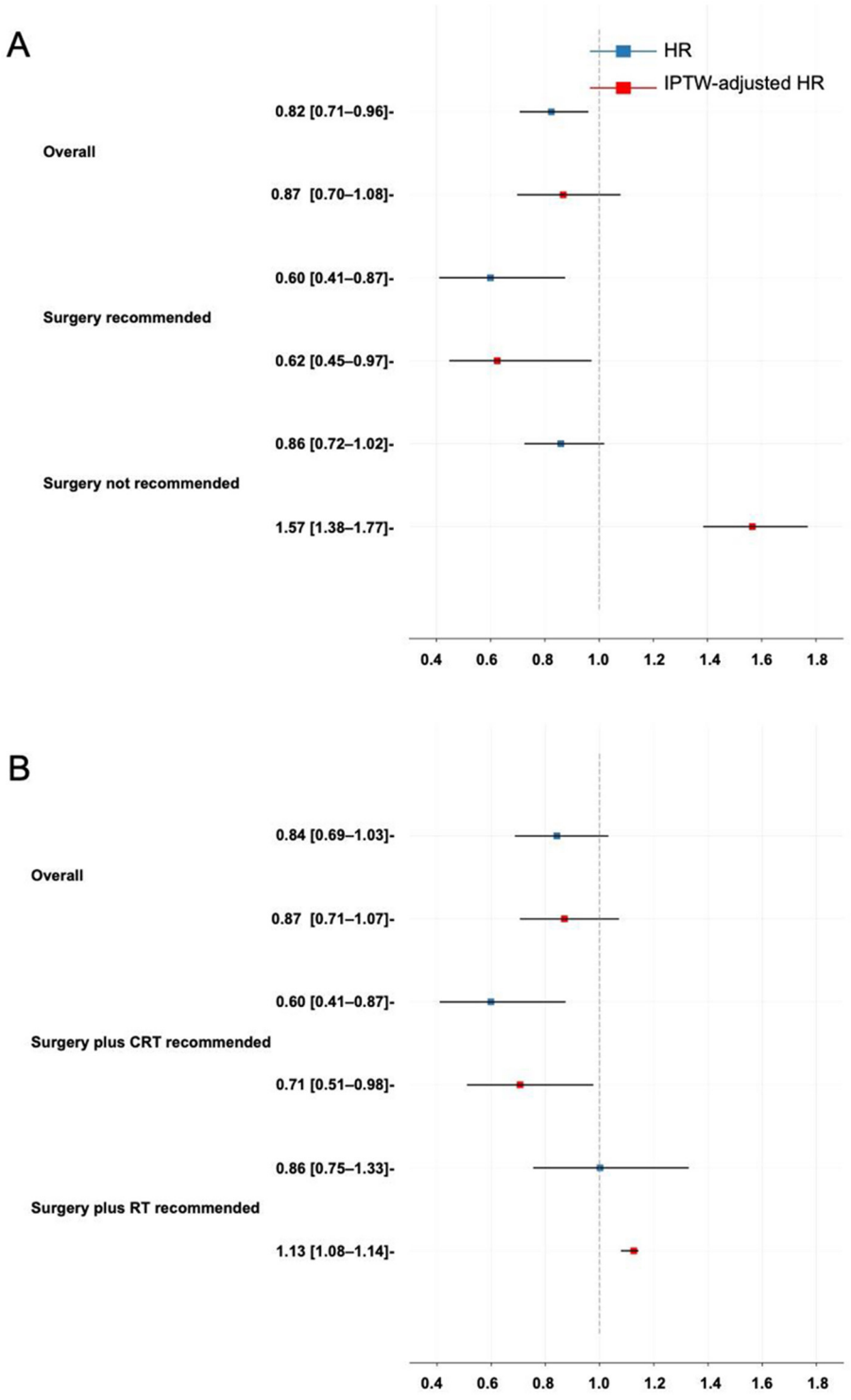

FIGURE 4
Treatment heterogeneity. **(A)** Treatment heterogeneity in the phase one recommendation; **(B)** Treatment heterogeneity in the phase two recommendation. HR, hazard ratio; IPTW, inverse probability treatment weighting.

95% CI: 1.13%−18.00%), and larynx (PD^e: 6.57%, 95% CI: 2.78%−10.40%) subsites, those with stage IVa (PD^e: 20.26%, 95% CI: 17.67%−22.85%), and those older than 60 years of age (PD^e: 29.00%, 95% CI: 26.40%−31.50%), with specific likelihood listed accordingly in the PD^e values. In contrast, the patients with tumors located at the base of the tongue (PD^e: −4.37%, 95% CI: −7.52%−1.21%), other parts of the tongue (PD^e: −7.86%, 95% CI: −12.43%−3.29%), and those aged 30 to 60 years (PD^e: −28.74%, 95% CI: −31.27%−26.21%) were less likely to be recommended for surgery.

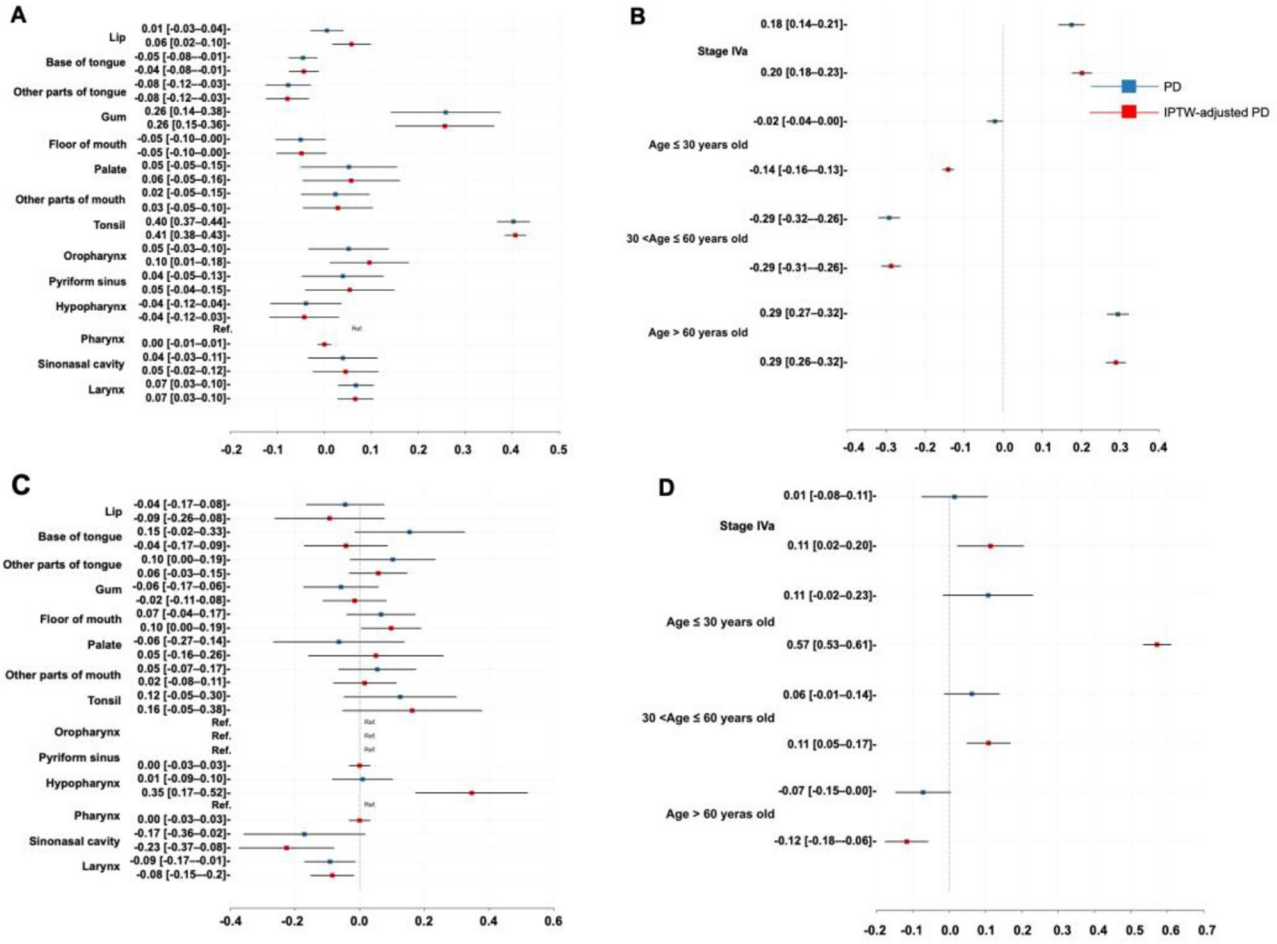

FIGURE 5
Therapeutic insights. **(A)** Probability difference regarding tumor location in the phase one recommendation; **(B)** Probability difference regarding age and TNM stage in the phase one recommendation; **(C)** Probability difference regarding tumor location in the phase two recommendation; **(D)** Probability difference regarding age and TNM stage in the phase two recommendation. PD, probability difference; IPTW, inverse probability treatment weighting.

For the phase two recommendation, factors such as floor of mouth carcinoma (PD^e: 9.68%, 95% CI: 0.40%−19.00%), hypopharyngeal carcinoma (PD^e: 34.6%, 95% CI: 17.20%−51.90%), stage IVa (PD^e: 11.34%, 95% CI: 2.17%−20.50%), age between 30 and 60 years (PD^e: 10.80%, 95% CI: 4.78%−16.90%), and age under 30 years (PD^e: 57.20%, 95% CI: 53.40%−61.10%) were associated with a greater likelihood of being recommended for surgery plus CRT. On the other hand, surgery plus RT was more likely to be recommended for the patients with sinonasal cancer (PD^e: −22.60%, 95% CI: −37.32%–−7.91%), laryngeal cancer (PD^e: −8.46%, 95% CI: −15.20%–−1.74%), and those older than 60 years (PD^e: −11.70%, 95% CI: −17.70%–−5.74%).

Figures 6A, B visualize the eight most important variables, sorted by the aggregated Shapley values, for the overall model outputs for the phase one and phase two recommendations using SurvSHAP(t). These results were calculated over 500 random observations in the testing set. The horizontal bars represent the number of observations for which the importance of the variable, represented by a given color, was ranked as first, second, and so on.

According to the phase one model, advanced T stage was the most important feature, followed by N stage, age, and treatment. N stage, age, and histological grade significantly affected the outputs of the phase two model.

Discussion

Surgery plus adjuvant RT is the classic therapy for patients with locally advanced HNSCC (3), while the use of adjuvant CRT has become increasingly popular (4). In terms of organ preservation, patients with advanced T stage or multiple lymph node involvement have been found to benefit from CRT (2). However, the treatment guidelines are still primarily population-based, and considering treatment heterogeneity, the optimal treatment plan for a patient needs to be considered at the individual level (8).

In this study, we developed and compared several models to provide individualized treatment recommendations for patients with locally advanced HNSCC. After thorough validation and bias control, BITES, a deep learning-based approach, demonstrated

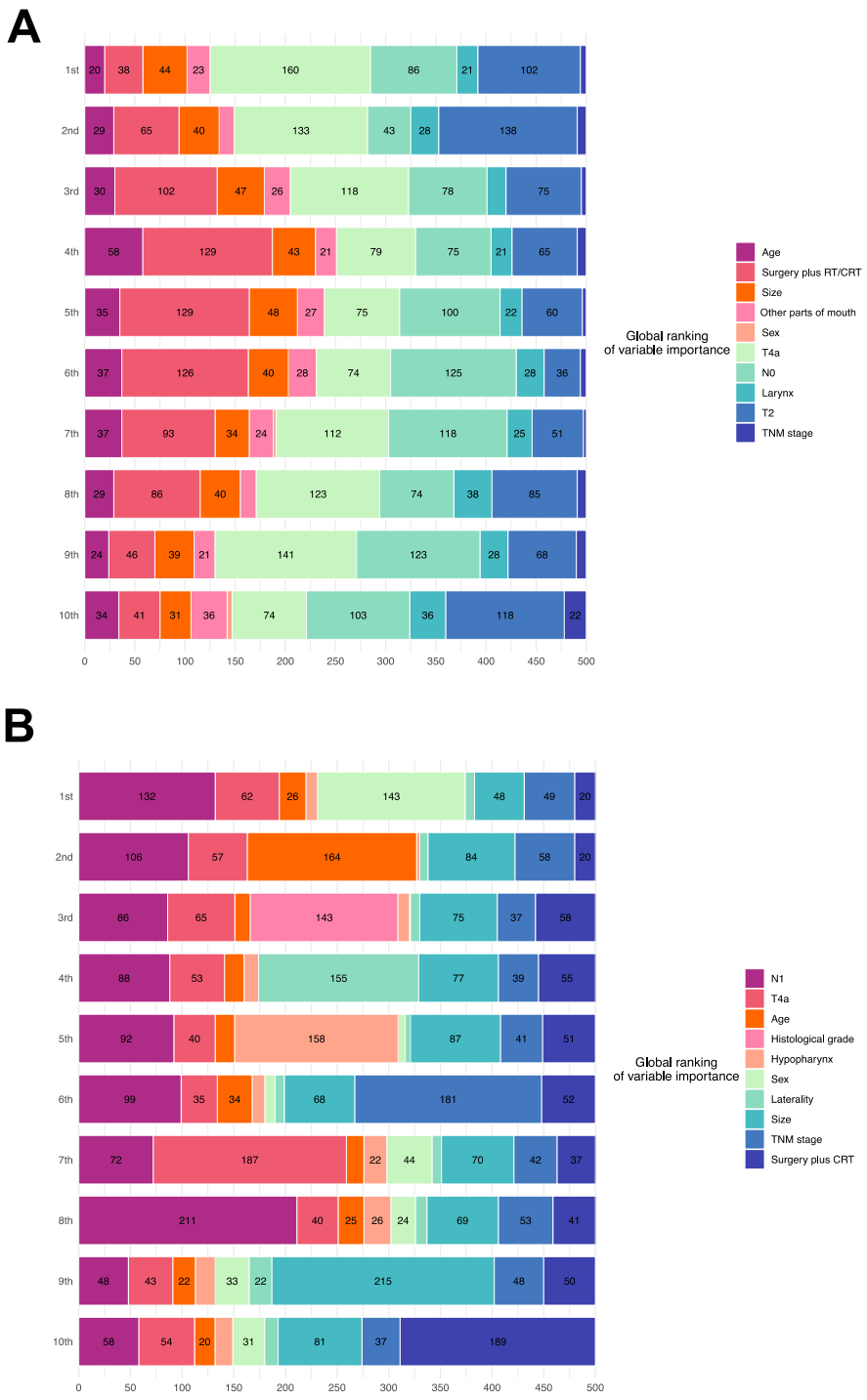

FIGURE 6
Model interpretation based on SurvSHAP(t). **(A)** Interpretation of the model of the phase one recommendation. **(B)** Interpretation of the model of the phase two recommendation. RT, radiation; CRT, chemoradiation.

the best performance, prolonging patient survival by 4 to 10 months over 5 years. It outperformed real-world physician choices, widely used models, and NCCN guidelines, showcasing its potential to improve clinical treatment decisions by addressing complex treatment heterogeneity and non-linear interactions more effectively than traditional models such as CPH and RSF (29, 30).

We believe the advantage of BITES lies in its superior feature extraction capability and its representation-based causal inference method#. Its deep learning framework captures complex non-linear relationships, surpassing the limitations of traditional models such as CPH, which relies on constant hazard ratio assumptions, and RSF, which struggles with high-dimensional data (30). Through

representation learning, it effectively balances covariates between treatment groups, reducing bias and improving ITE estimation (29), while traditional models are largely affected by selection bias in observational data#. In addition, BITES directly optimizes for the ITE, providing more precise treatment recommendations compared to DeepSurv, which focuses primarily on survival risk prediction (31). The shared and risk network architecture of BITES further enhances interpretability, making it particularly well-suited for clinical applications (29). These strengths position BITES as the most effective model for personalized treatment recommendations in this study and make it more suitable for individualized causal inference tasks.

Our quantitative results are consistent with the majority of the literature. In the phase one recommendation, we found that the patients older than 60 years were 29% more likely to be recommended for surgery than the remaining patients, which is supported by studies (32) indicating that the efficacy of chemotherapy decreases with the increasing age of the patient. Similar results were found in the patients with onset sites in the lip (33), gum (34), oropharynx (35), larynx (36), and tonsil (37), as well as in those with stage Iva (38). In addition, Foster et al. (39) found lower rates of osteonecrosis in tongue cancer patients treated with CRT, supporting the greater likelihood of them being recommended for CRT.

In the phase two recommendation, surgery plus RT was more frequently recommended for the older patients due to the reduced efficacy of chemotherapy (40). In addition, the better efficacy of this approach has been proven in patients with sinonasal cancer (41) and laryngeal cancer(36). Conversely, patients with stage Iva (42), onset sites in the hypopharynx (43), and floor of the mouth (44, 45) are found to benefit more from adjuvant CRT.

Maximizing patient survival and providing a satisfactory quality of life are priorities for physicians. Compared to conventional guidelines, DL models can not only personalize treatment but also quantify the benefits of each treatment and provide a visual platform for doctors and patients to communicate with each other. With the continuous improvement of DL models, the application can be extended to other areas, such as risk identification and imaging prediction, simplifying clinical diagnosis and treatment.

Limitations

The complete inclusion of variables and diverse outcomes is still an area of improvement. The SEER database lacks some important clinical variables, such as human papillomavirus status and vascular invasion, hindering more accurate modeling. In addition, other survival outcomes are also important considerations for patients when choosing a treatment plan, whereas our model solely focused on whether to perform organ preservation.

Conclusion

In this study, we developed a personalized treatment recommendation system for patients with locally advanced HNSCC using DL models. BITES demonstrated the ability to identify patients who can achieve organ preservation with CRT and to guide maximum survival. Comprehensive clinical data and further refinement of DL models can enable more accurate predictions in the future, ultimately achieving the potential of precision medicine.

Data availability statement

The datasets used in this study are available in online repositories. The original data can be accessed through the Surveillance, Epidemiology, and End Results (SEER) database at https://seer.cancer.gov/data/.

Ethics statement

The studies involving human participants were approved by the National Cancer Institution. Written informed consent for participation was not needed for this study in accordance with national legislation and institutional requirements. The studies were conducted in accordance with the local legislation and institutional requirements. The participants provided their written informed consent to participate in this study.

Author contributions

LZ: Conceptualization, Data curation, Formal analysis, Investigation, Methodology, Project administration, Resources, Supervision, Validation, Visualization, Writing – original draft, Writing – review & editing. EZ: Conceptualization, Data curation, Formal analysis, Methodology, Project administration, Resources, Software, Supervision, Validation, Visualization, Writing – original draft, Writing – review & editing. JSh: Formal analysis, Investigation, Methodology, Writing – original draft. XW: Formal analysis, Investigation, Writing – original draft. SC: Formal analysis, Writing – original draft. SH: Investigation, Writing – original draft. ZA: Funding acquisition, Supervision, Writing – review & editing. JSu: Funding acquisition, Supervision, Writing – review & editing.

Funding

The author(s) declare financial support was received for the research, authorship, and/or publication of this article. This research was supported by grants from the National Natural Science Foundation of China (Grant No. 81873715).

Conflict of interest

The authors declare that the research was conducted in the absence of any commercial or financial relationships that could be construed as a potential conflict of interest.

Publisher's note

All claims expressed in this article are solely those of the authors and do not necessarily represent those of

their affiliated organizations, or those of the publisher, the editors and the reviewers. Any product that may be evaluated in this article, or claim that may be made by its manufacturer, is not guaranteed or endorsed by the publisher.

Supplementary material

The Supplementary Material for this article can be found online at: https://www.frontiersin.org/articles/10.3389/fmed.2024.1478842/full#supplementary-material

References

1. Sung H, Ferlay J, Siegel RL, Laversanne M, Soerjomataram I, Jemal A, et al. Global cancer statistics 2020: GLOBOCAN estimates of incidence and mortality worldwide for 36 cancers in 185 countries. *CA Cancer J Clin.* (2021) 71:209–49. doi: 10.3322/caac.21660

2. Johnson DE, Burtness B, Leemans CR, Lui VWY, Bauman JE, Grandis JR. Head and neck squamous cell carcinoma. *Nat Rev Dis Primers.* (2020) 6:92. doi: 10.1038/s41572-020-00224-3

3. Caudell JJ, Gillison ML, Maghami E, Spencer S, Pfister DG, Adkins D, et al. NCCN guidelines® insights: head and neck cancers, version 1.2022. *J Natl Compr Canc Netw.* (2022) 20:224—34. doi: 10.6004/jnccn.2022.0016

4. Cooper JS, Pajak TF, Forastiere AA, Jacobs J, Campbell BH, Saxman SB, et al. Postoperative concurrent radiotherapy and chemotherapy for high-risk squamous-cell carcinoma of the head and neck. *N Engl J Med.* (2004) 350:1937–44. doi: 10.1056/NEJMoa032646

5. Chen AM, Daly ME, Farwell DG, Vazquez E, Courquin J, Lau DH, et al. Quality of life among long-term survivors of head and neck cancer treated by intensity-modulated radiotherapy. *JAMA Otolaryngol Head Neck Surg.* (2014) 140:129–33. doi: 10.1001/jamaoto.2013.5988

6. Campbell G, Glazer TA, Kimple RJ, Bruce JY. Advances in organ preservation for laryngeal cancer. *Curr Treat Options Oncol.* (2022) 23:594–608. doi: 10.1007/s11864-022-00945-5

7. Patel SA, Qureshi MM, Dyer MA, Jalisi S, Grillone G, Truong MT. Comparing surgical and nonsurgical larynx-preserving treatments with total laryngectomy for locally advanced laryngeal cancer. *Cancer.* (2019) 125:3367–77. doi: 10.1002/cncr.32292

8. Howard FM, Kochanny S, Koshy M, Spiotto M, Pearson AT. Machine learning-guided adjuvant treatment of head and neck cancer. *JAMA Netw Open.* (2020) 3:e2025881. doi: 10.1001/jamanetworkopen.2020.25881

9. Huang S, Yang J, Fong S, Zhao Q. Artificial intelligence in cancer diagnosis and prognosis: Opportunities and challenges. *Cancer Lett.* (2020) 471:61–71. doi: 10.1016/j.canlet.2019.12.007

10. Hosny A, Parmar C, Coroller TP, Grossmann P, Zeleznik R, Kumar A, et al. Deep learning for lung cancer prognostication: a retrospective multi-cohort radiomics study. *PLoS Med.* (2018) 15:e1002711. doi: 10.1371/journal.pmed.1002711

11. Hankey BF, Ries LA, Edwards BK. The surveillance, epidemiology, and end results program: a national resource. *Cancer Epidemiol Biomarkers Prev.* (1999) 8:1117–21.

12. von Elm E, Altman DG, Egger M, Pocock SJ, Gøtzsche PC, Vandenbroucke JP. The strengthening the reporting of observational studies in epidemiology (STROBE) statement: guidelines for reporting observational studies. *Lancet.* (2007) 370:1453–7. doi: 10.1016/S0140-6736(07)61602-X

13. Mazul AL, Naik AN, Zhan KY, Stepan KO, Old MO, Kang SY, et al. Gender and race interact to influence survival disparities in head and neck cancer. *Oral Oncol.* (2021) 112:105093. doi: 10.1016/j.oraloncology.2020.105093

14. Du X, Zhan W, Li X, Yin S, Chen Q, Huang J, et al. Marital status and survival in laryngeal squamous cell carcinoma patients: a multinomial propensity scores matched study. *Eur Arch Otorhinolaryngol.* (2022) 279:3005–11. doi: 10.1007/s00405-022-07252-7

15. van der Kamp MF, Halmos GB, Guryev V, Horvatovich PL, Schuuring E, van der Laan B, et al. Age-specific oncogenic pathways in head and neck squamous cell carcinoma - are elderly a different subcategory? *Cell Oncol (Dordr).* (2022) 45:1–18. doi: 10.1007/s13402-021-00655-4

16. Xu B, Salama AM, Valero C, Yuan A, Khimraj A, Saliba M, et al. The prognostic role of histologic grade, worst pattern of invasion, and tumor budding in early oral tongue squamous cell carcinoma: a comparative study. *Virchows Arch.* (2021) 479:597–606. doi: 10.1007/s00428-021-03063-z

17. Al Saad S, Al Shenawi H, Almarabheh A, Al Shenawi N, Mohamed AI, Yaghan R. Is laterality in breast Cancer still worth studying? Local experience in Bahrain. *BMC Cancer.* (2022) 22:968. doi: 10.1186/s12885-022-10063-y

18. Tsuge H, Kawakita D, Taniyama Y, Oze I, Koyanagi YN, Hori M, et al. Subsite-specific trends in mid- and long-term survival for head and neck cancer patients in Japan: a population-based study. *Cancer Sci.* (2024) 115:623–34. doi: 10.1111/cas.16028

19. Khalil C, Khoury M, Higgins K, Enepekides D, Karam I, Husain ZA, et al. Lymph node yield: impact on oncologic outcomes in oral cavity cancer. *Head Neck.* (2024) 46:1965–74. doi: 10.1002/hed.27656

20. Tsai MH, Chuang HC, Chien CY, Huang TL, Lu H, Su YY, et al. Lymph node ratio as a survival predictor for head and neck squamous cell carcinoma with multiple adverse pathological features. *Head Neck.* (2023) 45:2017–27. doi: 10.1002/hed.27428

21. Voss JO, Freund L, Neumann F, Mrosk F, Rubarth K, Kreutzer K, et al. Prognostic value of lymph node involvement in oral squamous cell carcinoma. *Clin Oral Investig.* (2022) 26:6711–20. doi: 10.1007/s00784-022-04630-7

22. Künzel SR, Sekhon JS, Bickel PJ, Yu B. Metalearners for estimating heterogeneous treatment effects using machine learning. *Proc Natl Acad Sci U S A.* (2019) 116:4156–65. doi: 10.1073/pnas.1804597116

23. Yao L, Chu Z, Li S, Li Y, Gao J, Zhang A. A survey on causal inference. *ACM Trans Knowl Discov Data (TKDD).* (2020) 15:1–46. doi: 10.1145/3444944

24. Schrod S, Schäfer A, Solbrig S, Lohmayer R, Gronwald W, Oefner PJ, et al. BITES: balanced individual treatment effect for survival data. *Bioinformatics.* (2022) 38:i60–i67. doi: 10.1093/bioinformatics/btac221

25. Nagpal C, Goswami M, Dufendach KA, Dubrawski AW. Counterfactual phenotyping with censored time-to-events. In: *Proceedings of the 28th ACM SIGKDD Conference on Knowledge Discovery and Data Mining* (2022).

26. Katzman J, Shaham U, Cloninger A, Bates J, Jiang T, Kluger Y. Deep survival: a deep cox proportional hazards network. *ArXiv* [preprint] abs/1606.00931. (2016).

27. Krzyzi'nski M, Spytek M, Baniecki H, Biecek P. SurvSHAP(t): time-dependent explanations of machine learning survival models. *Knowl Based Syst.* (2022) 262:110234. doi: 10.1016/j.knosys.2022.110234

28. Hernán M, Brumback B, Robins J. Marginal structural models to estimate the joint causal effect of nonrandomized treatments. *J Am Stat Assoc.* (2001) 96:440–8. doi: 10.1198/016214501753168154

29. Shalit U, Johansson FD, Sontag DA. Bounding and minimizing counterfactual error. (2016). *ArXiv* [preprint] abs/1606.03976.

30. Ishwaran H, Kogalur UB, Blackstone EH, Lauer MS. Random survival forests. *Ann Appl Stat.* (2008) 2:841–60. doi: 10.1214/08-AOAS169

31. Katzman JL, Shaham U, Cloninger A, Bates J, Jiang T, Kluger Y. DeepSurv: personalized treatment recommender system using a Cox proportional hazards deep neural network. *BMC Med Res Methodol.* (2018) 18:24. doi: 10.1186/s12874-018-0482-1

32. Lacas B, Carmel A, Landais C, Wong SJ, Licitra L, Tobias JS, et al. Meta-analysis of chemotherapy in head and neck cancer (MACH-NC): an update on 107 randomized trials and 19,805 patients, on behalf of MACH-NC Group. *Radiother Oncol.* (2021) 156:281–93. doi: 10.1016/j.radonc.2021.01.013

33. Kerawala C, Roques T, Jeannon JP, Bisase B. Oral cavity and lip cancer: United Kingdom National multidisciplinary guidelines. *J Laryngol Otol.* (2016) 130:S83–s89. doi: 10.1017/S0022215116000499

34. Bark R, Mercke C, Munck-Wikland E, Wisniewski NA, Hammarstedt-Nordenvall L. Cancer of the gingiva. *Eur Arch Otorhinolaryngol.* (2016) 273:1335–45. doi: 10.1007/s00405-015-3516-x

35. Park JO, Park YM, Jeong WJ, Shin YS, Hong YT, Choi IJ, et al. Survival benefits from surgery for stage IVa head and neck squamous cell carcinoma: a multi-institutional analysis of 1,033 cases. *Clin Exp Otorhinolaryngol.* (2021) 14:225–34. doi: 10.21053/ceo.2020.01732

36. Mesia R, Iglesias L, Lambea J, Martínez-Trufero J, Soria A, Taberna M, et al. SEOM clinical guidelines for the treatment of head and neck cancer (2020). *Clin Transl Oncol.* (2021) 23:913–21. doi: 10.1007/s12094-020-02533-1

37. Roden DF, Schreiber D, Givi B. Triple-modality treatment in patients with advanced stage tonsil cancer. *Cancer.* (2017) 123:3269–76. doi: 10.1002/cncr.30728

38. Kim D, Li R. Contemporary treatment of locally advanced oral cancer. *Curr Treat Options Oncol.* (2019) 20:32. doi: 10.1007/s11864-019-0631-8

39. Foster CC, Melotek JM, Brisson RJ, Seiwert TY, Cohen EEW, Stenson KM, et al. Definitive chemoradiation for locally-advanced oral cavity cancer: A 20-year experience. *Oral Oncol.* (2018) 80:16–22. doi: 10.1016/j.oraloncology.2018.03.008

40. Gyawali B, Shimokata T, Honda K, Ando Y. Chemotherapy in locally advanced head and neck squamous cell carcinoma. *Cancer Treat Rev.* (2016) 44:10–6. doi: 10.1016/j.ctrv.2016.01.002

41. Cracchiolo JR, Patel K, Migliacci JC, Morris LT, Ganly I, Roman BR, et al. Factors associated with a primary surgical approach for sinonasal squamous cell carcinoma. *J Surg Oncol.* (2018) 117:756–64. doi: 10.1002/jso.24923

42. Chen WC, Lai CH, Fang CC, Yang YH, Chen PC, Lee CP, et al. Identification of high-risk subgroups of patients with oral cavity cancer in need of postoperative adjuvant radiotherapy or chemo-radiotherapy. *Medicine (Baltimore).* (2016) 95:e3770. doi: 10.1097/MD.0000000000003770

43. Hinerman RW, Amdur RJ, Mendenhall WM, Villaret DB, Robbins KT. Hypopharyngeal carcinoma. *Curr Treat Options Oncol.* (2002) 3:41–9. doi: 10.1007/s11864-002-0040-1

44. Alabi RO, Youssef O, Pirinen M, Elmusrati M, Mäkitie AA, Leivo I, et al. Machine learning in oral squamous cell carcinoma: current status, clinical concerns and prospects for future-a systematic review. *Artif Intell Med.* (2021) 115:102060. doi: 10.1016/j.artmed.2021.102060

45. Di Rito A, Fiorica F, Carbonara R, Di Pressa F, Bertolini F, Mannavola F, et al. Adding concomitant chemotherapy to postoperative radiotherapy in oral cavity carcinoma with minor risk factors: systematic review of the literature and meta-analysis. *Cancers (Basel).* (2022) 14:15. doi: 10.3390/cancers14153704

frontiers | Frontiers in Pharmacology

TYPE Original Research
PUBLISHED 20 March 2025
DOI 10.3389/fphar.2025.1513948

OPEN ACCESS

EDITED BY
Fujun Han,
The First Hospital of Jilin University, China

REVIEWED BY
Luo Min,
Fudan University, China
Dongxin Zhao,
Chinese Academy of Sciences (CAS), China

*CORRESPONDENCE
Xudong Wei,
weixd93@lzu.edu.cn
Lei Tan,
lei.tan19800707@njmu.edu.cn
Xiaoya Ma,
maxy.dela@gmail.com

†These authors have contributed equally to this work

RECEIVED 19 October 2024
ACCEPTED 25 February 2025
PUBLISHED 20 March 2025

CITATION
Liu L, Wang B, Ma X, Tan L and Wei X (2025) A novel ubiquitin-related genes-based signature demonstrated values in prognostic prediction, immune landscape sculpture and therapeutic options in laryngeal cancer.
Front. Pharmacol. 16:1513948.
doi: 10.3389/fphar.2025.1513948

A novel ubiquitin-related genes-based signature demonstrated values in prognostic prediction, immune landscape sculpture and therapeutic options in laryngeal cancer

Lu Liu[1,2,3,4†], Bing Wang[5†], Xiaoya Ma[3,6*], Lei Tan[4,7,8*] and Xudong Wei[1,2*]

[1]The First Clinical Medical College of Lanzhou University, Lanzhou, China, [2]Department of E.N.T., Gansu Provincial Hospital, Lanzhou, China, [3]Center for Energy Metabolism and Reproduction, Institute of Biomedicine and Biotechnology, Shenzhen Institute of Advanced Technology, Chinese Academy of Sciences, Shenzhen, China, [4]Innovation Center of Suzhou Nanjing Medical University, Suzhou, China, [5]Pediatric Heart Disease Treatment Center, Jiangxi Provincial Children's Hospital, Nanchang, China, [6]Department of Cardiology, Shenzhen Guangming District People's Hospital, Shenzhen, China, [7]State Key Laboratory of Reproductive Medicine and Offspring Health, Nanjing Medical University, Nanjing, China, [8]National Center of Technology Innovation for Biopharmaceuticals, Suzhou, China

Background: Laryngeal cancer (LC) is characterized by high mortality and remains challenging in prognostic evaluation and treatment benefits. Ubiquitin-related genes (UbRGs) are widely involved in cancer initiation and progression, but their potential value in LC is unknown.

Methods: RNA-seq and clinical data of LC were obtained from TCGA and GEO. UbRGs that independently influenced the overall survival (OS) of LC patients were screened with differential expression, COX and LASSO regression analyses. A prognostic signature was then established and assessed for its predictive value, stability and applicability using Kaplan-Meier analysis and receiver operating characteristic curves. The nomogram was further generated in combination with the signature and clinical characteristics. Characterization of immune properties and prediction of drug sensitivity were investigated on the signature-based subgroups using a panel of *in silico* platforms. Verification of gene expression was conducted with Western blot, qRT-PCR and ELISA, ultimately.

Results: PPARG, LCK and LHX1 were identified and employed to construct the UbRGs-based prognostic signature, showing a strong ability to discriminate LC patients with distinct OS in TCGA-LC and GSE65858, and excellent applicability in most clinical conditions. The nomogram showed higher predictive value and net clinical benefit than traditional indicators. As evaluated, the low-risk group had a more activated immune function, higher infiltration of anti-cancer immune cells and stronger expression of immune-promoting cytokines than the high-risk group. Immune properties were also correlated with individual signature genes. PPARG and LHX1 were negatively correlated, whereas LCK positively correlated, with the immuno-promoting microenvironment. Additionally,

chemotherapy would be more effective in high-risk patients, while immune checkpoint inhibitors would be more effective in low-risk patients. Finally, dysregulation of the signature genes was confirmed in LC cell lines by Western blot, and PPARG knockdown significantly reduced the expression of the immunosuppressive cytokines IL6, TGFB1, TGFB2 and VEGFC by qRT-PCR and ELISA.

Conclusion: We have developed a UbRGs-based signature for LC prognostic evaluation that is valuable in clinical application, indicative of the immune microenvironment and beneficial for individualized treatment guidance.

KEYWORDS

laryngeal cancer, ubiquitin-related genes-based signature, prognosis prediction, immune landscape sculpture, therapeutic options

1 Introduction

As the most common malignant tumor of the head and neck, there are approximately 188,960 new cases of laryngeal cancer (LC) and 103,216 related deaths annually worldwide, according to the latest GLOBOCAN report (Bray et al., 2024). With the application of comprehensive treatment strategies combining surgery, radiotherapy, chemotherapy and immunotherapy, the 5-year survival rate for certain LC patients has improved. However, the proportion of patients dying from recurrence, metastasis and resistance is still as high as 30%–40% (Steuer et al., 2017; Egelmeer et al., 2011). To reduce patient mortality, accurate prognostic prediction is essential for better survival estimation and optimization of therapeutic strategies. Current assessments depend primarily on the pathological characteristics of the tumor, especially the TNM stage. Unfortunately, the predictive power of the TNM stage is only 57% for overall survival (OS) and 60% for progression-free survival in LC patients (Cui et al., 2020a; Cui et al., 2020b). Obviously, current prognostic strategies have already hampered the accurate prediction of tumor progression and therapeutic response, and consequently will rarely support improvements in treatment. Therefore, to achieve better prognosis and efficacy in LC therapies, there's an urgent need to establish new prognostic strategies and discover biomarkers of advantage.

It's well known that protein dysregulation and dysfunction are widespread in cancer cells (Díaz et al., 2021). As the pivotal regulatory machinery of protein homeostasis in eukaryotic cells, the ubiquitin-proteasome system is deeply involved in tumor initiation and progression (Sun et al., 2020). As reported by Wang et al., cell proliferation and radiotherapy resistance in LC were mediated by overexpression of UBR5, an E3 ubiquitin-protein ligase, through activation of the p38/MAPK signaling pathway (Wang et al., 2020). Another report on USP34, one of the deubiquitinating enzymes, indicated its role in enhancing LC cell growth and resistance to cisplatin by stabilizing SOX2 (Dai et al., 2020). In addition to direct effects on cancer cells, ubiquitin-related genes (UbRGs) also play an important role in facilitating cancer immune evasion (Çetin et al., 2021). For example, the E3 enzyme TRIM28 has been reported to induce the infiltration of myeloid-derived suppressor cells into small cell lung cancer, thereby promoting cancer progression through increased RIPK1 ubiquitination and activation of the downstream NF-κB pathway (Liang et al., 2023). During the anti-PD-1 treatments in colorectal cancer, its reactivity was impaired by a deubiquitinating enzyme USP14, which inhibited PD-1 expression and $CD8^+$ T cell infiltration by targeting the IDO1/TRP/KYN signaling axis (Shi et al., 2022). In short, multiple properties of cancer will be altered by the disrupted expression of UbRGs through a panel of distinct mechanisms. As a consequence, patient survival and therapeutic response may be affected, suggesting that UbRGs could be employed as candidate biomarkers to develop novel strategies for predicting LC prognosis. However, the studies of UbRGs in LC are still insufficient, which hinders the understanding of their functional role and application in prognosis.

In this study, we aimed to develop a UbRGs-based prognostic signature and nomogram, attempting to achieve risk stratification and individualized survival prediction in LC patients. Multi-dimensional evaluations were then carried out to recognize the correlation between the UbRGs-based signature and the immune properties of the LC microenvironment. Subsequently, the potential regulatory role of the signature genes in LC immunity was thoroughly investigated by panels of *in silico* prediction and experiment validation. Finally, drug sensitivity prediction was performed to provide clues for the individualized therapy of LC patients based on this gene signature. Overall, our study was the first design of UbRGs-based prognostic signature of LC and provided new insights to improve prognosis prediction, understand cancer immunity, and guide individualized medication, which will ultimately shed new light on prolonging patient survival.

2 Materials and methods

The entire procedure of this study was summarized in the flowchart shown in Figure 1. All websites and calculation tools employed are listed in Supplementary Table S1.

2.1 Data collection and preprocessing

RNA-Seq data and clinical information of 116 LC and 12 normal laryngeal tissues were downloaded from The Cancer Genomic Atlas (TCGA). Expression profiling data were normalized using the transcripts per kilobase of exon model per million mapped reads format, and relevant clinical analyses were performed on 105 cases

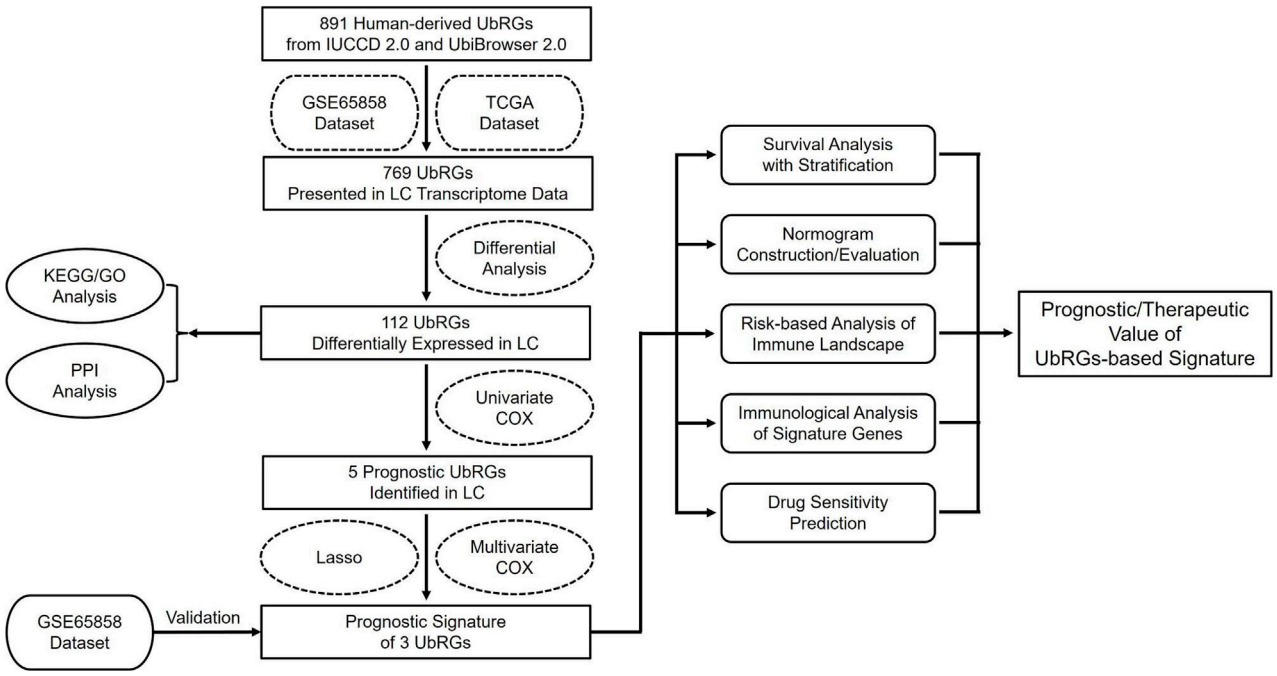

FIGURE 1
Flowchart of the current study.

after excluding samples with missing pathological and survival information. The TCGA-LC dataset was defined as the training set. For signature validation, the GSE65858 dataset was downloaded from the Gene Expression Omnibus (GEO), from which the expression matrix and clinical data of 46 LC patients were extracted. Those two datasets were uploaded in Supplementary Data 1.

2.2 Identification and annotation of differentially expressed ubiquitin-related genes

Ubiquitin-related genes were collected from two databases, iUUCD 2.0 and UbiBrowser 2.0. Differentially expressed UbRGs (DUbRGs) were then screened from the harvested genes using the "limma" R package with criteria of FDR <0.05 and |log2 fold change (FC) | > 1. Both genes and samples were clustered using the "Complete" clustering method and the "correlation" distance calculation approach. Subsequently, a heatmap was generated to visually present the top 20 DUBRGs.

Functional analyses of DUbRGs were carried out with the Sangerbox 3.0 online platform for either the Kyoto Encyclopedia of Genes and Genomes (KEGG) or Gene Ontology (GO), including cellular components (CC), molecular functions (MF) and biological processes (BP). FDR <0.05 was considered as the significance threshold for the enrichment of candidate pathways. The analysis of potential protein-protein interaction (PPI) among DUbRGs was performed in STRING, with a minimum interaction score of 0.4. Visualization of the PPI network proceeded using Cytoscape software.

2.3 Construction and validation of a prognostic signature based on UbRGs

Univariate Cox regression analysis was used to preliminarily screen for DUbRGs that significantly correlated with overall survival (OS) based on the gene expression profile data of individuals in the training set. These DUbRGs were shrunk based on the minimum lambda determined by 10-fold cross-validation in the least absolute shrinkage and selection operator (LASSO) regression analysis. Genes with independent prognostic value were further identified with multivariate COX regression analysis among the ones resulting from univariate Cox regression. The expression value will then be termed as Exp and incorporated into the prognostic signature. Meanwhile, the coefficient of gene expression value was also generated in the same analysis and termed as β. This value was employed to quantify the contribution of each gene to the risk rate and thus more accurately reflect its weight in the overall assessment. Subsequently, the patient risk score was formulated as below:

$$\text{Risk score} = \sum_{i=1}^{n} \beta_i \times Exp_i$$

Based on the median risk score, the individuals in the training set were divided into high- and low-risk groups. To assess the ability of the signature to discriminate OS in LC patients, Kaplan-Meier curves were plotted accordingly using the SRplot online platform. With this platform, receiver operating characteristic (ROC) curves were also plotted and the area under the curves (AUC) was calculated to evaluate the predictive efficacy of the signature in 1-, 2-, and 3-year OS of LC patients. In addition, the distribution characteristics were analyzed for the risk score, survival status and gene expression profiles. To assess the stability of the signature, the

validation set was employed. The median risk score of the training set was also used as the basis to group high- and low-risk. The numbers of high- and low-risk patients in the training and validation sets are shown in Supplementary Table S2.

To evaluate the clinical applicability of the signature under different clinical characteristics, Kaplan-Meier analysis was conducted on the subgroups retrieved from the training set, including age (</> 60 years old), gender (male/female), differentiation grade (1-2/3-4), T stage (1-2/3-4), N stage (0-1/2-3), M stage (0/1) and clinical stage (I-II/III-IV). The number of high- and low-risk patients in each subgroup was shown in Supplementary Table S2.

2.4 Establishment and evaluation of nomogram

Univariate and multivariate COX regression analyses were performed on the combination of risk score and clinical characteristics in the training set. To convert the results of complex regression equations into simple graphs, a nomogram was constructed using the "regplot" R package, which can efficiently predict the probability of an individual's outcome event according to the patient's specific situation, thus achieving individualized assessment in clinics (Balachandran et al., 2015). ROC curves were generated to evaluate the predictive efficacy of the nomogram, risk score and traditional prognostic indicators (T stage, N stage, M stage and clinical stage) for 3-year OS in LC patients. Calibration curves were synthesized to assess the consistency between the predicted and actual survival rates using the "rms" R package. To evaluate the net clinical benefit of the nomogram and traditional stage, decision curve analysis (DCA) was performed using the "ggDCA" R package.

2.5 Gene set enrichment analysis (GSEA)

KEGG- and GO-related gene sets were downloaded from the GSEA. To explore potentially enriched biological functions in the high- and low-risk groups, GSEA enrichment analysis was carried out on the training set using the R packages termed "limma" and "clusterProfiler". The enriched items were recognized with *p*-values lower than 0.05 and then ranked based on NES resulting from the normalization of enrichment scores. The top 5 enriched items were visualized as curves in GSEA plots, while pie charts were used to show the categories and percentages within all enriched items.

2.6 Analysis of immune landscape

To understand the potential correlation between the UbRGs-based prognostic signature and cancer immunity in LC, a panel of immune properties was calculated for individuals in the training set and then compared between the high- and low-risk groups as follows.

1) The activation degree of 13 immune-related pathways was assessed with the ssGSEA algorithm.
2) The TME scores (including stromal score, immune score and ESTIMATE score) were calculated using the ESTIMATE algorithm to determine the proportion of TME cells in LC.
3) The infiltration levels of immune cells were estimated using the CIBERSORT and ssGSEA algorithms, and the correlation between risk score and infiltration level of each cell type was further analyzed with the Chiplot online platform.
4) The expression levels of immune-related cytokines were analyzed using the Sangerbox 3.0 online platform.

2.7 Cell culture and CRISPR-based gene knockout

Human LC cell lines (TU686, TU212 and LCC) and a normal lung epithelial cell line (Bease-2B) were purchased from Meilun, Yihe, QuiCell and Aorisai Biotechnology Co., LTD respectively. They were cultured in RPMI 1640 or DMEM-H medium containing 10% fetal bovine serum and 1% penicillin/streptomycin. Cells were passaged at a ratio of 1:3 ratio upon reaching 80% confluence.

Plasmids containing control or PPARG-targeting sgRNAs were constructed based on the LentiCRISPR v2 vector (Addgene #52961) for stable gene knockout in cell lines. The lentivirus was then packaged into 293T cells and applied to infect TU212 and TU686 cells. After infection, continuous puromycin selection was performed at a concentration of 2 μg/mL to obtain stable cell lines for further experiments. The sgRNA sequences are listed in Supplementary Table S3.

2.8 Western blot (WB)

Western blot assays were performed using routine methods. Briefly, the cells were lysed with RIPA buffer on ice once reaching 80% confluence. After centrifugation at 4°C, 12,000 rpm for 30 min, protein samples were collected from the supernatant, mixed with 1×loading buffer, and then heated at 95°C for 30 min. The heated samples were further subjected to SDS-PAGE electrophoresis and antibody staining.

The expression levels of PPARG, LCK and LHX1 proteins were determined in TU686, TU212, LCC and Bease-2B cells. The knockout efficiency of PPARG was tested in TU212- and TU686-derived control and PPARG knockout cells. Hence, the primary antibodies used in this study included PPARG (Proteintect, 66936-1-Ig), LCK (Abcam, ab227975), LHX1 (Santa, sc-515631) and GAPDH (Proteintect, 66936-1-IG). 10494-1-AP). Goat Anti-Rabbit IgG-HRP (Affinity, S0001) and Goat Anti-Mouse IgG-HRP (Affinity, S0002) were adopted as secondary antibodies. The grayscale values of the protein bands were analyzed semi-quantitatively using ImageJ software.

2.9 Quantitative real-time polymerase chain reaction (qRT-PCR)

qRT-PCR was performed to analyze the mRNA expression levels of cytokines, including IL1A, IL6, IL18, CXCL11, CCL2, VEGFC, TGFB1, TGFB2, TGFB3, CSF1, FGF2 and PDGFC, in control and PPARG knockout groups derived from TU212 and TU686 cell lines.

Total RNA extraction, cDNA synthesis and qRT-PCR reaction were performed according to the kit manuals (Vazyme, R701-01; Takara, RR036A and RR820A). GAPDH was hired as the internal reference gene. Relative mRNA levels of cytokines were calculated by the $2^{-\Delta\Delta CT}$ method. Primer sequences are listed in Supplementary Table S4.

2.10 Enzyme-linked immunosorbent assay (ELISA)

Following the qRT-PCR results, the protein expression levels of IL6, VEGFC, TGFB1 and TGFB2 in the supernatants of control and PPARG knockout cells were examined using ELISA. The ELISA kits (RUIXIN BIOTECH; RX106126H, RX105005H, RX104768H, RX2D118026) were equilibrated at room temperature before the experiment. Operations were then performed following the instructions and the OD values were detected at 450 nm. The standard curves were subsequently plotted and the protein concentrations were calculated from the corresponding OD values.

2.11 Prediction of drug sensitivity in LC patients

The response of LC patients to immunotherapy was forecasted using the TIDE algorithm, and the expression levels of 48 immune checkpoints were further assessed with the Sangerbox 3.0 online platform.

Half inhibitory concentrations (IC50) for chemotherapy and targeted drugs were predicted using the "oncoPredict" R package. Briefly, drug sensitivity data valued as IC50 of tumor cell lines was retrieved from the Genomics of Drug Sensitivity in Cancer (GDSC) database, whereas the corresponding gene expression profiles were also obtained from the same source. They were used to build ridge regression models, which were applied on the training set mentioned in Section 2.1 to yield drug sensitivity predictions. These drug models were built after removing or summarizing gene duplication, homogenization (batch correction), and filtering low-variant genes. Subsequently, calcPhenotype function was applied to the proceeded, standardized and filtered clinical tumor expression data, yielding a drug sensitivity prediction for each patient. Averaged IC50 was ultimately calculated in either high- or low-risk groups respectively for each drug.

2.12 Statistical analysis

All statistical analyses were performed using R software (version 4.3.2), GraphPad Prism (version 9.0) and the online platforms mentioned above. Differences in gene expression, immune infiltration and IC50 predictions across the database were compared using the Wilcoxon signed-rank test. Spearman was employed for the correlation analysis. One-way ANOVA was used to compare differences in protein expression of signature genes among cell lines. The significance of differential cytokine expression was confirmed by t-test. $p < 0.05$ was considered statistically significant.

3 Results

3.1 A prognostic signature was constructed based on PPARG, LCK and LHX1 highlighted from UbRGs differentially expressed in LC

Initially, 1366 UbRGs were retrieved from iUUCD 2.0, including 27 E1 enzymes, 109 E2 enzymes, 1153 E3 enzymes, 164 deubiquitinating enzymes (DUBs), 396 ubiquitin/ubiquitin-like binding domains and 183 ubiquitin-like domains. Meanwhile, 417 E3 enzymes and 86 DUBs were obtained from UbiBrowser 2.0. After removing duplicates and non-human records, 891 human-derived UbRGs were obtained in combination (Supplementary Date 2). Of these, expression data were extracted for 766 UbRGs from both the training and validation sets (Figure 2A). 111 UbRGs were shown as differentially expressed between LC and normal laryngeal tissues in the training set, containing 100 upregulated and 11 downregulated ones, which were termed DUbRGs. The top 20 DUbRGs were presented in the heatmap (Figure 2B). The potential biological functions and protein interactions of these DUbRGs were revealed by KEGG, GO and PPI analyses (Supplementary Figure S1).

Out of 111 DUbRGs, 5 genes were highlighted with significant correlation to the OS of LC patients in univariate COX regression, including TRAF2, PPARG, KLHL17, LCK and LHX1 (Figure 3A). To avoid model overfitting, LASSO regression analysis was performed and these 5 DUbRGs remained when applying the minimum lambda (Figures 3B, C). To further determine the DUbRGs that independently influenced OS, multivariate Cox regression analysis was conducted. PPARG, LCK and LHX1 were subsequently identified as the genes highly correlated with the prognosis of LC patients (Figure 3D), while the other two genes were excluded due to $p > 0.05$. Of these, PPARG and LHX1 were indicated as risk genes with coefficients valued at 0.434 and 0.762 respectively, whereas LCK was indicated as a protective gene with a coefficient of −0.384. Also, such identity was confirmed by Kaplan-Meier analysis (Figures 3E–G). The shorter survival was correlated with high expression of PPARG and LHX1, while with low expression of LCK. Their differential expression in LC and normal lung epithelial cell lines was verified by Western blot, which was consistent with the RNA-seq results (Supplementary Figure S2).

A UbRGs-based prognostic signature was thus established as described in Section 2.3, where the risk score was formulated based on both gene expression levels and their corresponding coefficients:

$$\text{Risk Score} = 0.434 \times \text{PPARG} + 0.762 \times \text{LHX1} - 0.384 \times \text{LCK}$$

3.2 The effectiveness of UbRGs-based signature was proved and a related nomogram was established accordingly

To evaluate the effectivity of the UbRGs-based prognostic signature, a panel of calculations was carried out on the training set. At first, the median risk score was determined as 1.43 by the formulation in **3.1**, with which the high- and low-risk groups were

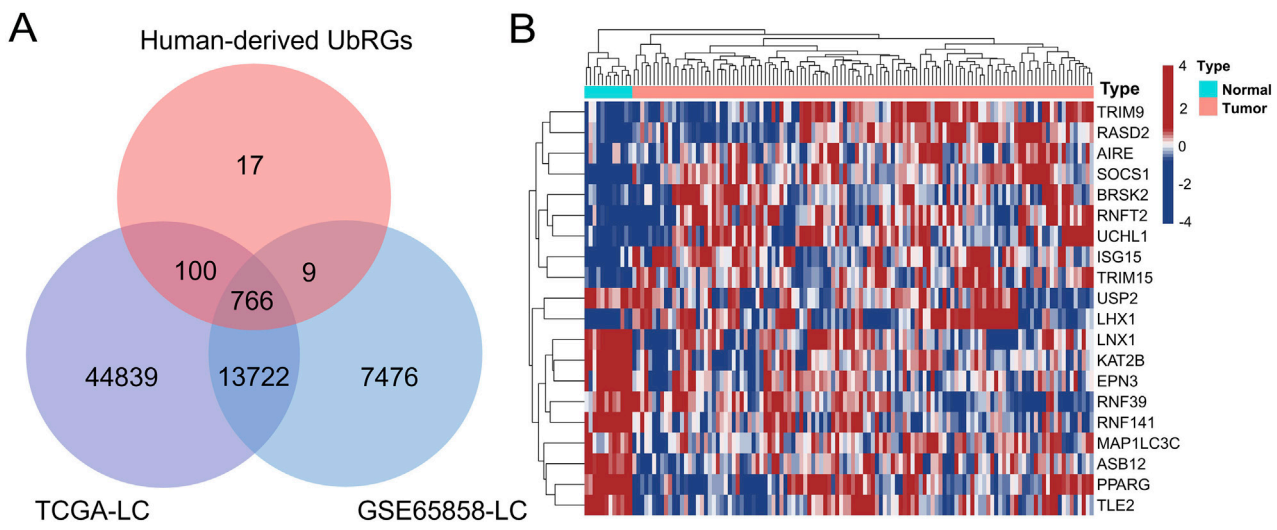

FIGURE 2
Screening of UbRGs differentially expressed in LC. **(A)** The Venn diagram showed 769 UbRGs retrieved from human-derived databases and presented in the TCGA-LC and GSE65858-LC datasets. **(B)** The heatmap of the top 20 differentially expressed UbRGs, with both genes and patients clustered.

then divided from the training set. The median survival time was defined as 22.85 months for the high-risk group and 88.87 months for the low-risk group with Kaplan-Meier analysis ($p < 0.0001$, Figure 4A), which demonstrated a significant difference in OS between the two groups. With the ROC curves of 1-, 2-, and 3-year OS, AUC values were calculated as 0.74, 0.81, and 0.81 respectively, indicating a good predictive efficacy of this signature (Figure 4B). Along with the increasing risk score (Figure 4C), the analysis of individual patients showed higher mortality (Figure 4D). Meanwhile, the expression levels of the risk genes, PPARG and LHX1, tended to be upregulated in high-risk patients; while the trend of protective gene LCK was downregulated (Figure 4E).

To assess the stability of the UbRGs-based signature, the same panel of analyses was subsequently conducted in the validation set. Worse OS was still significantly observed in the high-risk group ($p = 0.016$, Figure 4F). The AUC values were 0.72, 0.71 and 0.70 for 1-, 2-, and 3-year OS in LC patients respectively (Figure 4G), further confirming the effectiveness of the prediction. The correlation between the risk score and mortality as well as the expression trend of the signature genes were in good agreement with the results from the training set (Figures 4H–J).

To investigate the applicability of the UbRGs-based signature, Kaplan-Meier analysis was carried out across a range of clinical conditions. In the majority of cases (Figures 5A–J), shorter OS was significantly correlated with the high-risk group ($p < 0.05$), including age<60, age≥60, male, Grade 1-2, Grade 3–4, T3-4 stage, N0-1 stage, N2-3 stage, M0 stage and clinical stage III-IV. However, in the other four conditions (Supplementary Figure S3), namely, female ($p = 0.087$), T1-2 stage ($p = 0.083$), M1 stage ($p = 0.16$) and clinical stage I-II ($p = 0.13$), there was no significant difference in survival between the two groups.

To achieve individualized prediction, univariate and multivariate COX regression analyses were performed on the risk score and clinical characteristics. As the risk score ($p < 0.001$) and gender ($p = 0.001$) showed independent values in prognosis (Figures 6A, B), a nomogram was then constructed accordingly to visualize these results (Figure 6C). The probability of survival at 1, 2 and 3 years can be predicted more intuitively based on an individual's risk score and gender profile. When comparing the ROC curve of 3-year OS in LC patients, the AUC of the nomogram was 0.856, higher than that of the risk score (AUC = 0.810) and traditional indicators (T stage, AUC = 0.494; N stage, AUC = 0.641; M stage, AUC = 0.517; clinical stage, AUC = 0.542; Figure 6D). With the calibration curve, good consistency was indicated between the predicted and actual survival rates of the nomogram at 1, 2, and 3 years (Figure 6E). Additionally, the DCA curve demonstrated the nomogram as a better predictive tool than the clinical stage (Figure 6F).

In brief, the signature composed of PPARG, LHX1 and LCK was shown efficacious in the prognosis prediction of OS in LC patients and applicable in most clinical conditions. The nomogram combining risk score and gender provided an even better predictive efficiency than the signature and traditional indicators alone.

3.3 The UbRGs-based signature specified the status of the immune microenvironment in LC

For a better understanding of the UbRGs-based signature in prognosis prediction, biological processes differentially involved in the high- and low-risk groups were searched with GSEA enrichment analysis. By $p < 0.05$, 934 items were enriched with GO and 31 with KEGG (Supplementary Data 3). A prominent panel of immune-related processes was highlighted in the low-risk group. The top 5 enriched GO items included antigen processing and presentation, T-cell receptor complex, antigen binding, immunoglobulin receptor binding and immunoglobulin complex circulating (Figure 7A). Furthermore, 18 among top 20 enrichment in GO, and also

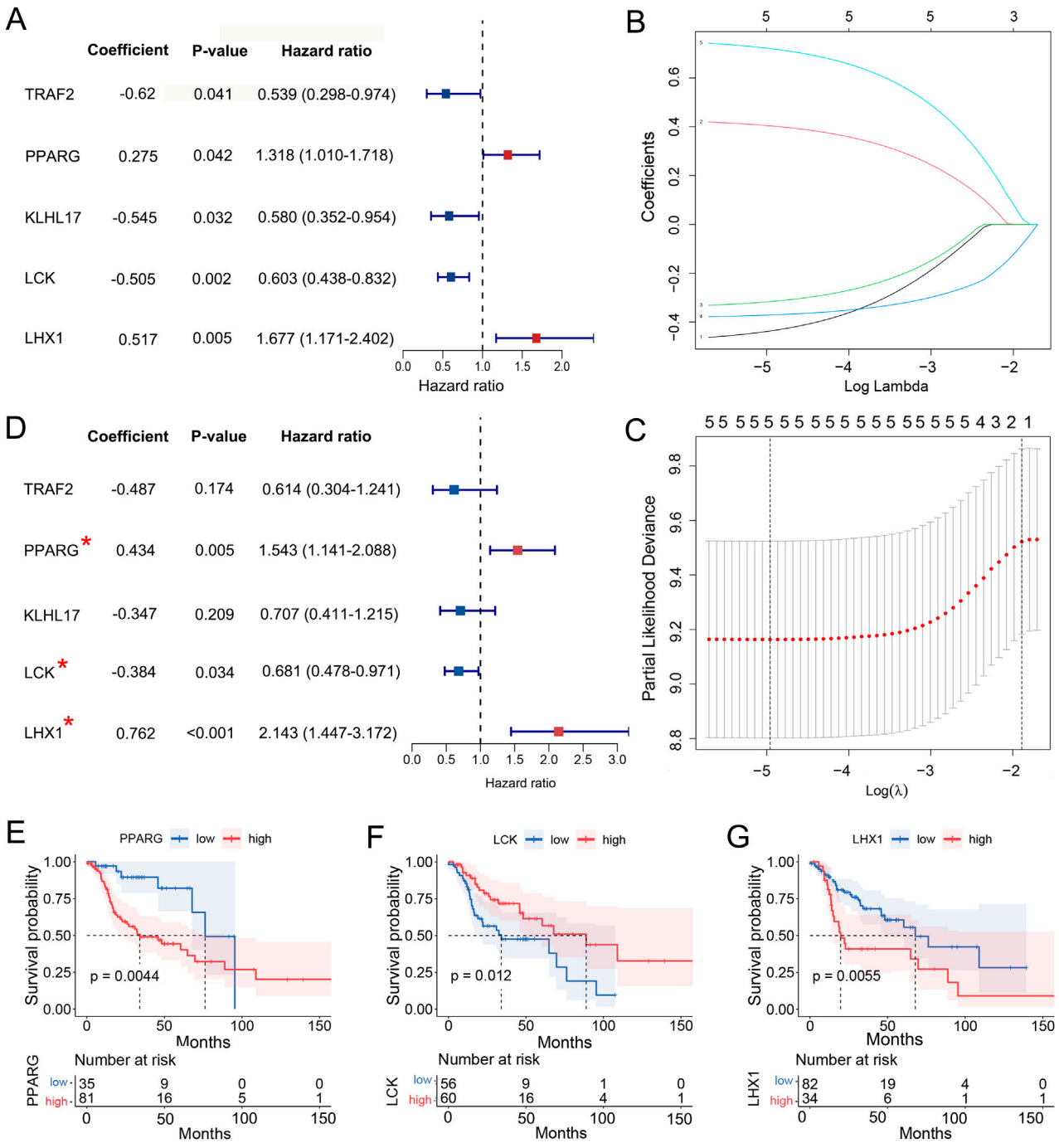

FIGURE 3
Identification of 3 UbRGs to construct the prognostic signature. **(A)** Univariate COX regression analysis of 5 UbRGs significantly associated with OS in LC patients, including TRAF2, PPARG, KLHL17, LCK and LHX1. **(B)** Coefficient profiles of these five UbRGs generated with LASSO regression analysis. **(C)** Determination of minimum lambda for 5 via 10-fold cross-validation in LASSO regression. **(D)** Multivariate Cox regression analysis of 3 UbRGs independently affected OS in LC patients, including PPARG, LCK and LHX1. **(E–F)** Kaplan-Meier analysis of identified UbRGs, **(E)** PPARG, **(F)** LCK and **(G)** LHX1.

26 among top 30, were occupied by the immune-related processes (Labeled in Supplementary Data 3 with yellow). A similar trend of enrichment was also highlighted in KEGG items, with top 5 enriched biological processes were: allograft rejection, type I diabetes mellitus, autoimmune thyroid disease, primary immunodeficiency, and antigen processing and presentation (Figure 7B, Supplementary Data 3). When the immune-related items were counted in all GO and KEGG enrichments, as visualized in Supplementary Figures S4A–D, high percentages were quantified as 46.15% in GO-CC, almost 100% in GO-MF, 74.01% in GO-BP and 69.23% in KEGG. However, in the high-risk group, it was failed to summarize a dominant module with clear and unique functional connotation

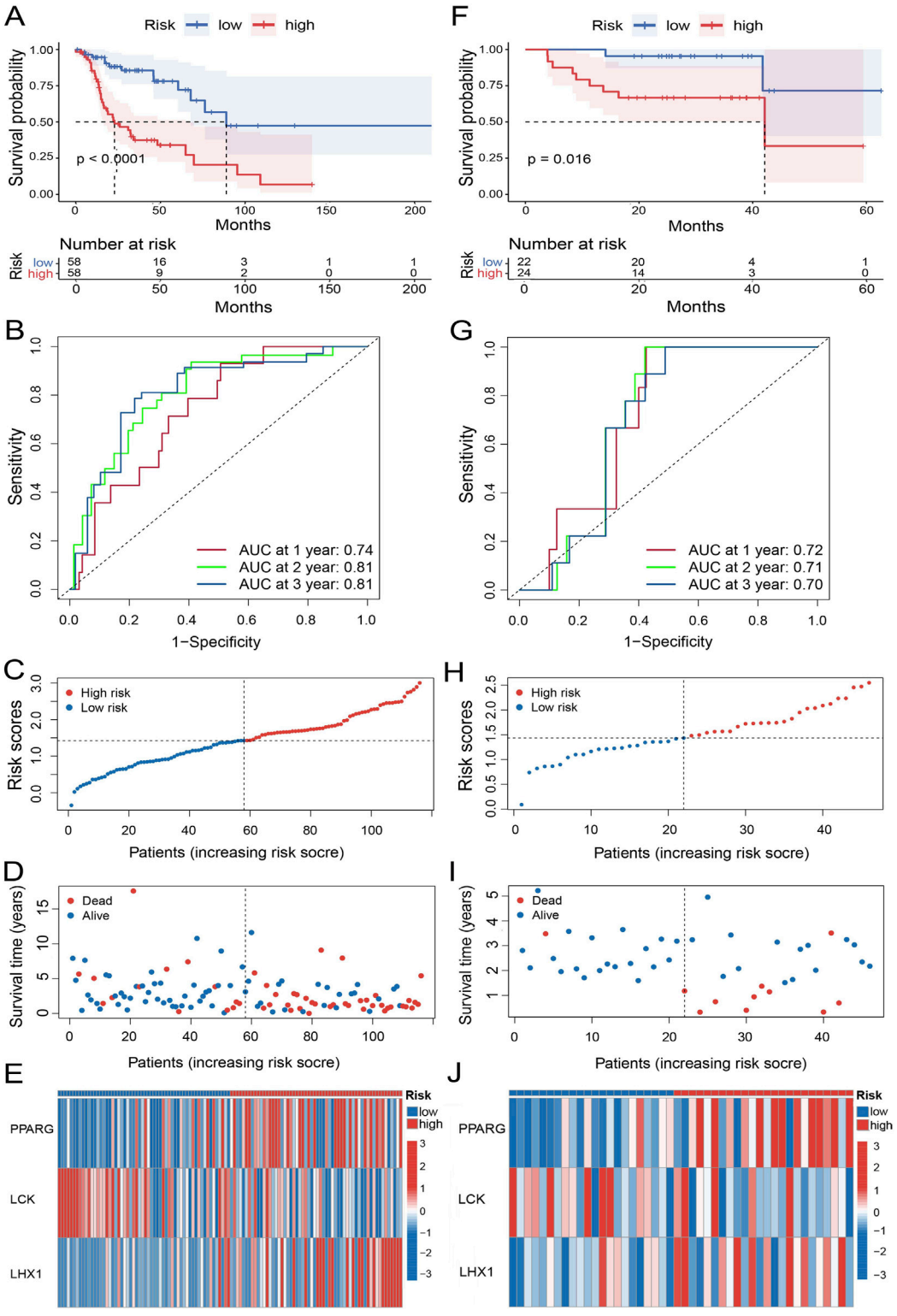

FIGURE 4
Evaluation of the prognostic performance of the UbRGs-based signature. **(A)** Kaplan-Meier analysis of OS in the high- and low-risk groups based on the training set. **(B)** ROC curves showing the predictive efficacy of this signature for 1-, 2-, and 3-year OS of patients in the training set. **(C–E)** Distribution of characteristics of individual patients in the training set, in-cluding **(C)** risk score, **(D)** survival status, and **(E)** expression profiles of 3 signature genes. **(F–J)** Evaluation of the UbRGs-based signature with the validation set for **(F)** Kaplan-Meier analysis of OS, **(G)** ROC curves of predictive efficacy in 1-, 2-, 3-year OS, and **(H)** risk score, **(I)** survival status, and **(J)** expression profiles of 3 signature genes in individual patients.

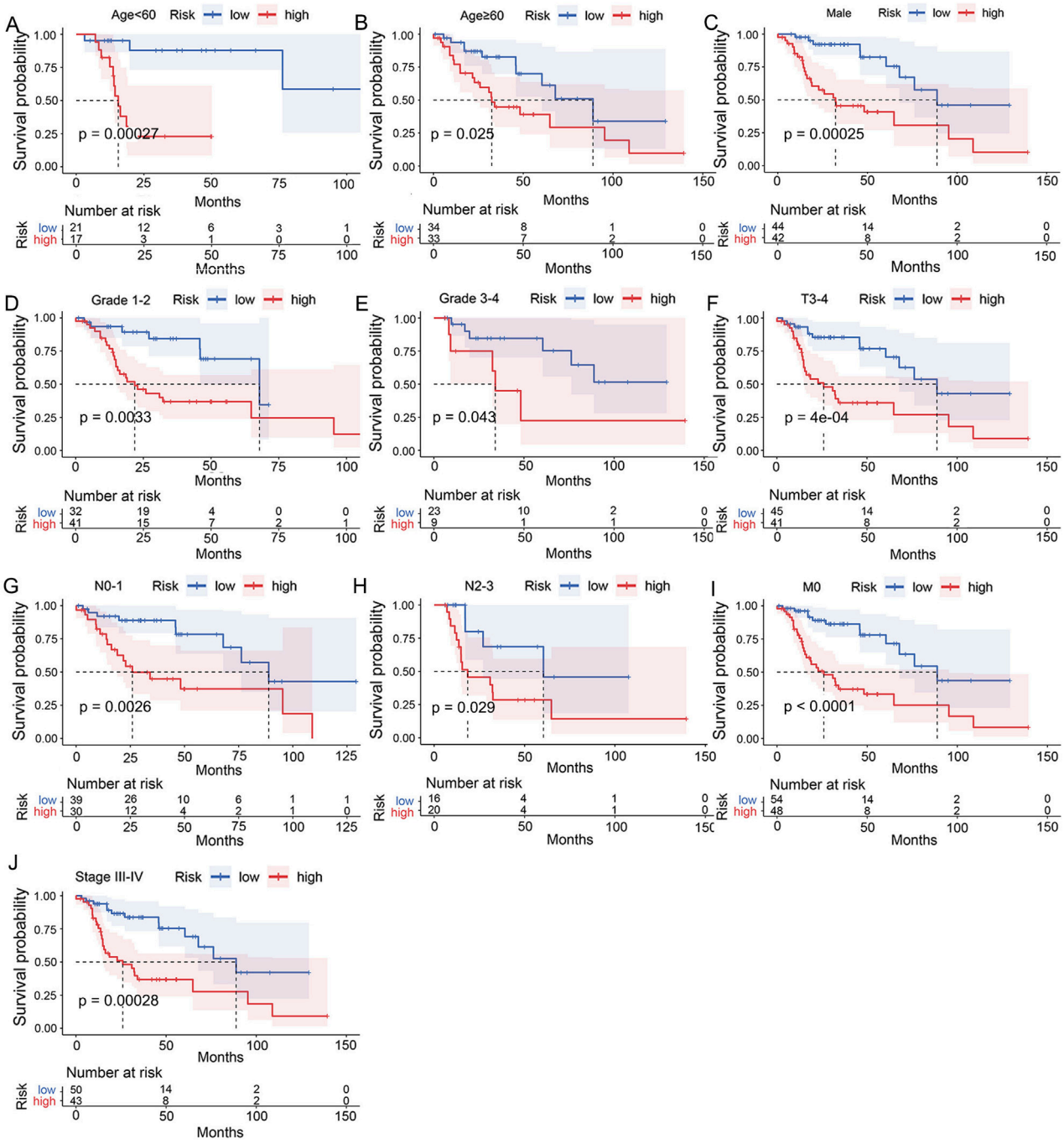

FIGURE 5
Assessment of the clinical applicability of the UbRGs-based signature. Significant dif-ferences in OS were exhibited between the high- and low-risk groups in conditions of **(A)** age<60, **(B)** age≥60, **(C)** male, **(D)** Grade 1-2, **(E)** Grade 3-4, **(F)** T3-4 stage, **(G)** N0-1 stage, **(H)** N2-3 stage, **(I)** M0 stage and **(J)** clinical stage III-IV by stratified Kaplan-Meier analysis.

from the GSEA results, either by GO or KEGG (Supplementary Figures S4E–H), especially, no significant enrichment of immune processes observed (Supplementary Figures S5A, B).

To investigate whether the effectiveness of the UbRGs-based signature was due to the distinct immune status in LC, the immune landscape was further explored in multiple dimensions. At first, functional groups of immune-related pathways were analyzed with the ssGSEA algorithm. In the low-risk group, functional modules of checkpoint, cytolytic activity, pro-inflammatory and T-cell co-stimulation were preferentially activated, whereas no functional modules were shown dominant in the high-risk group (Figure 7C). TME scores were then calculated for individuals with the ESTIMATE algorithm. Of the three TME scores, the immune score is the only one significantly higher in the low-risk group, rather than the stromal score and ESTIMATE score (Figure 7D), which confirmed a higher degree of immune cell

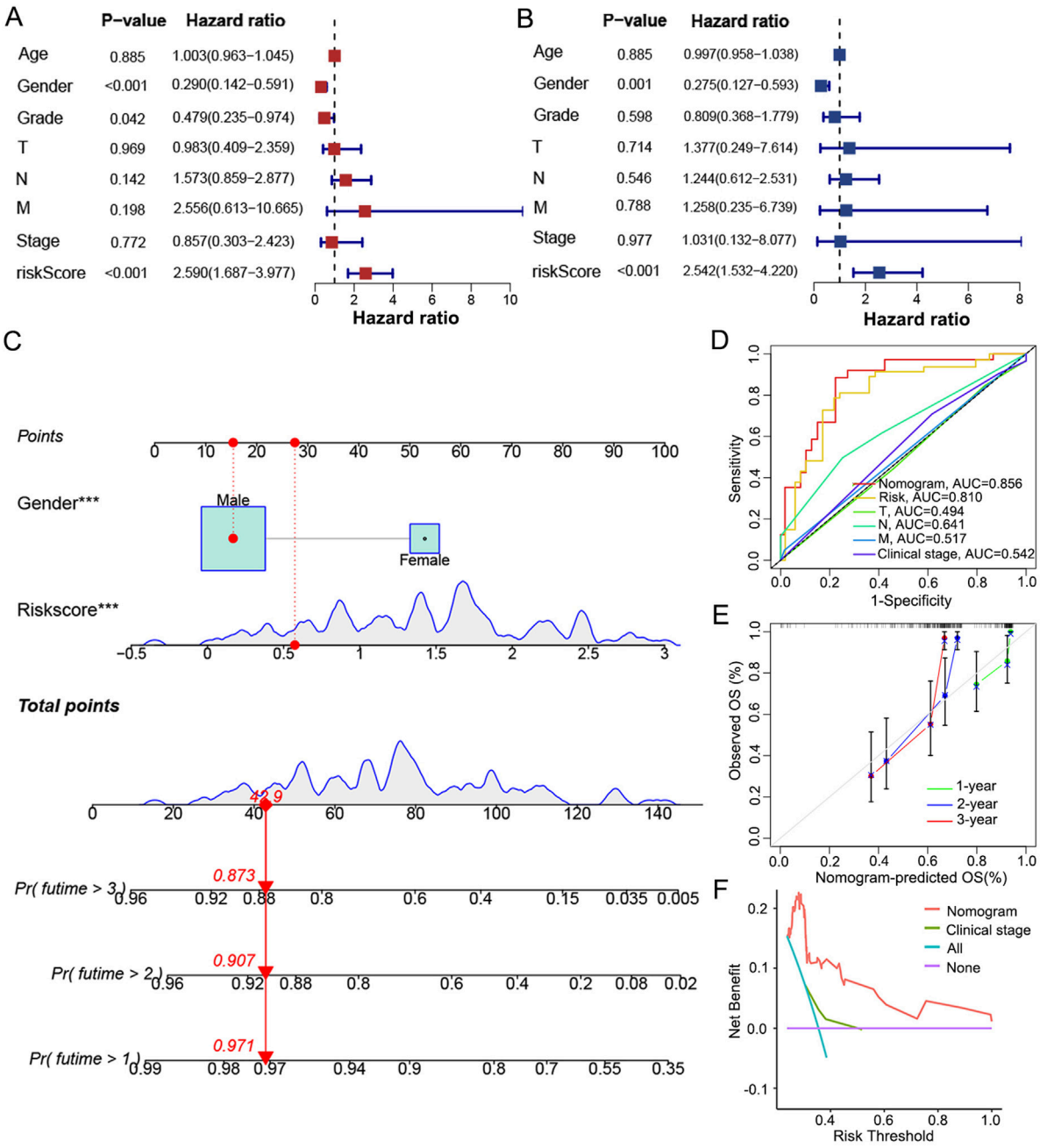

FIGURE 6
Establishment and evaluation of a nomogram integrating signature with gender. **(A)** Univariate and **(B)** multivariate COX regression analysis to highlight independent factors af-fecting OS in LC patients. **(C)** A nomogram constructed to predict the 1-, 2-, and 3-year OS in LC patients by combining the risk score with gender. **(D)** ROC curves based on the nomogram, risk score and traditional indicators to show the predictive efficacy of 3-year OS in LC patients. **(E)** Calibration curves of the consistency between the predicted and actual survival rates at 1, 2 and 3 years. **(F)** DCA showed the net clinical benefit of the nomogram and traditional stage.

infiltration in low-risk LC patients. With the CIBERSORT and ssGSEA algorithms, the infiltration level of each immune cell type was specifically speculated. The cell types with anti-tumor effects showed a higher degree of infiltration in the low-risk group (e.g., CD8 T cells, activated memory CD4 T cells, follicular helper T cells, activated B cells and natural killer T cells), while primitive or resting immune cell types (e.g., native CD4 T cells, resting memory CD4 T cells and M0 macrophages) were dominant in the high-risk group (Figure 7E; Supplementary Figure S5C). The correlation between cell types and risk score was consistent with the trend of immune cell infiltration (Figure 7F). As immune regulation was generally mediated by cytokines, the expression preference of cytokines was also analyzed. Higher levels of immune-promoting cytokines IL23A and IFNG were predicted in the low-risk group, whereas immune-suppressing

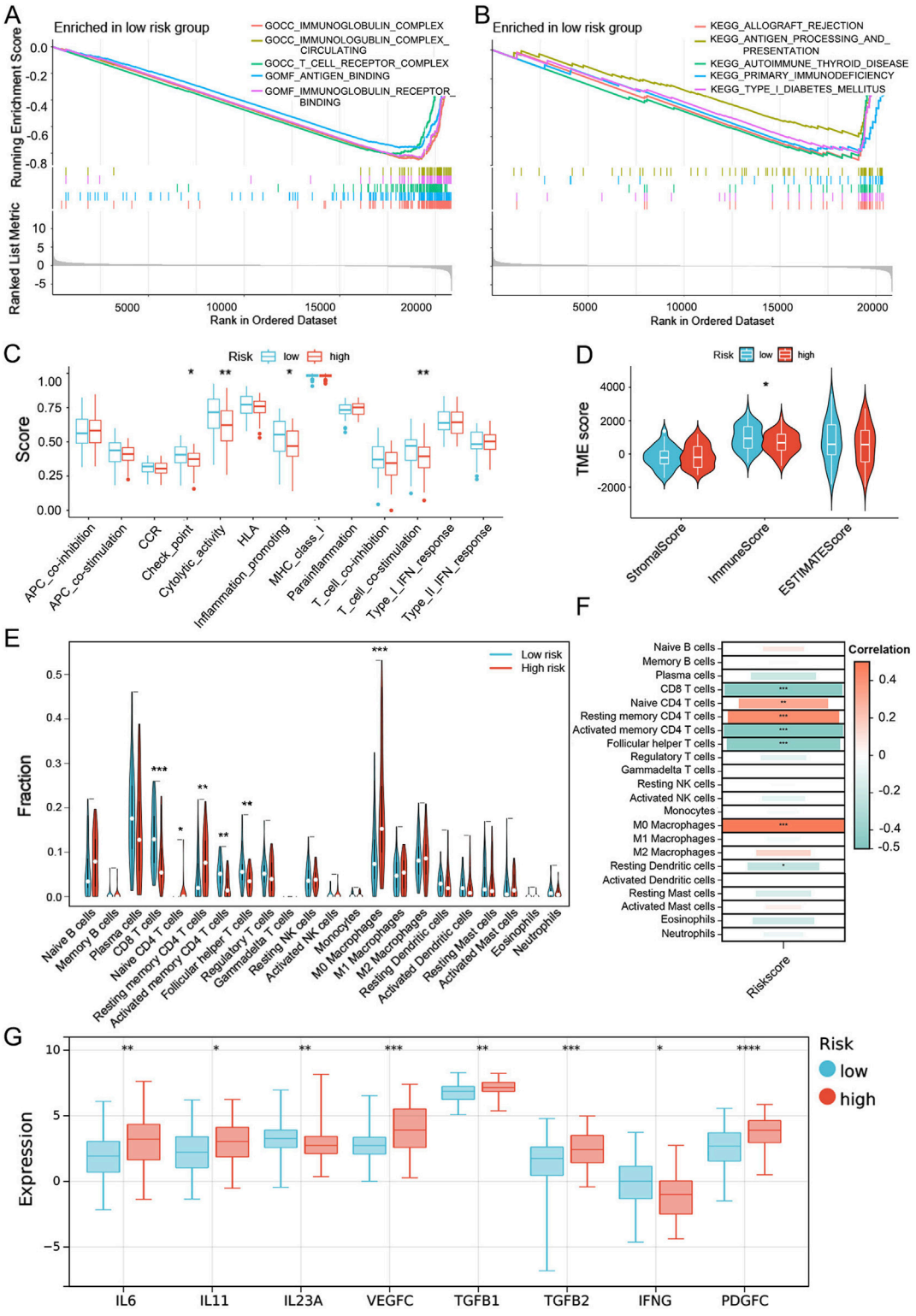

FIGURE 7
Evaluation of the immune microenvironment in the high- and low-risk groups dis-criminated by the UbRGs-based signature. **(A, B)** GSEA enrichment analysis in the low-risk group based on **(A)** GO- and **(B)** KEGG-related gene sets. **(C)** Differential activation of immune-related pathways in the high- and low-risk groups analyzed with the ssGSEA algorithm. **(D)** TME scores calculated by the ESTIMATE algorithm for both groups, in which the immune score was signifi-cantly different. **(E)** Estimation of immune cell infiltration levels via the CIBERSORT algorithm and 6 cell types highlighted with statistical significance. **(F)** Correlation between risk score and immune cell infiltration. **(G)** Immune-related cytokines differentially expressed between the high- and low-risk groups as predicted by the Sangerbox 3.0 online platform. *$p < 0.05$; **$p < 0.01$; ***$p < 0.001$; ****$p < 0.0001$.

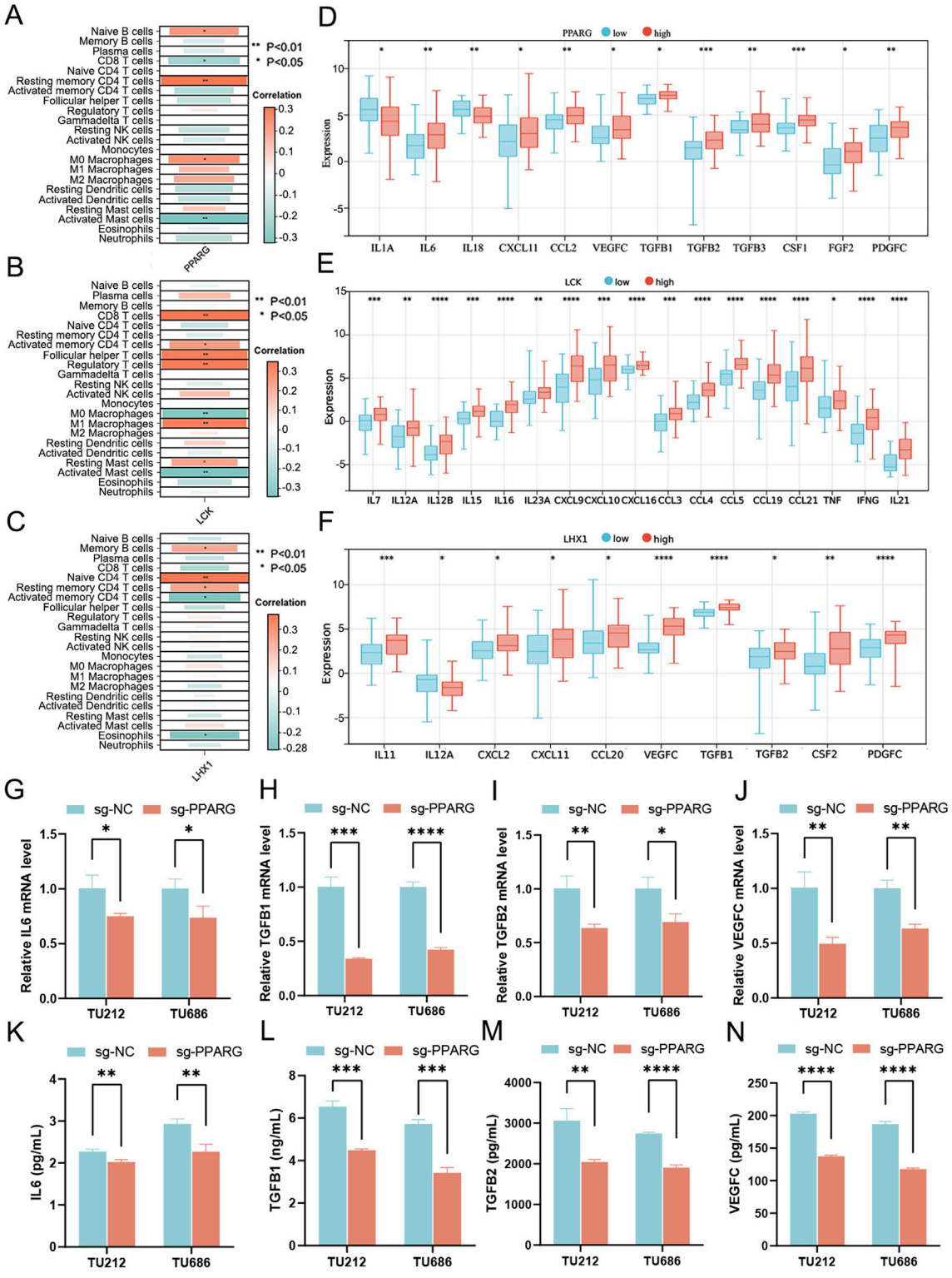

FIGURE 8
Investigation of the role played by signature genes in sculpting the immune landscape. **(A–C)** Correlation between immune cell infiltration and expression levels of 3 signature genes, **(A)** PPARG, **(B)** LCK and **(C)** LHX1. **(D–F)** Relationship between expression levels of immune-related cytokines and 3 signature genes, **(D)** PPARG, **(E)** LCK and **(F)** LHX1. **(G–I)** Cytokine mRNA levels quantified by qRT-PCR in PPARG knockout cells derived from LC cell lines TU212 and TU686, including **(G)** IL6, **(H)** TGFB1, **(I)** TGFB2 and **(J)** VEGFC. **(K–N)** Cytokine secretion levels meas-ured using ELISA in the supernatant of PPARG knockout LC cells, including **(K)** IL6, **(L)** TGFB1, **(M)** TGFB2 and **(N)** VEGFC. *$p < 0.05$; **$p < 0.01$; ***$p < 0.001$; ****$p < 0.0001$.

cytokines (e.g., IL6, IL11, VEGFC, TGFB1, TGFB2 and PDGFC) were preferentially expressed in the high-risk group (Figure 7G).

With a series of analyses, significant differences in the immune landscape were exhibited between the high- and low-risk groups, which was potentially one of the major origins of distinct outcomes in clinics and suggested the signature genes as immune regulators in LC.

3.4 Signature genes PPARG, LHX1 and LCK involved in sculpturing the LC immune microenvironment

To confirm the regulatory role of signature genes in the immunity of LC, the degree of immune cell infiltration and expression levels of cytokines relevant to each gene were predicted one by one. It was clearly visualized that the risk genes PPARG and LHX1 were negatively correlated with anti-tumor effectors (e.g., CD8 T cells and activated memory CD4 T cells), positively correlated with primitive or resting immune cells (e.g., naive B cells, memory B cells, naive CD4 T cells, resting memory CD4 T cells and M0 macrophages), while the protective gene LCK was positively correlated with anti-tumor effectors (CD8 T cells, activated memory CD4 T cells, follicular helper T cells and M1 macrophages; Figures 8A–C). Among the cytokines, immune activators (e.g., IL1A, IL18 and IL12A) were at lower levels and immune suppressors (e.g., IL6, CXCL11, CCL2, VEGFC, TGFB1, TGFB2, TGFB3, CSF1, FGF2, PDGFC, IL11, and CCL20) were at higher levels when PPARG and LHX1 were highly expressed (Figures 8D, F). Besides, another group of immune activators (e.g., IL7, IL12, IL15, IL16, IL23A, CXCL9, CXCL10, CXCL16, CCL3, CCL4, CCL5, CCL19, CCL21, TNF, IFNG, IL21) were overexpressed along with higher expression of LCK (Figure 8E).

Since PPARG showed the highest node index among three signature genes in the PPI network of DUbRGs (Supplementary Figure S1C), further validation was then carried out with PPARG knockout cells generated from TU212 and TU686 cell lines (Supplementary Figures S6A–D). 12 immune-related cytokines were assessed with qRT-PCR, including IL1A, IL6, IL18, CXCL11, CCL2, VEGFC, TGFB1, TGFB2, TGFB3, CSF1, FGF2 and PDGFC, which were predicted in relevance with PPARG expression. At the mRNA level, four immunosuppressive cytokines (IL6, TGFB1, TGFB2 and VEGFC) showed significant downregulation in both PPARG knockout cell lines (Figures 8G–J). Simultaneously, their secretion levels in the supernatant were decreased (Figures 8K–N), as confirmed using ELISA. The other four (e.g., CCL2, CSF1, PDGFC and TGFB3) were downregulated in PPARG knockout TU212 cells (Supplementary Figures S6E–H), while the rest (e.g., FGF2, IL1A, IL18 and CXCL11) mostly showed no significant change (Supplementary Figures S6I–L), as quantified by qRT-PCR.

3.5 The UbRGs-based signature provided insights to the personalized therapies in clinics

Since the distinct immune landscape in LC had been defined with the UbRGs-based signature and applied to the prognosis of OS, its instructiveness for immunotherapy was subsequently investigated. With the TIDE algorithm, a slight trend of higher response to immunotherapy was predicted in the low-risk group (41% vs. 31%), but unfortunately, no significance in statistics was shown (Supplementary Figure S7A). However, differential expression of immune checkpoint genes was exhibited with the ssGSEA algorithm (Figure 7C). The vast majority of immune checkpoints (e.g., PDCD1, CD244, CD27, ICOSLG, TNFRSF4, CD40LG, BTLA, TMIGD2, LAG3 and TNFRSF18) presented significant elevation of expression in the low-risk group, while only a few (e.g., ATIC, OLA1 and CD276) in the high-risk group ($p < 0.05$, Figure 9A). The differential expression data suggested that immune checkpoint inhibitor treatment may be more effective for LC patients with lower risk scores.

Alternatively, sensitivity to chemotherapy and targeted therapeutic agents was also analyzed. The reference tumor cell lines recorded in GDSC were employed as a reference to correlate gene expression signature and IC50 of drugs in a quantitative model. In high- and low-risk groups, the sensitivity to each drug was then evaluated via comparing the gene expression profiles of patients in either group with the reference tumor cell lines. The resultant IC50 values were presented in a 2D format similar to the volcano plot. For each drug, the Y-coordinate presented the $-\mathrm{Log2}(\mathrm{IC50}_{\text{high-risk}}/\mathrm{IC50}_{\text{low-risk}})$ value to show the difference of IC50 values between the two groups, while the -Log10(p-value) was projected as the X-coordinate to indicate the significance of the difference. A total of 48 agents were identified with a significant difference in sensitivity between the high- and low-risk groups ($p < 0.05$, Figure 9B). To find specific therapeutic agents suitable for either group, the IC50 ratio was set to >1.5 or <0.667 (displayed as $|\mathrm{Log2}(\mathrm{IC50}_{\text{high-risk}}/\mathrm{IC50}_{\text{low-risk}})| > 0.585$ in the plot), nine drugs were more sensitive in the high-risk group (gemcitabine, cytarabine, SCH772984, talazoparib, camptothecin, AZD6738, dasatinib, VX-11e and ERK-6604), and three drugs (TAF1-5496, AZD5991 and ABT737) in the low-risk group (Figure 9C; Supplementary Figures S7B–L). However, once the IC50 ratio was moved to 10 or 0.1 ($|\mathrm{Log2}(\mathrm{IC50}_{\text{high-risk}}/\mathrm{IC50}_{\text{low-risk}})| > 3.322$), only gemcitabine, a commonly used chemotherapy agent, remained in the high-risk group preferentially (Figure 9C).

4 Discussion

The incidence rate of LC is increasing yearly and has currently become the second most common head and neck cancer (Bray et al., 2024). Due to its insidious onset, easy recurrence and treatment resistance, the 5-year overall survival rate of LC patients is only 25%–60% (Steuer et al., 2017). To improve survival, it is crucial to develop effective strategies for accurate prediction of the prognosis in LC patients and personalized therapies in clinics. Based on the functional role of UbRGs in the homeostasis of substrate proteins, various cellular processes are affected by their dysregulation. As suggested by accumulating evidence, tumourigenesis will be promoted in turn (Sun et al., 2020). On the other side, UbRGs had been employed as the marker genes for the prognosis of cancers. The predictive efficacy of the related signatures was reported as 69% in ovarian cancer and 65% in melanoma, respectively (Luo et al., 2023; Zhang et al., 2023). Therefore, systematic investigations of

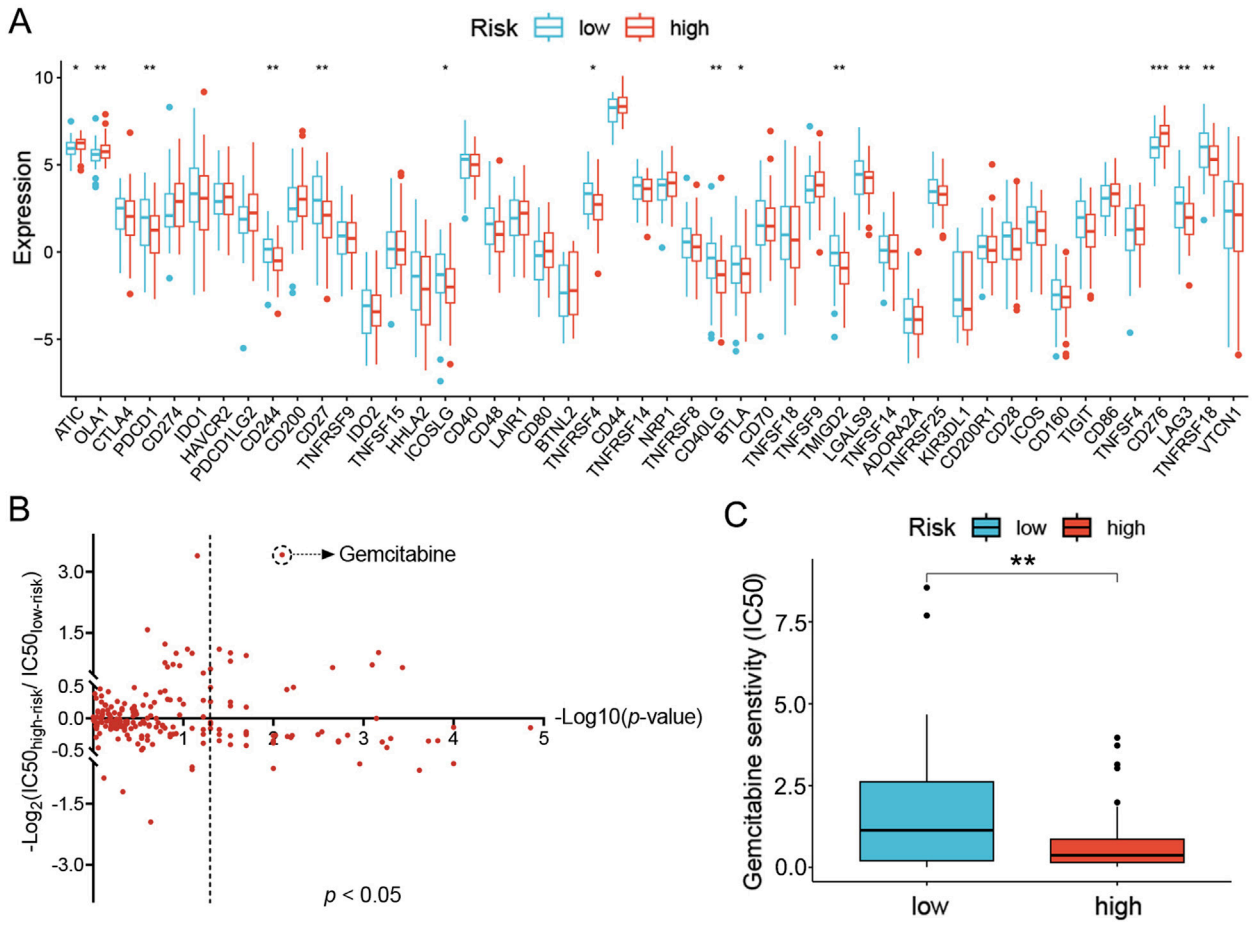

FIGURE 9
Prediction of sensitivity to clinical treatments for the high- and low-risk groups of LC patients. **(A)** Immune checkpoints differentially expressed in the high- and low-risk groups. **(B)** Predicted sensitivity to chemotherapy and targeted agents in the high- and low-risk groups. Data were plotted as -Log10(*p*-value) on the x-axis and -Log2($IC50_{high\text{-}risk}/IC50_{low\text{-}risk}$) on the y-axis. **(C)** Predicted IC50 for gemcitabine in both groups. $^{*}p < 0.05$; $^{**}p < 0.01$; $^{***}p < 0.001$.

UbRGs are valuable to reveal their prognostic potential and oncological characteristics, and will possibly benefit the development of new applications of UbRGs in the prognosis and treatment of LC.

In this study, a total of 111 differentially expressed UbRGs were identified in LC and 3 of them, PPARG, LHX1 and LCK, were highlighted as the independent prognostic markers. The signature generated based on these three genes effectively discriminated LC patients with different OS and showed excellent applicability in most clinical conditions. The performance of this signature for 3-year OS in LC patients reached 81% and 70% in the training and validation sets, respectively, which was more powerful than earlier reported UbRGs-based signatures in other cancers (Luo et al., 2023; Zhang et al., 2023). The nomogram incorporating risk score and gender showed considerable advantages over other factors, such as the TNM stage and clinical stage. The consequent model had stronger predictive power and higher clinical benefit for 3-year OS in LC patients. In one word, this UbRGs-based signature will not only satisfy the risk stratification of LC patients but also enable the individualized assessment of the prognosis.

The functional linkages behind the UbRGs-based signature were then excavated with GSEA enrichment and subsequent panels of prediction, through which a significant association with immune in LC was demonstrated. T- and B-cell-mediated immune processes were enriched in the low-risk group, whereas there was no significant enrichment of immune processes in the high-risk group. As reported, UbRGs can induce the formation of immunosuppressive TME by affecting the stability of proteins important in the anti-tumor immune process, thereby promoting the immune escape of tumors (Çetin et al., 2021). For Instance, the E2 enzyme UBE2T inhibited $CD8^{+}$ T-cell infiltration and expression of immune-promoting factors (IFN-γ, TNF-α and IL-2) in lung adenocarcinoma by activating the glycolytic pathway upon binding to FOXA1 (Pu et al., 2024). In colon cancer, a deubiquitinating enzyme USP4 suppressed anti-tumor immune responses by deubiquitinating TRAF6 and IRF3, hindering the nuclear localization of the latter protein and thus inhibiting cellular interferon responses and antigen presentation (Zhou et al., 2024). With further exploration of the immune microenvironment, it was observed that the low-risk group had a higher degree of infiltration of anti-tumor immune cells, more activated immune modules,

stronger expression of immune-promoting cytokines and lower expression of immune-suppressing cytokines. Therefore, the active immune landscape in low-risk rather than high-risk populations may be one of the major forces shaping the different clinical outcomes.

Besides the correlation between cancer immunity and the entire signature in our study, reviewing the correlation with selected individual UbRGs also provides valuable insights into understanding the effectiveness of this signature. In previous reports, PPARG was mainly a regulator of immune cell differentiation and cytokine secretion (Riaz et al., 2023; Zhao et al., 2024). The essentiality of PPARG was indicated in the differentiation of fetal monocytes into alveolar macrophages (Schneider et al., 2014). In mouse models of colitis, it was observed that PPARG agonists can shift the immune response from a Th1-type to a Th2-type, resulting in a decrease in the expression of Th1-associated transcription factors, cytokines, and chemokines, and simultaneously an increase in the expression of Th2-associated factors (Celinski et al., 2013; Saubermann et al., 2002). Deficiency of this gene in a similar mouse model was associated with a decreased number of $CD4^{+}Foxp3^{+}$ regulatory T cells (Guri et al., 2010). Additionally, PPARG was also observed to inhibit the secretion of pro-inflammatory cytokines (such as TNF-α and IL-1β) and promote anti-inflammatory cytokines (such as TGF-β and IL-10) (Riaz et al., 2023). In a cancerous context, Liu *et al* reported the accelerative role played by activated PPARG in KRAS-mutant pancreatic carcinogenesis. The tumor immune microenvironment was remodeled by PPARG via recruiting and promoting the M2 polarization of macrophages through the CCL2/CCR2 signaling axis (Liu et al., 2022). But the actual functional roles of PPARG playing in laryngeal cancer are still lack of investigation. Similar to our work, the other risk gene LHX1 was also adopted in a recent published prognostic signature of breast cancer. With consistence, correlation was observed between LHX1 and lymph node metastasis, infiltration of multiple immune cells (including $CD8^{+}$ T cells, B cells, dendritic cells, antigen-presenting cells, neutrophils and regulatory T cells) and enrichment of immune functions in patients (including B-cell receptor signaling pathway, PD-L1 expression, and the PD-1 checkpoint pathway) (Pan et al., 2024). However, the potential role of LHX1 was only suggested with the trend of dysregulation in cancer, but not yet by the functional assays in normal and oncogenic circumstance. Additionally, the protective gene LCK, one of the non-receptor tyrosine kinases in the Src family, was reported as a crucial player in T cell-mediated immune responses in previous reports (Wu et al., 2021; Lanz et al., 2024). It precisely regulated T cell activation and the subsequent cascade of immune reactions by initiating T cell receptor (TCR) signal transduction. Once TCR binding to the antigenic peptide-MHC complex, LCK was activated with the synergistic participation of co-receptors CD4 or CD8. The activated LCK prompted the subsequent phosphorylation of CD3 and ζ-chain immunoreceptor tyrosine-based activation motifs, recruiting and activating ZAP-70, and led to the formation of LAT signaling bodies through further phosphorylation of LAT and SLP-76. A panel of downstream signaling pathways were triggered consequently, including ERK and PI3K/Akt, and thus, the T cell-mediated immune responses were launched ultimately. Meanwhile, LCK can also indirectly connect ZAP-70 and LAT, and promote their phosphorylation, thus TCR signal transduction is enhanced (De Sanctis et al., 2024). Another report about Jurkat E6-1 leukemia cells by Wan *et al* demonstrated the expression of LCK was under the regulation of SMAD4, and affected the proliferation of chimeric antigen receptor-T cells through perturbation of PI3K/Akt signal (Wan et al., 2025). In multiple tumor cell lines, as reported by Ahn *et al*, the tumor surveillance was mediated by LCK-ERK signal through the activation of T cells (Ahn et al., 2025). These accumulating clues suggested the rationality of our choice of signature genes, and further, the derived risk signature for prognosis.

In our wet-lab works, the expression was validated for 12 cytokines predicted according to the according to the association with signature genes, either promotors and suppressors of cancer immunity. Among them, four immunosuppressors supported by PPARG were confirmed through CRISPR-based gene knockout, including IL6, TGFB1, TGFB2 and VEGFC, which was consistent with an earlier report (Riaz et al., 2023). Since then, the cytokine expression and functions in LCs are worthy of further investigation to provide more insights into our signature and help the stratification of patients.

Another potential value of this signature is to facilitate the optimization of clinical treatments for LC patients. Based on the properties of the immune microenvironment, the low-risk group tends to be “hot” tumors, while the high-risk group tends to be “cold” (Duan et al., 2020). Due to the presence of higher numbers of effector T cells in “hot” tumors, combined with the preferential expression of 10 checkpoint genes, treatment with immune checkpoint inhibitors will be more effective in the low-risk group (Cejuela et al., 2022). Of all the targets that predominate in the low-risk group, immune checkpoint inhibitors against PDCD1, CD27, CD40LG, BTLA and LAG3 have been approved for clinical use or trials in patients with other tumors (Sharma et al., 2024; Lutfi et al., 2021; Liu et al., 2021; Dalle et al., 2024; Ibrahim et al., 2023), and thus, worthy to be tried in LC patients. Additionally, the prediction of drug sensitivity showed little preference between the high- and low-risk groups scored with the UbRGs-based signature, except for gemcitabine, a traditional chemotherapy agent, which showed hypersensitivity in the high-risk group. This drug works through inhibition of DNA synthesis as pyrimidine antimetabolites and is commonly applied in pancreatic cancer but not LC (Han et al., 2022). However, based on our signature, at least a certain portion of LC patients in the high-risk group may benefit from the administration of gemcitabine, which will be a potential alternative choice for LC patients, like cisplatin and paclitaxel (Fang et al., 2023). Regardless, the UbRGs-based signature provides new insights into the choice of therapeutic agents and strategies for LC.

Despite the encouraging performance and advantages of the UbRGs-based prognostic signature, more investigations shall be carried out in the future. Firstly, due to the limited number of LC patients contained in the TCGA and GEO databases, larger clinical cohorts are necessary for comprehensive validation of this signature. Secondly, the oncological and immunological roles of PPARG, LHX1 and LCK should be explored in depth, particularly in LC, to specify their functions and prognostic values. Thirdly, the prediction of drug sensitivity based on the signature still requires extensive assessments in different models and ultimately in patients,

since the prediction was fundamentally based on the collection of gene expression profiles in cancer cell lines.

5 Conclusion

In conclusion, we systematically analyzed the molecular characteristics and prognostic potential of UbRGs in LC for the first time, and established a prognostic signature based on UbRGs. This signature demonstrated good clinical value in predicting the patients' prognosis, speculating the immune microenvironment and suggesting anticancer therapies, thus facilitating the risk stratification of clinical patients and providing new ideas for formulating individualized treatment.

Data availability statement

The datasets presented in this study can be found in online repositories. The names of the repository/repositories and accession number(s) can be found in the article/Supplementary Material.

Ethics statement

Ethical approval was not required for the studies on humans in accordance with the local legislation and institutional requirements because only commercially available established cell lines were used.

Author contributions

LL: Conceptualization, Formal Analysis, Investigation, Methodology, Software, Validation, Writing–original draft, Writing–review and editing. BW: Data curation, Validation, Visualization, Writing–original draft, Writing–review and editing. XM: Conceptualization, Supervision, Writing–review and editing. LT: Resources, Supervision, Writing–review and editing, Conceptualization, Writing–original draft, Funding acquisition. XW: Funding acquisition, Project administration, Resources, Supervision, Writing–review and editing.

Funding

The author(s) declare that financial support was received for the research, authorship, and/or publication of this article. This work was funded by the National Natural Science Foundation of China (No. 82260475); Natural Science Foundation of Gansu Province (No. 23JRRA1321); Research fund project of Gansu Provincial Hospital (No. 22GSSYD-12); National research project cultivation plan key project of Gansu Provincial Hospital (No. 19SYPYA-13); Gansu Province health industry science and technology innovation major research project (No. GSWSZD2024-02); Startup Foundation for New Faculty at the State Key Laboratory of Reproductive Medicine and Offspring Health, Nanjing Medical University (Grant No. NMUR20240018), and the Hundred Talents Program of the Chinese Academy of Sciences.

Acknowledgments

Thanks to all the participants who made this work possible and all the R software package developers.

Conflict of interest

The authors declare that the research was conducted in the absence of any commercial or financial relationships that could be construed as a potential conflict of interest.

Generative AI statement

The author(s) declare that no Generative AI was used in the creation of this manuscript.

Publisher's note

Supplementary material

The Supplementary Material for this article can be found online at: https://www.frontiersin.org/articles/10.3389/fphar.2025.1513948/full#supplementary-material

References

Ahn, J., Jang, S. H., Jang, S., Yoon, J. H., Lee, M. G., and Chi, S. G. (2025). XAF1 is secreted from stressed tumor cells to activate T cell-mediated tumor surveillance via Lck-ERK signaling. *Neoplasia* 59, 101094. doi:10.1016/j.neo.2024.101094

Balachandran, V. P., Gonen, M., Smith, J. J., and DeMatteo, R. P. (2015). Nomograms in oncology: more than meets the eye. *Lancet Oncol.* 16 (4), e173–e180. doi:10.1016/S1470-2045(14)71116-7

Bray, F., Laversanne, M., Sung, H., Ferlay, J., Siegel, R. L., Soerjomataram, I., et al. (2024). Global cancer statistics 2022: GLOBOCAN estimates of incidence and mortality worldwide for 36 cancers in 185 countries. *CA Cancer J. Clin.* 74 (3), 229–263. doi:10.3322/caac.21834

Cejuela, M., Vethencourt, A., and Pernas, S. (2022). Immune checkpoint inhibitors and novel immunotherapy approaches for breast cancer. *Curr. Oncol. Rep.* 24 (12), 1801–1819. doi:10.1007/s11912-022-01339-4

Celinski, K., Dworzanski, T., Fornal, R., Korolczuk, A., Madro, A., Brzozowski, T., et al. (2013). Comparison of anti-inflammatory properties of peroxisome proliferator-activated receptor gamma agonists rosiglitazone and troglitazone in prophylactic treatment of experimental colitis. *J. Physiol. Pharmacol.* 64 (5), 587–595.

Çetin, G., Klafack, S., Studencka-Turski, M., Krüger, E., and Ebstein, F. (2021). The ubiquitin-proteasome system in immune cells. *Biomolecules* 11 (1), 60. doi:10.3390/biom11010060

Cui, J., Wang, L., Tan, G., Chen, W., He, G., Huang, H., et al. (2020a). Development and validation of nomograms to accurately predict risk of recurrence for patients with laryngeal squamous cell carcinoma: cohort study. *Int. J. Surg.* 76, 163–170. doi:10.1016/j.ijsu.2020.03.010

Cui, J., Wang, L., Zhong, W., Chen, Z., Tan, X., Yang, H., et al. (2020b). Development and validation of nomogram to predict risk of survival in patients with laryngeal squamous cell carcinoma. *Biosci. Rep.* 40 (8), BSR20200228. doi:10.1042/BSR20200228

Dai, W. L., Yuan, S. X., and Cao, J. P. (2020). The deubiquitinase USP34 stabilizes SOX2 and induces cell survival and drug resistance in lar-yngeal squamous cell carcinoma. *Kaohsiung J. Med. Sci.* 36 (12), 983–989. doi:10.1002/kjm2.12285

Dalle, S., Verronese, E., N'Kodia, A., Bardin, C., Rodriguez, C., Andrieu, T., et al. (2024). Modulation of blood T cell polyfunctionality and HVEM/BTLA expression are critical determinants of clinical outcome in anti-PD1-treated metastatic melanoma patients. *Oncoimmunology* 13 (1), 2372118. doi:10.1080/2162402X.2024.2372118

De Sanctis, J. B., Garmendia, J. V., Duchová, H., Valentini, V., Puskasu, A., Kubíčková, A., et al. (2024). Lck function and modulation: immune cytotoxic response and tumor treatment more than a simple event. *Cancers* 16 (15), 2630. doi:10.3390/cancers16152630

Díaz, P., Sandoval-Bórquez, A., Bravo-Sagua, R., Quest, A. F. G., and Lavandero, S. (2021). Perspectives on organelle interaction, protein dysregulation, and cancer disease. *Front. Cell Dev. Biol.* 9, 613336. doi:10.3389/fcell.2021.613336

Duan, Q., Zhang, H., Zheng, J., and Zhang, L. (2020). Turning cold into hot: firing up the tumor microenvironment. *Trends Cancer* 6 (7), 605–618. doi:10.1016/j.trecan.2020.02.022

Egelmeer, A. G., Velazquez, E. R., De Jong, J. M., Oberije, C., Geussens, Y., Nuyts, S., et al. (2011). Development and validation of a nomogram for prediction of survival and local control in laryngeal carcinoma patients treated with radiotherapy alone: a cohort study based on 994 patients. *Radiother. Oncol.* 100 (1), 108–115. doi:10.1016/j.radonc.2011.06.023

Fang, Q., Xu, P., Cao, F., Wu, D., and Liu, X. (2023). PD-1 Inhibitors combined with paclitaxel (Albumin-bound) and cisplatin for larynx preservation in locally advanced laryngeal and hypopharyngeal squamous cell carcinoma: a retrospective study. *Cancer Immunol. Immunother.* 72 (12), 4161–4168. doi:10.1007/s00262-023-03550-z

Guri, A. J., Mohapatra, S. K., Horne, W. T. 2nd, Hontecillas, R., and Bassaganya-Riera, J. (2010). The role of T cell PPAR gamma in mice with experimental inflammatory bowel disease. *BMC Gastroenterol.* 10, 60. doi:10.1186/1471-230X-10-60

Han, H., Li, S., Zhong, Y., Huang, Y., Wang, K., Jin, Q., et al. (2022). Emerging pro-drug and nano-drug strategies for gemcita-bine-based cancer therapy. *Asian J. Pharm. Sci.* 17 (1), 35–52. doi:10.1016/j.ajps.2021.06.001

Ibrahim, R., Saleh, K., Chahine, C., Khoury, R., Khalife, N., and Cesne, A. L. (2023). LAG-3 inhibitors: novel immune checkpoint inhibitors changing the landscape of immunotherapy. *Biomedicines* 11 (7), 1878. doi:10.3390/biomedicines11071878

Lanz, A. L., Erdem, S., Ozcan, A., Ceylaner, G., Cansever, M., Ceylaner, S., et al. (2024). A novel biallelic LCK variant resulting in profound T-cell immune deficiency and review of the literature. *J. Clin. Immunol.* 44 (1), 1. doi:10.1007/s10875-023-01602-8

Liang, M., Sun, Z., Chen, X., Wang, L., Wang, H., Qin, L., et al. (2023). E3 ligase TRIM28 promotes anti-PD-1 resistance in non-small cell lung cancer by enhancing the recruitment of myeloid-derived suppressor cells. *J. Exp. Clin. Cancer Res.* 42 (1), 275. doi:10.1186/s13046-023-02862-3

Liu, Y., Deguchi, Y., Wei, D., Liu, F., Moussalli, M. J., Deguchi, E., et al. (2022). Rapid acceleration of KRAS-mutant pancreatic carcinogenesis via remodeling of tumor immune microenvironment by PPARδ. *Nat. Commun.* 13 (1), 2665. doi:10.1038/s41467-022-30392-7

Liu, Z., Liu, L., Guo, C., Yu, S., Meng, L., Zhou, X., et al. (2021). Tumor suppressor gene mutations correlate with prognosis and im-munotherapy benefit in hepatocellular carcinoma. *Int. Immunopharmacol.* 101 (Pt B), 108340. doi:10.1016/j.intimp.2021.108340

Luo, X., Wang, Y., Zhang, H., Chen, G., Sheng, J., Tian, X., et al. (2023). Identification of a prognostic signature for ovarian cancer based on ubiquitin-related genes suggesting a potential role for FBXO9. *Biomolecules* 13 (12), 1724. doi:10.3390/biom13121724

Lutfi, F., Wu, L., Sunshine, S., and Cao, X. (2021). Targeting the CD27-CD70 pathway to improve outcomes in both checkpoint immuno-therapy and allogeneic hematopoietic cell transplantation. *Front. Immunol.* 12, 715909. doi:10.3389/fimmu.2021.715909

Pan, Y., Zou, Q., Yin, W., Huang, Z., Zhao, Y., Mo, Z., et al. (2024). Development of lymph node metastasis-related prognostic markers in breast cancer. *J. Proteomics* 291, 105045. doi:10.1016/j.jprot.2023.105045

Pu, J., Zhang, D., Wang, B., Zhu, P., Yang, W., Wang, K., et al. (2024). FOXA1/UBE2T inhibits CD8+T cell activity by inducing mediates glycolysis in lung adenocarcinoma. *Front. Biosci. Landmark Ed.* 29 (4), 134. doi:10.31083/j.fbl2904134

Riaz, F., Wei, P., and Pan, F. (2023). PPARs at the crossroads of T cell differentiation and type 1 diabetes. *Front. Immunol.* 14, 1292238. doi:10.3389/fimmu.2023.1292238

Saubermann, L. J., Nakajima, A., Wada, K., Zhao, S., Terauchi, Y., Kadowaki, T., et al. (2002). Peroxisome proliferator-activated receptor gamma agonist ligands stimulate a Th2 cytokine response and prevent acute colitis. *Inflamm. Bowel Dis.* 8 (5), 330–339. doi:10.1097/00054725-200209000-00004

Schneider, C., Nobs, S. P., Kurrer, M., Rehrauer, H., Thiele, C., and Kopf, M. (2014). Induction of the nuclear receptor PPAR-γ by the cytokine GM-CSF is critical for the differentiation of fetal monocytes into alveolar macrophages. *Nat. Immunol.* 15 (11), 1026–1037. doi:10.1038/ni.3005

Sharma, N., Mazumder, R., Rai, P., and Debnath, A. (2024). Role of PD-1 in skin cancer: molecular mechanism, clinical applications, and resistance. *Chem. Biol. Drug Des.* 104 (3), e14613. doi:10.1111/cbdd.14613

Shi, D., Wu, X., Jian, Y., Wang, J., Huang, C., Mo, S., et al. (2022). USP14 promotes tryptophan metabolism and immune suppression by stabilizing Ido1 in colorectal cancer. *Nat. Commun.* 13 (1), 5644. doi:10.1038/s41467-022-33285-x

Steuer, C. E., El-Deiry, M., Parks, J. R., Higgins, K. A., and Saba, N. F. (2017). An update on larynx cancer. *CA Cancer J. Clin.* 67 (1), 31–50. doi:10.3322/caac.21386

Sun, T., Liu, Z., and Yang, Q. (2020). The role of ubiquitination and deubiquitination in cancer metabolism. *Mol. Cancer* 19 (1), 146. doi:10.1186/s12943-020-01262-x

Wan, R., Fu, B., Fu, X., Liu, Z., Simayi, N., Fu, Y., et al. (2025). SMAD4 regulates the expression of LCK affecting chimeric antigen receptor-T cells proliferation through PI3K/akt signaling pathway. *J. Cell Physiol.* 240 (1), e31520. doi:10.1002/jcp.31520

Wang, K., Tang, J., Liu, X., Wang, Y., Chen, W., and Zheng, R. (2020). UBR5 regulates proliferation and radiosensitivity in human laryngeal carcinoma via the p38/MAPK signaling pathway. *Oncol. Rep.* 44 (2), 685–697. doi:10.3892/or.2020.7620

Wu, J., Li, G., Li, L., Li, D., Dong, Z., and Jiang, P. (2021). Asparagine enhances LCK signalling to potentiate CD8+ T-cell activation and an-ti-tumour responses. *Nat. Cell Biol.* 23 (1), 75–86. doi:10.1038/s41556-020-00615-4

Zhang, L., Shi, Z., Zhang, F., Chen, B., Qiu, W., Cai, L., et al. (2023). Ubiquitination-related biomarkers in metastatic melanoma patients and their roles in tumor microenvironment. *Front. Oncol.* 13, 1170190. doi:10.3389/fonc.2023.1170190

Zhao, Y., Tan, H., Zhang, X., and Zhu, J. (2024). Roles of peroxisome proliferator-activated receptors in hepatocellular carcinoma. *J. Cell Mol. Med.* 28 (5), e18042. doi:10.1111/jcmm.18042

Zhou, Y., Li, H., Zhang, Y., Zhao, E., Huang, C., Pan, X., et al. (2024). Deubiquitinase USP4 suppresses an-titumor immunity by inhibiting IRF3 activation and tumor cell-intrinsic interferon response in colorectal cancer. *Cancer Lett.* 589, 216836. doi:10.1016/j.canlet.2024.216836

frontiers | Frontiers in Oncology

TYPE Case Report
PUBLISHED 31 March 2025
DOI 10.3389/fonc.2025.1549790

OPEN ACCESS

EDITED BY
Luis Abel Quiñones,
University of Chile, Chile

REVIEWED BY
Stephen B. Keysar,
University of Colorado Anschutz Medical Campus, United States
Luccas Lavareze,
State University of Campinas, Brazil

*CORRESPONDENCE
Shui-Hong Zhou
1190051@zju.edu.cn

RECEIVED 22 December 2024
ACCEPTED 13 March 2025
PUBLISHED 31 March 2025

CITATION
Fan J, Chen L, Li C-H, Xiao Z-Y and Zhou S-H (2025) Laryngeal sarcomatoid carcinoma: a case report and literature review on potential molecular targets for therapeutic opportunities.
Front. Oncol. 15:1549790.
doi: 10.3389/fonc.2025.1549790

Laryngeal sarcomatoid carcinoma: a case report and literature review on potential molecular targets for therapeutic opportunities

Jie Fan[1], Lun Chen[1], Chen-Hui Li[1], Zhong-Yong Xiao[1] and Shui-Hong Zhou[2*]

[1]Department of Otolaryngology, Head and Neck Surgery, Ningbo No.9 Hospital, Ningbo, China, [2]Department of Otolaryngology, Head and Neck Surgery, The First Affiliated Hospital of Medical College of Zhejiang University, Hangzhou, China

Laryngeal sarcomatoid carcinoma (LSC) is a rare variant of laryngeal malignancies characterized by an aggressive nature and poor prognosis, predominantly affecting older males. Although early diagnosis may facilitate organ preservation through adjuvant chemotherapy and radiation therapy, advanced stages of the disease, as classified by the TNM system, necessitate a deeper understanding of molecular interactions. This understanding could potentially yield improved molecularly targeted therapeutic opportunities and early diagnosis that likely support the treatment benefits in the LSC. Therefore, this study aims to identify possible molecular targets in LSC to better inform therapeutic options and prognostic markers for obtaining treatment benefits, alongside presenting a case study of a patient with LSC who was admitted to our department.

KEYWORDS

laryngeal sarcomatoid carcinoma, case report, molecular targets, therapeutical target, molecular markers

Introduction

Laryngeal sarcomatoid carcinoma (LSC) is a rare type of laryngeal malignancy that tends to have a poor prognosis, even when detected at early stages. It is considered a more aggressive variant of squamous cell carcinoma of the head and neck. This condition typically affects older males. The World Health Organization's 2017 Classification of Head and Neck Tumors states that LSC is a monoclonal neoplasm that originates from a non-committed stem cell, resulting in the development of both epithelial and mesenchymal components (1). Research indicates that the LSC defines the occurrence of epithelial-mesenchymal transition (2) and is recognized as a biphasic tumor consisting of two components: a squamous cell carcinoma and a malignant spindle cell component that

exhibits a mesenchymal phenotype (2). This malignancy originates from an epithelial cell clone that has undergone mutations. LSC is a rare form of malignant variant that comprises 2 to 3% of all laryngeal cancers (3). As mentioned, this type onsets more specifically in elderly patients with a significant smoking history. Treatment options such as adjuvant chemotherapy and adjuvant radiation therapy can preserve the organ to treat the selected laryngeal cancers, which opens a new door in the treatment of LSC. In addition, suspension laryngoscopy and CO2 laser resection have produced a significant impact on this field, especially in treating the early stages of larynx cancers (4). Radiation therapy has also been remarkably improved over the decades. However, the incidence of LSC has been decreasing in recent decades, with an increase in mortality. This may be due to the poor prognosis, suggesting that identifying possible molecular biomarkers as prognostic markers or therapeutical targets can significantly improve the treatment outcomes in the LSC. Therefore, this review aims to find molecular markers as potential prognostic markers and therapeutic targets for the LSC, along with presenting a case report. For that, we reported a 68-year-old male patient with laryngeal sarcomatoid carcinoma admitted to our department in addition to presenting relevant literature for the aim of understanding possible molecular therapeutical strategies for LSC.

Clinical case report

This case report presents a 68-year-old male patient diagnosed with LSC who was admitted to our department. The patient reported experiencing recurrent hoarseness over the past one year. He had a history of type 2 diabetes mellitus (T2DM), smoking habits for more than 30 years, and a history of alcohol consumption for the same duration. The onset of hoarseness occurred without an identifiable cause approximately one year prior and had progressively deteriorated since then. The patient encountered difficulties with vocalization, leading to a complete loss of voice; however, he had no difficulty in breathing or swallowing. Following treatment with anti-infective and anti-inflammatory therapies, there was an improvement in his hoarseness, but it was prone to recurrence. The patient's hoarseness persisted for one year, and it gradually intensified over the year.

Laryngoscopy

Local hyperplasia of the left vocal cord, cumulative anterior commissure, and rough surface were observed (Figure 1). Larynx tomography (CT) scan shows that the morphology of the right vocal cord was fixed with thickening, about 6mm, extending forward to the anterior commissure of the vocal cord and the anterior edge of the left vocal cord (Figure 2). After enhancement, there was significant enhancement in the arterial phase, and the enhancement in the venous phase was higher than in the surrounding tissue. The bone window shows local bone destruction of the thyroid cartilage. No signs of mass were observed in the posterior space of the ring. The soft tissue structure of the remaining neck was symmetrical, and there was no apparent mass or enlarged lymph node shadow. The trachea was centered, the thyroid gland was not enlarged, and the density was symmetrical and uniform on both sides. The laryngeal cavity shown was unobstructed, with epiglottic valleys and symmetrical on both

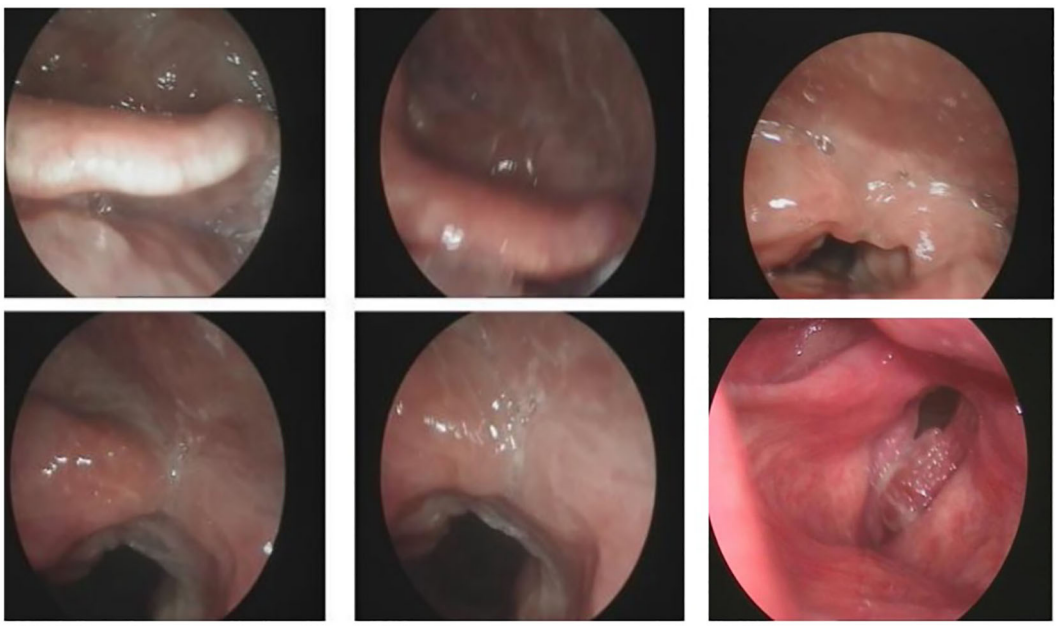

FIGURE 1
Laryngoscopy biopsy shows a malignant tumor with poor differentiation and necrosis (left vocal cord lesion, biopsy).

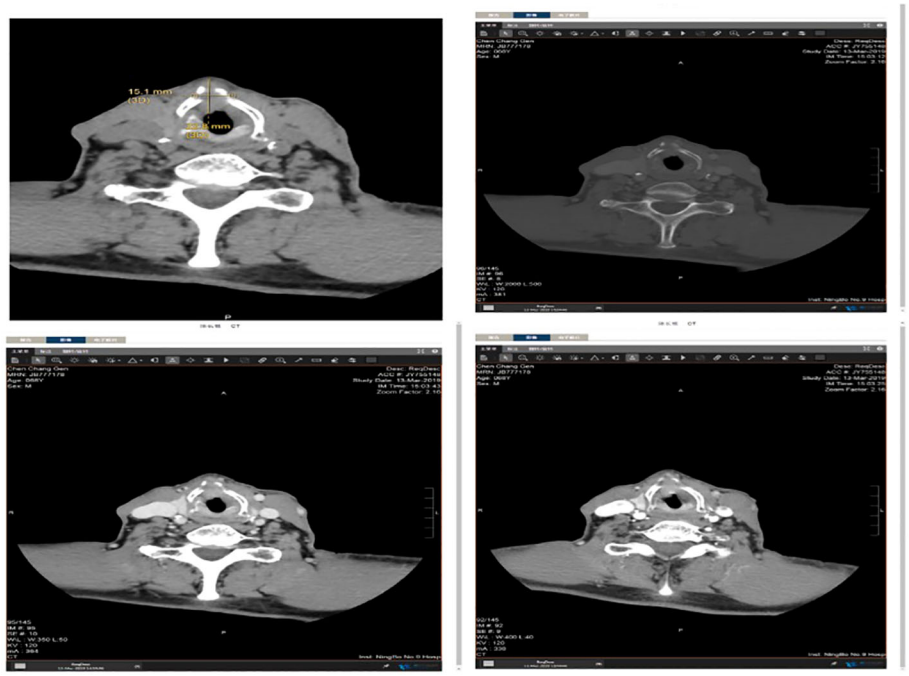

FIGURE 2
Larynx tomography (CT) scan showing that the morphology of the right vocal cord is fixed with thickening, about 6mm, extending forward to the anterior commissure of the vocal cord and the anterior edge of the left vocal cord.

sides. The standard laryngeal carcinoma classification is based on tumor size, lymph node affection, and metastasis (TNM). It is the classification scheme of the American Joint Committee on Cancer Staging (AJCC), and it is used in the same way for stage spindle cell carcinoma (SPCC).

Tumor classification of the patient

According to the tumor classification, the initial classification was given as T3N0MO. After excluding surgical contraindications, a supportive laryngoscopy biopsy was performed. The postoperative examination results revealed the presence of a malignant tumor characterized by poor differentiation and necrosis (identified in the left vocal cord lesion, biopsy). Further analysis through immunohistochemistry did not exclude the possibility of sarcomatoid carcinoma or a mesenchymal soft tissue spindle cell tumor. The immunohistochemical results indicated the following profiles: tumor cells CD34 (-) (Figure 3A), CK (pan) with a small amount of cells (+) (Figure 3B), CAM5.2 with a small amount of cells (+) (Figure 3C), (Figure 3D H&E staining of LSC), Calponin (+) (Figure 4A), SMA (+) (Figure 4B), Desmin (+) (Figure 4C), Ki-67 (+) 30% (Figure 4D) and S-100 (-) (Figure 4E). On March 16, 2019, a supracricoid laryngectomy combined with cricohyoidoepiglottopexy (CHEP) and left lymph node dissection (areas II, III, and IV) was performed under general anesthesia. The postoperative pathology report indicated the following findings: A malignant tumor was identified in the left ventricular zone, consistent with the prior biopsy suggesting a sarcomatoid carcinoma. The maximum tumor diameter was 1 cm, confined to the mucosal layer with adjacent striated muscle involvement; no evidence of vascular invasion or nerve infiltration was observed. During the operation, a frozen section was submitted for examination. (cut margin), left crease, right ROP, ring cartilage, epiglottis, and right arypedium were negative, and no tumor cells were found. Additionally, a malignant tumor was noted in the left sigmoid cartilage plate. The previous biopsy led to sarcomatoid carcinoma, with a maximum diameter of 0.5cm, confined to the mucosal layer, and no vasoma thrombus and nerve invasion. The left arypetis wrinkle, left ladle, right arypetis wrinkle, ring cartilage, epiglottis, and right arypep margin were negative. None of the submitted lymph nodes showed cancer metastasis: left cervical lymph node 2A: 0/1; left cervical lymph node 2B: 0/10; left cervical lymph node area 3:0/16; left cervical lymph node area 40/2. Opening closure was performed 1 year after surgery. After postoperative follow-up until January 2023, the tumor did not recur, and the patient died due to COVID-19 infection.

Methodology

To identify potential molecular targets within LSC for exploring therapeutic opportunities, a comprehensive literature search was conducted between January 2023 and November 2024. This search utilized various scientific databases, including PubMed, Google Scholar, and Web of Science. The primary objective was to delineate the molecular pathways and specific proteins involved in the molecular signaling associated with tumor progression. To

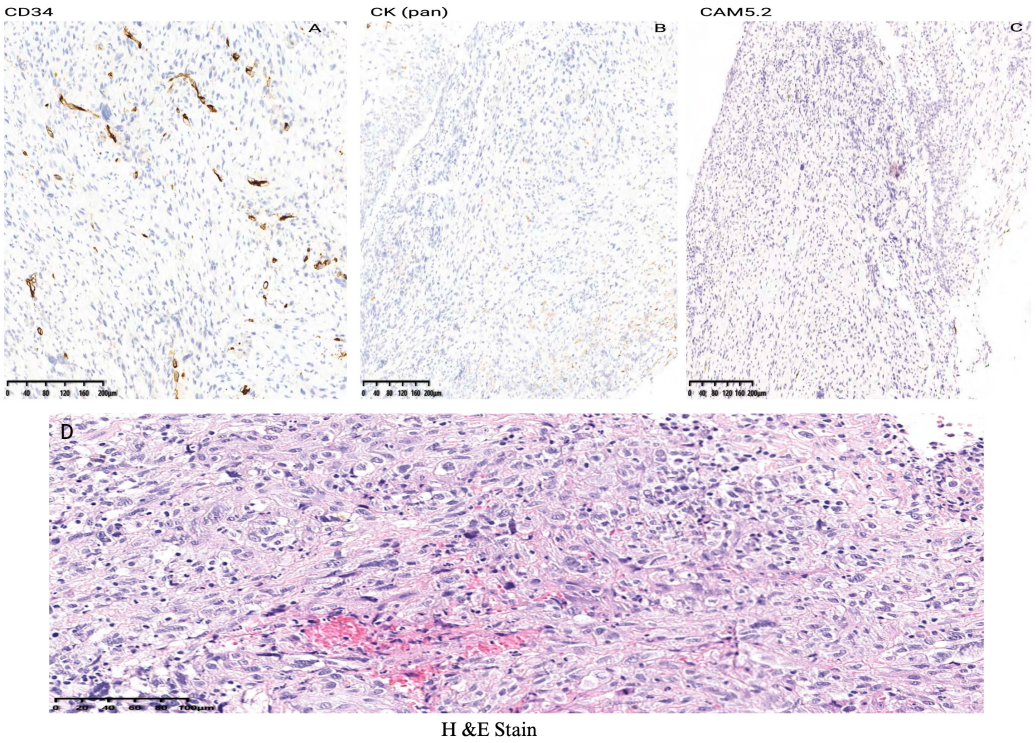

FIGURE 3
Immunohistochemical results indicated the following profiles of LSC case report: tumor cells CD34 (-) **(A)**, CK (pan) with a small amount of cells (+) **(B)**, CAM5.2 **(C)** and **(D)** H&E staining of LSC.

achieve this, specific keywords (Medical Subject Headings [MeSH] terms) related to "laryngeal sarcomatoid carcinoma and molecular signaling," "laryngeal sarcomatoid carcinoma and molecular targets" and "laryngeal sarcomatoid carcinoma and therapeutic opportunities" were employed. These keywords were systematically combined using Boolean operators (AND/OR) to curate articles directly addressing laryngeal sarcomatoid carcinoma and the relevant molecular signaling proteins. The selection process commenced with a review of article titles, followed by abstracts and full texts. Duplicate articles were identified and excluded after a meticulous evaluation of the titles by each author. In total, 350 articles were considered during the selection process. Of these, 300 articles were eliminated after preliminary assessment of the titles and abstracts. Subsequently, an additional 38 articles were excluded after a thorough full-text screening. Ultimately, 12 articles met the established criteria and were deemed relevant to the topic at hand. We included only the patient tissues that were directly utilized for identifying therapeutic possibilities, excluding cell line studies.

Results

We included a total of 12 studies related to molecular targets and their signaling pathways related to LSC aimed at exploring therapeutic possibilities and predicting them as prognostic markers for better clinical outcomes in LSC. Our observations indicate that the following molecular proteins may serve as significant targets in controlling tumor progression at various TNM stages of LSC development: TP53, CD1, Bcl2L12, P21, p27, EGFR, E-cadherin, β-catenin, FAK, NOTCH, FGFR1, PTEN, DJ-1, and TrkB. Most of the studies had male patients at higher proportions than females with smoking and alcohol consumption.

Discussion

Sarcomatoid carcinomas have ambiguous biological implications and pathogenesis because the tumor exploration is limited to immunohistochemical, ultrastructural, and phenotype biomarkers. Nevertheless, considering the current study`s patient's history of smoking and alcohol consumption for three decades, accompanied by symptoms of hoarseness and throat pain, the application of a traditional approach may facilitate the identification of a mass on the vocal cord. This approach would assist in tumor resection while preserving vocal function, and a biopsy could substantiate the diagnosis of Laryngeal Sarcomatoid Carcinoma (T2N0M0, Stage II). Additionally, several diagnostic challenges arise due to its rarity and histological complexity, which can lead to misdiagnosis. For instance, LSC closely resembles other spindle cell tumors, creating a diagnostic dilemma. Moreover, biopsy sampling may not capture the full spectrum of the tumor, particularly the epithelial component, which is crucial for diagnosis. This often results in misdiagnosis because these components are very small and difficult to locate. Therefore, thorough biopsies are necessary. Furthermore,

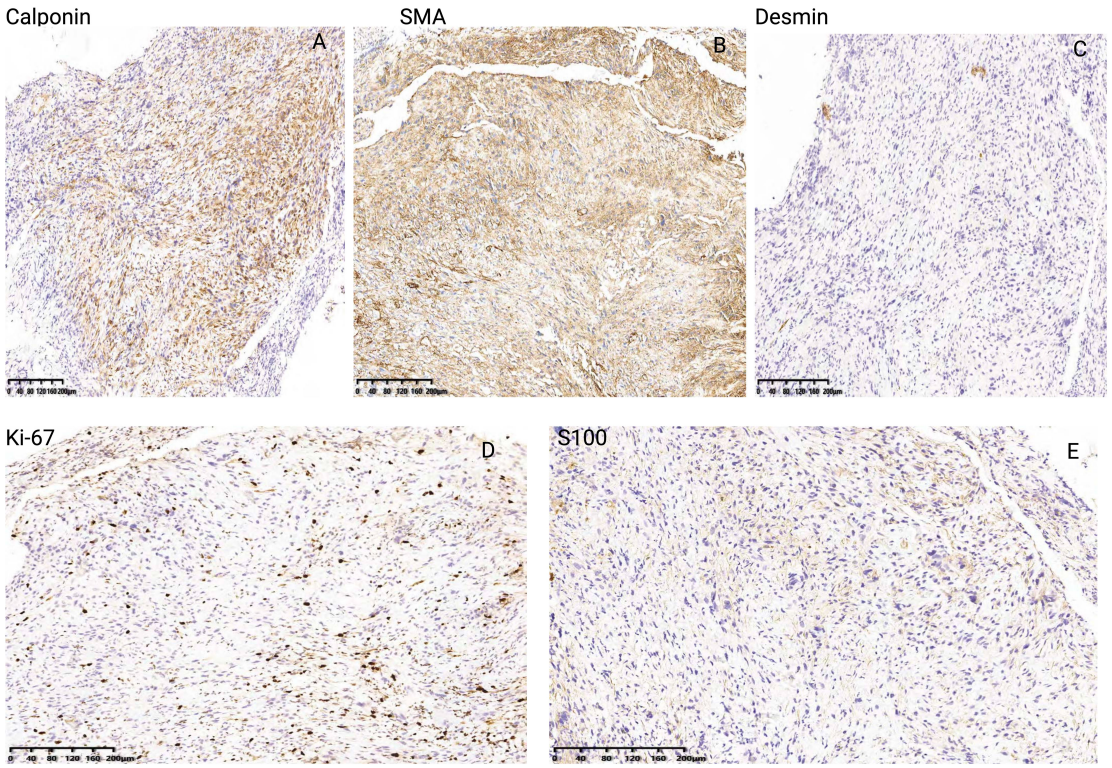

FIGURE 4
Immunohistochemical results of Calponin **(A)**, SMA **(B)**, Desmin **(C)**, Ki-67 **(D)** and S-100 **(E)** of LSC case report.

histopathological examination can reveal both squamous cell carcinoma and sarcomatous components, adding to the complexity of the diagnosis. Altogether, a definitive diagnosis of LSC requires a combination of meticulous histopathological examination, judicious use of immunohistochemical markers, and careful clinical assessment correlation.

Molecular markers discussed in this study would benefit patients because they are cost-effective, rapid, and easy to implement. Pathologists may prefer these markers as surrogate indicators. For example, markers such as p53 are straightforward to assess and can identify the early stages of cancer, as well as predict therapy responses and patient outcomes. Additionally, p53 immunohistochemical (IHC) staining could aid in diagnosing predisposed tumors. Moreover, markers like E-cadherin and β-catenin levels are found to be reduced in IHC analyses of cancer samples, and this reduction correlates with the development of invasive and metastatic phenotypes. Decreased levels of E-cadherin and β-catenin in IHC are associated with tumor stages. Markers like Notch1/2/3/4 expression may serve as prognostic indicators in high-risk subgroups of cancer patients. Therefore, assessing these molecular markers would be more sensitive and specific than older methods, and, as mentioned, they are easier to use and have clinical value. However, the accuracy of these markers is open to discussion; screening for these molecular markers would offer convenience, as it only requires blood, urine, or stool samples instead of tests that involve radiation or unpleasant procedures like colonoscopy. Therefore, using these molecular markers provides an opportunity for repeated testing among the general population. Consequently, this can enhance the tests' sensitivity and improve the chances of detecting early cancers.

Molecular targets for improving clinical significance

Although several genes are reported to induce LSC, how these genes orchestrate the molecular signaling to change the tumor microenvironment is ambiguous. Thus, pinpointing the molecular alterations could clarify the mechanism of LSC progression and aid in identifying these molecular proteins as key therapeutic targets in this field. We included the major molecular pathways from the literature that implicates with tumorigenesis, such as epidermal growth factor receptor (EGFR), tropomyosin-related kinase B receptor (TrkB), cyclin D1, D2, D3, and NOTCH1 (Table 1). These molecular proteins affect the cell cycle and induce significant changes in the tumor and around the microenvironment. For instance, TP53 plays a vital role in managing genomic functions by repairing DNA damage and preventing the accumulation of harmful mutations (Supplementary Figure 1). A mutation in this gene bypasses this protective mechanism, resulting in tumorigenesis. In terms of LSC, a mutation in TP53 influences the apoptotic protein BCl-xl, which then affects Cyclin D1 and promotes the phosphorylation of the Retinoblastoma tumor suppressor protein (RB), facilitating cell progression in LSC (5). Research indicates that approximately 37.9% of advanced larynx cancer cases feature TP53 mutations,

TABLE 1 Study characteristics of LSC patients and possible molecular targets as prognostic and diagnostic markers.

References	No of cases	Molecular target	Possible mechanism	Specific habbits	gender	TNM stages
Scheel et al., 2016 (5)	58patients	TP53	TP53 mutation affects the apoptotic protein BCl-xl, which then interferes Cyclin D1 and promotes the phosphorylation of RB for facilitating cell progression in LSC	Smoking habbits	Male (48)/ female (10)	Stage 3 (24) Stage 4 (34)
Zand et al., 2020 (6)	Out of 82, 75 were positive	CD1	Mutation in the CD1 alters the functions of RB and cellular activities such as DNA damage response checkpoint and cell cycle exit in the LSC	smoking	69 male and 13 female	(38 patients) are stage 2 and (10 patients) 4th stage
Giotakis et al., 2019 (7)	78	Bcl2L12	Cdk activity primarily inhibited by the proteins p21 and p27	Smoking	73 male/ 5 female	I (15/78) II (11/78) III (25/78) IV (27/78)
Pruneri et al., 1999 (8)	132	P21 and p27	P21 and P27 in (LSCC) can increase tumor aggression, advanced clinical stage, and metastasis via affecting Cdk activity. p21 expression correlates with elevated levels of Ki67, cyclin D, and cyclin E, while p27 is linked to accumulation of p53 and promote cell cycle progression	Smoking	129 male/ 3 (female)	Stage 1 and 2 (74) stage 3 and 4 (58)
Maurizi et al., 1996 (9)	140	EGFR	EGFR has been correlated with the anaplastic lymphoma kinase (ALK) ratio to induce neoplastic process in LSC.	–	Males (130)/ females(10)	–
García-Cabo et al., 2020 (10)	133	E-cadherin and -catenin	E-cadherin to N-cadherin significantly influences the characteristics of epithelial-mesenchymal transitions in LSC via affecting the expression of ZEB2.	Tobacco and alcohol consumption	127 (Men) 6 (women)	Stage 1 an 2 (9), stage 3 (17) and stage 4 (33)
Aronsohn et al., 2003 (11)	35	FAK	integrin β1 and FAK signaling facilitate invasion and metastasis in LSCC. FAK phosphorylation activates the paxillin and SATA1 pathways, resulting in increased expression of MMP-2 and MMP-26, and enhances cell invasiveness and migration in LSCC.	–	34 male 1 female	–
Dai et al., 2015 (12)	55	NOTCH 1 and 2	NOTCH2 or 3 receptors can also involve in the cell growth and survival and metastasis in the LSC.			–
Monico et al., 2018 (13)	80	FGFR1	Overexpression of FGFR1 is linked to lymph node metastasis and poor survival outcomes in LSC.	–	5 female/ 69 males	–
Bruine et al., 2019 (14)	52	PTEN	PTEN is decreased in LSCC, evidenced by the increase in tumor degree, indicating in the LSC.	–	11 female and 41 male	–
Shen et al., 2011 (15)	82	DJ-1 protein	The high level of DJ-1 expression might indicate worse T stage, pTNM pathologic stage and differentiation. Survivin and DJ-1 mediated mechanism inhibits the apoptosis by mitigating the PTEN via PI3K-AKT/ PKB pathways.	–	–	17 (stage 1), 16 (stage 2), 34 (stage 3), and 15 (stage 4),
Zhu et al., 2007 (16)	23	TrkB	Trk-B induce metastasis by suppressing anoikis	–	6 female and 17 male	–

making it a potential prognostic and diagnostic biomarker for predicting the survival of larynx cancer patients (5). Notably, 75% of mutations occur within the DNA-binding domain, while 30% are found in the "hotspot" codons, which contributes to cancer progression (5). Studies have reported that TP53 mutations decreased the survival rate in LSC patients (5), and this may be due to the poor response to radiotherapy and increased cellular differentiation and neck LNM. Nonetheless, TP53 mutations can also render cancer cells vulnerable because they struggle to manage extensive DNA damage, leading to cell death. Further investigation is needed to determine if drugs targeting TP53 could effectively address this issue.

Furthermore, mutation of cyclin D1, D2, D3, and Cyclin and cyclin-dependent kinase 4 and 6 (CDK4 and 6) genes are altered in the LSC, which further changes the functions of RB, altering cellular activities such as DNA damage response checkpoint and cell cycle exit (17). The upregulation of p63 is linked to the initial stages of laryngeal tumorigenesis. Bcl-2 and p53 are correlated with poor cellular differentiation, tumor progression, and lymph node metastasis (LNM), contributing to the advancement of the cancer phenotype. Pro-apoptotic isoforms like Bcl2L12 are associated with a reduced risk of patient death, whereas BCL2 and BAX do not correlate with the prognosis of LSCC patients (7). This suggests that Bcl2L12 could serve as a prognostic marker in the advanced stages of primary LSCC. CDK complexes are critical in regulating cell cycle progression, with Cdk activity primarily inhibited by the proteins p21 and p27. Notably, decreased levels of these inhibitors can impede cell cycle arrest and apoptosis, thereby facilitating cancer progression (16, 17). For example, diminished expression of p27 in LSC has been associated with increased tumor aggression, advanced clinical stage, and metastasis. Moreover, p21 expression correlates with elevated levels of Ki67, cyclin D, and cyclin E, while p27 is associated with the accumulation of p53 for promoting cell cycle progression (8). These findings suggest that p21 and p27 may be potential prognostic biomarkers for LSC. Proteins such as the EGFR have been implicated in developing LSC by modulating the epidermal growth factor/transforming growth factor α (EGF/TGFα) signaling pathway (8). Thus affecting cell transformation. Therapeutically, the level of EGFR has been correlated with the anaplastic lymphoma kinase (ALK) ratio, where EGFR overexpression is commonly observed in LSC patients presenting with poorly differentiated histological features and a low ALK ratio (8). Moreover, it has been established that EGFR, KRAS, and cyclin D1 interact synergistically to initiate neoplastic processes. Studies have reported that a decline in survival rates among LSC patients is associated with decreased levels of EGFR and cyclin D1, coupled with an increase in KRAS expression, which adversely influences prognosis (7, 8).

Molecular targets for cancer cell invasion and metastasis in the LSCC

Metastasis is a significant contributing factor to mortality in cancer patients, defined as the spreading of cancer cells to tissues and organs distant from the original tumor site. This metastatic process primarily involves several critical steps, including invasion, intravasation, and extravasation (18). A crucial aspect of metastasis is the loss of adhesion properties in cancer cells, which facilitates their invasion into the surrounding cellular or tissue environment. Various molecules and molecular pathways play vital roles in this process, with E-cadherin and catenins being notable examples (18). E-cadherin functions as a tumor suppressor; however, its diminished expression during the epithelial-to-mesenchymal transition (EMT) can enable cancer cells to acquire metastatic capabilities. The reduction of E-cadherin expression is associated with a loss of cellular polarity and cell adhesion, fostering migratory and invasive characteristics that contribute to tumor progression (8, 18). The ratio of E-cadherin to N-cadherin significantly influences the characteristics of epithelial-mesenchymal transitions (EMTs) across various cancer types, including head and neck squamous cell carcinomas. Notably, lower expressions of E-cadherin have been observed in the LSC and are primarily associated with poor tumor differentiation and advanced T-stage (18). Research indicates that both E-cadherin and β-catenin levels are reduced in immunohistochemical (IHC) analyses of LSC samples, and this reduction correlates with the occurrence of cervical metastases (18). This phenomenon may be attributed to the expression of Zinc finger E-box-binding homeobox (ZEB2), a transcriptional repressor that initiates EMTs by downregulating E-cadherin expression, thereby enhancing tumor invasiveness (Supplementary Figure 2). Consequently, ZEB2 expression may serve as a prognostic biomarker in LSC, alongside E-cadherin, which acts as an EMT biomarker reflecting oncogenesis, tumor development, and metastasis of LSC. Furthermore, targeting the TGF-β/Smads pathway may also represent a valuable prognostic biomarker as it plays a critical role in activating EMT (18).

Integrins are cell surface receptors that play a significant role in the migration and invasion of cancer cells, contributing to the phenomenon of drug resistance. Notably, integrin β1 has been implicated in promoting both invasion and radioresistance in LSC (19). Evidence suggests that the overexpression of integrin β1 in LSC correlates with a poor survival rate, suggesting that integrin β1 may serve as a potential therapeutic target for this malignancy. One proposed mechanism involves the mediating effects of integrin β1 and focal adhesion kinase (FAK) signaling pathways, which facilitate invasion and metastasis in LSC (19). Additionally, the interaction of integrin β1 with CD147 has been shown to rewire metabolic reprogramming that is crucial for tumor development (19). Furthermore, selectin-dependent invasion and metastasis have been associated with cancer progression (20). The knockdown of selectins has been observed to reduce metastatic formation in LSC (20). FAK expression is also linked to laryngeal dysplasia and subsequent invasion in LSC. It appears that ECM integrins activate FAK, thereby enhancing cell survival and proliferation. The FAK-Src complex interacts with Ras-GTPase activator protein SH3 domain-binding protein 1, which inhibits the apoptosis process through the activation of various signaling pathways, including Ras/MAPK, TGF-β/Smad, and Src/FAK, as well as p53 (20). FAK affects the expression of CDK inhibitors p21 and p27, ultimately facilitating tumor progression in LSC. In the context of tumor invasion and migration, FAK knockdown has been shown to inhibit these processes by reducing the activities of matrix metalloproteinases MMP-2 and MMP-9 (21). Studies have demonstrated that FAK phosphorylation activates the paxillin and SATA1 pathways, resulting in increased expression of MMP-2 and MMP-26. Thus, it enhances cell invasiveness and migration in LSCC (22, 23).

Next, the changes in the NOTCH signaling pathway affect tumor regulation (24). For example, NOTCH1 is linked to LNM and tumor progression in LSC patients. For example, the silence of NOTCH1 in the laryngeal carcinoma Hep-2 cell line affects the migration and invasion and promotes metastasis (25). In addition,

other NOTCH components like NOTCH2 or 3 receptors can also be involved in cell growth and survival, and metastasis in the LSC patients (25). Next, 5-hydroxytryptamine (serotonin) receptor 7 (HTR7) is involved in the progression of LSC via activating AKT pathway (26). For example, overexpression of HTR7 has decreased the survival rate of patients with laryngeal squamous cell cancer, suggesting that HTR7 can be an independent prognostic factor for LSC (26). Possibly, the phosphorylation of AKT by HTR7 is linked with the tumor progression. Noncoding RNAs such as miR-132 can promote laryngeal cancer proliferation and growth via targeting FOXO1, resulting in the activation of PI3K/AKT pathway (27). TRA2β is attributed to lymph node metastasis, proliferation, growth, and invasion and inhibits apoptosis in the LSC by activating PI3K/AKT (28). Fibroblast growth factor receptor 1 (*FGFR1)* plays a crucial role in the invasion, metastasis, and causing drug resistance to LSC, and FGFR1 can be an independent prognostic factor for LSC, mainly overexpression of FGFR1 is linked to lymph node metastasis and poor survival outcomes. Studies have shown that over-expression of FGFR1 is an important factor for malignant evolution and progression of laryngeal SCC (29). Another tumor suppressor gene PTEN that regulates several cellular functions such as proliferation, protein synthesis, and cell survival (29). A study has shown that PTEN is decreased in LSCC, evidenced by the increase in tumor degree, indicating that PTEN could be an important prognostic marker of LSCC tumor aggressiveness (30). PARK7 protein (DJ-1) is linked to various cancer types mainly; it influences the cancer cells transforming activity being with H-Ras/Myc, which primarily affects the S phase of the cell cycle by translocating from the cytoplasm to the nucleus (31). Studies have shown that increased levels of PARK7 in 85% of LSC patients are linked to poor survival and tumor recurrence in the LSC patients (15). A study has shown that silencing RNA targeting PARK7 significantly increased the PTEN expression, which resulted in an increase in cell death and decreased cell proliferation and invasion in the laryngeal cancer cells (32), and increase of PARK7 triggers the surviving expression, resulting in the inhibition of apoptosis and cell proliferation of laryngeal carcinoma cells (15). Tropomyosin-related kinase B receptor (TrkB) plays various roles in inducing tumor progression, such as increasing invasion, metastasis, and angiogenesis and inducing resistance against cancer treatments (32). TrkB overexpression is linked to metastatic laryngeal cancer cell lines, and it drives EMT by regulating c-Src-mediated activation of PI3K/AKT signal pathway, suggesting the therapeutical opportunity of TrkB to counteract metastasis in the LSC (33).

Genetic/molecular alterations involved in sarcomatoid transformation

Sarcomatoid carcinoma is a rare morphological variant with distinctive histological features. It can exist as either a sarcomatoid form or a typical squamous phenotype. Despite its aggressive behavior, poor survival rates, and higher levels of tumor programmed death-ligand 1 (PD-L1), the mechanisms behind its evolution and progression remain unknown. However, EMT is a widely accepted theory, with contrasting hypotheses regarding the development of these tumors as follows: a monoclonal origin from an undifferentiated stem cell that generates both mesenchymal and squamous components, and sarcomatoid carcinoma is a multiclonal origin where these components arise independently from different cell types. However, studies reported that these types of carcinomas from different cell types showed similar molecular and genetic features, supporting the monoclonal hypothesis, and the differentiation and morphogenesis of these carcinomas are organized by coordinated genetics and molecular events of both epithelial and mesenchymal elements, which can provide crucial information of sarcomatoid transformation. Although the underlying molecular events are unknown, the loss of heterozygosity in chromosome 17p, and subsequent molecular progression is responsible for sarcomatoid transformation (34). Tumor growth factor-β (TGF-β), epithelial growth factor (EGF), and insulin-like growth factor (IGF) have been linked to sarcomatoid transformation (35). For example, TGF-β promotes the EMT via MAPK through Hic-5, a focal adhesion protein that is crucial for maintaining the mesenchymal phenotype, accompanied by RhoA activation (36). Additionally, higher expression of Src is associated with sarcomatoid transformation. The activation of these molecular events alters mesenchymal morphology, increasing the motility and invasiveness of tumors. Mutations in the pathways of VENTX, HIF-1α, and SUMOylation induce DNA damage and drive proliferation toward EMT (37). For instance, sentrin/SUMO2/3-specific protease (SENP3) modifies the removal of SUMO2/3, which leads to increased cell proliferation, tumorigenesis, and EMT through STAT3 activation (38). Y-box binding protein 1 (YB-1) is a conserved protein that induces epithelial-to-mesenchymal transition and further metastasis by binding to HIF-1α and triggering the translation of HIF1A messages, enhancing metastatic capacity in sarcomatoid carcinoma (39). Moreover, other new mutations in sarcomatoid carcinoma, such as integrin cell surface interactions, WNT, MAPK, and BRAF signaling pathways, induce EMT phenotypes (37). For example, mutations in WNT drive the proliferation of mesenchymal stem cells through the TCF/β-catenin target gene CDC25A, which is crucial for cell cycle progression (40). Targeting these molecular proteins may offer viable clinical strategies.

Conclusion

Laryngeal sarcomatoid carcinoma is a rare type of cancer, and its clinical manifestations and imaging manifestations are not significantly specific, and it is confirmed only based on pathological examination. Treatment options are still controversial. The particular treatment regimen still depends on the specific condition of the patient. In this case, CHEP + left lymph node dissection was performed without chemoradiation, with no postoperative recurrence or metastasis. Regarding molecular proteins as prognostic and diagnostic markers in the LSC, we found TP53, CD1, Bcl2L12, P21, p27, EGFR, E-cadherin, β-catenin, FAK, NOTCH, FGFR1, PTEN, DJ-1, and TrkB are the

possible markers to inhibit the tumor stages as they are involved in the cell cycle progression and cell cycle arrest in the LSC. However, further research is warranted on these molecular markers to elucidate their dual nature, particularly their potential role in inducing DNA damage in cancer cells.

Data availability statement

The raw data supporting the conclusions of this article will be made available by the authors, without undue reservation.

Ethics statement

The studies involving humans were approved by Ningbo No.9 Hospital, Ningbo, China. The studies were conducted in accordance with the local legislation and institutional requirements. The participants provided their written informed consent to participate in this study. Written informed consent was obtained from the individual(s) for the publication of any potentially identifiable images or data included in this article.

Author contributions

JF: Conceptualization, Data curation, Methodology, Validation, Writing – original draft, Writing – review & editing. LC: Validation, Writing – review & editing. CL: Methodology, Writing – review & editing. ZX: Methodology, Software, Writing – review & editing. SZ: Conceptualization, Writing – original draft, Writing – review & editing.

Funding

The author(s) declare that no financial support was received for the research and/or publication of this article.

Conflict of interest

The authors declare that the research was conducted in the absence of any commercial or financial relationships that could be construed as a potential conflict of interest.

Generative AI statement

The author(s) declare that no Generative AI was used in the creation of this manuscript.

Publisher's note

Supplementary material

The Supplementary Material for this article can be found online at: https://www.frontiersin.org/articles/10.3389/fonc.2025.1549790/full#supplementary-material

SUPPLEMENTARY FIGURE 1
Molecular signaling pathways for improving clinical significance in LSC. P53 and p63 mutations induce LSC metastasis by affecting Bcl-xl, Ki67, Cyclin D1, D2, and cyclin E and Retinoblastoma (RB) phosphorylation.

SUPPLEMENTARY FIGURE 2
Potential Prognostic Biomarkers for Laryngeal sarcomatoid carcinoma (LSC). The blue arrows indicate the molecular signaling pathways involved in the induction of tumorigenesis, impacting apoptosis, cell proliferation, differentiation, and metastasis.

References

1. Sarradin V, Siegfried A, Uro-Coste E, Delord JP. Classification de l'OMS 2017 des tumeurs de la tête et du cou: principales nouveautés et mise à jour des méthodes diagnostiques [WHO classification of head and neck tumours 2017: Main novelties and update of diagnostic methods. *Bull Canc*. (2018) 105:596–602. doi: 10.1016/j.bulcan.2018.04.004

2. Ricciardiello F, Bocchetti M, Pellini R, Palladino R, Caraglia M, Boscaino A, et al. Sarcomatoid larynx carcinoma differential clinical evolution, on field statistical considerations. *Am J Otolaryngol*. (2021) 42:102934. doi: 10.1016/j.amjoto.2021.102934

3. Liberale C, Soloperto D, Marchioni A, Monzani D, Sacchetto L. Updates on larynx cancer: risk factors and oncogenesis. *Int J Mol Sci*. (2023) 24:12913. doi: 10.3390/ijms241612913

4. Rubinstein M, Armstrong WB. Transoral laser microsurgery for laryngeal cancer: a primer and review of laser dosimetry. *Lasers Med Sci*. (2011) 26:113–24. doi: 10.1007/s10103-010-0834-5

5. Scheel A, Bellile E, McHugh JB, Walline HM, Prince ME, Urba S, et al. Classification of TP53 mutations and HPV predict survival in advanced larynx cancer. *Laryngoscope*. (2016) 126:E292–9. doi: 10.1002/lary.25915

6. Zand V, Binesh F, Meybodian M, Safi Dahaj F, Alamdar Yazdi A. Cyclin D1 expression in patients with laryngeal squamous cell carcinoma. *Iran J Pathol*. (2020) 15:245–50. doi: 10.30699/ijp.2020.116579.2276

7. Giotakis AI, Lazaris AC, Kataki A, Kontos CK, Giotakis EI. Positive BCL2L12 expression predicts favorable prognosis in patients with laryngeal squamous cell carcinoma. *Cancer biomark*. (2019) 25:141–9. doi: 10.3233/CBM-181772

8. Pruneri G, Pignataro L, Carboni N, Buffa R, Di Finizio D, Cesana BM, et al. Clinical relevance of expression of the CIP/KIP cell-cycle inhibitors p21 and p27 in laryngeal cancer. *J Clin Oncol*. (1999) 17:3150–9. doi: 10.1200/JCO.1999.17.10.3150

9. Maurizi M, Almadori G, Ferrandina G, Distefano M, Romanini ME, Cadoni G, et al. Prognostic significance of epidermal growth factor receptor in laryngeal squamous cell carcinoma. *Br J Canc*. (1996) 74:1253–7. doi: 10.1038/bjc.1996.525

10. García-Cabo P, García-Pedrero JM, Villaronga MÁ, Hermida-Prado F, Granda-Díaz R, Allonca E, et al. Expresión de E-cadherina y -catenina en carcinomas de células escamosas de laringe e hipofaringe. *Acta Otorrinolaringol Esp*. (2020) 71:358–66. doi: 10.1016/j.otorri.2019.12.002

11. Aronsohn MS, Brown HM, Hauptman G, Kornberg LJ. Expression of focal adhesion kinase and phosphorylated focal adhesion kinase in squamous cell carcinoma of the larynx. *Laryngoscope*. (2003) 113:1944–8. doi: 10.1097/00005537-200311000-00017

12. Dai MY, Fang F, Zou Y, Yi X, Ding YJ, Chen C, et al. Downregulation of Notch1 induces apoptosis and inhibits cell proliferation and metastasis in laryngeal squamous cell carcinoma. *Oncol Rep*. (2015) 34:3111–9. doi: 10.3892/or.2015.4274

13. Monico J, Miller B, Rezeanu L, May W, Sullivan DC. Fibroblast growth factor receptor 1 amplification in laryngeal squamous cell carcinoma. *PloS One*. (2018) 13: e0186185. doi: 10.1371/journal.pone.0186185

14. Bruine de Bruin L, Wachters JE, Schrijvers ML, Slagter-Menkema L, Mastik MF, Langendijk JA, et al. PTEN is associated with worse local control in early stage supraglottic laryngeal cancer treated with radiotherapy. *Laryngoscope Investig Otolaryngol*. (2019) 4:399–404. doi: 10.1002/lio2.v4.4

15. Shen Z, Ren Y, Ye D, Guo J, Kang C, Ding H. Significance and relationship between DJ-1 gene and surviving gene expression in laryngeal carcinoma. *Eur J Histochem*. (2011) 55:e9. doi: 10.4081/ejh.2011.e9

16. Zhu L, Werner JA, Mandic R. Implications of tropomyosin-related kinase B (TrkB) in head and neck cancer. *Anticancer Res*. (2007) 27:3121–6.

17. Narasimha AM, Kaulich M, Shapiro GS, Choi YJ, Sicinski P, Dowdy SF. Cyclin D activates the Rb tumor suppressor by mono-phosphorylation. *Elife*. (2014) 3:e02872. doi: 10.7554/eLife.02872

18. Xu J, Lamouille S, Derynck R. TGF-β–induced epithelial to mesenchymal transition. *Cell Res*. (2009) 19:156–72. doi: 10.1038/cr.2009.5

19. Li L, Dong X, Peng F, Shen L. Integrin β1 regulates the invasion and radioresistance of laryngeal cancer cells by targeting CD147. *Cancer Cell Int*. (2018) 18:80. doi: 10.1186/s12935-018-0578-z

20. Valentiner U, Knips J, Pries R, Clauditz T, Münscher A, Sauter G, et al. Selectin binding sites are involved in cell adhesive properties of head and neck squamous cell carcinoma. *Cancers (Basel)*. (2019) 11:1672. doi: 10.3390/cancers11111672

21. Xiao W, Jiang M, Li H, Li C, Su R, Huang K. Knockdown of FAK inhibits the invasion and metastasis of Tca-8113 cells in *vitro*. *Mol Med Rep*. (2013) 8:703–7. doi: 10.3892/mmr.2013.1555

22. Huang Y, Sook-Kim M, Ratovitski E. Midkine promotes tetraspanin-integrin interaction and induces FAK-Stat1alpha pathway contributing to migration/invasiveness of human head and neck squamous cell carcinoma cells. *Biochem Biophys Res Commun*. (2008) 377:474–8. doi: 10.1016/j.bbrc.2008.09.138

23. Zhang Y, Sun X. Role of focal adhesion kinase in head and neck squamous cell carcinoma and its therapeutic prospect. *Onco Targets Ther*. (2020) 13:10207–20. doi: 10.2147/OTT.S270342

24. Li X, Yan X, Wang Y, Kaur B, Han H, Yu J. The Notch signaling pathway: a potential target for cancer immunotherapy. *J Hematol Oncol*. (2023) 16:45. doi: 10.1186/s13045-023-01439-z

25. Jiao J, Qin Z, Li S, Liu H, Lu Z. Potential role of Notch1 signaling pathway in laryngeal squamous cell carcinoma cell line Hep-2 involving proliferation inhibition, cell cycle arrest, cell apoptosis, and cell migration. *Oncol Rep*. (2009) 22:815–23. doi: 10.3892/or_00000504

26. Sheng X, Liu W, Lu Z, Xu M, Li R, Zhong R, et al. HTR7 promotes laryngeal cancer growth through PI3K/AKT pathway activation. *Ann Transl Med*. (2021) 9:840. doi: 10.21037/atm-21-1069

27. Lian R, Lu B, Jiao L, Li S, Wang H, Miao W, et al. Mir-132 plays an oncogenic role in laryngeal squamous cell carcinoma by targeting foxo1 and activating the pi3k/akt pathway. *Eur J Pharmacol*. (2016) 792:1–6. doi: 10.1016/j.ejphar.2016.10.015

28. Ni HS, Hu SQ, Chen X, Liu YF, Ni TT, Cheng L. Tra2beta silencing suppresses cell proliferation in laryngeal squamous cell carcinoma via inhibiting pi3k/akt signaling. *Laryngoscope*. (2019) 129:E318–28. doi: 10.1002/lary.27716

29. Kim EK, Cho YA, Koh YW, Shin HA, Cho BC, Yoon SO. Prognostic implications of Fibroblast growth factor receptor 1 (FGFR1) gene amplification and protein overexpression in hypopharyngeal and laryngeal squamous cell carcinoma. *BMC Canc*. (2020) 20:348. doi: 10.1186/s12885-020-06792-7

30. Mastronikolis NS, Tsiambas E, Papadas TA, Karameris A, Ragos V, Peschos D, et al. Deregulation of PTEN expression in laryngeal squamous cell carcinoma based on tissue microarray digital analysis. *Anticancer Res*. (2017) 37:5521–4. doi: 10.21873/anticanres.11983

31. Le Naour F, Misek DE, Krause MC, Deneux L, Giordano TJ, Scholl S, et al. Proteomics-based identification of RS/DJ-1 as a novel circulating tumor antigen in breast cancer. *Clin Cancer Res*. (2001) 7:3328–35.

32. Zhu XL, Sun W, Lei WB, Zhuang HW, Hou WJ, Wen WP. DJ-1-induced phosphatase and tensin homologue downregulation is associated with proliferative and invasive activity of laryngeal cancer cells. *Mol Med Rep*. (2015) 12:2003–8. doi: 10.3892/mmr.2015.3617

33. Jiang L, Wang Z, Liu C, Gong Z, Yang Y, Kang H, et al. TrkB promotes laryngeal cancer metastasis via activation PI3K/AKT pathway. *Oncotarget*. (2017) 8:108726–37. doi: 10.18632/oncotarget.21711

34. Choi HR, Sturgis EM, Rosenthal DI, Luna MA, Batsakis JG, El-Naggar AK. Sarcomatoid carcinoma of the head and neck: molecular evidence for evolution and progression from conventional squamous cell carcinomas. *Am J Surg Pathol*. (2003) 27:1216–20. doi: 10.1097/00000478-200309000-00004

35. Klebanov N, Reddy BY, Husain S, Silvers DN, Grossman ME, Tsao H. Cutaneous presentation of mesothelioma with a sarcomatoid transformation. *Am J Dermatopathol*. (2018) 40:378–82. doi: 10.1097/DAD.0000000000001023

36. Tumbarello DA, Turner CE. Hic-5 contributes to epithelial-mesenchymal transformation through a RhoA/ROCK-dependent pathway. *J Cell Physiol*. (2007) 211:736–47. doi: 10.1002/jcp.v211:3

37. Lin MC, Hsu CL, Lai SF, Huang YL, Hsieh MS, Chen TC, et al. Spindle cell carcinoma of the head and neck: clinical characteristics and molecular signatures. *Laryngoscope*. (2023) 133:2183–91. doi: 10.1002/lary.v133.9

38. Zhou Z, Wang M, Li J, Xiao M, Chin YE, Cheng J, et al. SUMOylation and SENP3 regulate STAT3 activation in head and neck cancer. *Oncogene*. (2016) 35:5826–38. doi: 10.1038/onc.2016.124

39. El-Naggar AM, Veinotte CJ, Cheng H, Grunewald TG, Negri GL, Somasekharan SP, et al. Translational activation of HIF1α by YB-1 promotes sarcoma metastasis. *Cancer Cell*. (2015) 27:682–97. doi: 10.1016/j.ccell.2015.04.003

40. Vijayakumar S, Liu G, Rus IA, Yao S, Chen Y, Akiri G, et al. High-frequency canonical Wnt activation in multiple sarcoma subtypes drives proliferation through a TCF/β-catenin target gene, CDC25A. *Cancer Cell*. (2011) 19:601–12. doi: 10.1016/j.ccr.2011.03.010

frontiers | Frontiers in Pharmacology

TYPE Original Research
PUBLISHED 29 May 2025
DOI 10.3389/fphar.2025.1541987

OPEN ACCESS

EDITED BY
Luis Abel Quiñones,
University of Chile, Chile

REVIEWED BY
Ashwin Kotnis,
All India Institute of Medical Sciences, Bhopal, India
Yabing Nan,
Department of Cancer Biology, Dana–Farber Cancer Institute, United States

*CORRESPONDENCE
Uday Venkat Mateti,
udayvenkatmateti@gmail.com

RECEIVED 09 December 2024
ACCEPTED 17 April 2025
PUBLISHED 29 May 2025

CITATION
Chaudhary RK, Patil P, Shetty VV, Mateti UV and Shetty P (2025) A multimodal approach for establishing *ACTL6A* and *ERCC1* as chemoresistance genes in locally advanced head and neck cancer.
Front. Pharmacol. 16:1541987.
doi: 10.3389/fphar.2025.1541987

A multimodal approach for establishing *ACTL6A* and *ERCC1* as chemoresistance genes in locally advanced head and neck cancer

Raushan Kumar Chaudhary[1], Prakash Patil[2], Vijith Vittal Shetty[3], Uday Venkat Mateti[1]* and Praveenkumar Shetty[2,4]

[1]Department of Pharmacy Practice, NGSM Institute of Pharmaceutical Sciences (NGSMIPS), Nitte (Deemed to be University), Mangalore, Karnataka, India, [2]Central Research Laboratory, K.S. Hegde Medical Academy (KSHEMA), Nitte (Deemed to be University), Mangalore, Karnataka, India, [3]Department of Medical Oncology, K.S. Hegde Medical Academy (KSHEMA), Justice K.S. Hedge Charitable Hospital (JKSHCH), Nitte (Deemed to be University), Mangalore, Karnataka, India, [4]Department of Biochemistry, K.S. Hegde Medical Academy (KSHEMA), Nitte (Deemed to be University), Mangalore, Karnataka, India

Background: DNA is generally considered the ultimate target of cisplatin, so DNA repair has become the hallmark for cisplatin chemoresistance that is attributed to the poor overall survival (50%) among patients with head and neck cancer (HNC). As the efficacy of cisplatin is dose-dependent, we conducted the first study in an Asian population to characterize the DNA repair genes *ACTL6A* and *ERCC1* based on the dosing of cisplatin-based chemoradiotherapy (CRT).

Methods: Locally advanced HNC (LAHNC) patients who were planning to undergo cisplatin-based CRT were enrolled in a prospective study to quantify the dose-dependent expressions of *ACTL6A* and *ERCC1* from peripheral blood mononuclear cells via quantitative polymerase chain reaction; these results were integrated with computational analysis and systematic review/meta-analysis to formulate evidence-based translation decisions. The Friedman test and Wilcoxon's test were used to compare the expressions of the two genes before and after CRT, and Spearman's rank correlation was used to find the correlation between *ACTL6A* and *ERCC1* expressions. All statistical analyses were performed using SPSS version 29.

Results: A total of 77 LAHNC patients were enrolled in this study, of which 96.1% were men and 3.9% were women with a mean age of 52.88 $\pm$ 9.68 years. The median expressions of *ERCC1* were significantly increased ($p < 0.001$) after 50% (0.19) and 100% CRT (0.23) compared to the baseline value (0.14), whereas *ACTL6A* expression decreased from 4.77 to 3.87 after 50% CRT ($p < 0.05$) and increased to 5.43 after 100% CRT. From the computational analysis, *ACTL6A* and *ERCC1* were found to be overexpressed among HNC patients and observed to regulate 10 repair pathways. Overexpressions of *ERCC1* and *ACTL6A* were predicted to infiltrate the tumors with $CD4^+$ cells, macrophages, dendritic cells, and B cells. The hazard ratios for overall survival were found to be 1.67 among the *ACTL6A* overexpressed and 1.82 among the *ERCC1* overexpressed HNC patients via computational analysis and meta-analysis, respectively. Furthermore, FDA-approved drugs like gemcitabine and

panobinostat were found to be the best candidates for downregulating *ERCC1* and *ACTL6A* expressions based on binding affinities of −3.707 and −4.198 kcal/mol, respectively.

Conclusion: The increased expressions of *ACTL6A* and *ERCC1* during/after cisplatin-based CRT are expected to mediate DNA repair leading to chemoresistance, which could result in poor overall survival in HNC patients. Thus, FDA-approved drugs like panobinostat and gemcitabine can be repurposed to target the chemoresistance genes *ACTL6A* and *ERCC1*, respectively.

KEYWORDS

chemoradiotherapy, chemoresistance, cisplatin, DNA repair, drug repurposing, evidence

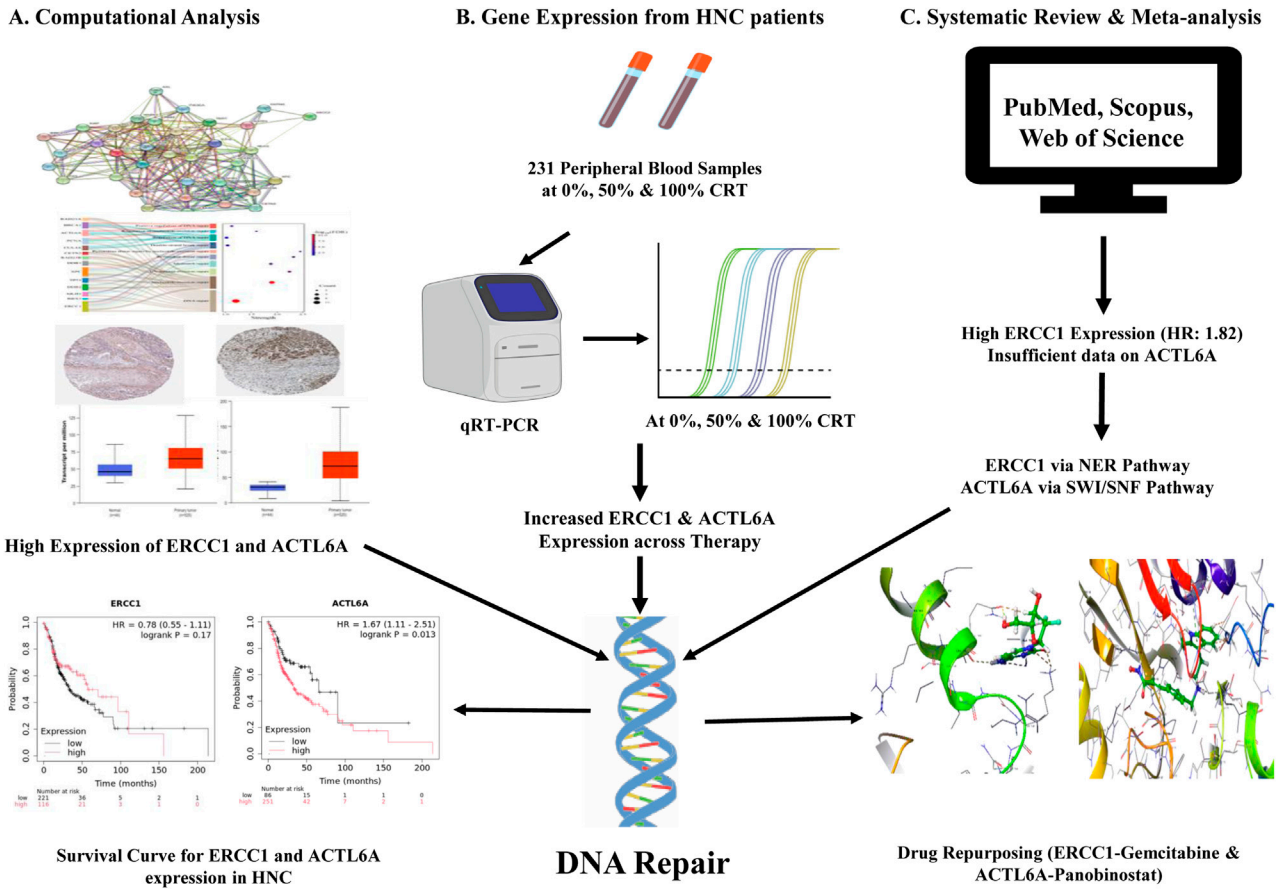

GRAPHICAL ABSTRACT

Highlights

- Of the 77 LAHNC patients in the study cohort, men outnumbered women and had a mean age of 52.88 ± 9.68 years.
- *ACTL6A* expression increased after CRT (5.43) compared to the baseline value (4.77).
- *ERCC1* expression significantly increased with CRT, indicating high nucleotide excision repair capacity.
- *ERCC1*/*ACTL6A* overexpressions were linked to poor overall survival (hazard ratio: 1.82/1.67).
- Gemcitabine and panobinostat can downregulate *ERCC1* and *ACTL6A*, respectively.

Abbreviations: DNA: deoxyribonucleic acid, HNC: head and neck cancer, ERCC1: excision repair cross-complementation group 1, ACTL6A: actin-like protein 6A, CRT: chemoradiotherapy, FDA: Food and Drug Administration, NER: nucleotide excision repair, SWI/SNF: switch/sucrose non-fermenting, LAHNC: locally advanced head and neck cancer, CCRT: concurrent chemoradiotherapy, R/MHNC: recurrent/metastatic head and neck cancer, HR: hazard ratio, TCR: transmission-coupled repair, GGR: global genome repair, PPI: protein–protein interaction, BP: biological process, CC: cellular component, MF: molecular function, IHC: immunohistochemistry, BMI: body mass index, OR: odds ratio.

1 Introduction

Head and neck cancer (HNC) refers to a group of heterogenous malignancies generally originating from the mucosal epithelial regions of the head and neck, such as the oral cavity, pharynx, larynx, oro/hypo/naso-pharynx, and salivary glands (Chaudhary et al., 2023). According to GLOBOCAN 2022, HNC has collectively secured the top spot among Indian patients in terms of incidence (17.53% or 247,924 new cases), 5-year prevalence (18.94% per 100,000 out of 613,841), and mortality (15.05% or 137,925) (Global Cancer Observatory, 2024: India Fact Sheet). Alcohol consumption, tobacco use (smoke/smokeless), poor oral hygiene, viral infections (human papilloma virus/Epstein–Barr virus), altered expressions of tumor suppressors, and oncogenes are the predominant etiopathophysiological factors associated with the development of HNC (Chaudhary et al., 2023). Localized/early-stage (stages I/II) HNCs are generally managed through surgery or radiation therapy, whereas locally advanced HNC (LAHNC) is generally managed using concurrent chemoradiotherapy (CCRT) with/without surgery (Chaudhary et al., 2023). Approximately 66.6% of the Indian population of HNC patients are diagnosed at the locally advanced stage, which makes CCRT with/without surgery as the popular choice of treatment among clinicians (Chaudhary et al., 2023; Mathur et al., 2020). Thus, chemotherapy serves as the cornerstone of the treatment strategy for managing HNC.

Cisplatin is the most widely preferred and broad-spectrum frontline dose-dependent antineoplastic drug in HNC that exerts its anticancer effects via the formation of interstrand and intrastrand cross-linking with nuclear/mitochondrial DNA at the N7 positions of adenine and guanine, thereby arresting the cell cycle at the G2 phase and causing apoptosis to interfere with DNA repair (Chaudhary et al., 2023; Ranasinghe et al., 2022). In addition, aqueous cisplatin is known to enhance the mitochondrial outer membrane permeabilization, which further induces the caspases and causes apoptosis of tumor cells through the release of protein cytochrome c into the cytoplasm (Kanno et al., 2021). Generally, once-weekly intravenous administration of cisplatin at 30–40 mg/m^2 for 6–7 weeks has been proven to be the best alternative to 3-weekly intravenous administration of cisplatin at 100 mg/m^2 as the former is associated with minimal toxicity (Chaudhary et al., 2023; NCCN Guidelines, 2024). Furthermore, cisplatin is often combined with other anticancer agents, such as paclitaxel, docetaxel, 5-fluorouracil (TPF regimen), hydroxyurea, etoposide, pembrolizumab, nivolumab, and cetuximab, to manage locally LAHNC and recurrent/metastatic HNC (R/MHNC) (Chaudhary et al., 2023; NCCN Guidelines, 2024). However, it is disheartening that almost 65% of LAHNC patients do not reap any benefits from such therapy, which is attributable to the recurrence, metastasis, and poor survival among LAHNC patients (Chaudhary et al., 2023; Mathur et al., 2020). Furthermore, approximately 70%–90% of R/MHNC patients do not respond to immunotherapy (Chaudhary et al., 2023). Collectively, these hurdles in the management of HNC have resulted in poor 5-year overall survival rates (50%) (Gormley et al., 2022). According to the Surveillance, Epidemiology, and End Results (SEER) registry, there has been a modest increase in the 5-year relative survival rate among HNC patients to approximately 65.25% between 2014 and 2020 (i.e., 5-year relative survival rates of oral cavity and pharynx cancer is 69% and larynx cancer is 61.5%) (SEER Cancer Stat Facts, 2024). The mortality rate of Indian patients accounts for approximately 71% of all HNC-related deaths in southeast Asia and 28% globally (Chauhan et al., 2018). The disease burden of HNC and its ineffective response to cisplatin have necessitated investigations into the causes behind the limited benefits of cisplatin therapy, which are achieved by exploring the possible biological markers involved in the molecular mechanisms of chemoresistance (Kanno et al., 2021).

Chemoresistance is a multifaceted condition that is often associated with increased DNA repair, deregulated influx/efflux pump, enzymatic inactivation of drugs, aberrant autophagy and apoptosis, regulation of EGFR/FAK/NF-kB pathways, cancer stem cells, and metabolic reprogramming (Ranasinghe et al., 2022; Kanno et al., 2021; Hu et al., 2023). As DNA is the ultimate target of cisplatin therapy, the pathways associated with repair of damaged DNA are crucially linked to cisplatin resistance. Nucleotide excision repair (NER) is a crucial DNA repair pathway that is responsible for clearing cisplatin-DNA adducts compared to other repair pathways, such as double-strand break repair, mismatch repair, and base excision repair (Kanno et al., 2021). NER is further subdivided into two important pathways, namely, the transcription-coupled repair (TCR-NER) and global genome repair (GGR-NER) pathways (KEGG Pathway, 2024: map03420). The current study explores the roles of the excision repair cross-complementation group1 (*ERCC1*) and actin-like protein 6A (*ACTL6A*) genes as attractive biological markers associated with DNA repair in HNC.

ERCC1 and ACTL6A are the core proteins of the NER pathway and switch/sucrose non-fermentable (SWI/SNF) complex, respectively (Kanno et al., 2021; Xiao et al., 2021). ERCC1 is a catalytically inactive protein that is capable of initiating DNA/protein–protein interaction (PPI) binds that can cause XPF activation and form the ERCC1-XPF1 heterodimer. Collectively, the ERCC1-XPF1 endonuclease protein complex is responsible for detection and repair of DNA damage. *ERCC1* is a high-capacity gene of the NER pathway that mediates cisplatin resistance in HNC patients (Prochnow et al., 2019). However, there exist controversies regarding its expression and clinical significance. Recently, the novel oncogene *ACTL6A* (a subunit of the SWI/SNF complex) has garnered attention for its DNA repair capacity (Xiao et al., 2021). Biologically, *ACTL6A* has been reported to be involved in chromatin remodeling and transcription regulation. *ACTL6A* encodes for the actin-related proteins comprising actin folds that are responsible for the binding and hydrolysis of adenosine triphosphate to remodel chromatin and promote gene expression by enhancing DNA accessibility (Xiao et al., 2021; Dang et al., 2020). Thus, *ACTL6A* mediates DNA repair via utilization of the SWI/SNF complex that might also promote such repair via NER (Dang et al., 2020). However, this mechanism remains unresolved.

The formation of DNA–cisplatin adducts as well as the anticancer efficacy of cisplatin are attributed to the therapeutic dose administered (Ranasinghe et al., 2022). Thus, it is crucial to determine the biomarkers for cisplatin resistance in relation to the therapeutic dose. Furthermore, investigating the expressions of the chemoresistance genes from blood samples before and after therapy is less invasive, inexpensive, easy, less

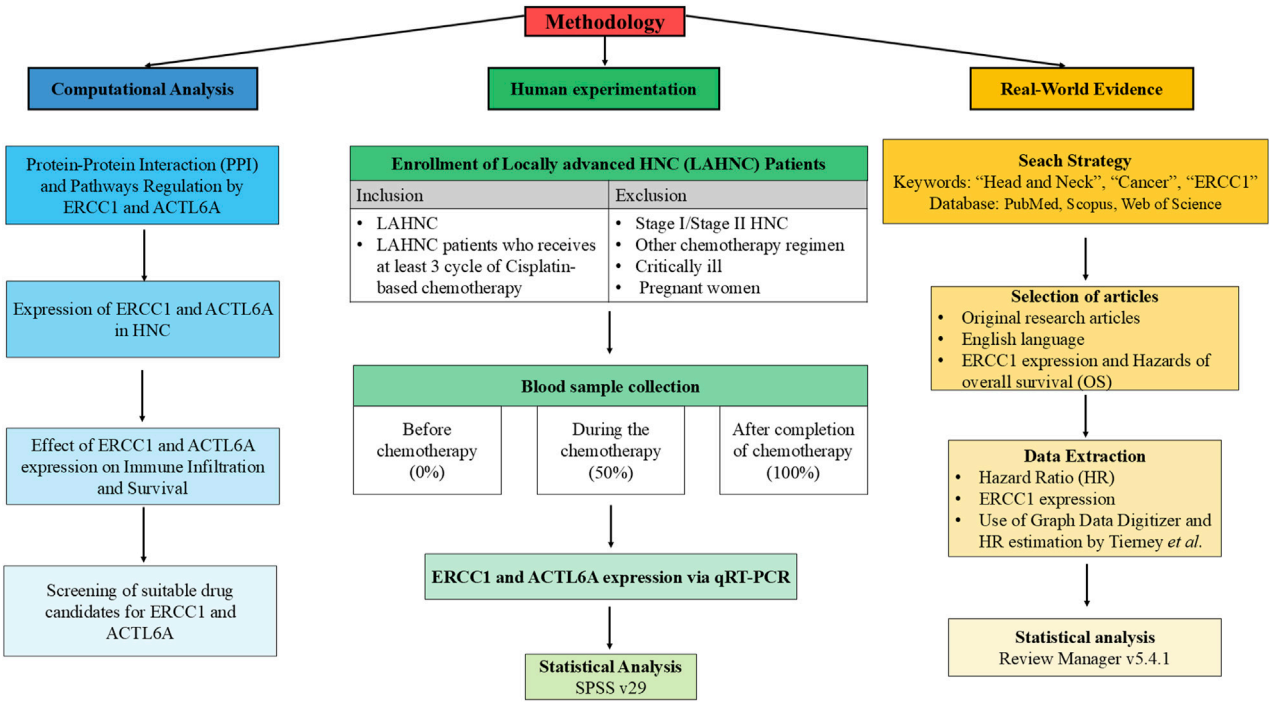

FIGURE 1
Detailed workflow showing integration of human experimentation with computational analysis and meta-analysis.

time-consuming, and ethically safe compared to using tissue samples that are difficult to obtain after therapy as this procedure may disturb the healing process or trigger recurrence, causing harm to the patient. Till date, there are no reported studies on detecting *ACTL6A* expression and very few studies on detecting *ERCC1* expression from blood samples. Furthermore, there are no available studies on characterizing the dose-dependent expressions of *ACTL6A* and *ERCC1* in HNC patients. Thus, to the best of our knowledge, this is the first study on Asian subjects to demonstrate the dose-dependent expressions of *ERCC1*/*ACTL6A* (zero cisplatin dose (zero cycle: 0 mg/m^2), after administration of 50% dose (3-cycle cisplatin: 90 mg/m^2), and after last cycle of cisplatin (4- or 5- or 6-cycle cisplatin: 120 or 150 or 180 mg/m^2)) and their correlations at these three phases. Additionally, computational analysis and meta-analysis were performed to investigate regulation of the repair pathways through *ACTL6A* and *ERCC1* interactions with the platinum resistance genes to understand their expression patterns and impacts on overall survival to establish *ACTL6A* and *ERCC1* as the chemoresistance genes. The detailed workflow of the present study is depicted in Figure 1.

2 Materials and methods

2.1 Computational analysis to investigate *ACTL6A* and *ERCC1* in cisplatin resistance

2.1.1 PPIs and pathway regulations of *ERCC1* and *ACTL6A*

In a previous study, we identified 21 genes that were regulated in the platinum drug resistance pathway (*ERCC1*, *MAPK1*, *MLH1*, *MDM2*, *PIK3CA*, *TP53*, *ERBB2*, *BAX*, *GSTM1*, *FAS*, *CASP8*, *FASLG*, *ABCC2*, *XIAP*, *BCL2*, *GSTP1*, *CDKN1A*, *TOP2A*, *CDKN2A*, *BRCA1*, and *BIRC2*) and five hub genes in cisplatin resistance (*CCND1*, *AXL*, *CDKN2A*, *TERT*, and *EZH2*), among which *ERCC1* was the only NER gene that was regulated for cisplatin resistance (Chaudhary et al., 2023). Furthermore, it has been reported that *ACTL6A* may contribute to DNA repair via the NER pathway, but its exact mechanism remains a mystery (Xiao et al., 2021). Thus, we investigated the interactions of *ACTL6A* with these 21 genes and the NER genes to clearly map the contributions of *ERCC1*/*ACTL6A* in DNA repair using STRING version 12.0 (https://string-db.org/). Furthermore, an unsupervised analysis was performed via K-means clustering to obtain similar protein clusters (https://string-db.org/) (Szklarczyk et al., 2023).

2.1.2 mRNA and tissue expressions of *ERCC1* and *ACTL6A* in HNC

Overexpression of the DNA repair genes could contribute to the development of cisplatin resistance. Thus, *ERCC1* and *ACTL6A* were investigated for their mRNA- and tissue-level expressions using the UALCAN database (https://ualcan.path.uab.edu/analysis.html) (Chandrashekar et al., 2022, 2017) and Human Protein Atlas (https://www.proteinatlas.org/; The Human Protein Atlas, 2024), respectively. Furthermore, the *ERCC1* and *ACTL6A* genes were queried as target inputs in the muTarget platform to identify the top-5 genes undergoing somatic mutations with prevalence rates of at least 1% among the HNC patients while significantly overexpressing *ERCC1* and *ACTL6A* (https://www.mutarget.com/; Nagy and Győrffy, 2021). Here, muTarget is a platform that links gene

expressions with the mutation statuses of the provided genes in solid cancers.

2.1.3 Effects of *ERCC1* and *ACTL6A* expressions on immune infiltration and survival

The infiltration of cancer cells is often linked to compromised tumor responses to anticancer agents, leading to poor clinical outcomes. Thus, the impacts of *ERCC1* and *ACTL6A* expressions on immune cell infiltration in HNC were predicted using TIMER 2.0 (http://timer.cistrome.org/; Li et al., 2020); further, their effects on the overall survival of LAHNC patients (stages III and IV) were investigated using the Kaplan–Meier plotter (https://kmplot.com/analysis/; Győrffy, 2024). The survival analysis was independent of therapy as the Kaplan–Meier plotter database does not have the option to restrict analysis based on treatment time framework, i.e., pre- and post-therapy.

2.1.4 Screening and binding of suitable drug candidates for *ERCC1* and *ACTL6A*

The DNA repair genes *ERCC1* and *ACTL6A* were screened for possible interactions with suitable FDA-approved or non-approved drug candidates using DGIbd (https://www.dgidb.org/; Cannon et al., 2024). Furthermore, the drug candidates were docked against their corresponding targets (*ERCC1* and *ACTL6A*) using Schrodinger version 2022-1 (https://www.schrodinger.com/) to investigate potential molecules other than platinum drugs that could downregulate *ERCC1* and *ACTL6A*. The protein structures of *ERCC1* (PDBID: 2A1I) and *ACTL6A* (PDBID: 9C4B) were obtained from protein data bank (https://www.rcsb.org/; RCSB PDB, 2024), and the structures of their corresponding drug candidates were obtained from PubChem database (https://pubchem.ncbi.nlm.nih.gov/; PubChem, 2024).

2.2 Human study for *ERCC1* and *ACTL6A* expressions among HNC patients

A prospective observational study was carried out at the Department of Oncology at a tertiary care hospital, where LAHNC patients above 18 years of age who were planning to undergo cisplatin-based CRT were enrolled after obtaining written informed consent. However, HNC patients with localized tumors (stage I/II) or those who were scheduled for other treatment modalities, critically ill patients, and pregnant women were excluded from the study. The study was initiated after obtaining approval from the Central Ethics Committee of the university (Ref. no. NU/CEC/2022/307 dated 21 September 2022 and revised on 31 January 2024 with Ref. no. NU/CEC/2024/526) and was also registered as a clinical trial in India (CTRI/2022/10/046142).

The sample size was calculated using the following formula for HNC prevalence of 30% (Dandekar et al., 2017; Prabhash et al., 2020) (P = 0.3) and marginal error of 9% (d = 0.09) at the 95% confidence interval (CI; $Z_{\alpha/2} = 1.96$). Thus, the total number of HNC patients was calculated to be 99.59 (rounded to 100). However, only 66.6% of the people in this population 100 belong to the LAHNC group (Mathur et al., 2020). Hence, the minimum sample size required for the study was 67 (N). The final sample size to be enrolled was estimated to be 77 after adjusting the study population for a 15% dropout rate.

$$N = \left(\frac{Z_{\alpha/2}}{d}\right)^2 P\,(1 - P)$$

2.2.1 Blood sampling and clinical data collection

All LAHNC patients who were enrolled in the study had been scheduled to receive CCRT, i.e., six cycles of cisplatin at 30 mg/m^2 weekly along with radiation of 60–70 Gy. After obtaining the informed consent and enrolling the participants, approximately 2 mL of peripheral blood sample was collected from each LAHNC patient in EDTA vacutainers and stored at −80°C. The patient blood was sampled at three different phases, i.e., zero cisplatin (before initiation of cisplatin-based CRT), after 50% of the planned cisplatin was administered (after third cycle of cisplatin therapy), and after completion or last cycle of cisplatin therapy. For patients who received only three cycles of cisplatin therapy, the third phase of blood sampling was conducted after completion of radiation therapy. Furthermore, we collected the demographic details and clinical characteristics of the patients.

2.2.2 Primer selection, verification, and confirmation for *ERCC1* and *ACTL6A* genes

The primers for the quantitative real-time polymerase chain reaction (qRT-PCR) were obtained from PrimerBank (https://pga.mgh.harvard.edu/primerbank/; PrimerBank-MGH-PGA, 2023) and verified with the protein-coding regions of the cDNA sequences for selected transcripts of *ERCC1* and *ACTL6A* from the Ensembl database (https://www.ensembl.org/; Ensembl genome browser, 2023). The amplicon size of the primer selected for *ERCC1* was 175 base pairs (forward: TTTGGCGACGTAATTCCCGAC; reverse: CCTGCTGGGGATCTTTCACA) and that for *ACTL6A* was 83 base pairs (forward: GACAGCATTTGCTAATGGTCGT; reverse: CATCGTGGACTGGAATTGCAG); further, the predesigned primer for β-actin (ACTB) had 249 base pairs (forward: CATGTACGTTGCTATCCAGGC; reverse: CTCCTTAATGTCACGCACGAT). The primers for *ERCC1* and *ACTL6A* along with the predesigned ACTB were confirmed experimentally via conventional PCR followed by DNA gel electrophoresis.

2.2.3 *ERCC1* and *ACTL6A* expressions via PCR

2.2.3.1 Total RNA extraction

The blood samples were centrifuged at 3,000 rpm to separate the plasma, followed by treatment of the blood cells with 1× RBC lysis solution. The mixture of blood cells and RBC lysis solution was left for 15–20 min to ensure RBC lysis and then centrifuged at 3,000 rpm to obtain Peripheral blood mononuclear cells (PBMC). The PBMC were used to extract the total RNA via the TRIzol reagent method using the RNAiso Plus kit (Takara, cat. no. 9109_v201904Da). The purity and concentration of the extracted RNA were confirmed via the nanodrop method.

2.2.3.2 cDNA synthesis

cDNA was synthesized from the total RNA using the PrimeScript™ RT reagent kit (Takara, cat. no. RR037A_v202008Da) in a thermal cycler (Prima 96, HiMedia, India), i.e., reverse transcription was performed at 55°C for 60 min,

followed by inactivation of reverse transcriptase at 87°C for 5 s and 4°C thereafter. The synthesized cDNA was stored at −20°C.

2.2.4 qRT-PCR

The expressions of *ERCC1* and *ACTL6A* were obtained using TB Green Premix EX Taq (Tli RNase H Plus, Takara, cat. no. RR820A_v201903Da) and quantified with the Applied Biosystems™ QuantStudio™ 6 RT-PCR System. The cDNA templates of the targets (*ERCC1* and *ACTL6A*) and reference (*ACTB*) were amplified using the QuantStudio™ system and SYBR Green PCR Master Mix fluorochrome dye. The qRT-PCR involved three stages: initial denaturation at 95°C for 3 min; PCR-based quantification at 95°C for 15 s followed by 60°C for 30 s and 72°C for 40 s (40 cycles); melting curve at 95°C for 15 s and 60°C for 1 min followed by 95°C for 15 s. The baseline and follow-up samples from a particular patient were processed together to avoid technical errors with the gene expressions. In addition, all samples were processed in duplicate along with RNAase-free water as the negative control.

3 Relative gene expressions and statistical analysis

The relative expressions of *ERCC1* and *ACTL6A* at baseline, after the third cycle of cisplatin therapy, and after the last cycle of cisplatin therapy were estimated by comparing the cycle threshold (Ct) value of a given sample for a particular gene of interest (GOI) (*ERCC1* and *ACTL6A*) with the Ct value of a given sample for the reference gene (*ACTB*). The relative expressions of the GOIs compared to the reference were calculated using the $2^{-\triangle CT}$ formula [$\triangle$CT = Ct (GOI) − Ct (ACTB)]. The patient data were analyzed using descriptive statistics (mean, standard deviation, frequency, percentage, and interquartile range) and were checked for normal distribution using the one-sample Kolmogorov–Smirnov test ($p < 0.05$). The *ERCC1* and *ACTL6A* expressions between the baseline and follow-ups were compared using the Friedman test. Furthermore, paired comparisons were performed via Wilcoxon's test. Correlations between *ERCC1* and *ACTL6A* expressions were examined using Spearman's rank test. All statistical analyses were performed using SPSS version 29 and figure was constructed using GraphPad Prism 8.0.2.

4 Real-world evidence for *ERCC1*/*ACTL6A* expressions and survival in HNC via meta-analysis

4.1 Research question and registration

Previous published meta-analyses by Xuelei et al. (2015) and Bišof et al. (2016) revealed that overexpression of *ERCC1* is the root cause of unfavorable overall survival outcomes (hazard ratio (HR): 2.14 and 1.95) among HNC patients, with the Asian population being the most affected victims (HR: 2.97 and 3.13, respectively). Thus, we conducted a further meta-analysis to update the predictive value of *ERCC1* on overall survival. This meta-analysis was registered prospectively with the International Prospective Register of Systematic Review (PROSPERO, 2024) under the title "Impact of ERCC1 expression on overall survival rate in head and neck cancer" with the registration ID CRD42024542859. However, data on the expression of *ACTL6A* and its impact on the survival of HNC patients are unavailable; thus, we could not conduct a meta-analysis for *ACTL6A*.

4.2 Search strategy

An electronic search was conducted for articles in the PubMed, Scopus, and Web of Science databases. The search strategy involved a combination of the following keywords: "Head and Neck," "ERCC1," "Cancer." Further, "Head and Neck," "ACTL6A," and "Cancer" were used as the keywords to retrieve articles related to the *ACTL6A* gene in HNC (see also the Supplementary File). In addition, the reference citations in these articles were manually checked for additional studies. Rayyan Software was used to import and manage the articles.

4.3 Eligibility criteria and selection process

The studies included in this meta-analysis/review were original research articles published in English language that evaluated the relationships between overall survival rate and expression of *ERCC1* or *ACTL6A* in HNC. After removing duplicate articles, the title and abstract were screened for eligibility by two independent authors. Any disagreements between these authors were resolved by a third author after a consensus discussion. Later, the selected studies were assessed for eligibility by two different authors based on the full text, and any disagreements were resolved by a third author. Articles without full text and ineligible articles were excluded from the study.

4.4 Data extraction

Data were extracted from eligible articles using the predesigned proforma containing the following information: author details, country, year of publication, sample size, gender, age, study design, disease details, TNCM/clinical staging, molecular technique used, *ERCC1* expression, and outcomes of the study. The data were extracted by two independent authors, and any disagreements were resolved by a third author. If the survival data were represented using the Kaplan–Meier curve, and then the relevant information was interpreted from the graph using Graph Data Digitizer 2.4. If the HR was not reported by the authors, then it was estimated using the method proposed by Tierney et al. (2007).

4.5 Statistical analysis

Review Manager software v5.4.1 (Cochrane Collaboration, Copenhagen, Denmark) was used to generate the forest plots, and the inverse variance method was used for pooled estimates. The outcome variables of all the included studies were represented in terms of the HR and 95% CI. The analyses were performed using RevMan calculator by incorporating the log(HR) with standard

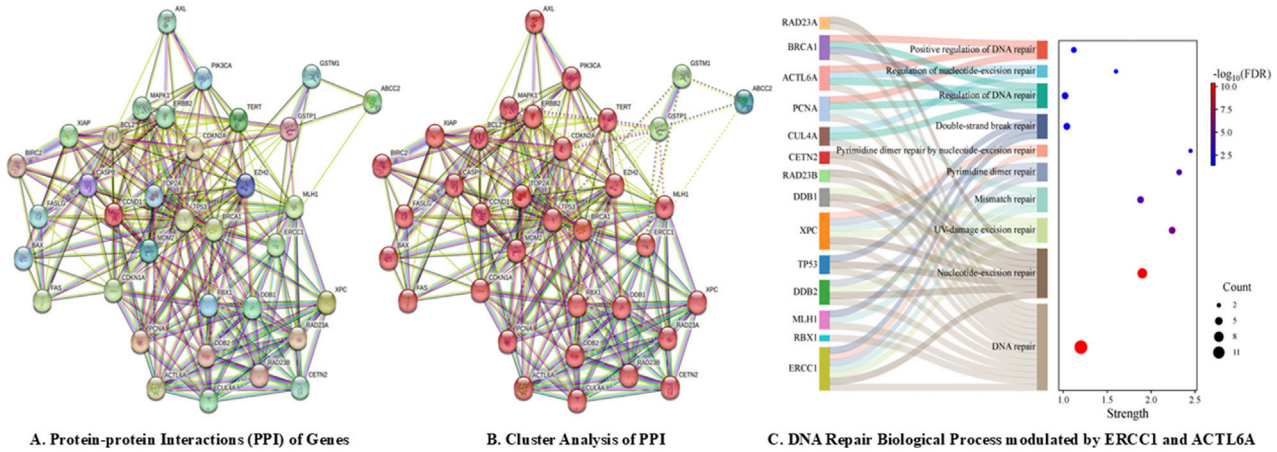

FIGURE 2
DNA repair pathways modulated by *ACTL6A* and *ERCC1* via computational analysis: **(A)** protein–protein interactions; **(B)** cluster analysis; **(C)** biological process modulations by *ERCC1* and *ACTL6A*.

error (SE), and the results were presented as HR with 95% CI. All results were presented graphically and numerically in the forest plot along with the weights imparted by the individual studies. The Higgins I^2 statistic and visual inspection were used to assess heterogenicity, and the percentage with *p*-value was used to represent interstudy variability. Both random and fixed effects were used; the fixed-effects model was used when the percentage of heterogenicity was $I^2 \leq 40\%$, whereas the random effects model was used when $I^2 > 40\%$. Furthermore, publication bias was assessed using funnel plots and Egger's regression test.

5 Results

5.1 Computational analysis to investigate cisplatin resistance in HNC via *ERCC1/ACTL6A*

5.1.1 PPIs associated with *ERCC1/ACTL6A* and enrichment analysis

A total of 35 genes were investigated for PPIs, including 21 genes for platinum drug resistance, *ACTL6A*, and eight genes for GGR-NER, with medium confidence (0.400); this revealed interactions between 30 nodes, resulting in a total of 260 edges at an average node degree of 14.9 and average local clustering coefficient of 0.737 (Figure 2A). The PPIs significantly enriched ($<1.0e^{-16}$) 177 biological process (BP), 17 cellular component (CC), and 15 molecular function (MF) terms of gene ontology along with four KEGG pathways that were modulated by *ERCC1* and/or *ACTL6A*. The *ACTL6A* gene was found to significantly modulate BPs such as DNA repair, regulation of DNA repair, positive regulation of DNA repair, and regulation of NER, whereas the *ERCC1* gene was found to modulate BPs like DNA repair, NER, UV damage excision repair, mismatch repair, pyrimidine dimer repair, pyrimidine dimer repair by NER, and double-strand break repair (Figure 2C). All these repair BPs were modulated via the PPIs of 14 identical genes belonging to the same cluster (red color), namely, *ACTL6A*, *ERCC1*, *PCNA*, *MLH1*, *BRCA1*, *TP53*, *XPC*, *CETN2*, *CUL4A*, *DDB1*, *DDB2*, *RAD23A*, *RAD23B*, and *RBX1* (Figure 2B). Additionally, the DNA repair and NER complexes were the CCs modulated by *ERCC1*. This shows that both *ERCC1* and *ACTL6A* are involved in DNA repair processes, particularly via the NER pathway.

5.1.2 mRNA and tissue expressions of *ERCC1* and *ACTL6A* in HNC

The median transcripts per million of *ERCC1* and *ACTL6A* were found to be significantly higher in primary tumors (64.801 and 71.98, respectively) than normal samples (46.256 and 30.826, respectively) (Figure 3A). Both *ERCC1* and *ACTL6A* were found to be overexpressed in advanced stages except stage III HNC patients (stage IV > stage II > stage III > stage I) (Figure 3B), particularly among African-American and Caucasian people compared to Asian patients. Furthermore, *ERCC1* was found to be overexpressed greatly among persons aged 61–80 years, followed by those in the age groups of 41–60 years, 81–100 years, and 21–40 years; however, *ACTL6A* was found to be overexpressed greatly among persons aged 41–60 years, followed by those in the age groups of 61–80 years, 21–40 years, and 81–100 years. Additionally, *ERCC1* is inconsistently expressed with advancing tumor grade (grade 3 > grade 2 > grade 4 > grade 1), whereas *ACTL6A* shows significant overexpression with the grade of tumor progression (grade 4 > grade 3 > grade 2 > grade 1) (see Supplementary Table S1 and Supplementary Figure S1). Thus, we can predict that both *ERCC1* and *ACTL6A* are upregulated in HNC patients, particularly in individuals with advanced stages and tumor grades and mostly in persons aged 40–80 years.

Furthermore, *ERCC1* and *ACTL6A* were found to show moderate and moderate-to-strong expressions, respectively. The immunohistochemistry (IHC) report of HNC tissue enclosed in HPA shows moderate expression of *ERCC1* at nuclear-level staining using antibodies, such as HPA029773, CAB004390, CAB072859, and CAB072860 (Figure 3B.I and Supplementary Figure S2). Furthermore, *ACTL6A* shows moderate-to-strong

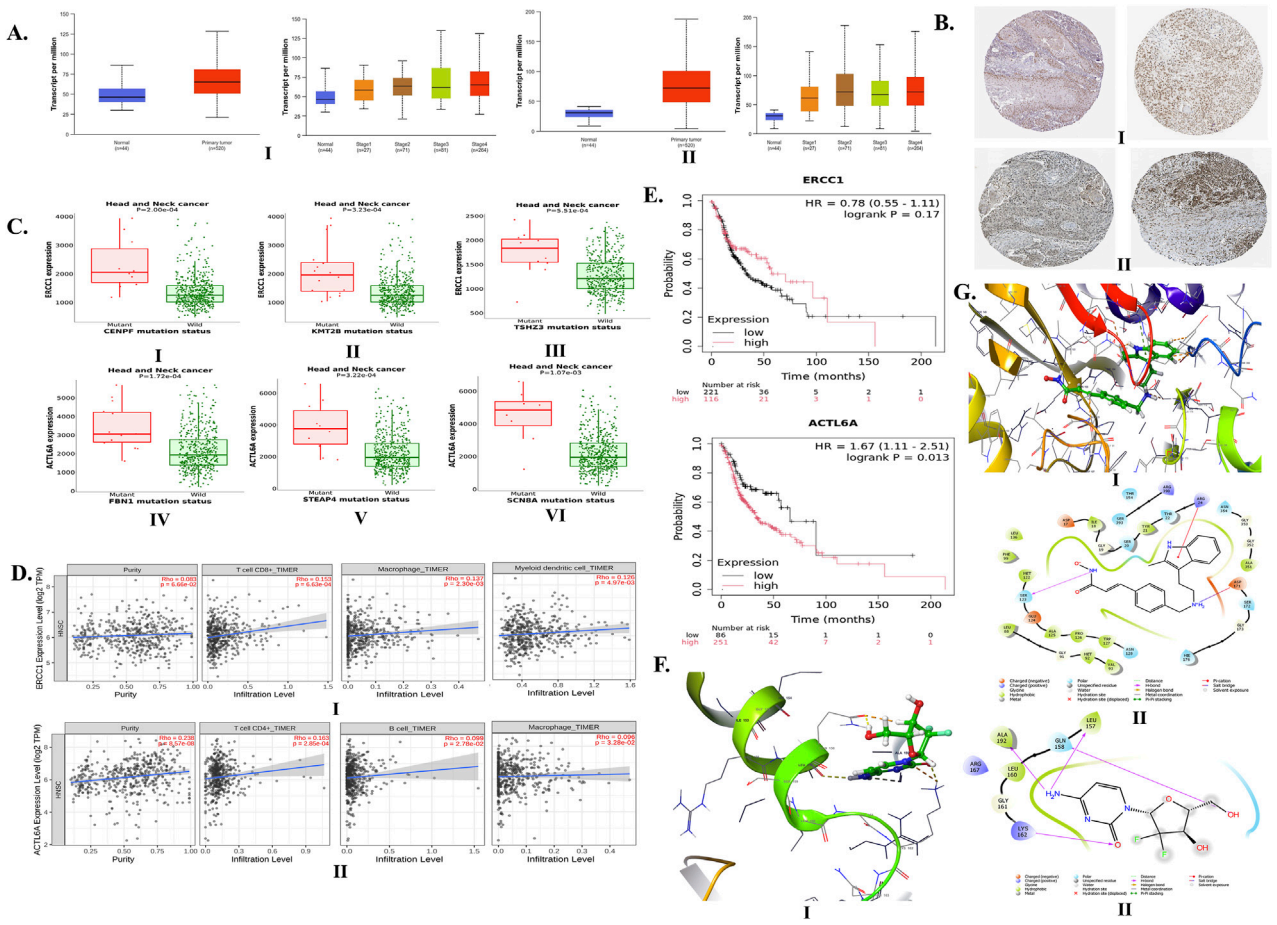

FIGURE 3
Expressions of *ERCC1* and *ACTL6A* in head and neck cancer (HNC) and their impacts on tumor infiltration and overall survival via computational analysis. **(A)** mRNA expressions of **(I)** *ERCC1* and **(II)** *ACTL6A* in tumor vs. normal samples based on stage of HNC. **(B)** Expressions of **(I)** *ERCC1* and **(II)** *ACTL6A* in tumor tissues via immunohistochemistry. **(C)** Gene mutations upregulating **(I–III)** *ERCC1* and **(IV–VI)** *ACTL6A* expressions. **(D)** Infiltration of **(I)** $CD8^+$ cells, macrophages, and myeloid dendritic cells by *ERCC1* expression and **(II)** $CD4^+$ cells, B cells, and macrophages by *ACTL6A* expression. **(E)** Impacts of *ERCC1* and *ACTL6A* expressions on overall survival. **(F)** **(I)** 3D and **(II)** 2D interactions of gemcitabine with *ERCC1*. **(G)** **(I)** 3D and **(II)** 2D interactions of panobinostat with *ACTL6A*.

expression at the nuclear- and cytoplasmic/membranous-nuclear-level staining using the CAB012188 antibody (Figure 3B.II, Supplementary Figure S2). These findings confirm the expressions of *ERCC1* and *ACTL6A* in various types of HNC tumor tissues. Moreover, there are certain mutations observed in HNC patients that can alter the expressions of *ERCC1* and *ACTL6A*. The top-5 genes undergoing somatic mutations with at least 1% prevalence rates contribute to the overexpressions of *ERCC1* (namely, *CASK*, *CENPF*, *KMT2B*, *TSHZ3*, and *DVL1*) and *ACTL6A* (namely, *FBN1*, *STEAP4*, *SCN8A*, *OR8H2*, and *CASZ1*) (Figure 3C, Supplementary Tables S2, S3, Supplementary Figures S3, S4).

5.1.3 Impacts of *ERCC1* and *ACTL6A* expressions on tumor cell infiltration and survival in HNC

The overexpressions of *ERCC1* and *ACTL6A* were found to significantly enhance the infiltration of $CD8^+$ T-cells, macrophages, dendritic cells, $CD4^+$ T-cells, and B-cells into HNC tumor cells (Figure 3D, Supplementary Figure S5). Overexpression of *ERCC1* was found to be linked with 22% less risk of death compared to reduced expression in HNC patients (HR: 0.78, $p = 0.17$), whereas overexpression of *ACTL6A* was found to be linked with 67% more risk of death among HNC patients (HR: 1.67, $p = 0.013$) (Figure 3E). Thus, computational analysis reveals that *ACTL6A* is a significant gene responsible for the poor survival of HNC patients.

5.1.4 Potential drug candidates and their binding affinities with *ERCC1* and *ACTL6A*

A total of 12 drug candidates, i.e., eight FDA-approved drugs (cyclosporine, carboplatin, cisplatin, 5-fluorouracil, doxorubicin hydrochloride, gemcitabine, paclitaxel, and thalidomide) and four drugs not approved by the FDA (staurosporine, herbimycin A, platinum, and platinum compound), were found to interact with the ERCC1 protein. Similarly, a total of four drug candidates (two FDA-approved drugs: panobinostat and cisplatin; two unapproved drugs: sphingosine-1-phosphate and sphingosylphosphorylcholine) were found to interact with the ACTL6A protein (Supplementary Table S4). In the case of cisplatin resistance, the predicted FDA-approved drug candidates other than platinum may be repurposed to downregulate both *ERCC1* and *ACTL6A* genes. Thus,

TABLE 1 Demographic details and clinical characteristics of the HNC patients in this study.

Parameters	Frequency	Percentage (%)
Gender		
Male	74	96.1
Female	3	3.90
Age Groups (52.88 ± 9.68 years)		
21–40 years	7	9.09
41–60 years	47	61.04
61–80 years	23	29.87
BMI Categories (19.39 ± 3.72)		
Overweight	5	6.49
Normal BMI	39	50.65
Underweight	33	42.86
Kuppuswamy Socioeconomic Class		
Lower Middle	30	38.96
Upper Lower	38	49.35
Upper Middle	9	11.69
Social Habits		
No habits	7	9.09
Alcohol consumption	45	58.44
Tobacco smoking	36	46.75
Tobacco chewing	30	38.96
Betel leaf or paan chewing	26	33.77
Areca nut or gutka chewing	26	33.77
Sharp Teeth Associated Injury		
Tongue bite	7	9.09
Cheek bite	5	6.49
Comorbidities		
No comorbidities	58	75.32
Hypertension	12	15.58
Diabetes mellitus	9	11.69
Cerebrovascular accident	4	5.19
Respiratory diseases: Asthma, COPD, and Old TB	2	2.60
Ischemic heart disease	1	1.30
Family History of Cancer		
No familial history of cancer	54	70.13
Patients with familial history of cancer	23	29.87
Breast	1	1.30
Breast and Brain	1	1.30
Hematological	3	3.90

(Continued on following page)

TABLE 1 (*Continued*) Demographic details and clinical characteristics of the HNC patients in this study.

Parameters	Frequency	Percentage (%)
HNC	13	16.88
HNC and Breast	1	1.30
Thyroid	1	1.30
Uterus	2	2.60
Brain	1	1.30
Histopathology		
Well differentiated (Grade 1)	27	35.06
Moderately differentiated (Grade 2)	43	55.84
Poorly differentiated (Grade 3)	7	9.09
8th Edition of the American Joint Committee on Cancer (AJCC) staging		
Stage III	16	20.78
Stage IV	61	79.22
Stage IVA	47	61.04
Stage IVB	14	18.18
Types of HNC		
Oral Cavity Cancer	40	51.95
Buccal mucosa cancer	13	16.88
Tongue cancer	18	23.38
Floor of the mouth	3	3.90
Gingivobuccal sulcus	1	1.30
Hard palate	1	1.30
Retromolar trigone	4	5.19
Laryngeal cancer	13	16.88
Supraglottic cancer	5	6.49
Aryepiglottic cancer	2	2.60
Epiglottic cancer	1	1.30
Vocal cord cancer	5	6.49
Hypopharynx cancer	11	14.29
Cricopharynx	2	2.60
Pyriform fossa	9	11.69
Oropharynx cancer	8	10.39
Base of tongue cancer	5	6.49
Soft palate	3	3.90
Cancer of unknown primary cause	3	3.90
Lymph node	2	2.60
Brachial cleft cyst	1	1.30
Nasopharynx cancer (Nasal cavity)	2	2.60
Treatment Modalities		

(Continued on following page)

TABLE 1 (*Continued*) Demographic details and clinical characteristics of the HNC patients in this study.

Parameters	Frequency	Percentage (%)
Total concurrent CRT (CCRT)	55	71.43
Concurrent CRT (CCRT)	46	59.74
CCRT with adjuvant chemotherapy	9	11.69
Surgery with adjuvant CCRT	22	28.57
Number of Cycles of Cisplatin Chemotherapy		
3	8	10.39
4	6	7.79
5	44	57.14
6	19	24.68
Radiation Dose		
60 Gy	17	22.08
66 Gy	43	55.84
70 Gy	17	22.08
Radiation Fraction		
30	23	29.87
33	37	48.05
35	17	22.08

gemcitabine (interaction score: 0.047) and paclitaxel (interaction score: 0.040) were found to have high interactions with *ERCC1*, whereas panobinostat (interaction score: 0.398) was found to interact with *ACTL6A*. From the molecular docking studies, we found that gemcitabine and panobinostat possessed higher binding affinities toward *ERCC1* and *ACTL6A* with binding energies of −3.707 kcal/mol (Figure 3F) and −4.198 kcal/mol (Figure 3G), respectively.

5.2 Human study for *ERCC1* and *ACTL6A* expressions among HNC patients

5.2.1 Demographic details and clinical characteristics of the HNC patients

A total of 77 LAHNC patients were enrolled in the study, of which 96.1% patients were men and 3.9% were women with a mean age of 52.88 ± 9.68 years. The majority of patients were in the age group of 41–60 years (61.04%), followed by 61–80 years (29.87%) and 21–40 years (9.09%). Nearly half of the enrolled patients (49.35%) were from the upper part of the lower socioeconomic class and had abnormal body mass index (BMI) values, i.e., they were underweight (42.86%) or overweight (6.49%). Most of the LAHNC patients (89.61%) had a history of social habits, such as drinking alcohol (58.44%), smoking tobacco (46.75%), or chewing tobacco (38.96%) or betel leaf (33.77%) or areca nut (33.77%). Approximately 16.88% of the patients reported both alcohol consumption and smoking. Furthermore, we observed that approximately 24.68% of the HNC patients had comorbidities, where hypertension (15.58%) and diabetes (11.69%) were the most prevalent types followed by cerebrovascular accidents (5.19%), respiratory diseases (2.60%), and ischemic heart disease (1.30%). We found that approximately 29.87% of patients had a history of cancer in their family. Surprisingly, HNC was the most commonly reported type of cancer (15.58%) in the family histories, which was attributed to prevailing social habits in their families (Table 1).

Clinically, the majority of the enrolled LAHNC patients belonged to grade 2 (55.84%) followed by grades 1 and 3 and were diagnosed at stage IV (79.22%) followed by stage III (20.78%). Approximately half of the HNC patients were diagnosed with carcinoma of the oral cavity (51.95%), followed by laryngeal cancer (16.88%), hypopharyngeal cancer (14.29%), oropharyngeal cancer (10.39%), cancer of unknown primary cause (3.90%), and nasopharyngeal cancer (2.60%). CCRT was the most popular choice of treatment (55.84%), followed by surgery with adjuvant CRT (32.47%) and CCRT with adjuvant chemotherapy (11.69%). All patients in the study cohort were scheduled to undergo six cycles of cisplatin therapy. However, approximately half of the patients received five cycles of cisplatin (57.14%), followed by six cycles (24.68%), three cycles (10.39%), and four cycles (7.79%). The dosage for radiation therapy ranged from

TABLE 2 Comparison of *ERCC1* and *ACTL6A* expressions across chemoradiotherapy.

Parameters	Median expressions of genes						
Genes	0% CRT	50% CRT	100% CRT	*p*-value (0% vs. 50%)	*p*-value (50% vs. 100%)	*p*-value (0% vs. 100%)	Overall *p*-value
ERCC1	0.14 (0.05, 0.41)	0.19 (0.06, 0.44)	0.23 (0.08, 0.68)	0.301	0.001**	0.011*	p < 0.001***
ACTL6A	4.77 (1.92, 12.065)	3.87 (1.00, 8.81)	5.43 (1.535, 9.26)	0.028*	0.459	0.362	0.729
Sociodemographic/ Clinical	Median Expression of *ERCC1* and *ACTL6A*						
Age Groups							
21–40 years *ERCC1*	0.12 (0.04, 0.36)	0.19 (0.08, 0.23)	0.12 (0.07, 0.32)	0.397	0.672	0.499	0.651
21–40 years *ACTL6A*	11.89 (1.12, 21.88)	6.39 (0.48, 9.82)	4.71 (1.42, 14.57)	0.128	0.612	0.499	0.565
41–60 years *ERCC1*	0.22 (0.05, 0.6)	0.17 (0.06, 0.48)	0.34 (0.13, 0.1.05)	0.782	0.005*	0.077	0.005*
41–60 years *ACTL6A*	4.49 (2.21, 11.73)	5.93 (2.61, 9.07)	6.78 (2.53, 9.95)	0.800	0.582	0.691	0.587
61–80 years *ERCC1*	0.01 (0.05, 0.32)	0.19 (0.04, 0.35)	0.21 (0.08, 0.37)	0.217	0.079	0.068	0.009*
61–80 years *ACTL6A*	4.76 (1.42, 11.98)	1.14 (0.77, 6.05)	2.06 (0.85, 7.16)	0.007	0.783	0.066	0.199
BMI							
Underweight *ERCC1*	0.11 (0.05, 0.385)	0.12 (0.06, 0.25)	0.2 (0.075, 0.56)	0.543	0.031*	0.136	0.029*
Underweight *ACTL6A*	5.19 (1.23, 11.55)	3.15 (0.81, 7.15)	4.37 (1.54, 8.90)	0.183	0.432	0.357	0.754
Normal *ERCC1*	0.15 (0.05, 0.6)	0.20 (0.06, 0.44)	0.26 (0.12, 0.88)	0.619	0.033*	0.121	0.021*
Normal *ACTL6A*	4.05 (2.14, 11.89)	4.25 (1.05, 8.84)	5.84 (1.17, 9.95)	0.264	0.596	0.967	0.975
Overweight *ERCC1*	0.27 (0.04, 0.345)	0.19 (0.085, 1.32)	0.51 (0.21, 2.975)	0.225	0.08	0.068	0.076
Overweight *ACTL6A*	21.59 (7.02, 25.62)	9.04 (5.89, 12.75)	6.78 (4.89, 12.89)	0.080	0.686	0.225	0.549
Social Habits							
No habits *ERCC1*	0.25 (0.09, 0.40)	0.10 (0.04, 0.14)	0.10 (0.05, 0.31)	0.236	0.610	0.917	0.772
Yes habits *ERCC1*	0.13 (0.05, 0.41)	0.19 (0.06, 0.45)	0.26 (0.097, 0.89)	0.153	0.001**	0.007*	p < 0.001***
No habits *ACTL6A*	11.73 (2.78, 21.59)	3.10 (1.14, 9.04)	8.37 (4.46, 10.63)	0.063	0.176	1.00	0.565
Yes habits *ACTL6A*	4.62 (1.67, 11.95)	3.88 (.937, 8.79)	5.41 (1.38, 9.14)	0.089	0.652	0.366	0.876
No smoking *ERCC1*	0.26 (0.085, 0.96)	0.17 (0.06, 0.44)	0.21 (0.095, 1.09)	0.559	0.003*	0.340	0.032
Smoking *ERCC1*	0.095 (0.05, 0.25)	0.195 (0.07, 0.44)	0.265 (0.08, 0.62)	0.016*	0.087	0.003*	0.001**
No Smoking *ACTL6A*	6.36 (2.66, 14.13)	4.87 (0.95, 9.06)	7.04 (3.19, 10.60)	0.013*	0.390	0.496	0.552
Smoking *ACTL6A*	3.68 (1.33, 9.71	3.315 (1.16, 7.62)	4.695 (1.09, 7.93)	0.530	0.888	0.599	1.000
No Alcohol consumption *ERCC1*	0.24 (0.09, 0.64)	0.11 (0.04, 0.38)	0.21 (0.07, 0.67)	0.206	0.014*	0.742	0.103
Alcohol consumption ERCC1	0.11 (0.04, 0.30)	0.19 (0.09, 0.30)	0.32 (0.125, 0.78)	0.011*	0.024*	0.002*	p < 0.001***
No alcohol consumption *ACTL6A*	4.27 (1.49, 11.52)	2.75 (0.84, 7.30)	5.26 (1.17, 9.82)	0.166	0.176	0.601	0.680
Alcohol consumption *ACTL6A*	6.27 (2.44, 13.72)	5.93 (1.48, 9.27)	5.59 (1.95, 8.17)	0.079	0.906	0.09	0.766
No tobacco chewing *ERCC1*	0.11 (0.04, 0.26)	0.19 (0.06, 0.29)	0.25 (0.08, 0.61)	0.137	0.002*	0.006*	p < 0.001***
Tobacco chewing *ERCC1*	0.28 (0.067, 0.89)	0.19 (0.06, 0.78)	0.22 (0.13, 1.17)	0.982	0.094	0.447	0.126
No tobacco chewing *ACTL6A*	4.05 (1.57, 11.98)	3.10 (1.05, 7.49)	5.15 (1.17, 8.78)	0.030*	0.174	0.608	0.722
Tobacco chewing *ACTL6A*	6.01 (2.54, 12.54)	6.74 (0.82, 11.45)	6.97 (1.89, 11.38)	0.441	0.586	0.417	0.905
No betel leaf chewing *ERCC1*	0.14 (0.05, 0.41)	0.19 (0.06, 0.29)	0.22 (0.08, 0.51)	0.927	0.007*	0.176	0.009*
Betel leaf chewing *ERCC1*	0.13 (0.037, .0397)	0.205 (0.06, 0.72)	0.44 (0.115, 1.32)	0.092	0.029*	0.014*	0.002*
No Betel leaf chewing *ACTL6A*	4.77 (1.41, 11.73)	3.77 (1.14, 8.42)	4.46 (1.17, 8.26)	0.033*	0.940	0.275	0.662
Betel leaf chewing *ACTL6A*	4.8 (3.21, 13.54)	6.1 (0.86, 9.04)	6.91 (3.53, 14.87)	0.439	0.382	0.929	0.832

(Continued on following page)

TABLE 2 (*Continued*) Comparison of *ERCC1* and *ACTL6A* expressions across chemoradiotherapy.

Sociodemographic/ Clinical	Median Expression of *ERCC1* and *ACTL6A*						
No areca nut or gutka chewing *ERCC1*	0.14 (0.05, 0.40)	0.17 (0.06, 0.44)	0.31 (0.14, 0.88)	0.234	0.010*	0.008*	p < 0.001***
Areca nut or gutka chewing *ERCC1*	0.12 (0.047, 0.537)	0.20 (0.045, 0.44)	0.195 (0.07, 0.61)	0.957	0.020*	0.493	0.137
No areca nut or gutka chewing *ACTL6A*	7.37 (2.68, 13.73)	5.50 (1.14, 9.47)	5.43 (1.29, 9.02)	0.034*	0.593	0.058	0.494
Areca nut or gutka chewing *ACTL6A*	3.26 (1.22, 6.61)	2.99 (0.85, 7.49)	5.49 (1.59, 11.56)	0.657	0.035*	0.209	0.173
Comorbidity							
No comorbidity *ERCC1*	0.13 (0.05, 0.465)	0.19 (0.077, 0.48)	0.225 (0.09, 0.97)	0.227	0.006*	0.038*	0.003*
No comorbidity *ACTL6A*	3.83 (1.42, 12.49)	3.82 (1.06, 8.93)	5.72 (1.59, 9.61)	0.277	0.619	0.642	0.852
Presence of comorbidity *ERCC1*	0.15 (0.03, 0.32)	0.12 (0.03, 0.23)	0.31 (0.05, 0.51)	0.948	0.036*	0.121	0.011*
Presence of comorbidity *ACTL6A*	5.19 (3.76, 11.73)	3.89 (0.96, 7.50)	5.33 (1.29, 8.27)	0.027*	0.601	0.398	0.229
Stages							
Stage III *ERCC1*	0.245 (0.08, 1.27)	0.21 (0.045, 0.43)	0.19 (0.08, 0.55)	0.535	0.211	0.623	0.867
Stage III *ACTL6A*	2.71 (0.90, 11.91)	3.83 (1.33, 8.54)	5.62 (3.47, 14.31)	0.756	0.148	0.469	0.269
Stage IV *ERCC1*	0.12 (0.05, 0.395)	0.19 (0.06, 0.435)	0.27 (0.095, 0.78)	0.153	0.002*	0.001**	p < 0.001***
Stage IV *ACTL6A*	5.11 (2.44, 12.82)	3.87 (.915, 8.91)	5.43 (1.35, 8.90)	0.027*	0.947	0.156	0.452
Histopathology							
Poorly differentiated *ERCC1*	0.29 (0.09, 1.15)	0.26 (0.14, 0.84)	0.25 (0.10, 1.57)	0.672	0.446	0.866	0.651
Poorly differentiated *ACTL6A*	2.68 (1.41, 7.73)	4.25 (2.89, 8.89)	3.85 (1.15, 8.78)	0.612	0.866	0.398	0.368
Moderately differentiated *ERCC1*	0.12 (0.05, 0.36)	0.15 (0.06, 0.40)	0.21 (0.09, 0.95)	0.974	0.001**	0.053	0.001**
Moderately differentiated *ACTL6A*	6.27 (2.93, 13.49)	3.15 (0.94, 8.78)	5.89 (1.93, 9.02)	0.001**	0.358	0.098	0.108
Well differentiated *ERCC1*	0.14 (0.04, 0.42)	0.20 (0.06, 0.43)	0.27 (0.08, 0.68)	0.082	0.237	0.038*	0.030*
Well differentiated *ACTL6A*	4.05 (1.25, 13.7)	6.05 (.75, 8.84)	5.18 (1.17, 13.90)	0.829	1.00	0.848	0.772
Type of HNC							
Oral cavity cancer *ERCC1*	0.13 (0.05, 0.69)	0.185 (0.06, 0.44)	0.29 (0.12, 1.03)	0.632	0.017*	0.050*	0.007*
Oral cavity cancer *ACTL6A*	7.57 (2.48, 13.72)	6.43 (1.97, 11.03)	7.33 (1.45, 14.40)	0.162	0.707	0.364	0.928
Laryngeal cancer *ERCC1*	0.22 (0.04, 0.36)	0.15 (0.05, 0.34)	0.22 (0.05, 0.43)	0.506	0.208	0.649	0.146
Laryngeal cancer *ERCC1*	4.77 (1.32, 9.55)	2.84 (0.94, 7.59)	5.33 (2.39, 6.94)	0.249	0.753	0.701	0.584
Hypopharyngeal cancer *ERCC1*	0.09 (0.04, 0.36)	0.10 (0.06, 0.70)	0.15 (0.06, 1.14)	0.046*	0.333	0.139	0.027*
Hypopharyngeal cancer *ERCC1*	3.38 (0.66, 7.36)	5.50 (0.80, 7.50)	4.46 (0.80, 8.78)	0.859	0.721	0.929	0.368
Oropharyngeal cancer *ERCC1*	0.085 (0.027, 0.24)	0.24 (0.19, 0.28)	0.20 (0.11, 0.76)	0.123	0.345	0.161	0.079
Oropharyngeal cancer *ACTL6A*	5.02 (2.33, 10.92)	1.49 (0.74, 2.64)	5.49 (1.75, 7.97)	0.123	0.017*	0.674	0.223
CUP *ERCC1*	0.39 (0.23, 0.42)	0.35 (0.02, 0.39)	0.62 (0.27, 0.68)	0.593	0.285	0.285	0.717
CUP *ACTL6A*	4.05 (3.03, 6.36)	1.75 (0.5, 8.84)	3.69 (1.09, 20.88)	0.593	0.285	1.00	0.717
Nasopharyngeal cancer *ERCC1*	0.91 (0.20, 1.16)	0.44 (0.03, 0.63)	0.81 (0.37, 1.17)	0.655	0.180	0.655	0.607
Nasopharyngeal cancer *ERCC1*	7.07 (2.085, 8.51)	6.88 (3.65, 6.67)	9.46 (.86, 13.33)	0.655	0.655	0.655	1.000
Therapy							
CCRT *ERCC1*	0.12 (0.05, 0.39)	0.19 (0.06, 0.29)	0.21 (0.09, 0.51)	0.418	0.010*	0.071	0.003*
CCRT *ACTL6A*	4.77 (1.71, 11.98)	3.25 (0.84, 7.66)	5.33 (1.42, 8.37)	0.053*	0.639	0.135	0.608
Surgery plus adjuvant CCRT *ERCC1*	0.165 (0.05, 0.465)	0.195 (0.057, 0.52)	0.345 (0.080, 1.34)	0.490	0.032*	0.044*	0.027*
Surgery plus adjuvant CCRT *ACTL6A*	4.90 (1.92, 13.59)	5.03 (2.59, 9.26)	7.40 (1.74, 15.84)	0.306	0.661	0.465	0.580

(Continued on following page)

TABLE 2 (*Continued*) Comparison of *ERCC1* and *ACTL6A* expressions across chemoradiotherapy.

Sociodemographic/ Clinical	Median Expression of *ERCC1* and *ACTL6A*						
Cycles of chemotherapy							
3 cycles *ERCC1*	0.185 (0.06, 0.38)	0.15 (0.075, 0.87)	0.29 (0.22, 1.88)	0.779	0.025*	0.233	0.093
3 cycles *ACTL6A*	3.89 (0.94, 8.59)	2.57 (0.80, 6.44)	8.75 (1.91, 13.9)	0.401	0.069	0.674	0.417
4 cycles *ERCC1*	0.105 (0.07, 0.28)	0.145 (0.05, 2.83)	0.21 (0.082, 1.85)	0.345	0.6	0.463	0.607
4 cycles *ACTL6A*	1.31 (1.16,12.60)	4.96 (1.59, 16.10)	8.18 (5.86, 9.23)	0.917	0.463	0.345	0.607
5 cycles *ERCC1*	0.14 (0.05, 0.55)	0.19 (0.053, 0.42)	0.29 (0.097, 0.67)	0.741	0.005*	0.083	0.007*
5 cycles *ACTL6A*	4.94 (1.82, 13.2)	4.38 (1.23, 9.36)	5.27 (1.38, 7.66)	0.327	0.462	0.143	0.853
6 cycles *ERCC1*	0.22 (0.03, 0.40)	0.17 (0.06, 0.44)	0.13 (0.07, 1.14)	0.354	0.176	0.212	0.055
6 cycles *ACTL6A*	5.75 (3.38,13.49)	4.25 (0.94,7.49)	5.18 (1.10,15.78)	0.022*	0.711	0.778	0.698

60 to 70 Gy and was administered in 30–35 fractions. The demographics and clinical characteristics of the LAHNC patients are depicted in Table 1.

5.2.2 *ERCC1* and *ACTL6A* expressions from peripheral blood samples via qPCR

Considering the expression of the reference gene as 1 (with >1 being high expression and <1 being low expression), *ERCC1* was highly expressed among 14.29% patients out of the total of 77 HNC patients while 85.71% of patients showed low expressions compared to the baseline. Furthermore, 9.09% and 20.78% of patients were observed to have higher expressions of *ERCC1* after 50% CCRT and 100% CCRT, respectively. Similarly, *ACTL6A* was highly expressed in 88.31% of the patients while 11.69% of the patients had low expressions compared to the baseline. After administration of 50% and 100% CCRT dosing, *ACTL6A* expressions were found to be highly expressed among 75.32% and 84.42% of the patients, respectively (Supplementary Table S5). This shows that cisplatin-based CCRT initially decreases the expressions of *ERCC1* (14.29%–9.09%) and *ACTL6A* (88.31%–75.32%) among HNC patients via initial response to therapy, whereas the expressions of *ERCC1* (9.09%–20.78%) and *ACTL6A* (75.32%–84. 42%) increase later to confer possible resistance to cisplatin therapy.

Comparative analyses on the impacts of cisplatin-based CCRT on the gene expressions showed that the overall median expression of *ERCC1* significantly increased ($p < 0.001$) by 1.64-fold compared to the baseline (from 0.14 to 0.19 and 0.23), signifying that *ERCC1* could potentially be involved in DNA repair (Table 2 and Figure 4.I). Similarly, the median expression of *ACTL6A* significantly decreased by 0.81-fold (from 4.77 to 3.87) after the initial three cycles of CCRT but later increased by 1.14-fold (from 3.87 to 5.43), showing the ability of *ACTL6A* to bounce back and mediate DNA repair (Table 2 and Figure 4.II). Furthermore, the subgroup analysis of variables showed that patients with advanced ages (40–80 years), advanced stages (stage IV), highly differentiated tumors (grades 1 and 2), low BMIs (underweight/normal), social habits (tobacco smoking, alcohol consumption, betel leaf chewing), oral cavity cancers, and hypopharyngeal cancer who received CCRT alone or five cycles of cisplatin are at high risk of developing ERCC1-mediated cisplatin resistance as ERCC1 was found to be significantly increased in these patients. In contrast, patients with no history of tobacco use or betel leaf chewing also showed significant increases in *ERCC1* expressions. Interestingly, we observed that *ACTL6A* expressions were significantly lower in patients with no history of tobacco smoking, alcohol consumption, or tobacco/betel leaf/areca nut/gutka chewing (Table 2). This indicates that patients with a history of social habits may be at a greater risk of developing chemoresistance to CCRT than patients without such history. Additionally, correlation analysis did not indicate any correlation in the baseline expressions of *ERCC1* and *ACTL6A* ($\rho = 0.201$, $p = 0.08$). However, the expressions of these genes were significantly ($\rho = 0.331$, $p = 0.003$) and marginally ($\rho = 0.215$, $p = 0.060$) correlated after receiving 50% and 100% cisplatin-based CCRT, indicating that *ACTL6A* could indirectly influence DNA repair via the NER pathways.

5.3 Real-world evidence for *ERCC1*/*ACTL6A* expressions and survival in HNC via meta-analysis

A total of 266 articles related to *ERCC1* and HNC were obtained by searching the three databases, of which only 12 articles met the criteria for meta-analysis (Supplementary Figure S6). Out of these 12 studies, only four were conducted prospectively while the remaining eight were conducted retrospectively. The aggregate sample size from all included studies was 2,041, of which 1,810 samples (high *ERCC1* expression: 911 patients, low *ERCC1* expression: 899 patients) were in our analysis (Table 3). Based on the random effects analysis of the pooled data of the 1,810 samples, we found that *ERCC1* expression was linked to poor overall survival among HNC patients, i.e., overexpression of the *ERCC1* gene significantly increased the risk of mortality among HNC patients by 82% (HR: 1.82, 95% CI: 1.26–2.63, $p = 0.0001$) compared to patients who had low expressions of *ERCC1*. However, the analysis showed moderate heterogenicity (X^2: 26.77, I^2: 56%, $p = 0.0005$) (Figure 5A). Subgroup analysis of the pooled data also showed that high *ERCC1* expression was significantly linked to poor survival rate among Asians (HR: 1.73, 95% CI: 1.16–2.59, $p = 0.007$) (Figure 5B). Additionally, the funnel plot of the pooled data showed symmetricity with an Egger regression coefficient of −0.152

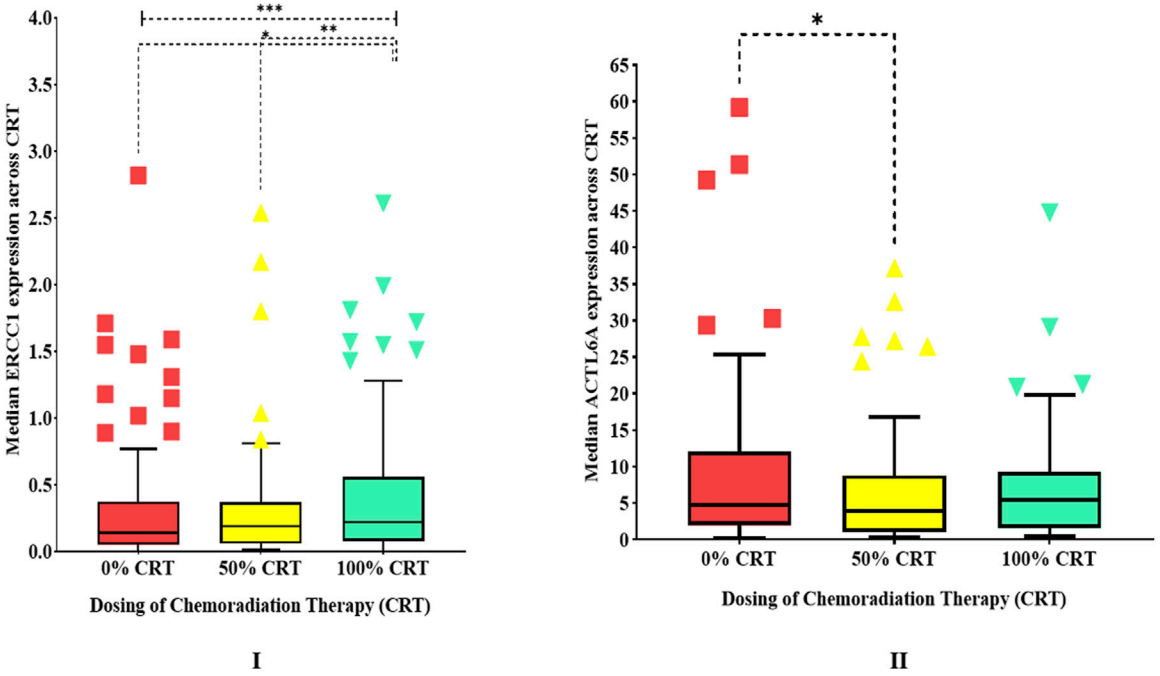

FIGURE 4
Human experimentation results showing box plots of **(I)** *ERCC1* expressions (outliers with median expressions >4 have been removed) and **(II)** *ACTL6A* expressions over the duration of chemoradiotherapy.

($p = 0.603$, 95% CI: −0.783 to 0.479), suggesting no publication bias. A total of 13 articles were identified from the three databases for *ACTL6A* and its association with HNC, of which only four articles were found to have the necessary information; however, none of these articles contained information on *ACTL6A* expression and its impact on survival. Thus, we were unable to conduct a meta-analysis for the *ACTL6A* gene.

6 Discussion

The increases in the median expressions of *ERCC1* and *ACTL6A* before and after CCRT as well as their associations with the poor overall survival outcomes in HNC patients (revealed by integrating computational analysis with meta-analysis) in the present study predict the chemoresistance of genotoxic regimens like cisplatin-based CCRT as these genes are reported to mediate DNA repair via the NER and/or SWI/SNF pathways (Figure 6). Sociodemographically, our findings are consistent with recent epidemiological studies from north India by Badola et al. (2023) and Chauhan et al. (2022), who reported that HNC is more prevalent in men than women, i.e., 87% vs. 13% and 89.4% vs. 10.6%, respectively. Furthermore, Chauhan et al. (2022) and a study on south Indians by SathiyaPriya et al. (2024) observed that nearly half of the study population (48% and 51%, respectively) was aged 40–60 years; in contrast to our study, Badola et al. (2023) and Bagal et al. (2023) found that most of the HNC patients were above 60 years of age followed by those aged 40–60 years. Furthermore, the socioeconomic classes and social habits of the patients in our study resemble those reported by SathiyaPriya et al. (2024), where most of the HNC patients were from the lower middle (62.3%) or lower (37.7%) socioeconomic class and were most commonly associated with tobacco smoking (47.6%) and alcohol consumption (42.4%) followed by tobacco chewing (30.6%) with betel leaf (27.3%) or areca nut (3.3%). Sharp teeth and teeth-mediated injuries to the oral mucosa or tongue have been infrequently linked to cancer of the oral cavity. Lateral tongue carcinoma (odds ratio (OR): 9.1) has been reported as a teeth-mediated injury (Singhvi et al., 2017), while another study reported that lesions due to trauma (OR: 4.5) were observed to be higher among oral cancer patients than lesions in the control group (Piemonte et al., 2018).

Clinically, a significant proportion of the patients in our study were underweight, so we hypothesize that low BMI may be associated with HNC occurrence; this is also supported by the findings from a Korean study, where the incidence of HNC was observed to be higher among underweight individuals (HR: 1.32) than normal weight and overweight patients (HR: 0.89). Furthermore, it was noted that tobacco smoking (HR: 1.448) and alcohol drinking (HR: 1.448) along with low BMI could impose a significantly higher ($p < 0.05$) risk of developing HNC (Kim et al., 2022). A study by Eytan et al. (2019) among 10,524 HNC patients in the United States showed that hypertension, hyperlipidemia, chronic obstructive pulmonary disease, and diabetes were the most common comorbidities at the time of diagnosis, which is consistent with the conditions among our population. Although HNC incidence is not believed to depend on a family history of cancer, we observed that

TABLE 3 Characteristics of all the studies included in the meta-analysis.

S. No.	Author Year	Country Continent	Sample size 2041–231 = 1810	Study Design	Cancer site	Stages	Assay	High vs. low *ERCC1* expression	HR	95% CI	*p*-value	Data extraction model
1	Liang et al. (2015)	China Asia	76 (M:59, F:17)	P	Nasopharynx	III, IVA	IHC	32 (42.1%) vs. 44 (57.89%)	1.43	0.49–4.16	-	KM survival curve
2	Ciaparrone et al. (2015)	Italy Europe	48 (M:39, F:9)	R	Head/Neck	III–IVB	IHC	36 (75%) vs. 12 (25%)	9.53	1.27–71.35	0.028	Multivariate
3	Lu et al. (2017)	China Asia	334 (M:244, F:90)	R	Nasopharynx	I–IVB	IHC	118 (35.32%) vs. 216 (64.7%)	2.65	1.16–6.05	-	KM survival curve
4	Xu et al. (2017)	China Asia	201 (M:132, F:69)	P	Nasopharynx	III–IV	IHC	136 (56.6%) vs. 65 (76.9%)	5.582	1.23–25.27	0.026	Multivariate KM survival curve
5	An et al. (2017)	Korea Asia	204 (M:173, F:31)	R	Head/Neck	I–IV	IHC	136 (66.66%) vs. 68 (33.33%)	1	0.52–1.93	0.99	Multivariate KM survival curve
6	Prochnow et al. (2019)	Germany Europe	453 (159 patients excluded) (M:335, F:118)	R	Head/Neck	I–III	IHC	135 (45.92%) vs. 159 (54.08%)	1.85	1.03–3.35	-	KM survival curve
7	Gong et al. (2019)	China Asia	156 (67 patients excluded) (M:87, F:69)	R	Oral cavity	III, IVA	IHC	41 (22.4%) vs. 48 (84.7%)	5.61	2.51–12.53	-	KM survival curve
8	Raturi et al. (2020)	India Asia	98 (M:98)	P	Larynx	III–IVB	RT-PCR	49 (50%) vs. 49 (50%)	1.26	0.73–2.20	-	KM survival curve
9	Aksoy et al. (2019)	Turkey Asia	33 (5 patients excluded) (M:24, F:9)	R	Nasopharynx	II–IVB	IHC	15 (53.57%) vs. 13 (46.43%)	1.63	0.40–6.68	-	KM survival curve
10	Chitapanarux et al. (2020)	Thailand Asia	262 (M:183, F:79)	R	Nasopharynx	I–IV	IHC	135 (51.52%) vs. 127 (48.48%)	1.08	0.79–1.47	0.647	Multivariate KM survival curve
11	Wang et al. (2021)	Taiwan Asia	98 (M:92, F:6)	R	Oral cavity	I–IV	IHC	58 (59.18%) vs. 40 (40.82%)	1.06	0.45–2.50	0.9	Multivariate KM survival curve
12	Hua et al. (2022)	China Asia	78 (M:59, F:19)	P	Nasopharynx	II	RT-PCR	20 (25.6%) vs. 58 (74.4%)	4.59	0.65–32.60	-	KM survival curve

Note: M: male, F: female, P: prospective, R: retrospective, IHC: immunohistochemistry, RT-PCR: real-time polymerase chain reaction, HR: hazard ratio, KM: Kaplan–Meier. A total of 231 patients were excluded from the analysis because Prochnow et al. and Aksoy et al. did not perform *ERCC1* expression analyses for 159 and 5 patients, respectively, whereas Gong et al. compared *ERCC1* low vs. high for only 89 patients.

10.3389/fphar.2025.1541987

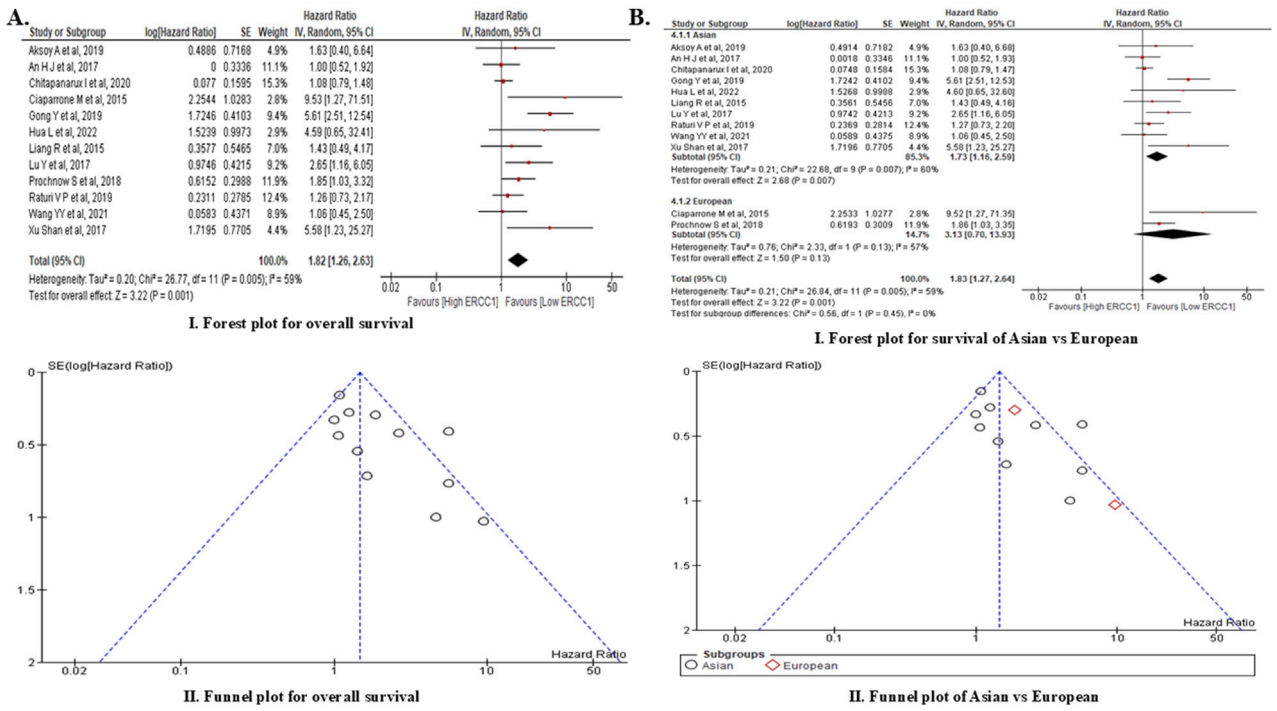

FIGURE 5
Meta-analysis of *ERCC1* expression and overall survival showing forest plot and funnel plot for **(A)** overall survival of HNC patients and **(B)** comparison of overall survival of Asian vs. European subjects.

approximately 29.87% of our HNC patients presented with such family history; of these, 16.88% reported a family history of HNC, which is a serious concern. A recent study by Pachuau et al. (2022) on north Indians reporting a family history of cancer among first-degree relatives showed that the risk of developing cancer was significantly higher (OR: 1.921, $p = 0.037$). Furthermore, another study by Li et al. (2021) revealed that the risk of developing HNC among family members increased by 2-fold if the parents/siblings developed HNC. Carcinomas of the oral cavity, larynx, and hypo/oro/nasopharynx were the most predominant types of HNC among our patients, which conform with the sites of HNC development reported from an analysis of 37 Indian cancer registries (Bagal et al., 2023); however, there is a slight disagreement with the findings of Badola et al. (2023) and Chauhan et al. (2022) who reported larynx cancer as the second most-common type after oral cavity cancer. The treatment strategies adopted for our patients (i.e., surgery and CCRT or CCRT alone) comply with the standard treatment guidelines for the management of LAHNC (NCCN Guidelines, 2024; Badola et al., 2023).

Till date, there is only one report of a European study on the dose-dependent expressions of NER genes (Psyrri et al., 2021) among 43 HNC patients, where 35 were responders (81.4%) and 8 were non-responders (18.60%) to cisplatin-based CRT; it was also found that DNA damage, oxidative stress, and NER pathway capacity were significantly higher ($p < 0.05$) in the cisplatin non-responders than responders owing to diminished apoptosis of the tumor cells among the non-responders. This is in agreement with the findings of our study that *ERCC1* expression was significantly increased by 1.64-fold after CCRT compared to the baseline, confirming the increase in NER capacity to clear damaged DNA-cisplatin adducts. Furthermore, approximately 20.78% of the patients in our study showed overexpression of *ERCC1* after 100% CCRT, which is nearly equal to that of the non-responder group reported by Psyrri et al. (2021). Although the DNA repair capacity of *ERCC1* was found increase with therapy, the overall median expression of *ERCC1* was lower than that of the reference gene in our study; this is in agreement with the findings of Psyrri et al. (2021) who observed downregulation of the NER genes, such as *ERCC1*, *ERCC2/XPD*, *XPA*, and *XPC*, among HNC patients. Even though we predicted no link between overexpression of *ERCC1* and overall survival via computational analysis, we found that upregulation of *ERCC1* is significantly linked to poor overall survival (HR: 1.82) through the meta-analysis of dose-independent expressions in *ERCC1* studies; this is consistent with the previously reported HRs (2.14 and 1.95) among *ERCC1* overexpressing HNC patients (Xuelei et al., 2015; Bišof et al., 2016). These findings are attributed to the increased NER capacity via *ERCC1*, which may be associated with CCRT resistance and poor clinical outcomes among HNC patients. Furthermore, nearly half of the HNC patients (50.33%) among the studies included in the meta-analysis showed high *ERCC1* expressions, which is comparatively higher than that observed in our study where 14.29% and 20.78% of the patients had high expressions at baseline and after 100% CCRT, respectively. The details of the studies included in the meta-analysis are outlined in Table 3 (Prochnow et al., 2019; Liang et al., 2015; Ciaparrone et al., 2015; Lu et al., 2017; Xu et al., 2017; An et al., 2017; Gong et al., 2019; Aksoy et al., 2019; Raturi et al., 2020; Chitapanarux et al., 2020; Wang et al., 2021; Hua et al., 2022).

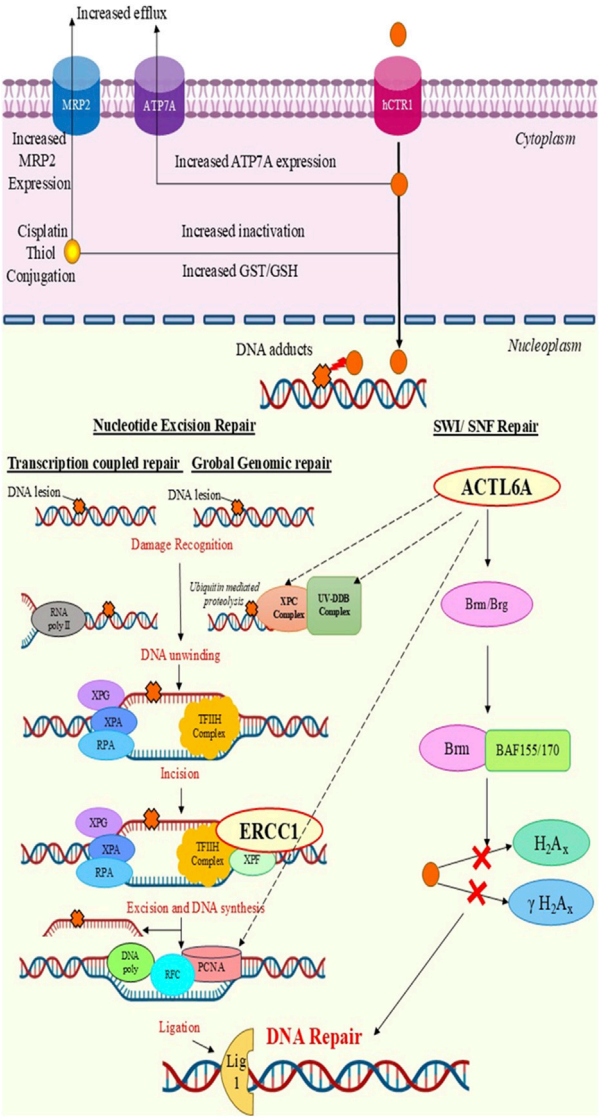

FIGURE 6
Chemoresistance mechanisms of *ERCC1* and *ACTL6A*. DNA repair is promoted by *ERCC1* via the nucleotide excision repair pathway and by *ACTL6A* through the SWI/SNF complex.

Presently, there are no available studies on evaluating the dose-dependent expression of *ACTL6A*. However, *ACTL6A* has been applauded as a novel gene responsible for cisplatin resistance in various cancers, such as ovarian, lung, and esophageal cancers (Xiao et al., 2021). Overexpression of *ACTL6A* is believed to mediate DNA repair via the SWI/SNF complex by regulating the expression of the Brahma related gene 1 (*Brg1*) or Brahma (*Brm*) and promoting its binding to BRAF155/BRAF170 to hinder cisplatin-mediated H2AX or γH2AX activation (Xiao et al., 2021). Out of the four documents that we retrieved through a systematic search, three studies used human tissue samples to explore *ACTL6A* as a biomarker for cell proliferation, invasion, or metastasis, leading to unfavorable/poor prognosis among HNC patients (Xiao et al., 2021; Liu et al., 2024; Dang et al., 2020; Saladi et al., 2017). A recently published Chinese study by Liu et al. (2024) reported that *ACTL6A* is significantly overexpressed in oral cancer tissues compared to normal tissues and proposed that tumor factors like E2F7, TP63, and microRNA has-mir-381 regulate *ACTL6A* expression to promote cell proliferation, migration, and invasion through the WNT and TP53 signaling pathways. It has also been reported that high *ACTL6A* expression is significantly linked to TP53 mutation rate, which could contribute to chemoresistance to CRT (Xiao et al., 2021). Similarly, studies by Dang et al. (2020) and Saladi et al. (2017) confirmed overexpression of *ACTL6A* in HNC, anticipating that *ACTL6A* interacts with P63 and activates the Yes-associated protein (YAP); this could lead to translocation of YAP into the nucleus, which promotes tumorigenesis via the Hippo-YAP signaling pathway (Dang et al., 2020; Saladi et al., 2017). These findings are correlated with those of our study, where we predicted and demonstrated *ACTL6A* overexpression in HNC via computational analysis and qPCR across the therapy. Furthermore, overexpression of *ACTL6A* was also predicted to be a significant contributor to poor overall survival. However, none of these studies have demonstrated the involvement of *ACTL6A* in DNA repair in HNC or its relation to NER. The present study indicates that *ACTL6A* interacts with the UV-DDB complex, XPC complex of GGR-NER, and PCNA of TCR-NER, thereby contributing to DNA repair. We also found significant and marginally significant correlations between *ERCC1* and *ACTL6A* expressions after 50% (p = 0.003) and 100% (p = 0.06) CCRT, respectively, among the HNC patients, which supports the hypothesis of ACTL6A-mediated NER activation.

Immune cell infiltration of the tumor cells and their interactions with the tumor microenvironment have been proposed to modulate the immune cells, leading to immunosuppression and chemoresistance, thereby resulting in poor clinical outcomes like metastasis and poor survival (Wondergem et al., 2020; Jumaniyazova et al., 2022). However, the inconsistencies in these findings pose conflicts for acceptability in clinical practice. Neutrophil-infiltrating tumor cells undergo polarization to form two phenotypes N1 and N2 that exhibit antitumor and protumor properties, respectively. Here, the N2 phenotype makes the tumor more aggressive by inducing genetic instabilities, angiogenesis, metastasis, and immunosuppression (Wondergem et al., 2020; Jumaniyazova et al., 2022). However, infiltration of the tumor cells by myeloid dendritic cells was reported to exert antitumor and anti-inflammatory effects via increased tumor leucocyte infiltration, whereas plasmacytoid dendritic cell infiltration was reported to be linked with unfavorable outcomes (Wondergem et al., 2020; Jumaniyazova et al., 2022). Similar to neutrophils, macrophages also polarize into M1 and M2 phenotypes, of which the M2 phenotype is linked with protumoral activities, such as tumor migration, invasion, metastasis, and poor survival (Wondergem et al., 2020; Jumaniyazova et al., 2022). To some extent, $CD8^+$ infiltration has been reported to be associated with favorable outcomes, whereas the effects of $CD4^+$ are yet to be clarified (Wondergem et al., 2020; Jumaniyazova et al., 2022). These findings may be important in chemoresistance as both *ERCC1* and *ACTL6A* expressions were found to increase the infiltration of immune cells, such as $CD4^+$ cells, macrophages, myeloid dendritic cells, and B cells.

Nevertheless, knockdown of DNA repair expression could reverse the chemoresistance of or restore sensitivity to the cisplatin or platinum drugs. Among the HNC patients with cisplatin-based CRT resistance or platinum drug resistance, FDA-approved drugs like cyclosporin, 5-fluorouracil, doxorubicin,

gemcitabine, paclitaxel, thalidomide, and panobinostat can be repurposed to downregulate *ERCC1* and *ACTL6A* genes. Although paclitaxel and 5-fluorouracil are used for the management of HNC (NCCN Guidelines, 2024), there are no data regarding the use of these anticancer agents against *ERCC1* and *ACTL6A* genes among HNC patients. Thus, we recommend the clinical investigation of these anticancer agents in combination with platinum therapy to mitigate platinum drug resistance or achieve better efficacy of CCRT among HNC patients. Moreover, E-X PPI2, E-X AS7, and panobinostat (a HDAC inhibitor) have been reported to silence *ERCC1* and *ACTL6A* expressions in melanoma and ovarian/lung cancers, respectively, via *in vitro* and preclinical experiments (Xiao et al., 2021; McNeil et al., 2015). Similarly, siRNA- and shRNA-transfected HNC cell lines have shown promising results for downregulating *ACTL6A* expressions (Liu et al., 2024; Dang et al., 2020; Saladi et al., 2017); these findings offer hope for tackling chemoresistance in cancer therapy.

7 Limitations and future directions

Although the present study was conducted with a unique methodology to decipher the dose-dependent expressions of chemoresistance genes and has the advantage of a molecularly sensitive technique like qPCR compared to IHC, we were unable to evaluate the tumor burden via the RECIST criteria, which should be addressed in the future to generalize our findings. However, the findings of the current study can also be utilized to conduct a novel clinical trial to investigate the dose-dependent expressions of *ERCC1* and *ACTL6A* among large HNC cohorts along with RECIST mapping of the tumor burden for clinical applicability. Furthermore, *ACTL6A* (Liu et al., 2024; Dang et al., 2020; Saladi et al., 2017) and *ERCC1* (Seetharam et al., 2010; Wang et al., 2017) can be targeted using siRNA and shRNA to silence their expressions to counteract chemoresistance. The present study also offers a hypothesis regarding the associations between chromatin remodeling genes and their DNA repair capacities via the SWI/SNF as well as NER pathways, which could motivate future research in this field.

8 Conclusion

We demonstrate that increased expressions of *ERCC1* and *ACTL6A* during and/or after cisplatin-based CRT can mediate DNA repair, leading to chemoresistance in HNC as well as poor overall survival thereof. *ERCC1* and *ACTL6A* are known to regulate several repair pathways that participate in DNA repair processes. *ACTL6A* is also known to promote DNA repair activity by interacting with the UV-DDB complex, XPC complex of GGR-NER, and PCNA of TCR-NER. Thus, *ERCC1* and *ACTL6A* are critical evolutionarily conserved core proteins with theranostic potential for cisplatin or cisplatin-based CRT resistance that can be detected via liquid biopsy. Furthermore, repurposing some of the available FDA-approved drugs for targeting *ERCC1* and *ACTL6A* is proposed as a novel approach to counteract chemoresistance in clinical practice.

Data availability statement

The original contributions presented in the study are included in the article/Supplementary Material, further inquiries can be directed to the corresponding author.

Ethics statement

The study involving humans was approved by the Central Ethics Committee (CEC) of Nitte (Deemed to be University) (Ref. no. NU/CEC/2022/307, revised ref. no. NU/CEC/2024/526) and was registered as a clinical trial in India (CTRI/2022/10/046142). The study was conducted in abeyance with all guidelines of the Declaration of Helsinki. The studies were conducted in accordance with the local legislation and institutional requirements. All participants provided their written informed consent to participate in this study. No potentially identifiable images or data are presented in this work.

Author contributions

RKC: conceptualization, data curation, formal analysis, investigation, methodology, project administration, writing – original draft, and writing – review and editing. PP: formal analysis, methodology, and writing – review and editing. VVS: project administration, resources, supervision, and writing – review and editing. UVM: conceptualization, resources, supervision, validation, and writing – review and editing. PS: formal analysis, resources, validation, and writing – review and editing.

Funding

The author(s) declare that no financial support was received for the research and/or publication of this article.

Acknowledgments

The authors wish to thank the late Dr. Jayarama Shetty. The authors also express their gratitude to the Central Research Laboratory, Nitte (Deemed to be University) along with Mrs. Shweta Shetty K, Mrs. Prajna Bhandary, and Dr. Ananthesh L for their support during the study. The authors are grateful to the Japanese Society of Medical Oncology for providing an opportunity to present the human experimentation part of this research work at the "22nd Annual Meeting of the Japanese Society of Medical Oncology (JSMO2025)" held from 6–8 March 2025 at Kobe, Japan. The abstract (no: 101030) might be included in the supplement of the Annals of Oncology. The graphical abstract was constructed using study images as well as images from free server bioicons.

Conflict of interest

The authors declare that the research was conducted in the absence of any commercial or financial relationships that could be construed as a potential conflict of interest.

Generative AI statement

The authors declare that no Generative AI was used in the creation of this manuscript.

Publisher's note

All claims expressed in this article are solely those of the authors and do not necessarily represent those of their affiliated organizations, or those of the publisher, the editors and the reviewers. Any product that may be evaluated in this article, or claim that may be made by its manufacturer, is not guaranteed or endorsed by the publisher.

Supplementary material

The Supplementary Material for this article can be found online at: https://www.frontiersin.org/articles/10.3389/fphar.2025.1541987/full#supplementary-material

References

Aksoy, A., Elkiran, E. T., Harputluoglu, H., Dagli, A. F., Isikdogan, A., and Urakci, Z. (2019). Is excision repair cross-complementation Group1 expression a biological marker in nasopharynx carcinoma? *J. Cancer Res. Ther.* 15 (3), 550–555. doi:10.4103/0973-1482.206865

An, H. J., Jo, H., Jung, C. K., Kang, J. H., Kim, M. S., Sun, D. I., et al. (2017). Prognostic implication of ERCC1 protein expression in resected oropharynx and oral cavity cancer. *Pathol. Res. Pract.* 213 (8), 949–955. doi:10.1016/j.prp.2017.05.006

Badola, A., Mehta, P., Mehra, S., and Sood, S. (2023). Epidemiology and survival analysis of head and neck cancer: results from comprehensive care center in North India. *Oral Oncol. Rep.* 6, 100022–109060. doi:10.1016/j.oor.2023.100022

Bagal, S., Budukh, A., Thakur, J. S., Dora, T., Qayyumi, B., Khanna, D., et al. (2023). Head and neck cancer burden in India: an analysis from published data of 37 population-based cancer registries. *Ecancermedicalscience* 17, 1603. doi:10.3332/ecancer.2023.1603

Bišof, V., Zajc Petranović, M., Rakušić, Z., Samardžić, K. R., and Juretić, A. (2016). The prognostic and predictive value of excision repair cross-complementation group 1 (ERCC1) protein in 1288 patients with head and neck squamous cell carcinoma treated with platinum-based therapy: a meta-analysis. *Eur. Arch. Otorhinolaryngol.* 273 (9), 2305–2317. doi:10.1007/s00405-015-3710-x

Cannon, M., Stevenson, J., Stahl, K., Basu, R., Coffman, A., Kiwala, S., et al. (2024). DGIdb 5.0: rebuilding the drug-gene interaction database for precision medicine and drug discovery platforms. *Nucleic Acids Res.* 52 (D1), D1227–D1235. doi:10.1093/nar/gkad1040

Chandrashekar, D. S., Bashel, B., Balasubramanya, S. A. H., Creighton, C. J., Ponce-Rodriguez, I., Chakravarthi, B. V. S. K., et al. (2017). UALCAN: a portal for facilitating tumor subgroup gene expression and survival analyses. *Neoplasia* 19 (8), 649–658. doi:10.1016/j.neo.2017.05.002

Chandrashekar, D. S., Karthikeyan, S. K., Korla, P. K., Patel, H., Shovon, A. R., Athar, M., et al. (2022). UALCAN: an update to the integrated cancer data analysis platform. *Neoplasia* 25, 18–27. doi:10.1016/j.neo.2022.01.001

Chaudhary, R. K., Khanal, P., Mateti, U. V., Shastry, C. S., and Shetty, J. (2023). Identification of hub genes involved in cisplatin resistance in head and neck cancer. *J. Genet. Eng. Biotechnol.* 21 (1), 9. doi:10.1186/s43141-023-00468-y

Chauhan, A. S., Prinja, S., Ghoshal, S., Verma, R., and Oinam, A. S. (2018). Cost of treatment for head and neck cancer in India. *PLoS One* 13 (1), e0191132. doi:10.1371/journal.pone.0191132

Chauhan, R., Trivedi, V., Rani, R., and Singh, U. (2022). A study of head and neck cancer patients with reference to tobacco use, gender, and subsite distribution. *South Asian J. Cancer* 11 (1), 46–51. doi:10.1055/s-0041-1740601

Chitapanarux, I., Lekawanvijit, S., Sripan, P., Mahanupab, P., Chakrabandhu, S., Onchan, W., et al. (2020). The prognostic value of excision repair cross-complementing Group 1 expression in nasopharyngeal cancer patients. *J. Res. Med. Sci.* 25, 34. doi:10.4103/jrms.JRMS_787_18

Ciaparrone, M., Caspiani, O., Bicciolo, G., Signorelli, D., Simonelli, I., de Campora, L., et al. (2015). Predictive role of ERCC1 expression in head and neck squamous cell carcinoma patients treated with surgery and adjuvant cisplatin-based chemoradiation. *Oncology* 89 (4), 227–234. doi:10.1159/000430447

Dandekar, M., Tuljapurkar, V., Dhar, H., Panwar, A., and Dcruz, A. K. (2017). Head and neck cancers in India. *J. Surg. Oncol.* 115 (5), 555–563. doi:10.1002/jso.24545

Dang, Y., Zhang, L., and Wang, X. (2020). Actin-like 6A enhances the proliferative and invasive capacities of laryngeal squamous cell carcinoma by potentiating the activation of YAP signaling. *J. Bioenerg. Biomembr.* 52 (6), 453–463. doi:10.1007/s10863-020-09855-3

Ensembl genome browser 112 (2023). Available online at: https://www.ensembl.org/index.html (Accessed on March 6, 2023).

Eytan, D. F., Blackford, A. L., Eisele, D. W., and Fakhry, C. (2019). Prevalence of comorbidities among older head and neck cancer survivors in the United States. *Otolaryngol. Head. Neck Surg.* 160 (1), 85–92. doi:10.1177/0194599818796163

Global Cancer Observatory (2024). India Fact sheet. Available online at: https://gco.iarc.who.int/media/globocan/factsheets/populations/356-india-fact-sheet.pdf (Accessed on June 1, 2024).

Gong, Y., Ju, H., Ren, G., and Wu, Y. (2019). Cisplatin based induction chemotherapy modified by ERCC1 improved the outcome of young adults with locally advanced oral squamous cell carcinoma. *J. Cancer* 10 (9), 2083–2090. doi:10.7150/jca.28959

Gormley, M., Creaney, G., Schache, A., Ingarfield, K., and Conway, D. I. (2022). Reviewing the epidemiology of head and neck cancer: definitions, trends and risk factors. *Br. Dent. J.* 233 (9), 780–786. doi:10.1038/s41415-022-5166-x

Győrffy, B. (2024). Integrated analysis of public datasets for the discovery and validation of survival-associated genes in solid tumors. *Innov. (Camb)* 5 (3), 100625. doi:10.1016/j.xinn.2024.100625

Hu, H., Li, B., Wang, J., Tan, Y., Xu, M., Xu, W., et al. (2023). New advances into cisplatin resistance in head and neck squamous carcinoma: mechanisms and therapeutic aspects. *Biomed. Pharmacother.* 163, 114778. doi:10.1016/j.biopha.2023.114778

Hua, L., Chen, S., Wei, M., Shen, Y., Long, J., Lin, Z., et al. (2022). Predictive value of ERCC1 mRNA level from receiver-operator characteristic and pretreatment EBV-DNA Virus load in stage II nasopharyngeal carcinoma patients receiving intensity-modulated radiotherapy with concurrent cisplatin. *Cancer Biother. Radiopharm.* 37 (1), 2–10. doi:10.1089/cbr.2020.4474

Jumaniyazova, E., Lokhonina, A., Dzhalilova, D., Kosyreva, A., and Fatkhudinov, T. (2022). Immune cells in head-and-neck tumor microenvironments. *J. Pers. Med.* 12 (9), 1521. doi:10.3390/jpm12091521

Kanno, Y., Chen, C. Y., Lee, H. L., Chiou, J. F., and Chen, Y. J. (2021). Molecular mechanisms of chemotherapy resistance in head and neck cancers. *Front. Oncol.* 11, 640392. doi:10.3389/fonc.2021.640392

KEGG Pathway: (2024). Nucleotide excision repair. Available online at: https://www.kegg.jp/pathway/map03420. Accessed on 1 . Accessed on 1 June 2024

Kim, C. S., Park, J. O., Nam, I. C., Park, S. J., Lee, D. H., Kim, H. B., et al. (2022). Associations of body mass index and waist circumference with the risk of head and neck cancer: a national population-based study. *Cancers (Basel)* 14 (16), 3880. doi:10.3390/cancers14163880

Li, T., Fu, J., Zeng, Z., Cohen, D., Li, J., Chen, Q., et al. (2020). TIMER2.0 for analysis of tumor-infiltrating immune cells. *Nucleic Acids Res.* 48 (W1), W509–W514. doi:10.1093/nar/gkaa407

Li, X., Koskinen, A. I., Hemminki, O., Försti, A., Sundquist, J., Sundquist, K., et al. (2021). Family history of head and neck cancers. *Cancers (Basel)* 13 (16), 4115. doi:10.3390/cancers13164115

Liang, R., Lin, Y., Liu, Z. H., Liao, X. L., Yuan, C. L., Liao, S. N., et al. (2015). Correlation between ERCC1 expression and concurrent chemotherapy and radiotherapy in patients with locally advanced nasopharyngeal cancer. *Genet. Mol. Res.* 14 (2), 5804–5811. doi:10.4238/2015.May.29.12

Liu, Y., Liu, Y., Li, Y., Wang, T., Li, B., Kong, X., et al. (2024). High expression of ACTL6A leads to poor prognosis of oral squamous cell carcinoma patients through promoting malignant progression. *Head Neck* 46 (6), 1450–1467. doi:10.1002/hed.27742

Lu, Y., Huang, H., Kang, M., Yi, M., Yang, H., Wu, S., et al. (2017). Combined Ki67 and ERCC1 for prognosis in non-keratinizing nasopharyngeal carcinoma underwent chemoradiotherapy. *Oncotarget* 8 (51), 88552–88562. doi:10.18632/oncotarget.19158

Mathur, P., Sathishkumar, K., Chaturvedi, M., Das, P., Sudarshan, K. L., Santhappan, S., et al. (2020). Cancer statistics, 2020: report from national cancer registry programme, India. *JCO Glob. Oncol.* 6, 1063–1075. doi:10.1200/GO.20.00122

McNeil, E. M., Astell, K. R., Ritchie, A. M., Shave, S., Houston, D. R., Bakrania, P., et al. (2015). Inhibition of the ERCC1-XPF structure-specific endonuclease to overcome

cancer chemoresistance. *DNA Repair (Amst)* 31, 19–28. doi:10.1016/j.dnarep.2015.04.002

Nagy, Á., and Győrffy, B. (2021). muTarget: a platform linking gene expression changes and mutation status in solid tumors. *Int. J. Cancer* 148 (2), 502–511. doi:10.1002/ijc.33283

NCCN Guidelines for Head and neck cancers, version 4. (2024). NCCN clinical practice guidelines in Oncology. Available online at: https://www.nccn.org/professionals/physician_gls/pdf/head-and-neck.pdf. Accessed 1, June 2024.

Pachuau, L., Zami, Z., Nunga, T., Zodingliana, R., Zoramthari, R., Lalnuntluanga, R., et al. (2022). First-degree family history of cancer can be a potential risk factor among head and neck cancer patients in an isolated Mizo tribal population, northeast India. *Clin. Epidemiol. Glob. Health* 13 (2213-3984), 100954. doi:10.1016/j.cegh.2021.100954

Piemonte, E., Lazos, J., Belardinelli, P., Secchi, D., Brunotto, M., and Lanfranchi-Tizeira, H. (2018). Oral cancer associated with chronic mechanical irritation of the oral mucosa. *Med. Oral Patol. Oral Cir. Bucal* 23 (2), e151–e160. doi:10.4317/medoral.22017

Prabhash, K., Babu, G., Chaturvedi, P., Kuriakose, M., Birur, P., Anand, A. K., et al. (2020). Indian clinical practice consensus guidelines for the management of very advanced disease of squamous cell carcinoma of head and neck. *Indian J. Cancer* 57 (Suppl. ment), S22–S25. doi:10.4103/0019-509X.278977

PrimerBank-MGH-PGA (2023). Available online at: https://pga.mgh.harvard.edu/primerbank/(Accessed on March 6, 2023).

Prochnow, S., Wilczak, W., Bosch, V., Clauditz, T. S., and Muenscher, A. (2019). ERCC1, XPF and XPA-locoregional differences and prognostic value of DNA repair protein expression in patients with head and neck squamous cell carcinoma. *Clin. Oral Investig.* 23 (8), 3319–3329. doi:10.1007/s00784-018-2751-0

PROSPERO (2024). International prospective register of systematic reviews. Available online at: https://www.crd.york.ac.uk/prospero/(Accessed on May 13, 2024).

Psyrri, A., Gkotzamanidou, M., Papaxoinis, G., Krikoni, L., Economopoulou, P., Kotsantis, I., et al. (2021). The DNA damage response network in the treatment of head and neck squamous cell carcinoma. *ESMO Open* 6 (2), 100075. doi:10.1016/j.esmoop.2021.100075

PubChem (2024). Available online at: https://pubchem.ncbi.nlm.nih.gov/(Accessed on June 8, 2024).

Ranasinghe, R., Mathai, M. L., and Zulli, A. (2022). Cisplatin for cancer therapy and overcoming chemoresistance. *Heliyon* 8 (9), e10608. doi:10.1016/j.heliyon.2022.e10608

Raturi, V. P., Wu, C. T., Mohammad, S., Hojo, H., Bei, Y., Nakamura, M., et al. (2020). Could excision repair cross-complementing group-1 mRNA expression from peripheral blood lymphocytes predict locoregional failure with cisplatin chemoradiation for locally advanced laryngeal cancer? *Asia Pac. J. Clin. Oncol.* 16 (2), e19–e26. doi:10.1111/ajco.13239

RCSB PDB (2024). Homepage. Available online at: https://www.rcsb.org/(Accessed on June 8, 2024).

Saladi, S. V., Ross, K., Karaayvaz, M., Tata, P. R., Mou, H., Rajagopal, J., et al. (2017). ACTL6A is Co-amplified with p63 in squamous cell carcinoma to drive YAP activation, regenerative proliferation, and poor prognosis. *Cancer Cell* 31 (1), 35–49. doi:10.1016/j.ccell.2016.12.001

SathiyaPriya, S., Shavi, G. R., Sanga, R., Shankar, S., Gunasekaran, L., Rahila, C., et al. (2024). Assessment of the prevalence of types of head and neck cancer in a tertiary cancer center at Madurai, Tamil Nadu: a cross-sectional study. *J. Cancer Res. Ther.* 20 (3), 959–965. doi:10.4103/jcrt.jcrt_2081_22

SEER Cancer Stat Facts (2024). Available online at: https://seer.cancer.gov/statfacts/(Accessed on July 15, 2024).

Seetharam, R. N., Sood, A., Basu-Mallick, A., Augenlicht, L. H., Mariadason, J. M., and Goel, S. (2010). Oxaliplatin resistance induced by ERCC1 up-regulation is abrogated by siRNA-mediated gene silencing in human colorectal cancer cells. *Anticancer Res.* 30 (7), 2531–2538.

Singhvi, H. R., Malik, A., and Chaturvedi, P. (2017). The role of chronic mucosal trauma in oral cancer: a review of literature. *Indian J. Med. Paediatr. Oncol.* 38 (1), 44–50. doi:10.4103/0971-5851.203510

Szklarczyk, D., Kirsch, R., Koutrouli, M., Nastou, K., Mehryary, F., Hachilif, R., et al. (2023). The STRING database in 2023: protein-protein association networks and functional enrichment analyses for any sequenced genome of interest. *Nucleic Acids Res.* 51 (D1), D638–D646. doi:10.1093/nar/gkac1000

The Human Protein Atlas (2024). Available online at: https://www.proteinatlas.org/(Accessed on June 5, 2024).

Tierney, J. F., Stewart, L. A., Ghersi, D., Burdett, S., and Sydes, M. R. (2007). Practical methods for incorporating summary time-to-event data into meta-analysis. *Trials* 8, 16. doi:10.1186/1745-6215-8-16

Wang, W., Zhang, L., Liu, L., Zheng, Y., Zhang, Y., Yang, S., et al. (2017). Chemosensitizing effect of shRNA-mediated ERCC1 silencing on a Xuanwei lung adenocarcinoma cell line and its clinical significance. *Oncol. Rep.* 37 (4), 1989–1997. doi:10.3892/or.2017.5443

Wang, Y. Y., Fang, P. T., Su, C. W., Chen, Y. K., Huang, J. J., Huang, M. Y., et al. (2021). Excision repair cross-complementing group 2 upregulation is a potential predictive biomarker for oral squamous cell carcinoma recurrence. *Oncol. Lett.* 21 (6), 450. doi:10.3892/ol.2021.12711

Wondergem, N. E., Nauta, I. H., Muijlwijk, T., Leemans, C. R., and van de Ven, R. (2020). The immune microenvironment in head and neck squamous cell carcinoma: on subsets and subsites. *Curr. Oncol. Rep.* 22 (8), 81. doi:10.1007/s11912-020-00938-3

Xiao, Y., Lin, F. T., and Lin, W. C. (2021). ACTL6A promotes repair of cisplatin-induced DNA damage, a new mechanism of platinum resistance in cancer. *Proc. Natl. Acad. Sci. U. S. A.* 118 (3), e2015808118. doi:10.1073/pnas.2015808118

Xu, S., Yu, Y., Rong, J., Hu, D., Zhang, L., Fu, S., et al. (2017). Expression of BRCA1 and ERCC1 as predictive clinical outcome after radiochemotherapy in patients with locoregionally moderate-advanced nasopharyngeal carcinoma. *Oncotarget* 8 (19), 31355–31367. doi:10.18632/oncotarget.15565

Xuelei, M., Jingwen, H., Wei, D., Hongyu, Z., Jing, Z., Changle, S., et al. (2015). ERCC1 plays an important role in predicting survival outcomes and treatment response for patients with HNSCC: a meta-analysis. *Oral Oncol.* 51 (5), 483–492. doi:10.1016/j.oraloncology.2015.02.094

frontiers | Frontiers in Oncology

TYPE Original Research
PUBLISHED 12 June 2025
DOI 10.3389/fonc.2025.1518587

OPEN ACCESS

EDITED BY
Luis Abel Quiñones,
University of Chile, Chile

REVIEWED BY
Zhengrui Li,
Shanghai Jiao Tong University, China
Luccas Lavareze,
State University of Campinas, Brazil

*CORRESPONDENCE
Yucheng Yang
yychxh@163.com

RECEIVED 28 October 2024
ACCEPTED 21 May 2025
PUBLISHED 12 June 2025

CITATION
Zhou S, Jiang Y, Xiong P, Li Z, Jia L, Yuan W, Liao X, An X, Hu J, Luo R, Mo H, Fang H and Yang Y (2025) Identification and prognostic analysis of propionate metabolism-related genes in head and neck squamous cell carcinoma. *Front. Oncol.* 15:1518587. doi: 10.3389/fonc.2025.1518587

Identification and prognostic analysis of propionate metabolism-related genes in head and neck squamous cell carcinoma

Shitong Zhou[1,2], Yu Jiang[1], Panhui Xiong[1], Zhongwan Li[2], Lifeng Jia[2], Wei Yuan[2], Xiufu Liao[2], Xiang An[2], Jie Hu[2], Rui Luo[2], Hailan Mo[2], Hongyan Fang[2] and Yucheng Yang[1*]

[1]Department of Otorhinolaryngology, The First Affiliated Hospital of Chongqing Medical University, Chongqing, China, [2]Department of Otorhinolaryngology Head and Neck Surgery, Chongqing General Hospital, Chongqing University, Chongqing, China

Introduction: Head and neck squamous cell carcinoma (HNSCC) is a highly heterogeneous malignancy with poor overall prognosis. Recent studies have suggested that propionate metabolism-related genes (PMRGs) may play key roles in tumor progression and immune regulation, yet their functions in HNSCC remain unclear.

Methods: Transcriptomic data from 502 HNSCC tumor samples and 44 normal tissue samples were obtained from the UCSC Xena database as the training set. Two independent datasets (GSE41613 and GSE6631) from the GEO database were used for validation. Differentially expressed genes (DEGs), key module genes identified via weighted gene co-expression network analysis (WGCNA), and PMRGs were intersected to identify candidate genes. A prognostic model was constructed using Cox regression and LASSO analysis. Immune infiltration, somatic mutations, and drug sensitivity were compared between high- and low-risk groups. Gene expression was further validated by RT-qPCR using clinical samples.

Results: A total of 42 intersecting genes were identified, and four feature genes (PRKAA2, SLC7A5, GRIP2, CHGB) were selected to build the prognostic model. The model effectively stratified patients into high- and low-risk groups with significant survival differences in both the training and validation cohorts. The high-risk group exhibited marked differences in immune cell infiltration, immune checkpoint expression, and cancer immune cycle activity. Mutation burden and drug sensitivity also varied significantly between risk groups. A nomogram combining risk score and pathological N stage showed strong predictive performance.

Discussion: This study highlights the potential role of PMRGs in immune regulation and tumor progression in HNSCC. The proposed four-gene signature provides a novel tool for prognosis prediction and offers new insights for risk stratification and individualized therapy. Further multicenter validation and mechanistic studies are warranted.

KEYWORDS

propionate metabolism-related genes, head and neck squamous cell carcinoma, prognostic risk model, metabolic reprogramming, immune evasion

1 Introduction

Head and neck squamous cell carcinoma (HNSCC) is the sixth most common cancer globally, with 5-year survival rates consistently ranging from 40% to 60% over the past few decades (1–3). Clinically, HNSCC is divided into HPV-positive and HPV-negative subtypes based on the presence of human papillomavirus (HPV), each with distinct etiologies, molecular profiles, therapeutic responses, and prognoses (4). HPV-positive HNSCC typically arises in the oropharynx, is more prevalent among nonsmokers, demonstrates relatively stable molecular features, and responds well to chemoradiotherapy, resulting in a favorable prognosis. In contrast, HPV-negative HNSCC is strongly associated with tobacco and alcohol use, displays considerable molecular heterogeneity, and is linked to poorer outcomes, including increased resistance to treatment and higher rates of local recurrence (4, 5). Current precision medicine strategies for HNSCC face two major challenges: the lack of reliable molecular biomarkers for prognostic prediction and significant individual variability in response to chemotherapeutic agents such as docetaxel and methotrexate (6). These issues highlight the urgent need for further exploration of molecular mechanisms to improve risk stratification and therapeutic approaches.

Recent research has emphasized the pivotal roles of tumor metabolic reprogramming and immune evasion. Metabolic reprogramming, for example, has been shown to influence the expression of immune checkpoint molecules such as PD-L1 (7). Tumor cells can increase PD-L1 expression through the activation of transcription factors like HIF-1α, thus suppressing T cell activity and enabling immune escape (8). Additionally, alterations in short-chain fatty acid (SCFA) metabolism, particularly propionate, have been implicated in tumorigenesis and progression (9, 10). Propionate, a key SCFA produced primarily through gut microbial fermentation of dietary fiber, not only contributes to energy metabolism but also plays pivotal roles in immunomodulation, epigenetic regulation, and cellular signaling (11). Growing evidence suggests that disturbances in propionate metabolism are closely associated with malignant progression and metastasis in various cancers (12). For instance, propionate promotes the differentiation of regulatory T cells (Tregs) and inhibits proinflammatory Th17 cells by activating G-protein-coupled receptors (GPR43/41) and suppressing HDAC activity, thereby fostering an immunosuppressive tumor microenvironment (TME) (13). Moreover, metabolites such as methylmalonic acid (MMA) can induce $CD8^+$ T-cell exhaustion and enhance PD-L1 expression, further contributing to tumor immune evasion (14). In colorectal cancer and melanoma, disrupted propionate metabolism has been linked to the polarization of M2-type tumor-associated macrophages (TAMs) and the recruitment of myeloid-derived suppressor cells (MDSCs), suggesting a role in immune escape (15). Despite these findings, the biological functions and clinical significance of propionate metabolism-related genes (PMRGs) in HNSCC remain largely unexplored.

This study identified key genes associated with propionate metabolism in HNSCC and developed a prognostic model based on these genes. A comprehensive analysis of clinical features, immune cell infiltration, immune checkpoint expression, immune cycle dynamics, and drug sensitivity differences between high- and low-risk patient groups was performed. In summary, the findings of this study uncover potential therapeutic targets linked to propionate metabolism in HNSCC and offer novel insights that may aid in the development of precision treatment strategies for this challenging malignancy.

2 Materials and methods

2.1 Data source and tissues

Transcriptome sequencing data from 502 HNSCC tumor tissue samples and 44 normal tissue samples were retrieved from the UCSC Xena database (https://xenabrowser.net/datapages/) to serve as the training set. Two additional HNSCC datasets (GSE41613 and GSE6631) were sourced from the GEO database (https://www.ncbi.nlm.nih.gov/gds). The validation set included 97 oral tissue samples from patients with HPV-negative HNSCC from GSE41613 (platform GPL570). For expression verification, 22 tissue samples from patients with HNSCC and 22 normal tissue samples from GSE6631 (platform GPL8300) were utilized. A total of 603 PMRGs were obtained from the GeneCards database (https://www.genecards.org/). Real-time quantitative reverse transcription polymerase chain reaction (RT-qPCR) validation was conducted on tumors and adjacent normal tissues from 24

patients at the Department of Otolaryngology, Chongqing General Hospital. Histological evaluation was performed on each sample, and all participants provided written informed consent. The study was approved by the Ethics Committee of Chongqing General Hospital (Approval No. KY S2023-102-01).

2.2 Acquisition of intersecting genes

Gene expression data were standardized by converting probe IDs into gene identifiers and eliminating duplicate entries for the same gene in each sample to ensure a single representation per gene. Subsequently, differential expression analysis was performed using the "limma" package (v 3.58.1) (16) in the training set, identifying differentially expressed genes (DEGs) with a threshold of | Fold Change (FC)| ≥ 1 and adj. $p< 0.05$. Weighted gene coexpression network analysis (WGCNA) was conducted using the "WGCNA" package (v 1.70-3) (17) to identify the most relevant modules for HNSCC in the training set. Hierarchical clustering was initially performed to detect outliers, with any identified outlier samples excluded. The optimal soft threshold was determined based on the scale-free fit index (signed R^2) and average connectivity (targeting a value close to 0). Genes were then grouped into modules using the hybrid dynamic tree-cutting algorithm. The correlation between these modules and the HNSCC phenotype was calculated, and the modules with the strongest correlations were defined as key modules. Genes within these key modules were identified as key module genes. Intersecting genes were derived by overlapping DEGs, key module genes, and PMRGs. To explore the biological functions and pathways involved in the intersecting genes, Gene Ontology (GO) and Kyoto Encyclopedia of Genes and Genomes (KEGG) enrichment analyses were performed using the clusterProfiler package (v 4.2.2) (18). Protein–protein interactions (PPI) among the intersecting genes were assessed using the STRING database (https://cn.string-db.org/).

2.3 Prognostic risk model

Univariate Cox regression analysis was performed on the intersecting genes in the training set to calculate the p-values, hazard ratios (HRs), and their 95% confidence intervals (CIs) for each gene ($p< 0.05$, HRs ≠ 1). Genes identified by univariate Cox regression were further analyzed using the Least Absolute Shrinkage and Selection Operator (LASSO) with the "glmnet" package (v 4.1-2) (19). Tenfold crossvalidation was conducted using the cv.glmnet function, and candidate genes were selected based on the lambda.min value that minimized the prediction error. These candidate genes were then subjected to multivariate Cox regression analysis ($p< 0.05$) and proportional hazards (PH) testing ($p > 0.05$) to identify feature genes. The risk score for each patient in the training set was calculated using the following formula: $\sum_n^n = 1(coefi*Xi)$. The median risk score was used to categorize the samples into high- and low-risk groups. Survival analysis was then conducted, and the Kaplan–Meier (K-M) curve was generated using the "survival" package (v 3.3-1) (20) ($p< 0.05$). Receiver operating characteristic (ROC) analysis was performed using the plotROC package (v 2.3.1) (21), and ROC curves for 1-, 3-, and 5-year survival were plotted, with the area under the curve (AUC) calculated (AUC > 0.7). Additionally, principal component analysis (PCA) was performed to evaluate the discriminative ability of the risk score in the training set. The same methodology was applied to validate the risk model in the validation set. The Wilcoxon test was used to assess differences in the expression of feature genes between HNSCC and control samples in both the training set and the validation set (GSE6631) ($p< 0.05$), with heatmaps generated to visualize the expression patterns.

2.4 Relationship between risk scores and clinical characteristics

Differential expression of feature genes across various clinical characteristics and risk groups was analyzed. The distribution of samples among each clinical characteristic group in the two risk groups was also examined. Additionally, differences in risk scores across clinical feature subgroups were evaluated, and survival differences between different risk subgroups within each clinical characteristic subgroup were computed.

2.5 Construction and evaluation of the nomogram model

Univariate and multivariate Cox regression analyses, based on risk scores, age, gender, stage, pathological T, pathological N, and grade, were performed using the "survival" package (v 3.3-1) to identify independent prognostic factors. The rms package (v 6.8-1) (21) was then employed to construct a nomogram based on the independent prognostic factors. The nomogram's predictive performance was assessed using calibration and decision curves.

2.6 Differential expression analysis

To explore the differential gene expression between the high- and low-risk groups, differential expression analysis was performed using the DESeq2 package (v 1.34.0) (16) in the training set with the threshold set at $|\log_2 FC| \geq 1$ and adj. $p< 0.05$. GO and KEGG enrichment analyses were conducted on the DEGs between the two risk groups using the clusterProfiler package (v 4.2.2) (18). Single-sample Gene Set Enrichment Analysis (ssGSEA) for KEGG pathways was performed across all samples in the training set, identifying pathways that differed between the high- and low-risk groups.

2.7 Somatic cell mutation, drug sensitivity, immune microenvironment, and immune cycle analyses

Somatic mutations in patients with HNSCC were analyzed and visualized using the maftool package (v 2.10.5). Mutation categories, types, and the frequency of the top 25 mutated genes were examined in both the high- and low-risk groups.

Chemotherapeutic agents for HNSCC were obtained from the GDSC database (https://www.cancerrxgene.org). The IC_{50} values for common chemotherapeutic and molecularly targeted drugs in each HNSCC sample were calculated using the R package pRRophetic (v 0.5) (22). Differences in IC_{50} values between the high- and low-risk groups were assessed using the Wilcoxon rank-sum test. Subsequently, ssGSEA of 16 immune cell types, eight immune functions, 19 immune checkpoints, and seven immune cycles was performed for both groups in the training set using the GSVA package (v 1.42.0) (16). The estimate package (v 1.0.13) (18) was used to calculate stromal, immune, and ESTIMATE scores for each HNSCC sample in the training set, and differences in these scores were compared between the high- and low-risk groups.

2.8 RNA isolation, RT-PCR, semi-quantitative PCR, and qPCR

Total RNA was extracted from cell lines and tissues using TRIzol Reagent (Invitrogen, Carlsbad, CA, USA) following the manufacturer's protocol. The RNA was quantified through spectrophotometry and stored at − 80°C. Primer sequences are listed in Table 1.

For qPCR, SYBR Green (Thermo Fisher Scientific, Hong Kong, China) was used according to the manufacturer's instructions, with amplification performed on a 7500 Real-Time PCR System (Applied Biosystems, Foster City, CA, USA). GAPDH served as the internal control. Gene expression levels were calculated using the $2^{-\Delta\Delta Ct}$ method, with all samples analyzed in triplicate.

2.9 Statistical analysis

Statistical analyses were performed using GraphPad Prism 9.0 (GraphPad Software Inc., CA, USA) and SPSS 23.0 (IL, USA). All experiments were conducted in triplicate, and data are presented as the mean ± standard deviation. Normality and equality of variance were assessed using the Shapiro–Wilk and Levene tests, respectively. For normally distributed data, comparisons between groups were made using Student's *t*-test, with Welch's correction for unequal variances. For non-normally distributed data, the Mann–Whitney *U* test was employed. The Wilcoxon rank-sum test was used to compare ssGSEA scores between groups. The Cox regression model was tested for PH assumptions, and survival analysis was conducted using the log-rank test.

TABLE 1 Primer sequences in the RT-qPCR experiment.

Genes	Forward primer (5′–3′)	Reverse primer (5′–3′)
PRKAA2	TCAATCGTTCTGTCGCCA	CGTTAGCATCATAGGAAGGG
CHGB	GACCACCATTCAACCCAC	CCCAACTCTCCTCACTCTG
SLC7A5	GCCGAGGAGAAGGAAGA	TGCCCGAGCCGATAATG
GRIP2	CCCTCGTGTGCTTCATCG	GCTTCCTCCATAGTCCC

3 Results

3.1 Intersecting genes were related to fatty acid metabolic processes

A total of 10,185 DEGs were identified in the training set, with 6,298 genes upregulated and 3,887 genes downregulated in HNSCC (Figures 1A, B). WGCNA revealed the green module, comprising 993 genes, as the most highly correlated with HNSCC (Cor = 0.43, adj. $p = 2 \times 10^{-22}$) (Figure 1C). Forty-two intersecting genes were derived by overlapping the 10,185 DEGs, 993 key module genes, and 603 PMRGs (Figure 1D). GO analysis of these intersecting genes highlighted pathways such as fatty acid metabolic processes and protein-lipid complex binding (Figure 1E). KEGG pathway analysis further identified involvement in pathways such as alanine, leucine, and isoleucine degradation (Figure 1F), suggesting that these genes may influence HNSCC by modulating fatty acid metabolism. To investigate potential gene interactions, a PPI network was constructed. Genes such as ACADM and ACADS, ACHE and MAPT, as well as ACSS3 and AOX1, showed significant interactions (Figure 1G).

3.2 Prognostic risk models were constructed based on PRKAA2, SLC7A5, GRIP2, and CHGB

Univariate Cox regression analysis identified five genes (TAC1, PRKAA2, SLC7A5, GRIP2, CHGB) with $p< 0.05$ and HR ≠ 1 (Figure 2A). Four feature genes (PRKAA2, SLC7A5, GRIP2, CHGB) were selected through LASSO and multivariate Cox regression analysis (Figures 2B, C). Based on these feature genes, risk scores for patients with HNSCC in the training set were calculated. Patients were stratified into high- (n = 250) and low-risk (n = 251) groups based on the median risk score. As the risk score increased, mortality rates also increased (Figure 2D), with patients in the low-risk group exhibiting significantly longer survival (Log-rank test $p< 0.0001$) (Figure 2E). The AUC values for the 1-, 3-, and 5-year ROC curves of the risk model were all greater than 0.6, indicating strong model performance (Figure 2F). PCA demonstrated that the risk scores effectively distinguished between samples in the training set (Figure 2G). External validation in the GSE41613 dataset yielded consistent results with the training set (Figures 3A–D). The Wilcoxon test confirmed that the expression trends of feature genes in control and disease samples were consistent across both datasets, with SLC7A5 showing significant upregulation in HNSCC samples ($p< 0.01$) (Figures 3E–H).

3.3 Nomogram diagram could effectively predict the risk profile of patients with HNSCC

The expression of feature genes across different subgroups is shown in Figure 4A. The distribution of clinical characteristics in

10.3389/fonc.2025.1518587

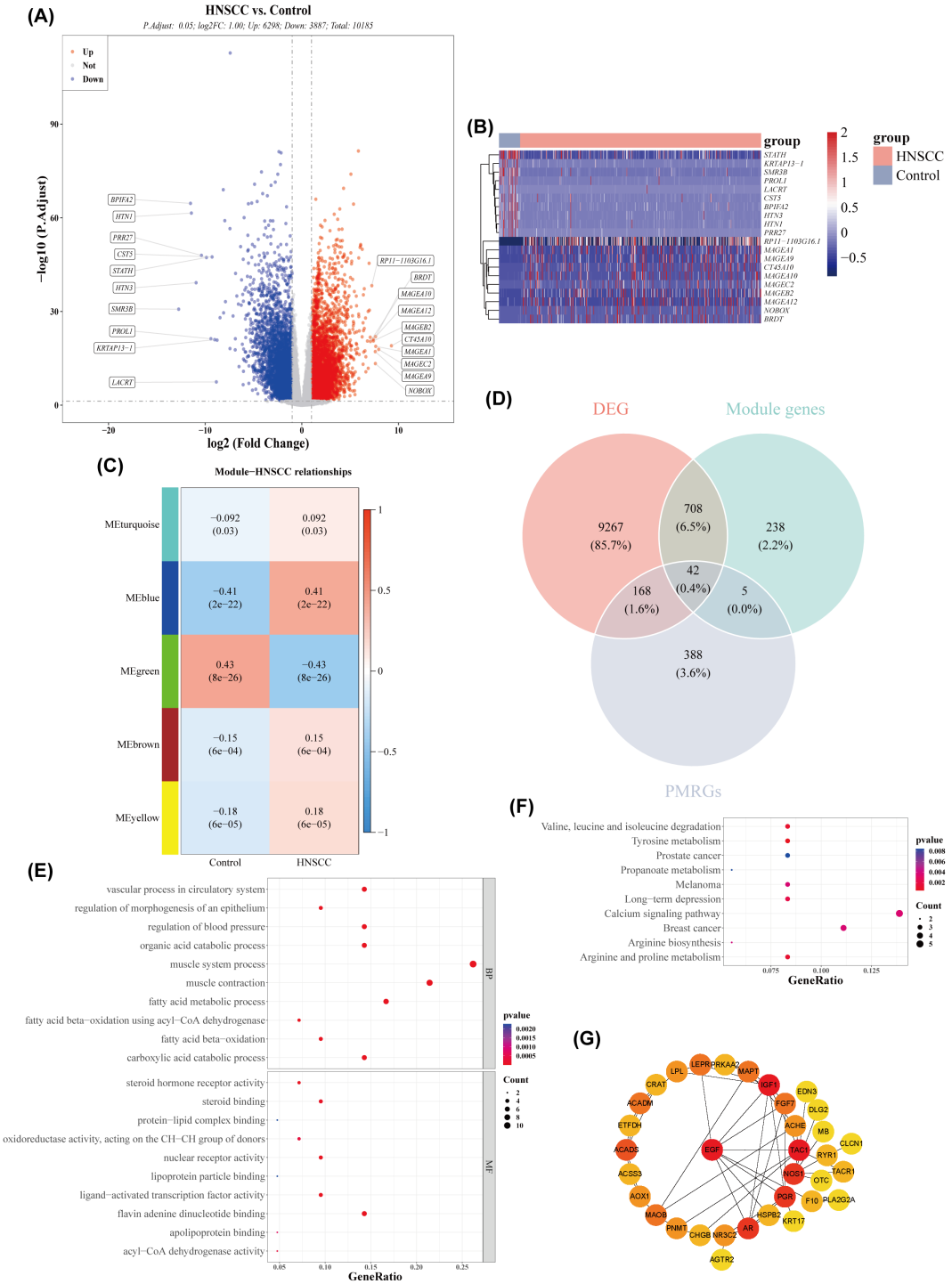

FIGURE 1
Acquisition of differentially expressed genes (DEGs) and key module genes. **(A)** Volcano plot of DEGs between HNSCC and normal samples ($|\log_2 FC| > 0.5$ and p-value< 0.05). **(B)** Heatmap of the top 20 DEGs between HNSCC and normal samples. **(C)** Correlation heatmap between gene modules and disease status. **(D)** Venn diagram showing the overlap of module genes, DEGs, and propionate metabolism-related genes (PMRGs) for screening PMRG-DEGs. **(E)** GO enrichment bubble plot. **(F)** KEGG enrichment bubble plot. **(G)** PPI network.

the high- and low-risk groups is presented in Figure 4B. Risk scores significantly differed between tumor grading and pathological stage T subgroups, but not between age, gender, tumor grading, tumor stage, and pathological stage N subgroups, indicating that risk scores are more closely associated with tumor grading and pathological stage T (Figure 4C). Significant survival differences between high- and low-risk groups were observed across 12 subgroups: age (≤ 60, > 60), gender (women, men), tumor grade (G2, G3), tumor stage (stage II, stage IV), pathological stage N (N1, N2), and pathological stage T (T2, T4) (Figure 4D).

10.3389/fonc.2025.1518587

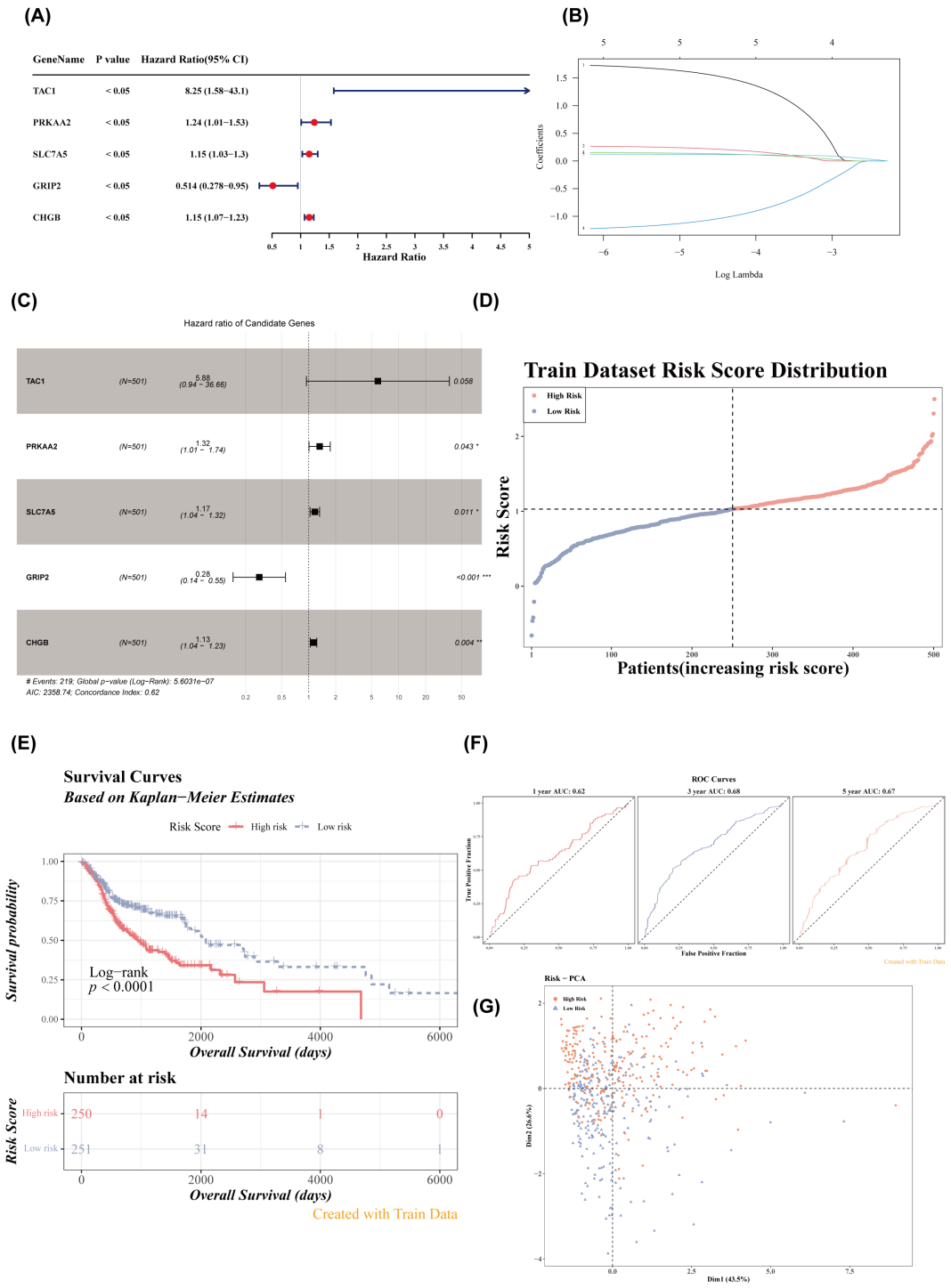

FIGURE 2
Risk model construction and evaluation in the training set. **(A)** Forest plot of univariate Cox analysis. **(B)** Regression coefficient-lambda plot. **(C)** Forest plot of multivariate Cox analysis. **(D)** Risk score distribution in the training dataset. **(E)** Survival curves of high- and low-risk groups in the training set. **(F)** ROC curves for 1-, 3-, and 5-year survival based on the training set. **(G)** PCA dendrogram.

Univariate and multivariate Cox regression analysis identified two independent prognostic factors: pathological stage N and risk score (Figures 5A, B). A nomogram was constructed based on these two factors (Figure 5C). The calibration curves for 1-, 3-, and 5-year survival showed slopes close to 1 (Figure 5D), indicating that the nomogram has high predictive accuracy. Furthermore, the 1-, 3-, and 5-year ROC curves for the nomogram demonstrated AUC values greater than 0.6 (Figure 5E), suggesting excellent prediction performance. In conclusion, the nomogram developed in this study exhibits favorable accuracy in predicting 1-, 3-, and 5-year overall survival (OS) in patients with HNSCC.

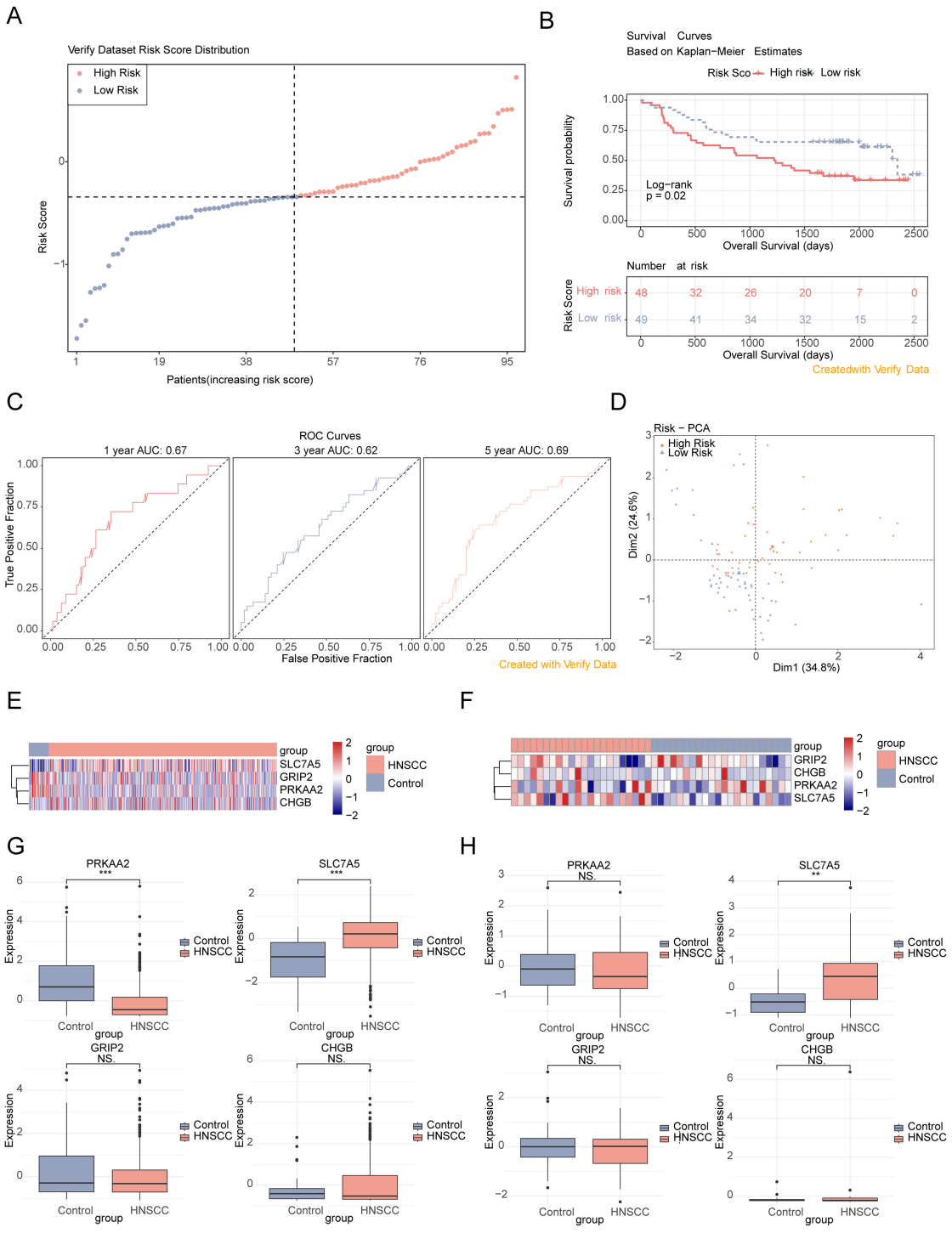

FIGURE 3
Validation of the risk model in the verification set. **(A)** Risk score distribution in the verification dataset. **(B)** Survival curves of high- and low-risk groups in the verification set. **(C)** ROC curves for 1-, 3-, and 5-year survival based on the verification set. **(D)** PCA dendrogram. **(E, F)** Heatmaps of model gene expression (training and verification datasets). **(G, H)** Box plots of feature gene expression in the training set and verification set (GSE6631). ns, $p > 0.05$; **$p < 0.01$; ***$p < 0.001$.

3.4 DEGs were related to immunity

A total of 1,336 DEGs were identified between the high- and low-risk groups, with 277 genes upregulated and 1,059 genes downregulated in the high-risk group (Figure 6A). GO analysis of these DEGs highlighted pathways such as adaptive immune response and immune system processes (Figure 6B). KEGG pathway analysis identified involvement in pathways such as primary immunodeficiency and the intestinal immune network for IgA production (Figure 6C), suggesting that these DEGs may

10.3389/fonc.2025.1518587

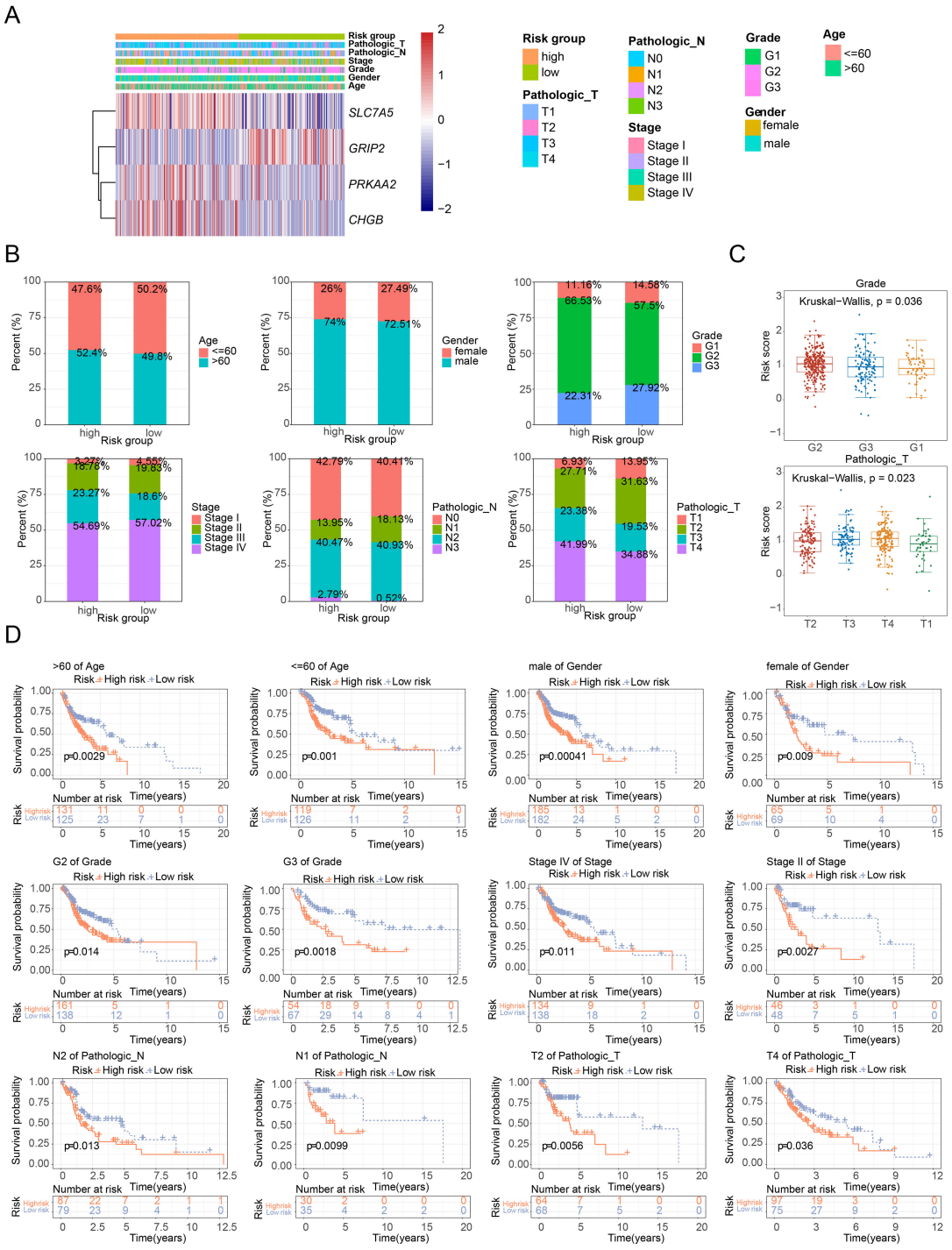

FIGURE 4
Analysis of risk scores across clinical subgroups. **(A)** Heatmap of model gene expression across different clinical groups. **(B)** Distribution of clinical characteristics in high- and low-risk groups. **(C)** Boxplot of risk scores among different clinical characteristic subgroups. **(D)** Survival curves of high- and low-risk groups across different clinical characteristic subgroups.

influence risk scores through modulation of immune responses. The ssGSEA scores for seven of the 186 pathways showed significant differences between the two groups (Figure 6D), with the high-risk group exhibiting generally lower scores in these pathways.

3.5 High-risk high-mutation rate

In this study, 96.79% of samples in the high-risk group and 93.9% of samples in the low-risk group exhibited mutations in the top 25

10.3389/fonc.2025.1518587

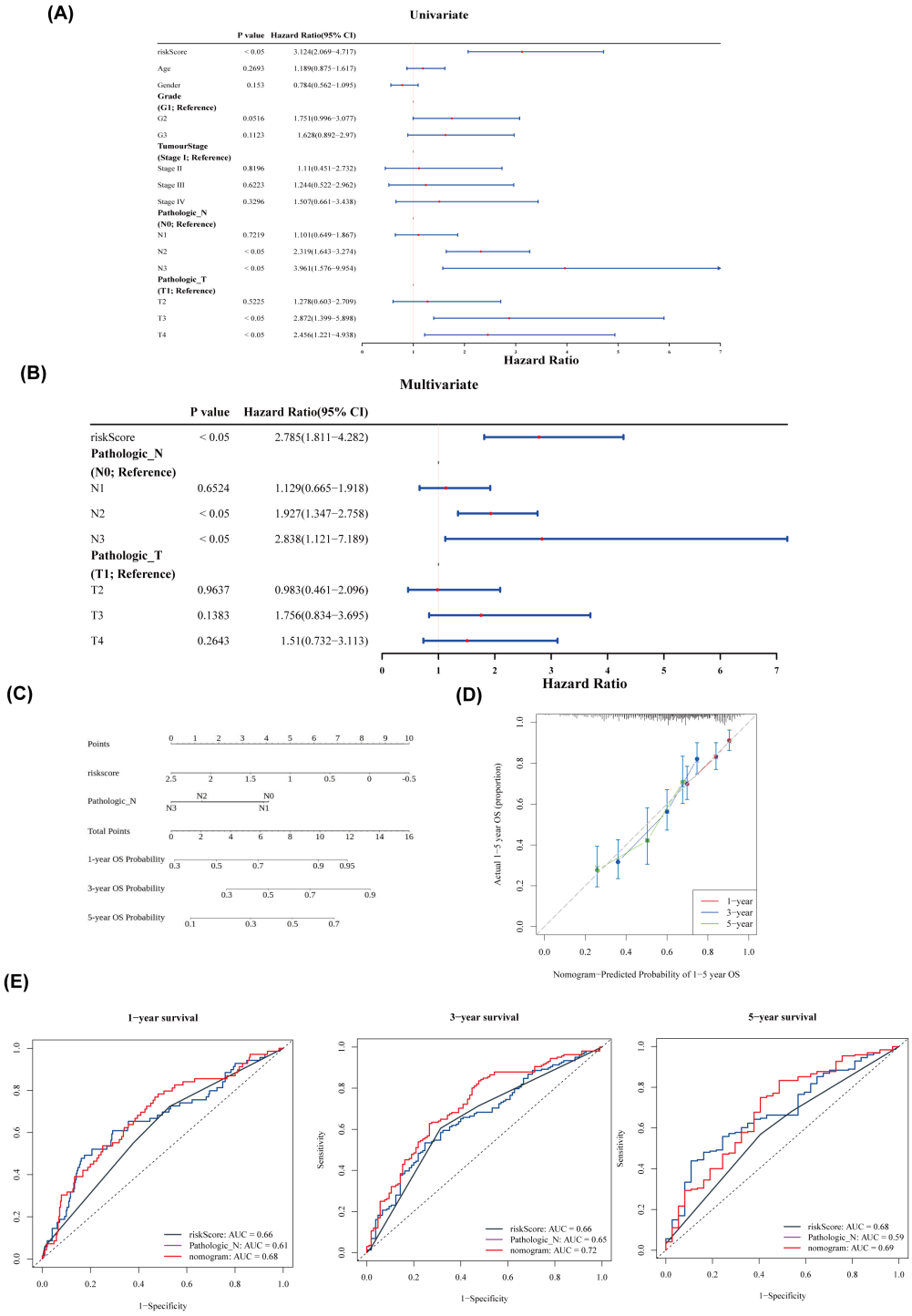

FIGURE 5
Nomogram construction and evaluation. **(A)** Forest plot of univariate Cox analysis. **(B)** Forest plot of multivariate Cox analysis. **(C)** Nomogram of independent prognostic factors. **(D)** Predicted probabilities of 1–5-year overall survival (OS) based on the nomogram. **(E)** ROC curves for 1-, 3-, and 5-year survival.

most frequently mutated genes (Figure 7A). The most common mutation type was missense mutation (SNP), with TP53 showing the highest mutation frequency across samples (Figure 7B). Additionally, 12 drugs displayed significant differences in sensitivity between the high- and low-risk groups, such as dasatinib, lenalidomide, and lapatinib (Figure 7C).

3.6 Significant differences in immune cells, immune checkpoints, and immune cycles

The heatmap of ssGSEA scores for 16 immune cell types is shown in Figure 8A. Except for macrophages, the remaining 15 immune cell types exhibited significant differences in scores between the high- and

10.3389/fonc.2025.1518587

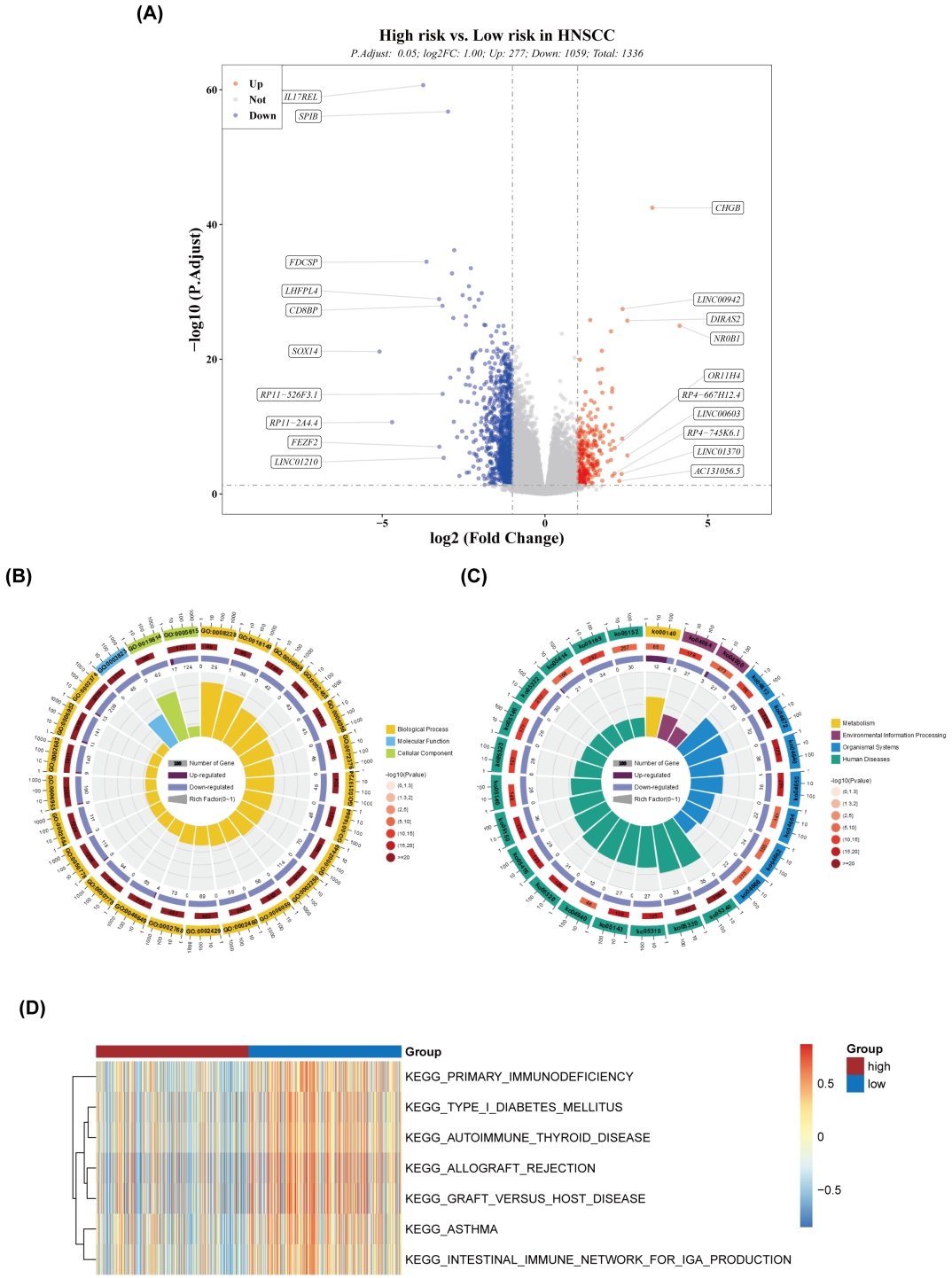

FIGURE 6
Differential expression and pathway analysis. **(A)** Volcano plot of differentially expressed genes. **(B)** Circular plot of GO enrichment. **(C)** Circular plot of KEGG enrichment. **(D)** Heatmap of ssGSEA scores for the pathways.

low-risk groups (Figure 8B). There was a negative correlation between risk scores and the scores of immune cells, with the strongest correlation observed between risk scores and $CD8^+$ T cells (Figure 8C). Significant differences in immune scores and ESTIMATE scores were found between the two groups, while stromal scores showed no significant differences (Figure 8D). The ssGSEA scores for four immune functions were significantly different between the groups (Figure 8E), and 16 immune checkpoints also exhibited significant differences (Figure 8F). All seven cancer immune cycle scores differed significantly between the high- and low-risk groups (Figure 8G). Furthermore, these cancer immune cycle scores were negatively correlated with risk scores, with STEP 3 showing the strongest correlation (Figure 8H).

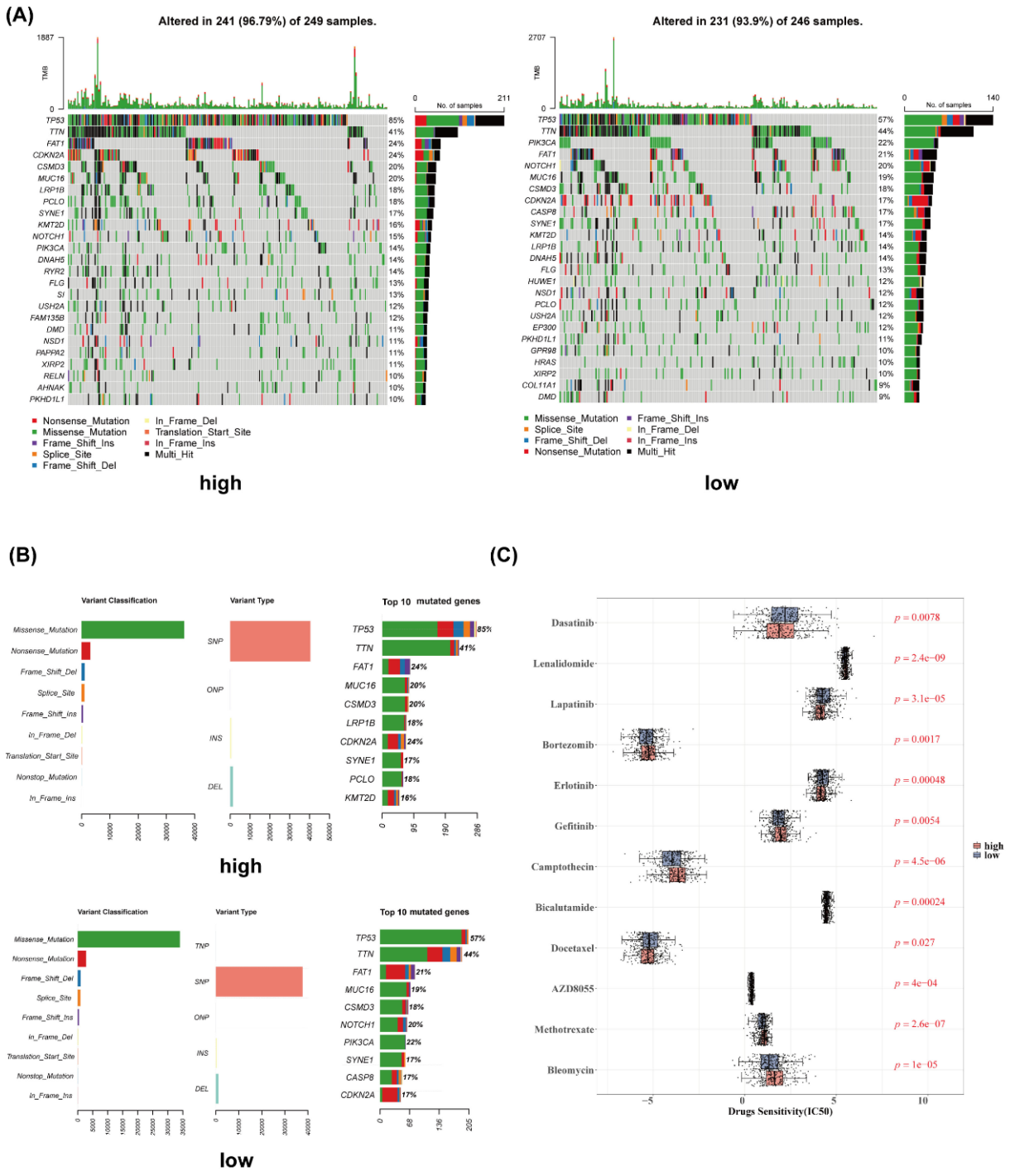

FIGURE 7
Gene mutation analysis and drug sensitivity. **(A)** Waterfall plot of gene mutation analysis (high- and low-risk groups). **(B)** Gene mutation cartogram (high- and low-risk groups). **(C)** Boxplot of differential drug sensitivity analysis.

3.7 Validation of the mRNA expression of four genes (PRKAA2, GRIP2, CHGB, SLC7A5) in HNSCC

To validate the expression changes of the feature genes in HNSCC, 24 pairs of tumor and adjacent noncancerous tissues were collected, and qPCR was performed for verification. The results showed no significant expression changes for PRKAA and GRIP2 in head and neck tumors (Figures 9A, B), whereas CHGB exhibited a noticeable upregulation, and SLC7A5 showed downregulation in head and neck tumors (Figures 9C, D).

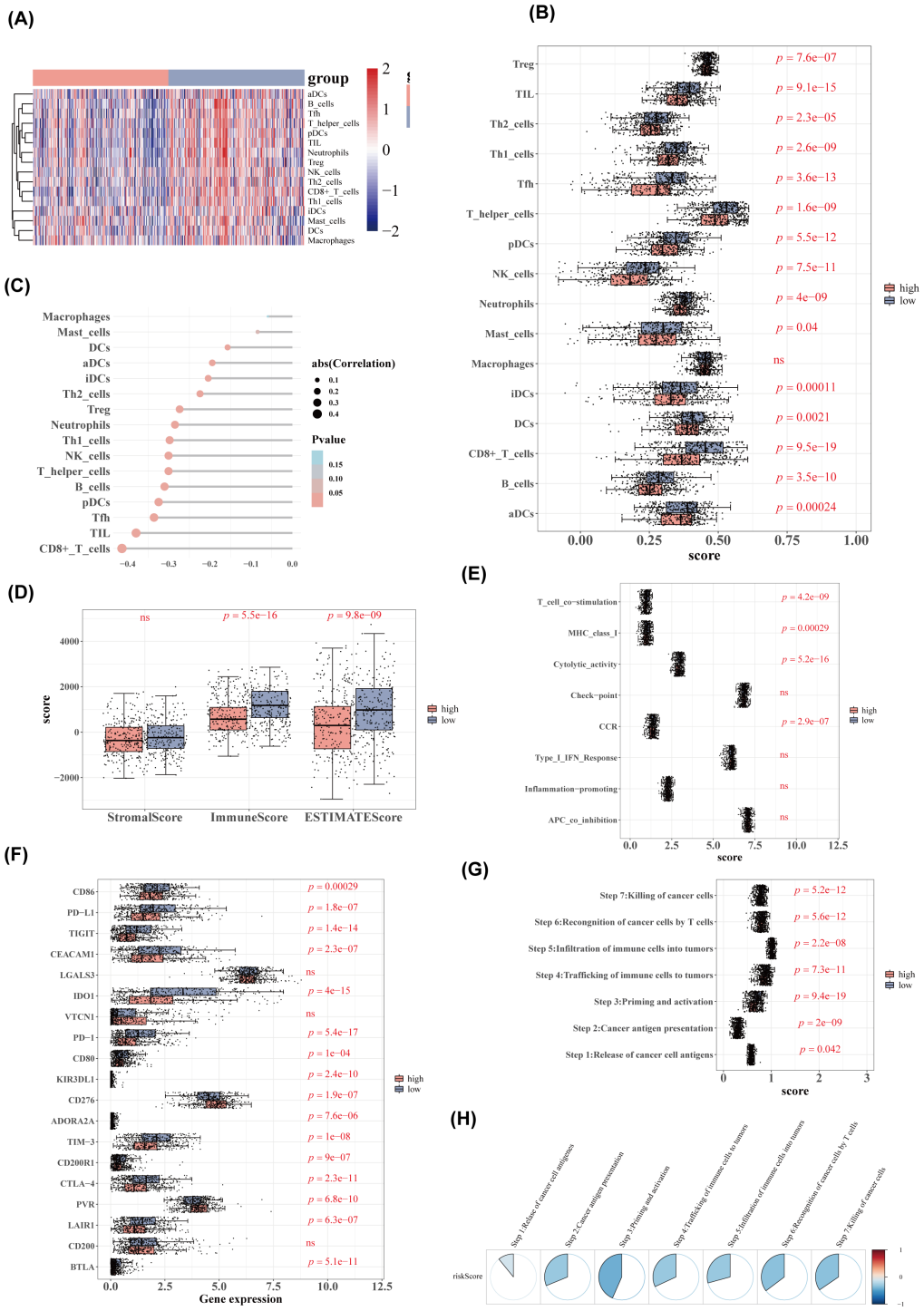

FIGURE 8
Immune cell and immune function analysis. **(A)** Heatmap of immune cell ssGSEA scores. **(B)** Boxplot of immune cell ssGSEA scores. **(C)** Lollipop diagram of correlation analysis between risk scores and immune cell scores. **(D)** Boxplot of stromal, immune, and ESTIMATE scores between high- and low-risk groups. **(E)** ssGSEA scores for immune function between high- and low-risk groups. **(F)** Boxplot of immune checkpoint inhibitor expression. **(G)** Boxplot of cancer immune cycle scores. **(H)** Correlation analysis between cancer immune cycle scores and risk scores.

4 Discussion

HNSCC is a highly heterogeneous malignancy whose development is strongly linked to HPV infection and immunometabolic reprogramming within the TME (23). Recent studies have highlighted the involvement of SCFAs, particularly propionate, as microbial metabolites that regulate energy metabolism and influence tumor progression through epigenetic modifications and immunomodulatory pathways (24). However, the exact mechanisms of PMRGs in HNSCC remain poorly understood. In this study, four

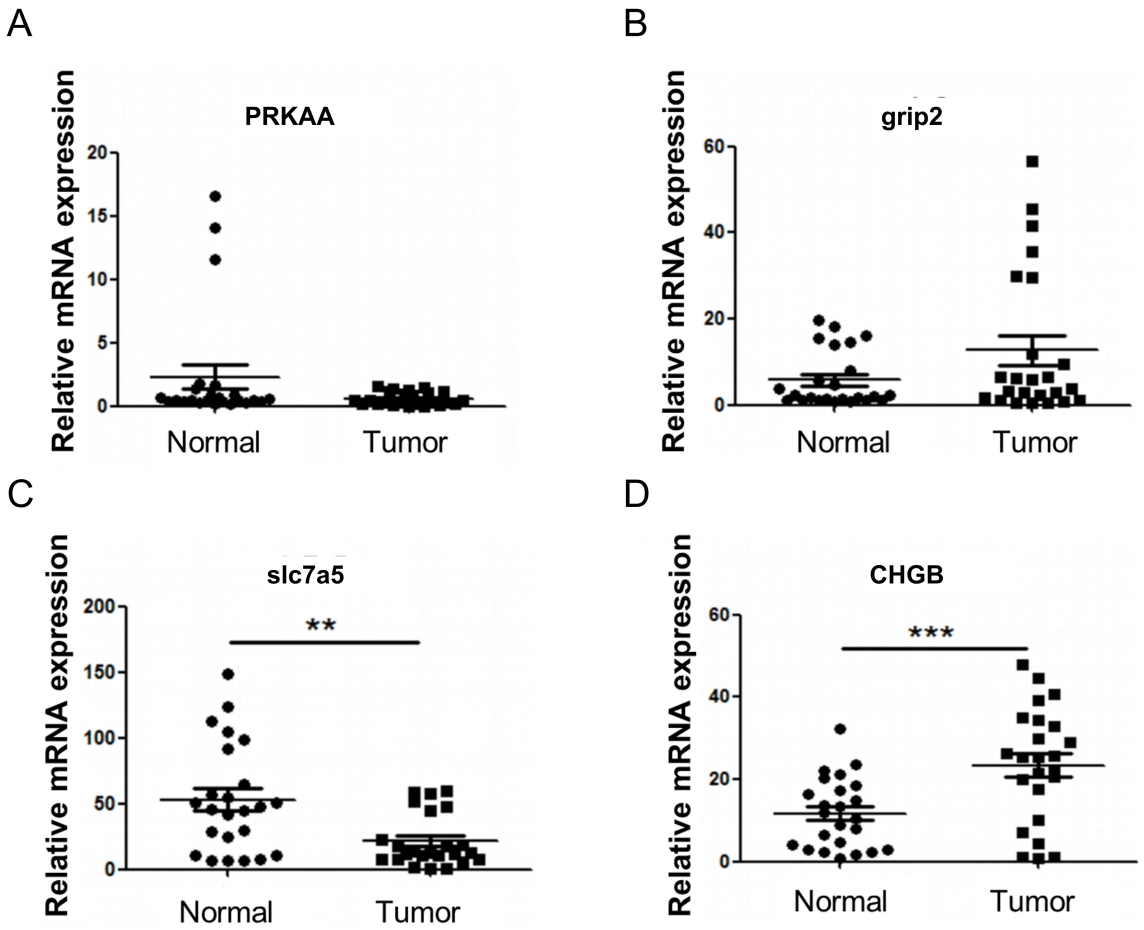

FIGURE 9
RT-qPCR verification of model genes. **(A)** Expression of PRKAA. **(B)** Expression of GRIP2. **(C)** Expression of CHGB. **(D)** Expression of SLC7A5. Compared with Normal, $^{**}P<0.01$, $^{***}P<0.001$.

characteristic genes associated with propionate metabolism in HNSCC—PRKAA2, SLC7A5, GRIP2, and CHGB—were identified through bioinformatics analysis, and their potential roles were explored, providing new theoretical insights for future research on HNSCC.

PRKAA2, also known as AMPKα2, encodes the catalytic α2 subunit of AMP-activated protein kinase (AMPK) (25). It regulates glucose metabolism, which affects tumor cell growth and energy supply (26). Notably, PRKAA2 expression is significantly elevated in hepatoblastoma (HB), where it acts as an oncogenic factor by promoting cell proliferation and inhibiting ferroptosis (27). In non-small cell lung cancer (NSCLC), PRKAA2 enhances tumor growth and suppresses ferroptosis via the SLC7A11/GSH/GPX4 pathway (28). These findings suggest that PRKAA2 may similarly influence tumor cell proliferation and survival in HNSCC.

SLC7A5 (LAT1) facilitates the cellular uptake of neutral amino acids, including leucine and glutamine (29). Its transport of leucine activates the mTORC1 signaling pathway, thereby promoting protein synthesis to support rapid tumor cell proliferation (30). Tumor cells can modulate SLC7A5 expression to alter immune cell function and evade immune surveillance (31, 32). Li et al. identified SLC7A5 as a potential prognostic biomarker in HNSCC associated with immune infiltration (33), suggesting that therapeutic targeting of SLC7A5 may offer a novel strategy for treatment.

GRIP2 encodes a PDZ domain-containing protein that binds GluR2 to anchor AMPA receptors within neuronal signaling complexes, playing pivotal roles in synaptic transmission and plasticity (34). Given the frequent dysregulation of signaling pathways in cancer cells (35), GRIP2 may influence HNSCC progression by modulating key tumorigenic pathways. Interestingly, GRIP2 has been linked to variations in innate $CD8^+$ T cells (36), suggesting its potential immunomodulatory effects in HNSCC progression. Thus, GRIP2 may regulate both tumor signaling pathways and immune cell function, making it a promising therapeutic target.

CHGB is a highly conserved eukaryotic protein involved in secretory regulation (37). While CHGB genetic variants have been associated with cardiovascular disease risk (38) and the protein regulates ion channels to maintain secretory granule homeostasis (37), its role in cancer remains poorly understood and warrants further investigation.

Drug sensitivity analysis identified 12 compounds, including dasatinib, lenalidomide, and lapatinib, with significantly different IC_{50} values between high- and low-risk groups, suggesting their potential clinical applications. Dasatinib, a multi-target tyrosine kinase inhibitor, may enhance treatment response in high-risk patients by inhibiting SRC family kinases and exerting immunomodulatory effects (39–41). The immunomodulator lenalidomide could improve the TME and increase sensitivity to chemoradiotherapy (42, 43). Lapatinib, an oral tyrosine kinase inhibitor targeting the EGFR/HER2 pathways, may provide precision therapy for specific molecular subtypes (44). These observed differences in drug sensitivities support the rationale for molecular classification and personalized treatment strategies in HNSCC. Validation through *in vitro* experiments and clinical cohorts is essential, alongside exploration of combination therapies with existing treatments, such as immune checkpoint inhibitors, to refine and optimize precision treatment regimens.

Significant differences in the expression of 16 immune checkpoint genes, including PD-L1, were identified between risk groups. Previous studies have shown that HNSCC cells often overexpress PD-L1, which binds to PD-1 on T cells, thereby suppressing their activation and function, enabling immune evasion (45–47). This immunosuppression is a key mechanism driving HNSCC progression (48). Furthermore, PD-L1 overexpression is associated with poorer prognosis in patients with HNSCC (49), likely due to reduced survival rates from PD-L1-mediated immune suppression. The elevated expression of PD-L1 in high-risk patients observed in this study supports these immune escape mechanisms and offers valuable insights for understanding prognostic differences and developing novel immunotherapies.

In summary, this study identified four characteristic genes associated with propionate metabolism through bioinformatics analysis and established a risk model based on these genes. These findings provide new insights for prognostic assessment and the development of innovative therapeutic strategies for HNSCC. However, several limitations must be acknowledged. The current sample size necessitates further validation through multicenter studies with larger cohorts to confirm the clinical applicability of the model. Additionally, while these metabolic genes have been identified as potential therapeutic targets, their precise mechanisms in modulating the immune microenvironment require further functional studies and clinical trials. Future research should refine this risk stratification system and investigate metabolism-targeted combination therapies to develop more precise treatment strategies for patients with HNSCC.

Data availability statement

The raw data supporting the conclusions of this article will be made available by the authors, without undue reservation.

Ethics statement

The studies involving humans were approved by the Ethics Committees of Chongqing General Hospital. The studies were conducted in accordance with the local legislation and institutional requirements. The participants provided their written informed consent to participate in this study.

Author contributions

SZ: Conceptualization, Funding acquisition, Writing – original draft, Writing – review & editing. YJ: Conceptualization, Investigation, Supervision, Writing – review & editing. PX: Data curation, Formal Analysis, Methodology, Resources, Software, Validation, Visualization, Writing – review & editing. ZL: Investigation, Writing – review & editing. LJ: Investigation, Writing – review & editing. WY: Investigation, Supervision, Writing – review & editing. XL: Investigation, Writing – review & editing. XA: Investigation, Writing – review & editing. JH: Investigation, Methodology, Writing – review & editing. RL: Investigation, Writing – review & editing. HM: Investigation, Writing – review & editing. HF: Investigation, Supervision, Writing – review & editing. YY: Supervision, Writing – review & editing.

Funding

The author(s) declare that financial support was received for the research and/or publication of this article. This study was supported by a joint project between the Chongqing Science and Technology Bureau and Municipal Health Commission (2023MSXM120).

Conflict of interest

The authors declare that the research was conducted in the absence of any commercial or financial relationships that could be construed as a potential conflict of interest.

Generative AI statement

The author(s) declare that no Generative AI was used in the creation of this manuscript.

Publisher's note

References

1. Mody MD, Rocco JW, Yom SS, Haddad RI, Saba NF. Head and neck cancer. *Lancet*. (2021) 398:2289–99. doi: 10.1016/S0140-6736(21)01550-6

2. Ruffin AT, Li H, Vujanovic L, Zandberg DP, Ferris RL, Bruno TC. Improving head and neck cancer therapies by immunomodulation of the tumour microenvironment. *Nat Rev Cancer*. (2023) 23:173–88. doi: 10.1038/s41568-022-00531-9

3. Leemans CR, Snijders PJF, Brakenhoff RH. The molecular landscape of head and neck cancer. *Nat Rev Cancer*. (2018) 18:269–82. doi: 10.1038/nrc.2018.11

4. Liu L, Xie Y, Yang H, Lin A, Dong M, Wang H, et al. HPVTIMER: A shiny web application for tumor immune estimation in human papillomavirus-associated cancers. *Imeta*. (2023) 2:e130. doi: 10.1002/imt2.v2.3

5. Krsek A, Baticic L, Sotosek V, Braut T. The role of biomarkers in HPV-positive head and neck squamous cell carcinoma: towards precision medicine. *Diagnostics (Basel) 14*. (2024) 14:1448. doi: 10.3390/diagnostics14131448

6. Johnson DE, Burtness B, Leemans CR, Lui VWY, Bauman JE, Grandis JR. Head and neck squamous cell carcinoma. *Nat Rev Dis Primers*. (2020) 6:92. doi: 10.1038/s41572-020-00224-3

7. Muralidharan S, Sehgal M, Soundharya R, Mandal S, Majumdar SS, Yeshwanth M, et al. PD-L1 activity is associated with partial EMT and metabolic reprogramming in carcinomas. *Curr Oncol*. (2022) 29:8285–301. doi: 10.3390/curroncol29110654

8. Shi Z, Hu C, Zheng X, Sun C, Li Q. Feedback loop between hypoxia and energy metabolic reprogramming aggravates the radioresistance of cancer cells. *Exp Hematol Oncol*. (2024) 13:55. doi: 10.1186/s40164-024-00519-1

9. Mann ER, Lam YK, Uhlig HH. Short-chain fatty acids: linking diet, the microbiome and immunity. *Nat Rev Immunol*. (2024) 24:577–95. doi: 10.1038/s41577-024-01014-8

10. Tejero J, Lazure F, Gomes AP. Methylmalonic acid in aging and disease. *Trends Endocrinol Metab*. (2024) 35:188–200. doi: 10.1016/j.tem.2023.11.001

11. Gomes AP, Ilter D, Low V, Drapela S, Schild T, Mullarky E, et al. Altered propionate metabolism contributes to tumour progression and aggressiveness. *Nat Metab*. (2022) 4:435–43. doi: 10.1038/s42255-022-00553-5

12. Ramesh V, Gollavilli PN, Pinna L, Siddiqui MA, Turtos AM, Napoli F, et al. Propionate reinforces epithelial identity and reduces aggressiveness of lung carcinoma. *EMBO Mol Med*. (2023) 15:e17836. doi: 10.15252/emmm.202317836

13. Du Y, He C, An Y, Huang Y, Zhang H, Fu W, et al. The role of short chain fatty acids in inflammation and body health. *Int J Mol Sci 25*. (2024) 25:7379. doi: 10.3390/ijms25137379

14. Li S, Duan Y, Luo S, Zhou F, Wu Q, Lu Z. Short-chain fatty acids and cancer. *Trends Cancer*. (2024) 11:154–68. doi: 10.1016/j.trecan.2024.11.003

15. Chen L, Zhou X, Wang Y, Wang D, Ke Y, Zeng X. Propionate and butyrate produced by gut microbiota after probiotic supplementation attenuate lung metastasis of melanoma cells in mice. *Mol Nutr Food Res*. (2021) 65:e2100096. doi: 10.1002/mnfr.202100096

16. Ritchie ME, Phipson B, Wu D, Hu Y, Law CW, Shi W, et al. limma powers differential expression analyses for RNA-sequencing and microarray studies. *Nucleic Acids Res*. (2015) 43:e47. doi: 10.1093/nar/gkv007

17. Langfelder P, Horvath S. WGCNA: an R package for weighted correlation network analysis. *BMC Bioinf*. (2008) 9:559. doi: 10.1186/1471-2105-9-559

18. Yu G, Wang LG, Han Y, He QY. clusterProfiler: an R package for comparing biological themes among gene clusters. *Omics*. (2012) 16:284–7. doi: 10.1089/omi.2011.0118

19. Ramsay IS, Ma S, Fisher M, Loewy RL, Ragland JD, Niendam T, et al. Model selection and prediction of outcomes in recent onset schizophrenia patients who undergo cognitive training. *Schizophr Res Cognit*. (2018) 11:1–5. doi: 10.1016/j.scog.2017.10.001

20. Lei J, Qu T, Cha L, Tian L, Qiu F, Guo W, et al. Clinicopathological characteristics of pheochromocytoma/paraganglioma and screening of prognostic markers. *J Surg Oncol*. (2023) 128:510–8. doi: 10.1002/jso.v128.4

21. Sachs MC. plotROC: A tool for plotting ROC curves. *J Stat Softw*. (2017) 79:2. doi: 10.18637/jss.v079.c02

22. Gibson JM, Doniach I. Correlation of dose of x-radiation to the rat thyroid gland with degree of subsequent impairment of response to goitrogenic stimulus. *Br J Cancer*. (1967) 21:524–30. doi: 10.1038/bjc.1967.62

23. Xie C, Ji N, Tang Z, Li J, Chen Q. The role of extracellular vesicles from different origin in the microenvironment of head and neck cancers. *Mol Cancer*. (2019) 18:83. doi: 10.1186/s12943-019-0985-3

24. Martin-Gallausiaux C, Marinelli L, Blottière HM, Larraufie P, Lapaque N. SCFA: mechanisms and functional importance in the gut. *Proc Nutr Soc*. (2021) 80:37–49. doi: 10.1017/S0029665120006916

25. Shariq M, Khan MF, Raj R, Ahsan N, Kumar P. PRKAA2, MTOR, and TFEB in the regulation of lysosomal damage response and autophagy. *J Mol Med (Berl)*. (2024) 102:287–311. doi: 10.1007/s00109-023-02411-7

26. Zhang Q, Hong Z, Zhu J, Zeng C, Tang Z, Wang W, et al. miR-4999-5p predicts colorectal cancer survival outcome and reprograms glucose metabolism by targeting PRKAA2. *Onco Targets Ther*. (2020) 13:1199–210. doi: 10.2147/OTT.S234666

27. Xie Y, Cui Z, Fang S, Zhu G, Zhen N, Zhu J, et al. Anti-ferroptotic PRKAA2 serves as a potential diagnostic and prognostic marker for hepatoblastoma. *J Gastrointest Oncol*. (2023) 14:1788–805. doi: 10.21037/jgo-23-110

28. Wei Z, Zhou Z, Zhang Y, Wang J, Huang K, Ding Y, et al. PRKAA2 promotes tumor growth and inhibits ferroptosis through SLC7A11/GSH/GPX4 pathway in non-small cell lung cancer. *Biotechnol Appl Biochem*. (2024). doi: 10.1002/bab.2710

29. Lu X. The role of large neutral amino acid transporter (LAT1) in cancer. *Curr Cancer Drug Targets*. (2019) 19:863–76. doi: 10.2174/1568009619666190802135714

30. Bharadwaj R, Jaiswal S, Velarde de la Cruz EE, Thakare RP. Targeting solute carrier transporters (SLCs) as a therapeutic target in different cancers. *Dis 12*. (2024) 12:63. doi: 10.3390/diseases12030063

31. Branchi V, Hosni R, Kiwitz L, Ng S, van der Voort G, Bambi N, et al. Expression of the large amino acid transporter SLC7A5/LAT1 on immune cells is enhanced in primary sclerosing cholangitis-associated cholangiocarcinoma and correlates with poor prognosis in cholangiocarcinoma. *Hum Pathol*. (2024) 153:105670. doi: 10.1016/j.humpath.2024.105670

32. Zhang C, Wang Y, Guo X, Wang Z, Xiao J, Liu Z. SLC7A5 correlated with Malignancies and immunotherapy response in bladder cancer. *Cancer Cell Int*. (2024) 24:182. doi: 10.1186/s12935-024-03365-7

33. Li C, Chen S, Jia W, Li W, Wei D, Cao S, et al. Identify metabolism-related genes IDO1, ALDH2, NCOA2, SLC7A5, SLC3A2, LDHB, and HPRT1 as potential prognostic markers and correlate with immune infiltrates in head and neck squamous cell carcinoma. *Front Immunol*. (2022) 13:955614. doi: 10.3389/fimmu.2022.955614

34. Mao L, Takamiya K, Thomas G, Lin DT, Huganir RL. GRIP1 and 2 regulate activity-dependent AMPA receptor recycling via exocyst complex interactions. *Proc Natl Acad Sci U.S.A*. (2010) 107:19038–43. doi: 10.1073/pnas.1013494107

35. Nisar S, Hashem S, Macha MA, Yadav SK, Muralitharan S, Therachiyil L, et al. Exploring dysregulated signaling pathways in cancer. *Curr Pharm Des*. (2020) 26:429–45. doi: 10.2174/1381612826666200115095937

36. Jo Y, Balmer L, Lee B, Shim JA, Ali LA, Morahan G, et al. Variants of innate CD8 (+) T cells are associated with Grip2 and Klf15 genes. *Cell Mol Immunol*. (2020) 17:1007–9. doi: 10.1038/s41423-019-0357-3

37. Yadav GP, Wang H, Ouwendijk J, Cross S, Wang Q, Qin F, et al. (CHGB) is dimorphic and responsible for dominant anion channels delivered to cell surface via regulated secretion. *Front Mol Neurosci*. (2023) 16:1205516. doi: 10.3389/fnmol.2023.1205516

38. Zhang K, Rao F, Wang L, Rana BK, Ghosh S, Mahata M, et al. Common functional genetic variants in catecholamine storage vesicle protein promoter motifs interact to trigger systemic hypertension. *J Am Coll Cardiol*. (2010) 55:1463–75. doi: 10.1016/j.jacc.2009.11.064

39. Hasinoff BB, Patel D. Mechanisms of the cardiac myocyte-damaging effects of dasatinib. *Cardiovasc Toxicol*. (2020) 20:380–9. doi: 10.1007/s12012-020-09565-7

40. Lindauer M, Hochhaus A. Dasatinib. *Recent Results Cancer Res*. (2018) 212:29–68. doi: 10.1007/978-3-319-91439-8_2

41. Yu GT, Mao L, Wu L, Deng WW, Bu LL, Liu JF, et al. Inhibition of SRC family kinases facilitates anti-CTLA4 immunotherapy in head and neck squamous cell carcinoma. *Cell Mol Life Sci*. (2018) 75:4223–34. doi: 10.1007/s00018-018-2863-3

42. McDaniel JM, Pinilla-Ibarz J, Epling-Burnette PK. Molecular action of lenalidomide in lymphocytes and hematologic Malignancies. *Adv Hematol*. (2012) 2012:513702. doi: 10.1155/2012/513702

43. Gribben JG, Fowler N, Morschhauser F. Mechanisms of action of lenalidomide in B-cell non-hodgkin lymphoma. *J Clin Oncol*. (2015) 33:2803–11. doi: 10.1200/JCO.2014.59.5363

44. Nolting M, Schneider-Merck T, Trepel M. Lapatinib. *Recent Results Cancer Res*. (2014) 201:125–43. doi: 10.1007/978-3-642-54490-3_7

45. Tahara M, Lim DW, Keam B, Ma B, Zhang L, Wang C, et al. Management approaches for recurrent or metastatic head and neck squamous cell carcinoma after anti-PD-1/PD-L1 immunotherapy. *Cancer Treat Rev*. (2025) 136:102938. doi: 10.1016/j.ctrv.2025.102938

46. Mishra PS, Sidhu A, Dwivedi G, Mulajker DS, Awasthi S. Determining PD-L1 expression in head and neck squamous cell carcinoma using immunohistochemistry. *Indian J Cancer*. (2022) 59:474–9. doi: 10.4103/ijc.IJC_920_19

47. Zheng A, Li F, Chen F, Zuo J, Wang L, Wang Y, et al. PD–L1 promotes head and neck squamous cell carcinoma cell growth through mTOR signaling. *Oncol Rep*. (2019) 41:2833–43. doi: 10.3892/or.2019.7053

48. Chen Y, Ding X, Bai X, Zhou Z, Liu Y, Zhang X, et al. The current advances and future directions of PD-1/PD-L1 blockade in head and neck squamous cell carcinoma (HNSCC) in the era of immunotherapy. *Int Immunopharmacol*. (2023) 120:110329. doi: 10.1016/j.intimp.2023.110329

49. Wang Q, Zhao Y, Chen Y, Chen Y, Song X, Zhang L, et al. High PD-L1 expression associates with low T-cadherin expression and poor prognosis in human papillomavirus-negative head and neck squamous cell carcinoma. *Head Neck*. (2023) 45:1162–71. doi: 10.1002/hed.27329

frontiers | Frontiers in Pharmacology

TYPE Original Research
PUBLISHED 24 June 2025
DOI 10.3389/fphar.2025.1602276

OPEN ACCESS

EDITED BY
Luis Abel Quiñones,
University of Chile, Chile

REVIEWED BY
Mariana Magalhães,
University of Coimbra, Portugal
Hong Sun,
Fudan University, China

*CORRESPONDENCE
Youlin Dong,
22235441@qq.com

†These authors have contributed equally to this work

RECEIVED 29 March 2025
ACCEPTED 09 June 2025
PUBLISHED 24 June 2025

CITATION
Gao W, Xia Z, Zhou T and Dong Y (2025) Adverse event profile of five anti head and neck squamous cell carcinoma drugs: a descriptive analysis from WHO-VigiAccess.
Front. Pharmacol. 16:1602276.
doi: 10.3389/fphar.2025.1602276

Adverse event profile of five anti head and neck squamous cell carcinoma drugs: a descriptive analysis from WHO-VigiAccess

Weimin Gao[1†], Zhigang Xia[1†], Tingfeng Zhou[2] and Youlin Dong[1*]

[1]Department of Otolaryngology, The Second Affiliated Hospital of Jiaxing University, Jiaxing, China, [2]Department of Otolaryngology, The First Affiliated Hospital of Wenzhou Medical University, Wenzhou, China

Background: Head and neck squamous cell carcinoma (HNSCC) remains a significant global health concern, with treatment outcomes for advanced or metastatic stages being suboptimal despite the availability of various targeted therapies and immunotherapies. This study evaluates five FDA-approved anti-HNSCC drugs—cetuximab, pembrolizumab, nivolumab, atezolizumab, and durvalumab—focusing on the adverse drug reactions (ADRs) associated with their use as reported in the WHO VigiAccess database.

Methods: A retrospective analysis was conducted on ADR reports from the WHO-VigiAccess database, focusing on demographic information (age, gender, and geographical distribution) and ADR classification. The disproportionality analysis was used to identify ADRs through Reporting Odds Ratios (ROR) and Proportional Reporting Ratios (PRR). ADRs were categorized into 27 system organ classes (SOCs) for comparison across the five drugs.

Results: A total of 145,678 ADR reports were analyzed. Cetuximab exhibited the highest incidence of skin and subcutaneous tissue disorders (20.88%), while durvalumab showed elevated respiratory system disorders (18.53%). Pembrolizumab and nivolumab had notable immune-related adverse events, with malignant neoplasm progression reported at 5.56% and 4.23%, respectively. Atezolizumab was primarily associated with blood and lymphatic system disorders (5.51%). Disproportionality analysis revealed significant safety concerns for each drug, such as skin toxicity for cetuximab, respiratory complications for durvalumab, and reproductive system risks for nivolumab.

Conclusion: This comparative pharmacovigilance study highlights the diverse safety profiles of the five anti-HNSCC drugs. Clinicians should consider these ADRs when treating patients, especially elderly individuals or those with comorbidities. Personalized monitoring strategies should be developed to minimize risks and optimize therapeutic outcomes for HNSCC patients.

KEYWORDS

HNSCC, WHO-vigiaccess, anti-HNSCC drugs, adverse drug reactions, disproportionality analysis

1 Introduction

Head and neck squamous cell carcinoma (HNSCC) is a malignant tumor originating from the mucosal epithelium of the oral cavity, pharynx, larynx, and other regions of the upper digestive tract (Jiang et al., 2025). With an annual incidence exceeding 600,000 cases worldwide, HNSCC demonstrates significant geographical variations in disease prevalence (Wang and Anderson, 2022). HNSCC remains a major global health concern, with an estimated 946,456 new cases and 482,001 deaths reported annually worldwide (Bray et al., 2024). Despite advancements in diagnostic imaging and multimodal therapies, the 5-year survival rate for HNSCC remains relatively low, with fewer than 50% of patients surviving beyond this period (Ferlay et al., 2019). The incidence is generally higher in males than in females, likely due to higher rates of tobacco and alcohol consumption among men (Jiang et al., 2024). A similar sex-based disparity is observed in mortality rates. The treatment of HNSCC typically requires multidisciplinary comprehensive therapy, including surgery, radiotherapy, and chemotherapy (Cao et al., 2024). These treatment methods not only cause physical suffering to patients but also impose a heavy economic burden. The direct medical costs associated with HNSCC include hospitalization, surgery, chemoradiotherapy, and various diagnostic procedures. Indirect costs arise from productivity loss due to illness and treatment, as well as caregiving-related expenses borne by family members (Haddad et al., 2019). Moreover, the high recurrence rate of HNSCC further increases treatment complexity and economic burden (Umbreit et al., 2016). A deeper understanding of the therapeutic landscape, associated adverse events is therefore essential to guide clinical decision-making and improve outcomes in HNSCC management.

In the treatment landscape of HNSCC, five major systemic agents—cetuximab, pembrolizumab, nivolumab, atezolizumab, and durvalumab—have received clinical approval based on their demonstrated efficacy and safety profiles. These drugs fall into two main therapeutic categories: targeted therapy and immune checkpoint inhibitors. Cetuximab, a monoclonal antibody against the epidermal growth factor receptor (EGFR), has historically played a key role in the EXTREME regimen (cetuximab + platinum + 5-fluorouracil), which was considered the first-line standard of care for recurrent/metastatic (R/M) HNSCC prior to the introduction of immunotherapy (Vasiliadou et al., 2021). The standard cetuximab dosing protocol consists of an initial loading dose of 400 mg/m^2 followed by 250 mg/m^2 weekly (Chen et al., 2013). With the advent of immune checkpoint inhibitors, particularly anti-PD-1 antibodies, treatment strategies have evolved significantly. Pembrolizumab, as demonstrated in the KEYNOTE-048 trial, has become a first-line standard for R/M HNSCC either as monotherapy in patients with PD-L1 Combined Positive Score ≥1, or combination with platinum-based chemotherapy in those with more aggressive disease (Fan et al., 2020). The recommended dosage of pembrolizumab is either 200 mg every 3 weeks or 400 mg every 6 weeks (Haas et al., 2023). Nivolumab is approved for patients with R/M HNSCC who experience disease progression on or after platinum-based therapy, typically administered at 240 mg every 2 weeks or 480 mg every 4 weeks (Cohen et al., 2019). Although atezolizumab and durvalumab are not yet standard treatments for HNSCC, they have received regulatory approval in other solid tumors such as non-small cell lung cancer and urothelial carcinoma, and are currently being explored in head and neck cancers through ongoing clinical trials (Sodji et al., 2017). Atezolizumab is typically dosed at 1200 mg every 3 weeks, while durvalumab is administered at 10 mg/kg every 2 weeks (Prelaj et al., 2022). Treatment decisions for HNSCC are influenced by a variety of clinical and demographic factors, including patient age, performance status, comorbidities, and prior treatment history (Klinghammer et al., 2022). Understanding the mechanism of action, approved indications, dosing regimens, and real-world application of these agents is essential for optimizing individualized treatment strategies.

The utilization of real-world data (RWD) and spontaneous reporting systems (SRS) constitutes a validated approach for pharmacovigilance assessment (Jo et al., 2021). Since the 1960s, SRS has served as the cornerstone of pharmacovigilance, enabling early detection of adverse drug reactions and population-level safety evaluation (Srba et al., 2012). The WHO Collaborating Centre for International Drug Monitoring (Uppsala Monitoring Centre) maintains a global adverse drug reactions (ADRs) database critical for comparative drug safety analytics (Shetti et al., 2011). These data repositories play pivotal roles in enhancing HNSCC drug safety profiles and refining therapeutic protocols. Expanded therapeutic applications necessitate intensified safety surveillance.

This study evaluates five FDA-approved anti-HNSCC agents: cetuximab, pembrolizumab, nivolumab, atezolizumab, and durvalumab. These therapeutics demonstrate validated efficacy in advanced/recurrent HNSCC through multicenter clinical trials. However, treatment tolerance diminishes in elderly patients due to tumor progression, physiological decline, and immunosenescence (Song et al., 2024). Age-related pharmacodynamic alterations increase vulnerability to immunotherapy/targeted therapy toxicities, exacerbated by tumor heterogeneity and therapeutic complexity (Su et al., 2023). Geriatric treatment disparities manifest as reduced therapeutic response, amplified adverse effects, and compromised disease management (Schupack et al., 2022). Therapeutic efficacy in advanced disease is constrained by immune evasion mechanisms, tumor microenvironment dynamics, and patient performance status. This necessitates personalized therapeutic regimens tailored to individual patient profiles. We conducted a descriptive analysis of the spontaneously reported adverse events recorded in the VigiAccess database, aiming to compare the differences in adverse reactions associated with the five anti-HNSCC drugs. By analyzing the types and frequencies of adverse events, we sought to identify key safety concerns that may impact drug use, providing valuable insights for future clinical practice.

2 Methods

2.1 Drug samples

This study analyzes five therapeutic agents for HNSCC: cetuximab, pembrolizumab, nivolumab, atezolizumab, and durvalumab. Selection criteria (Table 1) prioritized clinical utility in HNSCC management and mechanistic targeting of immune evasion pathways. This study selected five anti-HNSCC drugs for analysis based on the following considerations: (1) Widespread Clinical Adoption: These agents are among the most commonly

TABLE 1 Overview of five anti-HNSCC drugs.

Drug Name	Structure	Target	Indications	First Marketed year
Cetuximab	Monoclonal antibody (IgG1, chimeric)	EGFR	HNSCC, Metastatic colorectal cancer, Squamous cell carcinoma of head and neck	2004
Pembrolizumab	Monoclonal antibody (IgG4, humanized)	PD-1	HNSCC, Melanoma, Non-small cell lung cancer (NSCLC), Hodgkin lymphoma, Gastric cancer	2014
Nivolumab	Monoclonal antibody (IgG4, fully human)	PD-1	HNSCC, Melanoma, NSCLC, Renal cell carcinoma, Hodgkin lymphoma	2014
Atezolizumab	Monoclonal antibody (IgG1, humanized)	PD-L1	HNSCC, Urothelial carcinoma, NSCLC, Triple-negative breast cancer	2016
Durvalumab	Monoclonal antibody (IgG1, human)	PD-L1	HNSCC, Locally advanced or metastatic urothelial carcinoma, NSCLC	2017

used drugs in clinical practice for HNSCC treatment, particularly for recurrent or metastatic HNSCC (Goel et al., 2022; Taberna et al., 2019). (2) Representative Mechanisms of Action: These drugs exemplify the two primary therapeutic strategies for HNSCC—EGFR inhibition and PD-1/PD-L1 immune checkpoint blockade (Wang et al., 2024). Their inclusion provides a comprehensive overview of ADR profiles associated with current HNSCC treatment paradigms. (3) Guideline Recommendations: These agents are recommended for HNSCC treatment in authoritative guidelines such as the NCCN (Cohen et al., 2019). (4) Clinical Trial Evidence: Robust clinical trial data support the use of these drugs in HNSCC management, establishing a solid foundation for this study (Yao et al., 2025). (5) Data Accessibility: Selection of these drugs ensures sufficient sample size within the VigiBase database, enhancing the reliability of study findings.

2.2 Search strategy and data source

The WHO-VigiAccess database was queried in March 2025 for adverse event reports associated with HNSCC immunotherapies. Accessible via https://www.vigiaccess.org, the platform provides aggregated global data including demographic parameters (age, gender) and geographical distributions. The Uppsala Monitoring Centre (UMC) maintains this pharmacovigilance data through its WHO Programme for International Drug Monitoring (PIDM) portal (Hussain et al., 2021). VigiAccess interfaces with VigiBase - the world's largest pharmacovigilance database established in 1968, initially comprising 10 participating nations. By March 2022, VigiBase encompassed 155 full members and 21 associate members under PIDM. Member states submit validated Individual Case Safety Reports (ICSRs) from healthcare professionals, patients, and manufacturers through national regulatory agencies (Ke et al., 2024). Toxicity profiles were characterized using MedDRA classification (System Organ Class [SOC] and Preferred Term [PT]) for adverse event categorization. The analysis focused on 27 symptom-relevant SOCs and PT-level frequency patterns for each agent's ADRs. Severity stratification utilized outcome codes: fatal outcomes, hospitalization-requiring events, and life-threatening incidents. Agent-specific search filters ensured precise data extraction. WHO-VigiAccess enhances pharmacovigilance research through transparent global ADR data sharing.

2.3 Disproportionality analysis

This study implemented disproportionality analysis using the Reporting Odds Ratio (ROR) and Proportional Reporting Ratio (PRR) to evaluate immunotherapy-associated adverse events (AEs) in HNSCC treatment (Rothman et al., 2004; Evans et al., 2001). These quantitative methods are standard pharmacovigilance tools for AE signal detection. ROR quantifies the probability of disproportionate reporting (PDRAE) for specific drug-AE combinations relative to comparator medications (Rahman et al., 2017). The algorithm incorporates four contingency table elements: a (target drug-AE pairs), b (target drug non-AE reports), c (non-target drug AE reports), and d (non-target drug non-AE reports). Minimum case requirement (a≥5) ensures statistical stability in ROR computation. Significant disproportionality signals were defined as ROR>2. The formula provides the ROR.:

$$\mathrm{ROR} = \frac{a/c}{b/d}$$

PRR provides a complementary assessment of reporting imbalance through incidence ratio comparison. PRR analysis applied an equivalent case threshold (≥5 reports) for validity. PRR≥2 with $\chi^2 \geq 4$ (equivalent to $p < 0.05$) and ≥3 cases defined statistically significant signals. These thresholds minimize false-positive signals from random reporting variation. Dual-methodology analysis enabled robust detection of disproportionate AE patterns across five HNSCC immunotherapeutics. The generated safety signals contribute essential pharmacovigilance intelligence for risk mitigation strategies. The formula provides the PRR.:

$$\mathrm{PRR} = \frac{a/(a+b)}{c/(c+d)}$$

2.4 Statistical analysis

This study adopts a retrospective quantitative research method, exploring past situations by analyzing current results. We used Excel to analyze the gender, age, and regional characteristics of victims of ADR from five anti-HNSSC drugs. The data sources include current status, case reports, case series, etc. The ADR reporting rate for each drug is defined by dividing the number of ADR symptoms for that

10.3389/fphar.2025.1602276

TABLE 2 Five anti-HNSCC drugs adverse reports' Demographic data.

	Cetuximab	Pembrolizumab	Nivolumab	Atezolizumab	Durvalumab
First Report Year	2003	2009	2012	2012	2014
Number of ADR reports	49,527	88,762	100,907	28,583	15,382
Female	15,289 (30.87%)	39,855 (44.90%)	30,720 (30.44%)	9067 (31.72%)	4310 (28.02%)
Male	31,001 (62.59%)	44,059 (49.64%)	61,164 (60.61%)	16,492 (57.70%)	9036 (58.74%)
Unknown	3237 (6.54%)	4848 (5.46%)	9023 (8.94%)	3024 (10.58%)	2036 (13.24%)
<18	49 (0.10%)	134 (0.15%)	277 (0.27%)	26 (0.09%)	9 (0.06%)
18–44	3219 (6.50%)	4596 (5.18%)	5528 (5.48%)	1065 (3.73%)	254 (1.65%)
45–64	17,704 (35.75%)	21,649 (24.39%)	26,996 (26.75%)	7468 (26.13%)	3333 (21.67%)
65–74	11,288 (22.79%)	20,191 (22.75%)	24,662 (24.44%)	7890 (27.60%)	4197 (27.29%)
>75	5003 (10.10%)	13,473 (15.18%)	14,259 (14.13%)	4544 (15.90%)	2238 (14.55%)
Unknown	12,264 (24.76%)	28,719 (32.36%)	29,185 (28.92%)	7590 (26.55%)	5351 (34.79%)
Africa	767 (1.55%)	1048 (1.18%)	286 (0.28%)	142 (0.50%)	151 (0.98%)
Americas	24,403 (49.27%)	26,142 (29.45%)	32,983 (32.69%)	6394 (22.37%)	3343 (21.73%)
Asia	11,763 (23.75%)	35,556 (40.06%)	33,466 (33.17%)	13,943 (48.78%)	7282 (47.34%)
Europe	12,109 (24.45%)	24,030 (27.07%)	31,377 (31.09%)	7654 (26.78%)	4201 (27.31%)
Oceania	485 (0.98%)	1986 (2.24%)	2795 (2.77%)	450 (1.57%)	405 (2.63%)
2025	756 (1.53%)	2896 (3.26%)	1189 (1.18%)	530 (1.85%)	694 (4.51%)
2024	5151 (10.40%)	27,021 (30.44%)	22,283 (22.08%)	8403 (29.40%)	7108 (46.21%)
2023	4521 (9.13%)	14,037 (15.81%)	10,358 (10.26%)	5327 (18.64%)	1713 (11.14%)
2022	4429 (8.94%)	10,419 (11.74%)	9829 (9.74%)	4384 (15.34%)	823 (5.35%)
2021	3322 (6.71%)	7326 (8.25%)	8749 (8.67%)	2766 (9.68%)	1207 (7.85%)
2020	2836 (5.73%)	5524 (6.22%)	7572 (7.50%)	2431 (8.51%)	1190 (7.74%)
2019	2567 (5.18%)	8274 (9.32%)	13,390 (13.27%)	2668 (9.33%)	1819 (11.83%)
2018	2208 (4.46%)	6688 (7.53%)	11,928 (11.82%)	1286 (4.50%)	613 (3.99%)
2017	2914 (5.88%)	3930 (4.43%)	9528 (9.44%)	679 (2.38%)	148 (0.96%)
2016	1972 (3.98%)	1555 (1.75%)	4840 (4.80%)	75 (0.26%)	51 (0.33%)
Before 2015	18,851 (38.06%)	1092 (1.23%)	1241 (1.23%)	34 (0.12%)	16 (0.10%)

drug by the total number of ADR reports. We calculated the incidence rate of ADR symptoms reported for each drug and performed a descriptive comparative analysis. To obtain meaningful conclusions, we categorized descriptive variables using frequencies and percentages. Statistical significance was set at a p-value of less than 0.05.

3 Result

3.1 Case description of the study

According to the WHO-VigiAccess database statistics, as of March 2025, the global ADR reports for five drugs show the following characteristics: Cetuximab (first reported in 2003) has a total of 49,527 reports, with a significant male proportion (62.59%), females accounting for 30.87%, and unknown gender making up 6.54%. The age distribution is dominated by the 45–64 years group (35.75%), followed by 65–74 years (22.79%). Regionally, the Americas account for the highest proportion (49.27%), followed by Europe (24.45%) and Asia (23.75%). Historical data shows that 38.06% of the reports were concentrated before 2015, with reports from 2024 accounting for 10.40% (5,151 cases). Pembrolizumab (first reported in 2009) has a total of 88,762 reports, with a relatively balanced gender distribution (female 44.90%, male 49.64%). The age groups are mainly 45–64 years (24.39%) and 65–74 years (22.75%), with a higher reporting rate in the elderly population (>75 years) at 15.18%. Asia is its primary reporting region (40.06%), followed by Europe (27.07%). The report volume surged in 2024, accounting for 30.44% (27,021 cases), reflecting a significant increase in safety concerns in recent years. Nivolumab (first reported in 2012) has the highest report volume (100,907 cases), with 60.61% male and

10.3389/fphar.2025.1602276

TABLE 3 Cetuximab, Pembrolizumab, Nivolumab, Atezolizumab, and Durvalumab's report rates for 27 SOCs.

System organ class	Cetuximab	Pembrolizumab	Nivolumab	Atezolizumab	Durvalumab
Blood and lymphatic system disorders	4009 (3.62%)	6678 (3.30%)	5527 (2.57%)	3240 (5.51%)	1279 (4.65%)
Cardiac disorders	2021 (1.82%)	4453 (2.20%)	4790 (2.23%)	1288 (2.19%)	619 (2.25%)
Congenital, familial, and genetic disorders	30 (0.03%)	79 (0.04%)	58 (0.03%)	22 (0.04%)	16 (0.06%)
Ear and labyrinth disorders	175 (0.16%)	342 (0.17%)	525 (0.24%)	122 (0.21%)	52 (0.19%)
Endocrine disorders	61 (0.06%)	8544 (4.22%)	12,527 (5.83%)	1699 (2.89%)	901 (3.28%)
Eye disorders	1083 (0.98%)	2177 (1.08%)	2518 (1.17%)	421 (0.72%)	221 (0.80%)
Gastrointestinal disorders	12,444 (11.23%)	18,912 (9.35%)	23,603 (10.98%)	6087 (10.36%)	2371 (8.62%)
General disorders and administration site conditions	14,449 (13.04%)	28,775 (14.22%)	31,947 (14.86%)	10,520 (17.90%)	3726 (13.55%)
Hepatobiliary disorders	626 (0.57%)	4624 (2.29%)	6643 (3.09%)	1755 (2.99%)	739 (2.69%)
Immune system disorders	3465 (3.13%)	1644 (0.81%)	1735 (0.81%)	526 (0.90%)	185 (0.67%)
Infections and infestations	5977 (5.39%)	8832 (4.37%)	10,844 (5.04%)	3535 (6.01%)	1497 (5.44%)
Injury, poisoning and procedural complications	10,551 (9.52%)	18,039 (8.92%)	14,102 (6.56%)	3877 (6.60%)	1681 (6.11%)
Investigations	5978 (5.39%)	13,590 (6.72%)	11,888 (5.53%)	4551 (7.74%)	1917 (6.97%)
Metabolism and nutrition disorders	4221 (3.81%)	7316 (3.62%)	8994 (4.18%)	2468 (4.20%)	776 (2.82%)
Musculoskeletal and connective tissue disorders	1393 (1.26%)	8362 (4.13%)	10,222 (4.75%)	2155 (3.67%)	1051 (3.82%)
Neoplasms benign, malignant and unspecified (incl cysts and polyps)	3042 (2.74%)	14,634 (7.23%)	13,269 (6.17%)	1541 (2.62%)	1732 (6.30%)
Nervous system disorders	4429 (4.00%)	10,178 (5.03%)	10,940 (5.09%)	2860 (4.87%)	1111 (4.04%)
Pregnancy, puerperium and perinatal conditions	6 (0.01%)	31 (0.02%)	96 (0.05%)	9 (0.02%)	1 (0.00%)
Psychiatric disorders	934 (0.84%)	2824 (1.40%)	2376 (1.11%)	568 (0.97%)	278 (1.01%)
Renal and urinary disorders	1085 (0.98%)	5331 (2.63%)	5144 (2.39%)	1934 (3.29%)	442 (1.61%)
Reproductive system and breast disorders	166 (0.15%)	530 (0.26%)	360 (0.17%)	94 (0.16%)	43 (0.16%)
Respiratory, thoracic and mediastinal disorders	6937 (6.26%)	14,799 (7.31%)	17,807 (8.28%)	4635 (7.89%)	5097 (18.53%)
Skin and subcutaneous tissue disorders	23,146 (20.88%)	12,239 (6.05%)	14,529 (6.76%)	3064 (5.21%)	1308 (4.76%)
Social circumstances	72 (0.07%)	585 (0.29%)	175 (0.08%)	20 (0.03%)	20 (0.07%)
Surgical and medical procedures	943 (0.85%)	4645 (2.30%)	989 (0.46%)	112 (0.19%)	67 (0.24%)
Vascular disorders	3530 (3.19%)	3678 (1.82%)	3219 (1.50%)	1635 (2.78%)	348 (1.27%)
Product issues	69 (0.06%)	513 (0.25%)	190 (0.09%)	42 (0.07%)	25 (0.09%)

30.44% female. The 45–64 years age group accounts for 26.75%, followed by 65–74 years (24.44%). The geographic distribution is concentrated in the Americas (32.69%) and Europe (31.09%). Report volumes from 2021 to 2023 remained relatively high (8.67%–13.27%), with the 2024 report volume accounting for 22.08% (22,283 cases). Atezolizumab (first reported in 2012) has a total of 28,583 reports, with 57.70% male and 31.72% female. The 65–74 years group is the most prevalent age group (27.60%), with Asia accounting for nearly half of the reports (48.78%). The report volume for 2024 accounted for 29.40% (8,403 cases), with 2023 also showing a relatively high proportion (18.64%). Durvalumab (first reported in 2014) has the least number of reports (15,382 cases), with 58.74% male and 28.02% female. The 65–74 years group accounts for 27.29%, with Asia being the primary reporting region (47.34%). The report volume for 2024 saw a sharp increase, accounting for as high as 46.21% (7,108 cases). Table 2 presents the details.

3.2 Distribution tables of 27 SOCs for five anti-HNSCC drugs

As delineated in Table 3, the ADR reporting rates varied markedly across SOCs for the five anti-HNSCC drugs: Cetuximab, Pembrolizumab, Nivolumab, Atezolizumab, and Durvalumab. Cetuximab exhibited the highest reporting rate for skin and subcutaneous tissue disorders (20.88%), significantly exceeding other agents (Pembrolizumab: 6.05%; Nivolumab: 6.76%; Atezolizumab: 5.21%; Durvalumab: 4.76%). In contrast, Durvalumab demonstrated a disproportionately elevated

TABLE 4 Top 20 adverse reactions for five anti-HNSCC drugs.

Cetuximab		Pembrolizumab		Nivolumab		Atezolizumab		Durvalumab	
ADR	Report rate	ADR	Report rate	ADR	Report rate	ADR	Report rate	ADR	Report rate
Off label use	5.98%	Malignant neoplasm progression	5.56%	Malignant neoplasm progression	4.23%	Off label use	3.99%	Pneumonitis	8.28%
Rash	5.74%	Death	2.44%	Death	4.03%	Death	3.20%	Death	4.29%
Death	2.21%	Inappropriate schedule of product administration	2.33%	Diarrhoea	2.36%	No adverse event	2.78%	Malignant neoplasm progression	3.11%
Pruritus	2.21%	Fatigue	1.78%	Interstitial lung disease	1.90%	Pyrexia	1.89%	Interstitial lung disease	2.98%
Diarrhoea	2.14%	Diarrhoea	1.71%	Off label use	1.84%	Disease progression	1.72%	Radiation pneumonitis	2.44%
Acne	1.87%	Interstitial lung disease	1.67%	Fatigue	1.76%	Diarrhoea	1.71%	Diarrhoea	1.72%
Nausea	1.83%	Hypothyroidism	1.58%	Hypothyroidism	1.61%	Fatigue	1.64%	Dyspnoea	1.59%
Dyspnoea	1.77%	Product use in unapproved indication	1.56%	Intentional product use issue	1.52%	Asthenia	1.36%	Pneumonia	1.51%
Infusion related reaction	1.62%	Off label use	1.50%	Pyrexia	1.52%	Interstitial lung disease	1.30%	Off label use	1.44%
Vomiting	1.49%	Rash	1.25%	Rash	1.45%	Pneumonitis	1.26%	Fatigue	1.43%
Malignant neoplasm progression	1.36%	Product use issue	1.19%	Colitis	1.37%	Pneumonia	1.22%	Asthenia	1.32%
Dermatitis acneiform	1.32%	Nausea	1.17%	Asthenia	1.24%	Dyspnoea	1.22%	Pyrexia	1.25%
Pyrexia	1.24%	Pyrexia	1.09%	Pneumonitis	1.22%	Anaemia	1.21%	Rash	1.16%
Erythema	1.20%	Asthenia	1.09%	Pruritus	1.21%	Decreased appetite	1.18%	Hypothyroidism	1.05%
Dry skin	1.18%	Pneumonia	1.02%	Adrenal insufficiency	1.18%	Nausea	1.15%	Pruritus	1.02%
Hypotension	1.11%	Pneumonitis	1.01%	Dyspnoea	1.17%	Rash	1.15%	Cough	1.01%
Neutropenia	1.04%	Dyspnoea	0.92%	Nausea	1.16%	Febrile neutropenia	1.08%	Colitis	0.99%
Hypersensitivity	1.02%	Decreased appetite	0.91%	Decreased appetite	1.00%	Hypertension	1.08%	Nausea	0.92%
Asthenia	0.99%	Pruritus	0.87%	Pneumonia	0.97%	Neutropenia	1.02%	Anaemia	0.87%
Disease progression	0.97%	Drug ineffective	0.85%	Arthralgia	0.82%	Pruritus	1.01%	Febrile neutropenia	0.84%

incidence of respiratory, thoracic, and mediastinal disorders (18.53%), which was 2.2–3.5-fold higher than other drugs (Cetuximab: 6.26%; Pembrolizumab: 7.31%; Nivolumab: 8.28%; Atezolizumab: 7.89%). Pembrolizumab, Nivolumab, and Atezolizumab are associated with higher rates of systemic and administration site diseases (14.22%, 14.86%, and 17.90%, respectively). In the SOC of gastrointestinal disorders, ADRs were relatively high: cetuximab (11.23%), pembrolizumab (9.35%), nivolumab (10.98%), atezolizumab (10.36%), and durvalumab (8.62%). These findings underscore distinct toxicity patterns among the agents.

3.3 The most common adverse reactions of five anti-HNSCC drugs

The ADR profiles of five anti-HNSCC drugs—cetuximab, pembrolizumab, nivolumab, atezolizumab, and

TABLE 5 Common adverse reactions of five anti-HNSCC drugs.

System organ classes	ADRs	Signal N
Blood and lymphatic system disorders	Leukopenia, Febrile neutropenia, Thrombocytopenia,Pancytopenia, Neutropenia,Anaemia	6
Cardiac disorders	Cardiac arrest, Myocardial infarction, Atrial fibrillation, Cardiac failure, Tachycardia	4
Neoplasms benign, malignant and unspecified (incl cysts and polyps)	Neoplasm progression, Malignant neoplasm progression	2
Eye disorders	Vision blurred	1
Gastrointestinal disorders	Abdominal pain upper, Abdominal distension, Dysphagia,Diarrhoea, Vomiting,Ascites, Constipation,Colitis, Abdominal pain, Nausea,Stomatitis,Dry mouth, Dyspepsia	13
General disorders and administration site conditions	Peripheral swelling, Asthenia,Condition aggravated, Pain,Drug ineffective, Multiple organ dysfunction syndrome, Death,Chest pain, Malaise,Illness, Fatigue,Oedema peripheral, Swelling,Pyrexia, Chills,Oedema, Disease progression, General physical health deterioration, Mucosal inflammation	18
Hepatobiliary disorders	Hepatic failure	1
Immune system disorders	Hypersensitivity, Anaphylactic reaction	2
Infections and infestations	Sepsis, Infection,Nasopharyngitis, Pneumonia,Influenza, Pneumonia aspiration, Urinary tract infection, Septic shock, Cellulitis	9
Injury, poisoning and procedural complications	Toxicity to various agents,Off label use,Infusion related reaction, Fall,Product use in unapproved indication	5
Investigations	Weight decreased, Aspartate aminotransferase increased, Blood creatinine increased, Platelet count decreased, Oxygen saturation decreased, Haemoglobin decreased, Neutrophil count decreased, Alanine aminotransferase increased, Blood alkaline phosphatase increased, Blood bilirubin increased, White blood cell count decreased	11
Metabolism and nutrition disorders	Dehydration, Hypokalaemia,Hyperglycaemia, Decreased appetite, Hyponatraemia,Hyperkalaemia	6
Musculoskeletal and connective tissue disorders	Neck pain, Muscular weakness, Muscle spasms, Back pain, Arthralgia,Pain in extremity, Myalgia	7
Skin and subcutaneous tissue disorders	Hyperhidrosis, Skin toxicity, Rash,Erythema,Dry skin, Dermatitis,Urticaria, Alopecia,Pruritus, Rash pruritic, Skin disorder	10
Nervous system disorders	Headache, Paraesthesia,Dizziness, Tremor,Somnolence, Hypoaesthesia,Syncope, Cerebrovascular accident, Seizure,Neuropathy peripheral	10
Psychiatric disorders	Confusional state, Insomnia,Anxiety	3
Renal and urinary disorders	Acute kidney injury, Renal impairment, Renal failure	3
Respiratory, thoracic and mediastinal disorders	Respiratory failure, Oropharyngeal pain, Interstitial lung disease, Pneumothorax,Dyspnoea, Cough,Pulmonary embolism, Haemoptysis,Pleural effusion, Dysphonia,Hypoxia, Pneumonitis	10
Vascular disorders	Thrombosis, Hypotension,Deep vein thrombosis, Flushing,Haemorrhage, Hypertension	6

durvalumab—were analyzed using the WHO-VigiAccess database, revealing distinct toxicity patterns across SOCs.Table 4 lists the 20 most frequently reported adverse reactions for the five anti-HNSCC drugs, presented as preferred terms within the SOCs. Cetuximab exhibited a predominant dermal toxicity profile, with rash (5.74%) and off-label use (5.98%) as the most frequently reported ADRs. Cutaneous events, including pruritus (2.21%), acne (1.87%), and erythema (1.20%), collectively accounted for 12.45% of reports. Pembrolizumab demonstrated a higher incidence of immune-related adverse events (irAEs), notably malignant neoplasm progression (5.56%). Nivolumab shared similar irAE patterns, with malignant neoplasm progression (4.23%). It is worth noting that Atezolizumab showed outstanding Off-label use (3.99%) and Death (3.20%). Durvalumab displayed a unique safety signal: pneumonitis (8.28%) and radiation pneumonitis (2.44%) were reported at rates 2.2–8.2-fold higher than other agents (nivolumab: 1.22%; pembrolizumab: 1.01%).

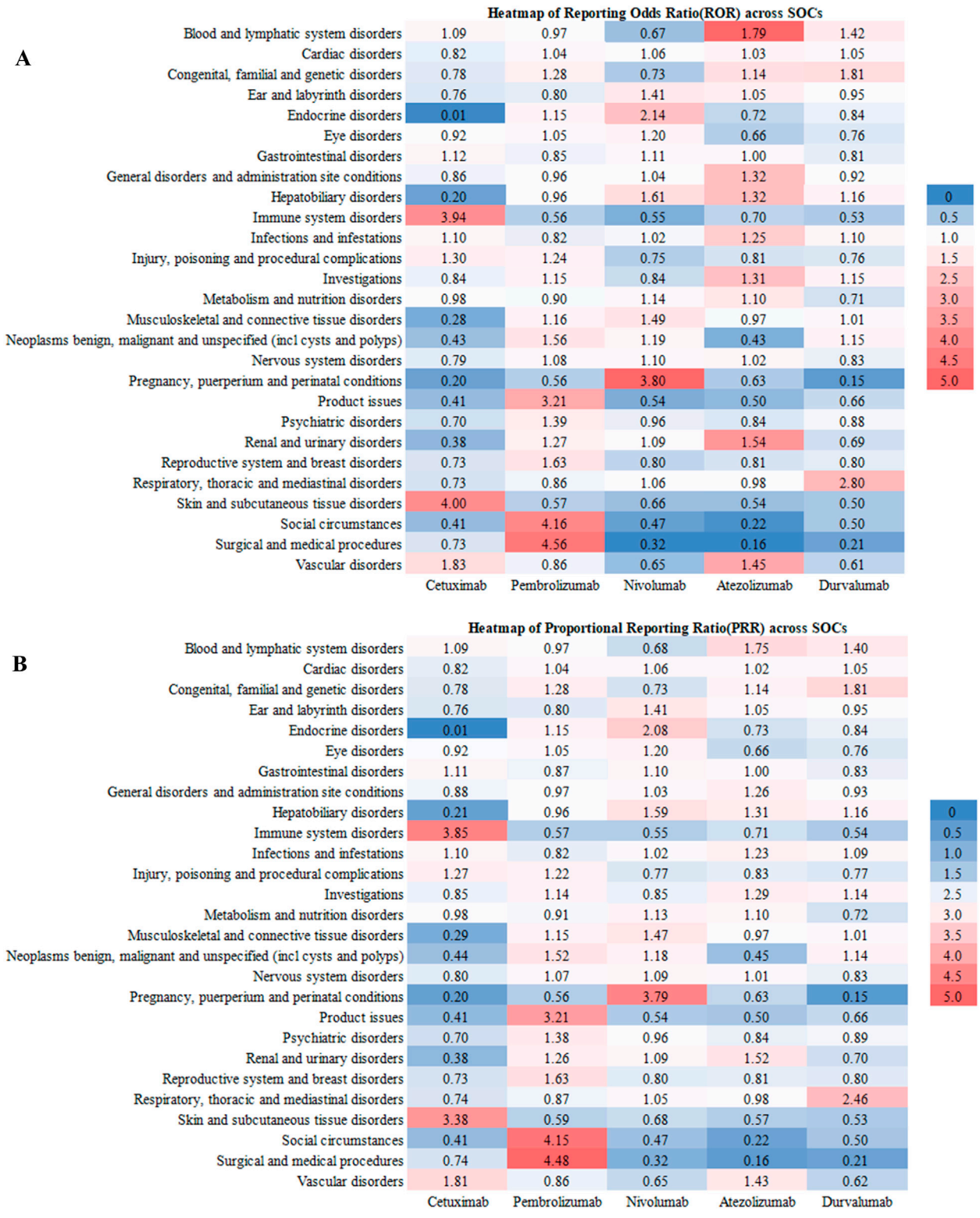

FIGURE 1
The RoR **(A)** and PRR **(B)** heatmap illustrates the safety profiles of the five anti-HNSCC drgus across different SOCs, highlighting specific areas of elevated risk for each drug.

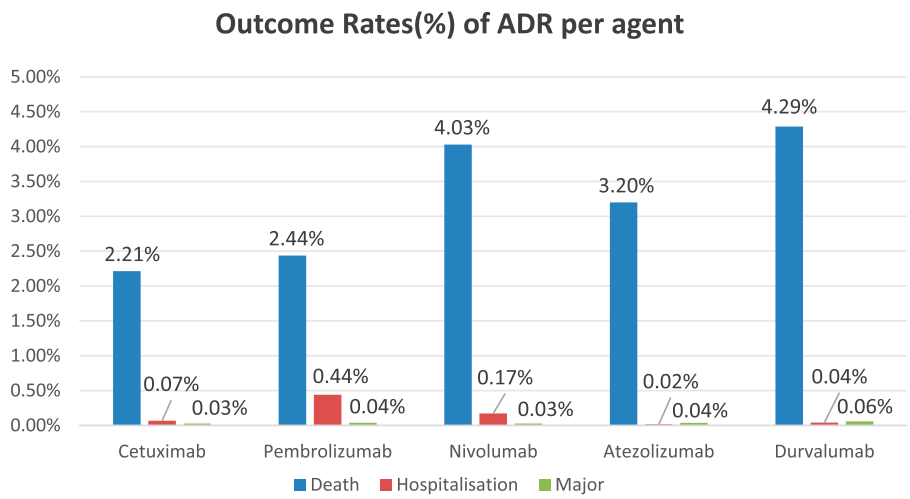

FIGURE 2
Major adverse event rates for five anti-HNSCC drgus.

3.4 Commonalities in the most common adverse reactions of five anti-HNSCC drugs

As delineated in Table 5, The analysis of common adverse reactions across five anti-HNSCC agents (Cetuximab, Pembrolizumab, Nivolumab, atezolizumab, Durvalumab) demonstrated that systemic and administration site-related events (Signal N = 18) were the most frequently reported, primarily including disease progression, death, multi-organ dysfunction, and nonspecific symptoms (e.g., pyrexia, fatigue, and mucosal inflammation). Gastrointestinal toxicities (Signal N = 13) were prominently observed, with diarrhea, vomiting, and abdominal pain as the predominant manifestations. Laboratory abnormalities (Signal N = 11) focused on cytopenias (e.g., leukopenia and thrombocytopenia) and elevated hepatic enzymes. Cutaneous reactions (Signal N = 10), neurologic events (Signal N = 10), and respiratory disorders (Signal N = 10) manifested as rash, headache, and dyspnea, respectively, while infection-related complications (Signal N = 9) included sepsis, pneumonia, and urinary tract infections. Notably, low-frequency but severe events were identified, encompassing cardiac toxicity (e.g., myocardial infarction, Signal N = 4), acute kidney injury (Signal N = 3), and hepatic failure (Signal N = 1).

3.5 Disproportionality analysis

As delineated in Figure 1, The risk stratification analysis based on the SOC reveals the unique safety characteristics of different immunotherapy drugs, specifically as follows: Cetuximab shows significant risk signals in immune system diseases (RoR = 3.94; PRR = 3.85), with its risk level far exceeding the other four drugs. Additionally, its high-risk features in the skin and subcutaneous tissue diseases (RoR = 4.00; PRR = 3.38) suggest that it may cause severe skin toxicity (such as rashes or mucositis). Pembrolizumab's main risks are concentrated in complications related to surgery and medical procedures (RoR = 4.56; PRR = 4.48), with its risk intensity being 4–5 times that of other systems. Nivolumab's reproductive system risk features are particularly distinctive, with abnormal increases in risk signals in pregnancy-related diseases (RoR = 3.80; PRR = 3.79). Atezolizumab's most prominent risks are in the blood and lymphatic systems (RoR = 1.79; PRR = 1.75), possibly increasing the risk of anemia or thrombocytopenia. Durvalumab's respiratory system toxicity is significantly higher than that of other drugs (RoR = 2.80; PRR = 2.46), necessitating caution regarding the risk of interstitial pneumonia. Furthermore, its higher risk in congenital diseases (RoR = 1.81; PRR = 1.81) suggests that potential genetic toxicity requires further investigation.

3.6 Serious adverse events of five anti-HNSCC drugs

Incidence of severe adverse events (including mortality, hospitalization, and life-threatening incidents) among five anti-HNSCC agents: Cetuximab: Mortality (2.21%), Hospitalization (0.07%), Major Events (0.03%); Pembrolizumab: Mortality (2.44%), Hospitalization (0.44%), Major Events (0.04%); Nivolumab: Mortality (4.03%), Hospitalization (0.17%), Major Events (0.03%); Atezolizumab: Mortality (3.20%), Hospitalization (0.02%), Major Events (0.04%); Durvalumab: Mortality (4.29%), Hospitalization (0.04%), Major Events (0.06%). The bar chart demonstrates comparative incidence rates of primary adverse events across therapeutic agents (Figure 2).

4 Discussion

The global health burden of HNSCC continues to rise, particularly among high-risk groups associated with smoking and alcohol consumption. If left untreated, HNSCC can lead to severe health consequences, including death (Chintala et al., 2022).In

recent years, novel immunotherapies and targeted treatments have offered more options for patients, but the potential ADRs of these therapies remain a major challenge in clinical application.his study analyzes data from the WHO-VigiAccess database, with a particular focus on ADRs associated with five promising anti-HNSCC drugs—cetuximab, pembrolizumab, nivolumab, atezolizumab, and durvalumab—highlighting their overall ADR profiles, distribution across different SOCs, and disproportionality in immune-related ADRs.The results show that different drugs exhibit significantly heterogeneous safety profiles due to differences in mechanisms of action and indications, underscoring the need for personalized monitoring strategies. These findings not only reveal the challenges in anti-HNSCC drug therapies but also provide important reference points for clinical practice.

Global ADR data analysis reveals a significant number of ADR reports associated with these five anti-HNSCC drugs, totaling 145,678 reports. In terms of gender distribution, ADRs reported by male patients are dominant, which could be linked to male patients' treatment needs and pharmacokinetic differences. Studies have shown that male patients often experience more significant treatment responses and ADRs than female patients across many types of cancer, possibly due to differences in hormone levels, immune responses, and drug metabolism (Dai et al., 2025). For example, males generally have a higher drug clearance rate, which may lead to fluctuations in drug concentrations in the body, thereby increasing the risk of ADRs (Venturini et al., 2011). For instance, the activity of certain cytochrome P450 enzymes might be higher in males than in females, accelerating drug metabolism and thereby affecting drug efficacy (Tran et al., 1998). Additionally, smoking and alcohol consumption are major risk factors for HNSCC, with males typically having higher rates of these behaviors than females (Johnson et al., 2020). These lifestyle factors may influence drug metabolism and efficacy, increasing the risk of ADRs.The age distribution shows that the 45–64 age group has the highest proportion of ADRs. Patients in this age group are typically middle-aged and elderly, often with comorbid conditions, and long-term exposure to carcinogenic environmental factors (such as smoking and drinking) further increases their risk of HNSCC. Elderly populations, in particular, are more likely to experience immune-related adverse events when undergoing immune checkpoint inhibitor therapy, which is associated with age-related immune system decline and enhanced autoimmune responses (Wang et al., 2021). Additionally, older patients may experience more drug interactions due to comorbidities or polypharmacy, thereby increasing the risk of ADRs (Yadesa et al., 2021). The immune system ages with increasing age, leading to a decline in immune function, which may affect the efficacy and toxicity of immune checkpoint inhibitors (Baik et al., 2017). Furthermore, geographic distribution data show that the highest ADR reports come from the Americas and Europe. This phenomenon may reflect differences in drug availability, healthcare systems, and pharmacovigilance practices. The disparities in drug accessibility across regions may lead to patients being exposed to different treatment regimens, which can influence ADR reporting. For example, in the Americas and Europe, regulatory systems for drugs are relatively well-established, and pharmacovigilance measures are effectively implemented, resulting in a higher number of ADR reports (Valinciute-Jankauskiene and Kubiliene, 2021). In contrast, in some low-income countries and regions, the limited availability of drugs and insufficient resources may lead to fewer ADR reports, potentially underestimating the actual incidence (Onyije et al., 2024). These geographic differences and patient population characteristics provide a more comprehensive understanding of the safety and tolerability of anti-HNSCC drugs, helping further optimize treatment strategies and pharmacovigilance practices.

The five anti-HNSCC drugs evaluated in this study exhibit distinct safety profiles influenced by their pharmacological mechanisms, treatment settings, and patient characteristics. Cetuximab, as an EGFR inhibitor, has been used for a long time in the treatment of HNSCC (Elmusrati et al., 2021). It can be used alone or in combination with chemotherapy drugs to enhance treatment efficacy, especially for tumors with high EGFR expression (Pirker, 2015). However, despite its good effectiveness in treating HNSCC, Cetuximab's ADRs related to skin and subcutaneous tissue diseases account for as much as 20.88%, mainly manifested as rash (5.74%), pruritus (2.21%), and acneiform dermatitis (1.87%). Skin toxicities such as rash and mucositis are common treatment-related side effects and typically manifest as rashes on the face, neck, and upper chest, closely related to the pharmacological effects of the drug (Puthenpurail et al., 2021). These ADRs are closely related to the abnormal differentiation of keratinocytes caused by EGFR signaling blockade, reflecting the typical skin toxicity of EGFR inhibitors (Nowaczyk et al., 2023). By inhibiting the EGFR signaling pathway, Cetuximab blocks the proliferation and repair of these cells, leading to skin cell damage and adverse reactions (Parikh et al., 2014). Clinically, preventive use of moisturizers and close monitoring of skin reactions is essential. Pembrolizumab, as a PD-1 inhibitor, blocks the interaction between PD-1 and its ligand PD-L1, restoring T-cell function and enhancing the immune system's ability to recognize and eliminate cancer cells (Gu et al., 2024). ICIs—including Pembrolizumab, Nivolumab, Atezolizumab, and Durvalumab—achieve anti-tumor effects by enhancing T-cell activity through PD-1/PD-L1 pathway inhibition (Zhong et al., 2020; Tekiki et al., 2021; Schomberg, 2019). In this study, gastrointestinal disorders (GI) emerged as a common category of ADRs across all five drugs. The relatively high prevalence of GI-related ADRs is consistent with known toxicities such as mucositis, diarrhea, colitis, and nausea. For Cetuximab, mucositis and diarrhea may result from EGFR inhibition in the GI epithelium, which impairs mucosal repair and absorption (Hintelmann et al., 2020). For ICIs, colitis and diarrhea are well-documented irAEs resulting from loss of immune tolerance in the intestinal mucosa, likely mediated by T-cell overactivation and cytokine release (Lau et al., 2021). In addition to GI toxicity, Pembrolizumab was linked to elevated risks of surgical and medical complications (RoR: 4.56; PRR: 4.48), possibly due to its impact on wound healing and infection control in the post-surgical setting (Xu et al., 2023). Nivolumab was associated with a significantly increased risk of pregnancy-related disorders (RoR: 3.80; PRR: 3.79), suggesting potential disruption of maternal-fetal immune tolerance via enhanced T-cell activity. Atezolizumab demonstrated a notable risk in the hematologic system, with 5.51% of ADRs affecting blood and lymphatic tissues (RoR: 1.79; PRR: 1.75). This may reflect

immune-mediated bone marrow suppression or autoimmunity targeting hematopoietic cells (Falette Puisieux et al., 2022). Immune checkpoint inhibitors may activate autoimmune responses, leading to attacks on normal blood cells, especially when the patient's immune function is activated, causing immune cells to mistakenly attack normal hematopoietic tissue or blood cells, leading to hematologic adverse reactions (Zhang et al., 2021). Durvalumab, in contrast, showed the highest respiratory system toxicity (18.53%), primarily pneumonia (8.28%) and radiation pneumonitis (2.44%). These effects are likely enhanced by its use in post-chemoradiation consolidation therapy for NSCLC, where radiotherapy exacerbates lung tissue susceptibility. Routine pulmonary evaluation and radiographic monitoring are critical during treatment. Finally, both Pembrolizumab and Nivolumab—commonly used in advanced or refractory HNSCC—showed the highest rates of malignant neoplasm progression reports (Pembrolizumab: 5.83%, Nivolumab: 4.23%). This may reflect the drugs' widespread use in late-stage disease, where tumor immune escape mechanisms can evolve in response to prolonged immune activation. Immune reprogramming of the tumor microenvironment might enable cancer cells to resist immune surveillance and promote progression or metastasis.

ICIs have demonstrated significant efficacy in the treatment of various malignancies, particularly HNSCC. The occurrence of specific irAEs may be related to the expression patterns of immune checkpoints and the immunological microenvironment in affected organs. For example, PD-1/PD-L1 expression in pulmonary tissue may lead to excessive T-cell activation, resulting in pneumonitis (Ebinama et al., 2023). Similarly, in the gastrointestinal tract, ICIs may disrupt immune tolerance and induce colitis. Endocrine organs are also susceptible, with irAEs manifesting as thyroiditis, hypophysitis, or type 1 diabetes (Takada et al., 2020). Pre-existing immune status may influence the likelihood of irAEs. Elevated levels of autoantibodies or inflammatory cytokines have been associated with increased risk (Basnet et al., 2024). In addition, the gut microbiome plays a crucial role in regulating immune responses. Studies have indicated that specific microbial compositions may be linked to irAE risk. For instance, the presence of certain bacterial strains may enhance immune activation and thereby increase susceptibility to irAEs (Naqash et al., 2021).

Although the overall incidence of SAEs—including mortality, hospitalization, and life-threatening complications—was relatively low across the five agents, their clinical significance should not be underestimated. Each drug exhibited a distinct adverse event profile. Previous studies have suggested that the risk of SAEs may be influenced by cumulative dosage and duration of treatment (Llopis-Salvia et al., 2010). However, there is currently a lack of robust data analyzing the specific causes leading to SAE outcomes. Therefore, it is essential to implement effective monitoring strategies in clinical practice. These include early recognition of symptoms and timely administration of immunosuppressive agents such as corticosteroids when indicated. Furthermore, stratifying patients based on comorbidities, PD-L1 expression, and prior treatment history may help reduce the likelihood of severe complications and improve treatment safety.

This study is limited by the inherent biases of spontaneous reporting systems. First, underreporting may disproportionately affect lower-grade toxicities, potentially underestimating their true incidence. Secondly, the lack of clinical variables such as treatment duration and dosing plan can hinder risk stratification and confuse ADR attribution. To address these limitations, future research should integrate existing adverse reaction reporting systems with hospital electronic medical record systems for analysis, to capture underreported low-level ADRs and clinical confounding factors. Additionally, the pharmacovigilance database lacked consistent data on whether ADRs occurred with monotherapy or combination regimens, limiting the assessment of each drug's independent safety profile. Importantly, while HNSCC comprises clinically distinct subtypes (e.g., oropharyngeal, hypopharyngeal, laryngeal carcinomas) with potential variations in tumor biology and treatment response, the WHO-VigiAccess database lacks subtype-specific ADR data. Future research should integrate electronic health records and real-world evidence platforms to dynamically track the impact of dosage, treatment duration, and concomitant medications on ADRs, while also exploring the correlation between biomarkers (e.g., PD-L1 expression levels) and toxicity risks. Despite these limitations, new immunotherapies continue to evolve, demonstrating promising prospects. For instance, ongoing research on anti-PD-1 drugs and combination immunotherapies has shown high efficacy and good tolerability in early clinical trial results. While these immunotherapy drugs show broad potential for clinical application, more Phase III clinical trials and long-term safety evaluations are still needed.

4.1 Clinical practice recommendations

Based on the study findings, individualized management strategies should be developed for different drugs: Considering the impact of gender and age on pharmacokinetics and pharmacodynamics, individualized dosing regimens should be developed based on factors such as the patient's gender, age, physiological functions, and comorbidities to enhance efficacy and reduce the risk of ADRs. In clinical trial design, gender and age factors should be fully considered, with stratified analysis performed to more accurately assess drug efficacy and safety. For patients receiving Cetuximab, heightened attention to dermatologic toxicity is warranted. Prophylactic skin care education, along with early intervention for rash and potential infections, is essential to manage the high incidence of cutaneous adverse events. In patients treated with ICIs such as Pembrolizumab or Nivolumab, comprehensive baseline assessments—including thyroid function, pulmonary function tests, and gastrointestinal evaluation—should be performed. Regular follow-up monitoring is recommended to promptly identify irAEs, such as thyroiditis, pneumonitis, or colitis. Prior to initiating Durvalumab therapy, pulmonary imaging should be conducted to exclude subclinical interstitial lung disease. For patients with a history of thoracic radiotherapy, extended post-treatment surveillance is advised to detect delayed-onset pulmonary complications, including radiation-induced pneumonitis. During Atezolizumab treatment, complete blood

counts should be monitored regularly, with particular attention to hemoglobin levels and leukocyte differentials. Early signs of anemia or infection should be promptly addressed to ensure hematologic safety. These mechanism-driven and agent-specific strategies aim to enhance therapeutic benefit while reducing preventable ADRs. Personalized monitoring protocols guided by pharmacological risk profiles are critical for improving treatment outcomes in patients with HNSCC.

5 Conclusion

This study analyzed ADRs associated with five major anti-HNSCC drugs based on data from the WHO-VigiAccess database, revealing the distinct safety profiles of these drugs in treating HNSCC. Ongoing long-term safety monitoring of these drugs, along with adjustments to clinical practice based on real-world data, will be crucial for the success of future HNSCC treatments.

Data availability statement

Publicly available datasets were analyzed in this study. This data can be found here: https://www.vigiaccess.org.

Author contributions

WG: Resources, Methodology, Writing – original draft, Software, Conceptualization. ZX: Formal Analysis, Data curation, Project administration, Writing – original draft. TZ: Writing – original draft, Formal Analysis, Investigation, Visualization. YD: Funding acquisition, Writing – review and editing, Validation, Supervision.

Funding

The author(s) declare that financial support was received for the research and/or publication of this article. This work is supported by the Jiaxing Science and Technology Plan Project (2024AD30090).

Acknowledgments

We are sincerely grateful to those who created and maintained the public database - the WHO-VigiAccess. Finally, the authors would like to thank all researchers who participated in this study.

Conflict of interest

The authors declare that the research was conducted in the absence of any commercial or financial relationships that could be construed as a potential conflict of interest.

Generative AI statement

The author(s) declare that no Generative AI was used in the creation of this manuscript.

Publisher's note

All claims expressed in this article are solely those of the authors and do not necessarily represent those of their affiliated organizations, or those of the publisher, the editors and the reviewers. Any product that may be evaluated in this article, or claim that may be made by its manufacturer, is not guaranteed or endorsed by the publisher.

References

Baik, C. S., Rubin, E. H., Forde, P. M., Mehnert, J. M., Collyar, D., Butler, M. O., et al. (2017). Immuno-oncology clinical trial design: limitations, challenges, and opportunities. *Clin. Cancer Res.* 23 (17), 4992–5002. doi:10.1158/1078-0432.CCR-16-3066

Basnet, A., Sharma, N. R., Gautam, S., Lamichhane, S., Kansakar, S., Tiwari, K., et al. (2024). Immune checkpoint inhibitor-induced myasthenia gravis, myocarditis, and myositis: a case report. *Clin. Case Rep.* 12 (6), e8968. doi:10.1002/ccr3.8968

Bray, F., Laversanne, M., Sung, H., Ferlay, J., Siegel, R. L., Soerjomataram, I., et al. (2024). Global cancer statistics 2022: GLOBOCAN estimates of incidence and mortality worldwide for 36 cancers in 185 countries. *CA Cancer J. Clin.* 74 (3), 229–263. doi:10.3322/caac.21834

Cao, L. M., Zhong, N. N., Chen, Y., Li, Z. Z., Wang, G. R., Xiao, Y., et al. (2024). Less is more: exploring neoadjuvant immunotherapy as a de-escalation strategy in head and neck squamous cell carcinoma treatment. *Cancer Lett.* 598, 217095. doi:10.1016/j.canlet.2024.217095

Chen, Y., Moon, J., Pandya, K. J., Lau, D. H., Kelly, K., Hirsch, F. R., et al. (2013). A pilot study (SWOG S0429) of weekly cetuximab and chest radiotherapy for poor-risk stage III non-small cell lung cancer. *Front. Oncol.* 3, 219. doi:10.3389/fonc.2013.00219

Chintala, S., Quist, K. M., Gonzalez-DeWhitt, P. A., and Katzenellenbogen, R. A. (2022). High expression of NFX1-123 in HPV positive head and neck squamous cell carcinomas. *Head. Neck* 44 (1), 177–188. doi:10.1002/hed.26906

Cohen, E. E. W., Bell, R. B., Bifulco, C. B., Burtness, B., Gillison, M. L., Harrington, K. J., et al. (2019). The Society for Immunotherapy of Cancer consensus statement on immunotherapy for the treatment of squamous cell carcinoma of the head and neck (HNSCC). *J. Immunother. Cancer* 7 (1), 184. doi:10.1186/s40425-019-0662-5

Dai, N., Zhao, Y. Q., Wu, W. J., Shen, Z. L., Xu, Y. H., Wu, X. Y., et al. (2025). Multidisciplinary approach improves eradication rate and safety in refractory *Helicobacter pylori* infection. *Clin. Transl. Gastroenterol.* 16 (2), e00804. doi:10.14309/ctg.0000000000000804

Ebinama, U., Sheshadri, A., Anand, K., and Swaminathan, I. (2023). Pulmonary immune-related adverse events of PD-1 versus PD-L1 checkpoint inhibitors: a retrospective review of pharmacovigilance. *J. Immunother. Precis. Oncol.* 6 (4), 177–184. doi:10.36401/JIPO-22-38

Elmusrati, A., Wang, J., and Wang, C. Y. (2021). Tumor microenvironment and immune evasion in head and neck squamous cell carcinoma. *Int. J. Oral Sci.* 13 (1), 24. doi:10.1038/s41368-021-00131-7

Evans, S. J., Waller, P. C., and Davis, S. (2001). Use of proportional reporting ratios (PRRs) for signal generation from spontaneous adverse drug reaction reports. *Pharmacoepidemiol Drug Saf.* 10 (6), 483–486. doi:10.1002/pds.677

Falette Puisieux, M., Pellat, A., Assaf, A., Ginestet, C., Brezault, C., Dhooge, M., et al. (2022). Therapeutic management of advanced hepatocellular carcinoma: an updated review. *Cancers (Basel)* 14 (10), 2357. doi:10.3390/cancers14102357

Fan, D., Kang, J. J., Fan, M., Wang, H., Lee, A., Yu, Y., et al. (2020). Last-line local treatment with the Quad Shot regimen for previously irradiated head and neck cancers. *Oral Oncol.* 104, 104641. doi:10.1016/j.oraloncology.2020.104641

Ferlay, J., Colombet, M., Soerjomataram, I., Mathers, C., Parkin, D. M., Pineros, M., et al. (2019). Estimating the global cancer incidence and mortality in 2018: GLOBOCAN sources and methods. *Int. J. Cancer* 144 (8), 1941–1953. doi:10.1002/ijc.31937

Goel, B., Tiwari, A. K., Pandey, R. K., Singh, A. P., Kumar, S., Sinha, A., et al. (2022). Therapeutic approaches for the treatment of head and neck squamous cell carcinoma-An update on clinical trials. *Transl. Oncol.* 21, 101426. doi:10.1016/j.tranon.2022.101426

Gu, L., Chen, H., Xia, Z., Qing, B., and Yuan, Y. (2024). Efficacy of combined surgery and pembrolizumab for the treatment of pulmonary large cell carcinoma: a case report. *Front. Immunol.* 15, 1500996. doi:10.3389/fimmu.2024.1500996

Haas, M., Lein, A., Fuereder, T., Schnoell, J., Brkic, F. F., Liu, D. T., et al. (2023). Early on-treatment C-reactive protein and its kinetics predict survival and response in recurrent and/or metastatic head and neck cancer patients receiving first-line pembrolizumab. *Invest New Drugs* 41 (5), 727–736. doi:10.1007/s10637-023-01388-x

Haddad, R., Guigay, J., Keilholz, U., Clement, P. M., Fayette, J., de Souza Viana, L., et al. (2019). Afatinib as second-line treatment in patients with recurrent/metastatic squamous cell carcinoma of the head and neck: subgroup analyses of treatment adherence, safety and mode of afatinib administration in the LUX-Head and Neck 1 trial. *Oral Oncol.* 97, 82–91. doi:10.1016/j.oraloncology.2019.08.004

Hintelmann, K., Kriegs, M., Rothkamm, K., and Rieckmann, T. (2020). Improving the efficacy of tumor radiosensitization through combined molecular targeting. *Front. Oncol.* 10, 1260. doi:10.3389/fonc.2020.01260

Hussain, R., Hassali, M. A., Hashmi, F., and Akram, T. (2021). Exploring healthcare professionals' knowledge, attitude, and practices towards pharmacovigilance: a cross-sectional survey. *J. Pharm. Policy Pract.* 14 (1), 5. doi:10.1186/s40545-020-00287-3

Jiang, S., Ou, L., Wang, Y., Su, K., Chen, Z., He, L., et al. (2025). CircPRMT5, a potential salivary biomarker, facilitates the progression of head and neck squamous cell carcinoma via the IGF2BP3-SERPINE1 pathway. *Int. J. Nanomedicine* 20, 1597–1613. doi:10.2147/IJN.S502400

Jiang, W. J., Wang, C., Hu, Z. H., Jiang, X. Z., and Hu, W. M. (2024). Construction of a novel tumor mutation burden-related mRNA signature for prognosis prediction in laryngeal squamous cell carcinoma. *Med. Baltim.* 103 (44), e40431. doi:10.1097/MD.0000000000040431

Jo, H. G., Jeong, K., Ryu, J. Y., Park, S., Choi, Y. S., Kwack, W. G., et al. (2021). Fatal events associated with adverse drug reactions in the Korean national pharmacovigilance database. *J. Pers. Med.* 12 (1), 5. doi:10.3390/jpm12010005

Johnson, D. E., Burtness, B., Leemans, C. R., Lui, V. W. Y., Bauman, J. E., and Grandis, J. R. (2020). Head and neck squamous cell carcinoma. *Nat. Rev. Dis. Prim.* 6 (1), 92. doi:10.1038/s41572-020-00224-3

Ke, H., Zhang, Z., Yu, Z., Zhang, B., Chen, R., Zhou, Q., et al. (2024). Characteristics of adverse reactions of three anti-glioma drugs in WHO-VigiAccess. *Front. Pharmacol.* 15, 1485067. doi:10.3389/fphar.2024.1485067

Klinghammer, K., Lorini, L., Nevens, D., Simon, C., Machiels, J. P., and Bossi, P. (2022). Treatment stratification in first-line recurrent or metastatic head and neck cancer, on behalf of the EORTC young investigator head and neck cancer group. *Front. Oncol.* 12, 730785. doi:10.3389/fonc.2022.730785

Lau, H. C. H., Sung, J. J., and Yu, J. (2021). Gut microbiota: impacts on gastrointestinal cancer immunotherapy. *Gut Microbes* 13 (1), 1–21. doi:10.1080/19490976.2020.1869504

Llopis-Salvia, P., Sarrio-Montes, G., Garcia-Llopis, P., and Bargues-Ruiz, A. (2010). Chemotherapy dose intensity reductions due to adverse drug reactions in an oncology outpatient setting. *J. Oncol. Pharm. Pract.* 16 (4), 256–261. doi:10.1177/1078155209355848

Naqash, A. R., Kihn-Alarcon, A. J., Stavraka, C., Kerrigan, K., Maleki Vareki, S., Pinato, D. J., et al. (2021). The role of gut microbiome in modulating response to immune checkpoint inhibitor therapy in cancer. *Ann. Transl. Med.* 9 (12), 1034. doi:10.21037/atm-20-6427

Nowaczyk, J., Fret, K., Kaminska-Winciorek, G., Rudnicka, L., and Czuwara, J. (2023). EGFR inhibitor-induced folliculitis decalvans: a case series and management guidelines. *Anticancer Drugs* 34 (8), 942–948. doi:10.1097/CAD.0000000000001494

Onyije, F. M., Dolatkhah, R., Olsson, A., Bouaoun, L., Deltour, I., Erdmann, F., et al. (2024). Risk factors for childhood brain tumours: a systematic review and meta-analysis of observational studies from 1976 to 2022. *Cancer Epidemiol.* 88, 102510. doi:10.1016/j.canep.2023.102510

Parikh, S. A., Patel, V. A., and Ratner, D. (2014). Advances in the management of cutaneous squamous cell carcinoma. *F1000Prime Rep.* 6, 70. doi:10.12703/P6-70

Pirker, R. (2015). Epidermal growth factor receptor-directed monoclonal antibodies in nonsmall cell lung cancer: an update. *Curr. Opin. Oncol.* 27 (2), 87–93. doi:10.1097/CCO.0000000000000162

Prelaj, A., Boeri, M., Robuschi, A., Ferrara, R., Proto, C., Lo Russo, G., et al. (2022). Machine learning using real-world and translational data to improve treatment selection for NSCLC patients treated with immunotherapy. *Cancers (Basel)* 14 (2), 435. doi:10.3390/cancers14020435

Puthenpurail, A., Rathi, H., Nauli, S. M., and Ally, A. (2021). A brief synopsis of monoclonal antibody for the treatment of various groups of diseases. *World J. Pharm. Pharm. Sci.* 10 (11), 14–22.

Rahman, M. M., Alatawi, Y., Cheng, N., Qian, J., Plotkina, A. V., Peissig, P. L., et al. (2017). Comparison of brand versus generic antiepileptic drug adverse event reporting rates in the U.S. Food and Drug Administration Adverse Event Reporting System (FAERS). *Epilepsy Res.* 135, 71–78. doi:10.1016/j.eplepsyres.2017.06.007

Rothman, K. J., Lanes, S., and Sacks, S. T. (2004). The reporting odds ratio and its advantages over the proportional reporting ratio. *Pharmacoepidemiol Drug Saf.* 13 (8), 519–523. doi:10.1002/pds.1001

Schomberg, J. (2019). Identification of targetable pathways in oral cancer patients via random forest and chemical informatics. *Cancer Inf.* 18, 1176935119889911. doi:10.1177/1176935119889911

Schupack, D. A., Mars, R. A. T., Voelker, D. H., Abeykoon, J. P., and Kashyap, P. C. (2022). The promise of the gut microbiome as part of individualized treatment strategies. *Nat. Rev. Gastroenterol. Hepatol.* 19 (1), 7–25. doi:10.1038/s41575-021-00499-1

Shetti, S., Kumar, C. D., Sriwastava, N. K., and Sharma, I. P. (2011). Pharmacovigilance of herbal medicines: current state and future directions. *Pharmacogn. Mag.* 7 (25), 69–73. doi:10.4103/0973-1296.75905

Sodji, Q., Klein, K., Sravan, K., and Parikh, J. (2017). Predictive role of PD-L1 expression in the response of renal Medullary carcinoma to PD-1 inhibition. *J. Immunother. Cancer* 5 (1), 62. doi:10.1186/s40425-017-0267-9

Song, W., Shi, J., Zhou, B., Meng, X., Liang, M., and Gao, Y. (2024). Nomogram predicting overall and cancer specific prognosis for poorly differentiated lung adenocarcinoma after resection based on SEER cohort analysis. *Sci. Rep.* 14 (1), 22045. doi:10.1038/s41598-024-73486-6

Srba, J., Descikova, V., and Vlcek, J. (2012). Adverse drug reactions: analysis of spontaneous reporting system in Europe in 2007-2009. *Eur. J. Clin. Pharmacol.* 68 (7), 1057–1063. doi:10.1007/s00228-012-1219-4

Su, H., Geng, H., Cai, L., Xu, M., Xing, W., Long, W., et al. (2023). Immune-check blocking combination multiple cytokines shown curative potential in mice tumor model. *Cancer Med.* 12 (12), 13573–13585. doi:10.1002/cam4.6053

Taberna, M., Oliva, M., and Mesia, R. (2019). Cetuximab-containing combinations in locally advanced and recurrent or metastatic head and neck squamous cell carcinoma. *Front. Oncol.* 9, 383. doi:10.3389/fonc.2019.00383

Takada, S., Hirokazu, H., Yamagishi, K., Hideki, S., and Masayuki, E. (2020). Predictors of the onset of type 1 diabetes obtained from real-world data analysis in cancer patients treated with immune checkpoint inhibitors. *Asian Pac J. Cancer Prev.* 21 (6), 1697–1699. doi:10.31557/APJCP.2020.21.6.1697

Tekiki, N., Fujita, M., Okui, T., Kawai, H., Oo, M. W., Kawazu, T., et al. (2021). Dynamic contrast-enhanced MRI as a predictor of programmed death ligand-1 expression in patients with oral squamous cell carcinoma. *Oncol. Lett.* 22 (5), 778. doi:10.3892/ol.2021.13039

Tran, C., Knowles, S. R., Liu, B. A., and Shear, N. H. (1998). Gender differences in adverse drug reactions. *J. Clin. Pharmacol.* 38 (11), 1003–1009. doi:10.1177/009127009803801103

Umbreit, C., Erben, P., Faber, A., Hofheinz, R. D., Schultz, J. D., Hoermann, K., et al. (2016). Lapatinib-induced mesenchymal-epithelial transition in squamous cell carcinoma cells correlates with unexpected alteration of beta-catenin expression. *Oncol. Lett.* 11 (4), 2715–2724. doi:10.3892/ol.2016.4293

Valinciute-Jankauskiene, A., and Kubiliene, L. (2021). Adverse drug reaction reporting by patients in 12 European countries. *Int. J. Environ. Res. Public Health* 18 (4), 1507. doi:10.3390/ijerph18041507

Vasiliadou, I., Breik, O., Baker, H., Leslie, I., Sim, V. R., Hegarty, G., et al. (2021). Safety and treatment outcomes of nivolumab for the treatment of recurrent or metastatic head and neck squamous cell carcinoma: retrospective multicenter cohort study. *Cancers (Basel)* 13 (6), 1413. doi:10.3390/cancers13061413

Venturini, C. D., Engroff, P., Ely, L. S., Zago, L. F., Schroeter, G., Gomes, I., et al. (2011). Gender differences, polypharmacy, and potential pharmacological interactions in the elderly. *Clin. (Sao Paulo)* 66 (11), 1867–1872. doi:10.1590/s1807-59322011001100004

Wang, C. W., Biswas, P. K., Islam, A., Chen, M. K., and Chueh, P. J. (2024). The use of immune regulation in treating head and neck squamous cell carcinoma (HNSCC). *Cells* 13 (5), 413. doi:10.3390/cells13050413

Wang, J., Ji, Q., Dong, S., Zhao, S., Li, X., Zhu, Q., et al. (2021). Factors influencing vaccine hesitancy in China: a qualitative study. *Vaccines (Basel)* 9 (11), 1479. doi:10.3390/vaccines9121479

Wang, Z., and Anderson, K. S. (2022). Therapeutic targeting of FGFR signaling in head and neck cancer. *Cancer J.* 28 (5), 354–362. doi:10.1097/PPO.0000000000000615

Xu, C., Zhang, Y., Wang, W., Wang, Q., Li, Z., Song, Z., et al. (2023). Chinese expert consensus on the diagnosis and treatment of thymic epithelial tumors. *Thorac. Cancer* 14 (12), 1102–1117. doi:10.1111/1759-7714.14847

Yadesa, T. M., Kitutu, F. E., Deyno, S., Ogwang, P. E., Tamukong, R., and Alele, P. E. (2021). Prevalence, characteristics and predicting risk factors of adverse drug reactions among hospitalized older adults: a systematic review and meta-analysis. *SAGE Open Med.* 9, 20503121211039099. doi:10.1177/20503121211039099

Yao, Z., Wang, J., Jiang, Y., Zhang, Y., Liu, J., Dai, L., et al. (2025). Pembrolizumab plus cetuximab with neoadjuvant chemotherapy for head and neck squamous cell carcinoma. *Head. Neck* 47 (1), 289–299. doi:10.1002/hed.27915

Zhang, W., Kong, X., Ai, B., Wang, Z., Wang, X., Wang, N., et al. (2021). Research progresses in immunological checkpoint inhibitors for breast cancer immunotherapy. *Front. Oncol.* 11, 582664. doi:10.3389/fonc.2021.582664

Zhong, S., Cui, Y., Liu, Q., and Chen, S. (2020). CAR-T cell therapy for lung cancer: a promising but challenging future. *J. Thorac. Dis.* 12 (8), 4516–4521. doi:10.21037/jtd.2020.03.118

frontiers | Frontiers in Oncology

TYPE Original Research
PUBLISHED 15 July 2025
DOI 10.3389/fonc.2025.1584061

OPEN ACCESS

EDITED BY
Luis Abel Quiñones,
University of Chile, Chile

REVIEWED BY
Seetha Harilal,
Kerala University of Health Sciences, India
Luccas Lavareze,
State University of Campinas, Brazil

*CORRESPONDENCE
Xiaohong Chen
trchxh@163.com

†These authors have contributed equally to this work and share first authorship

RECEIVED 26 February 2025
ACCEPTED 19 June 2025
PUBLISHED 15 July 2025

CITATION
Wang M, Shi M, Ding Y, Zhang Z, Ge Y, Li Z, Jing Y, Hu H and Chen X (2025) High cGAS-STING expression associates with improved efficacy of neoadjuvant chemo-immunotherapy in head and neck squamous cell carcinoma. *Front. Oncol.* 15:1584061. doi: 10.3389/fonc.2025.1584061

High cGAS-STING expression associates with improved efficacy of neoadjuvant chemo-immunotherapy in head and neck squamous cell carcinoma

Miao Wang[1†], Menglin Shi[1†], Yiming Ding[1], Zishanbai Zhang[1], Yuze Ge[2], Zhixin Li[3], Yixin Jing[1], Honglian Hu[1] and Xiaohong Chen[1*]

[1]Department of Otolaryngology-Head and Neck Surgery, Beijing Tongren Hospital, Capital Medical University, Beijing, China, [2]Department of Biochemistry and Molecular Biology, Capital Medical University, Beijing, China, [3]Department of Oncology Center, Beijing Tongren Hospital, Capital Medical University, Beijing, China

Purpose: Neoadjuvant chemo-immunotherapy (NACI) has demonstrated significant clinical advantages in head and neck squamous cell carcinomas (HNSCC), while clinical responses vary in different patients. This study investigated the correlation between the cyclic GMP-AMP synthase (cGAS, *CGAS*) and the stimulator of interferon genes (STING, *STING1*) expressions and the efficacy of NACI in HNSCC.

Methods: The correlation between *CGAS* and *STING1* expressions and chemotherapy/immunotherapy drug sensitivity was analyzed using the GDSC and TCIA dataset. The study enrolled 38 HNSCC patients receiving NACI, with protein expressions of cGAS and STING evaluated via immunohistochemistry. The T cell abundance and tumor-T cell interactions in different *CGAS* and *STING1* expression groups were analyzed using bulk RNA-seq and scRNA-seq data from open databases.

Results: The mRNA expressions of *CGAS* and *STING1* were negatively correlated with the IC50 of docetaxel and positively correlated with the efficacy of anti-PD-1 treatment ($p<0.05$). In the real-world cohort, cGAS and STING expressions were both positively related to NACI efficacy ($p<0.05$). The mRNA expressions of *CGAS* and *STING1* were positively correlated with the abundance of Act-CD4 (*CGAS*: rho=0.416, p<2.21e-16; *STING1*: rho=0.26, p=1.82e-09), Act-CD8 (*CGAS*: rho=0.089, p=0.0425; *STING1*: rho=0.303, p=1.98e-12), NKT cell (*CGAS*: rho=0.255, p=0.3.78e-09; *STING1*: rho=0.375, p=2.2e-6). Tumor cells with increased expression of *CGAS* or *STING1* showed enhanced interactions with T cells.

Conclusion: This study confirms the positive correlation between cGAS and STING expressions and NACI efficacy, suggesting their role in immune activation and potential as biomarkers for predicting NACI efficacy in HNSCC.

KEYWORDS

head and neck squamous cell carcinoma, neoadjuvant chemoimmunotherapy, cGAS-STING, predictive markers, T cells

1 Introduction

Head and neck cancer ranks as the eighth most prevalent malignancy globally, with an estimated 890,000 new cases and 450,000 deaths annually in 2022. Among these, head and neck squamous cell carcinomas (HNSCC) are the most common type (1). The combination of surgery, chemotherapy, and radiation therapy maximizes treatment efficacy, yet the 5-year overall survival (OS) remains only 50%. Once the disease has recurred, the 1-year OS rate is approximately 15%, with a median OS of 10 to 14 months (2). In recent years, the rise of immunotherapy has significantly improved patient outcomes. KEYNOTE 040, CheckMate 141, and KEYNOTE 048 trials have shown that immunotherapy demonstrates encouraging efficacy in metastatic/recurrent (R/M) HNSCC, with response rates ranging from 15% to 23% (3–5). Previous preclinical studies suggest that immunotherapy is more effective in the neoadjuvant setting than the adjuvant setting (6). Multiple trials on NACI can achieve a pathological complete response rate of approximately 33.3% to 55.6% in HNSCC patients (7–9). Therefore, identifying predictive biomarkers for therapeutic efficacy to select patient subgroups amenable to precision treatments has become a critical priority in NACI.

The stimulator of interferon genes (STING, *STING1*) pathway, activated by the cyclic GMP-AMP synthase (cGAS, *CGAS*) detection of aberrant double-stranded DNA (dsDNA), leading to a type-I interferon (IFN) response (10). The most effective regimen for neoadjuvant treatment of locally advanced HNSCC is confirmed as chemotherapy combined with immunotherapy (11). Chemotherapeutic agents, such as cisplatin, can activate the STING pathway, enhance cytotoxic T cell infiltration and increasing sensitivity to immunotherapy (12, 13). However, STING knockout has been demonstrated to significantly enhance resistance to cisplatin in HNSCC (14). Moreover, deletion of cGAS and STING reverses the anti-tumor effects of chemo-immunotherapy in small cell lung cancer (15). These findings suggest that the expression levels of cGAS and STING may serve as predictive biomarkers for response to chemo-immunotherapy.

This study evaluates the association between cGAS-STING expression and NACI efficacy in HNSCC. It also explores the immunological function of cGAS-STING and its potential as a predictive biomarker for therapeutic response.

2 Materials and methods

2.1 Open-database sources

CGAS and *STING1* expression levels in HNSCC from The Cancer Genome Atlas database (TCGA, http://portal.gdc.cancer.gov/) were analyzed. Regarding the high/low grouping, we dichotomized samples into high-expression and low-expression groups using the median value. The correlation between CGAS and STING expression and IC50 values for common chemotherapeutic drugs (cisplatin, docetaxel, and 5-Fluorouracil) was analyzed using the Genomics of Drug Sensitivity in Cancer (GDSC, http://www.cancerrxgene.org/) and processed with the R package 'oncoPredict. Additionally, immunotherapy data from The Cancer Immunome Atlas (TCIA, http://tcia.at/) was analyzed to assess the effectiveness of immunotherapy between the cGAS-STING high and low expression groups within the TCGA-HNSC cohort. The correlation between cGAS and STING expression and the abundance of immune cells was analyzed by TISIDB (http://cis.hku.hk/TISIDB/). Tumor-T cell interactions were explored using scRNA-seq data from the GEO database.

2.2 Clinical patients

This study enrolled HNSCC patients who received NACI at Beijing Tongren Hospital, Capital Medical University. Between June 2019 and April 2024, 38 patients received NACI. Eligibility criteria were as follows: (1) age ≥18 years, (2) pathologically confirmed squamous cell carcinoma, (3) no prior treatments before neoadjuvant therapy, and (4) at least one measurable or evaluable lesion according to Response Evaluation Criteria in Solid Tumors 1.1 (RECIST 1.1) (16).

2.3 Data collection

Clinicopathological characteristics, including age, gender, anatomical subsite, TNM staging (according to the 8th edition of the American Joint Committee on Cancer Staging Manual), histological classification (poorly, moderately, well differentiated),

smoking history, and alcohol consumption, were retrieved from the medical records system at Beijing Tongren Hospital, Capital Medical University.

2.4 Treatment regimes

The NACI group received pembrolizumab or tislelizumab in combination with the TP, PF, or TPF regimens. The TP regimen comprised paclitaxel 135 mg/m² and cisplatin 100 mg/m² on day 1, while the TPF regimen incorporated 5-fluorouracil 1000 mg/m² from days 1 to 5. The PF regimen consisted of cisplatin 100 mg/m² on day 1 and 5-fluorouracil 1000 mg/m² from days 1 to 5.

2.5 Efficacy assessment

The efficacy of NACI was evaluated based on the clinical and pathological responses. Clinical responses were evaluated based on radiologic evaluation of tumor size by magnetic resonance imaging (MRI) before and after neoadjuvant therapy according to RECIST, version 1.1 (16). Patients were classified as responders (complete response (CR) plus partial response (PR)) or non-responders (stable disease (SD)), and progressive disease (PD). Pathological responses were evaluated based on the percentage of residual viable tumor (RVT). We classified patients into major pathologic response (MPR) (defined as ≤10% RVT in the resected tumor specimen, including pathological complete response (pCR) (no RVT)), or incomplete pathologic response (IPR; defined as >10% RVT in the resected tumor specimens.

2.6 IHC analysis

Fixed tissue samples were deparaffinized with xylene and graded ethanol, followed by antigen retrieval using EDTA (pH 9.0) or sodium citrate buffer (pH 6.0). Samples were then treated with 30% hydrogen peroxide for 10 minutes at room temperature, blocked with goat serum for 1 hour at 37°C, and incubated overnight at 4°C with primary antibodies: cGAS (Cell Signaling Technology, 79978S, 1:100), STING (ProteinTech, 19851-1-AP, 1:2000). Horseradish peroxidase activity was detected using a PV two-step IHC kit. Negative controls used rabbit or mouse IgG. Staining intensity was analyzed using ImageJ software, and images were captured using a Leica microscope.

2.7 Statistical analysis

Data are presented as mean ± SD or mean ± SEM unless otherwise stated. To assess the predictive performance of cGAS and STING, receiver operating characteristic (ROC) curves were constructed, and the areas under the curves (AUCs) were calculated. ROC curves were plotted using the 'pROC' package. Group comparisons were performed using a two-tailed unpaired Student's t-test. A p-value of less than 0.05 was considered statistically significant. All analyses were conducted using GraphPad Prism 8.3.0 or R 4.2.3 software.

3 Results

3.1 cGAS-STING expressions were positively related to chemotherapy and immunotherapy efficacy in TCGA-HNSC cohort

Sensitivity differences of cisplatin, docetaxel, and 5-fluorouracil in the TCGA-HNSC cohort was conducted. Higher IC50 values indicate worse chemotherapy efficacy. The results showed that the *CGAS* high-expression group had lower IC50 values of cisplatin and docetaxel, suggesting increased sensitivity to these chemotherapy treatments (Figure 1A). No significant difference in 5-fluorouracil treatment response was observed between high- and low-expression groups (Figure 1A). Additionally, elevated *STING1* expression was related to higher docetaxel sensitivity, and was not associated with the efficacy of cisplatin and 5-fluorouracil (Figure 1B).

To assess the predictive value of cGAS-STING pathway expression for immunotherapy, we evaluated the IPS scores for anti-programmed cell death protein 1 (PD-1) and anti-cytotoxic T lymphocyte antigen 4 (CTLA-4) therapies. Higher scores indicate better outcomes. Individuals with elevated *CGAS* expression showed higher IPS scores for anti-PD-1 monotherapy alone or combined with anti-CTLA-4 treatment, suggesting a stronger response (Figure 1C). High *STING1* expression was associated with increased IPS for anti-PD-1 alone or combined with anti-CTLA-4 treatment (Figure 1D).

3.2 cGAS and STING expression levels were positively correlated with NACI response in HNSCC patients

Based on our analysis suggesting that cGAS and STING may influence chemotherapy and immunotherapy efficacy, we established a retrospective cohort of HNSCC patients treated with NACI to further investigate our findings. Baseline characteristics are presented in Table 1. A total of 38 patients were enrolled and received NACI therapy, 31 of whom proceeded to surgical resection, while 7 received non-surgical therapy. Among the 19 responders, 10 achieved pathological complete response (pCR). Over 75% had a history of smoking or alcohol use. The most common primary tumor sites were the hypopharynx (50.00%), followed by oropharynx (23.68%), larynx (21.05%), and nasal cavity and sinus (5.26%). Histological classification included poorly differentiated (44.74%), moderately differentiated (31.58%), and well

10.3389/fonc.2025.1584061

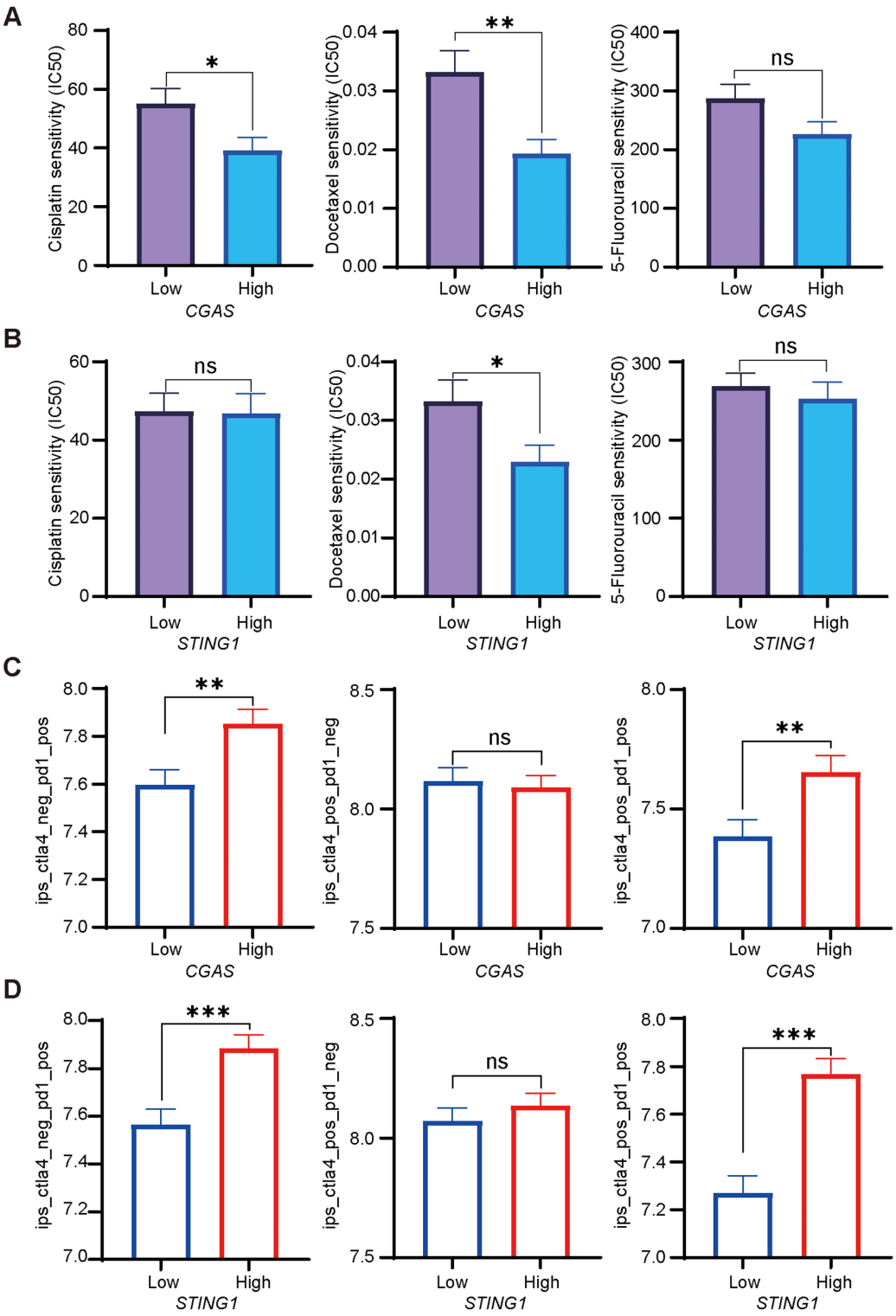

FIGURE 1
Chemotherapeutic and immunotherapy responses based on cGAS-STING expression in HNSCC. **(A, B)**. Relationships between high and low *CGAS* or *STING1* expression groups and IC50 of cisplatin, docetaxel, and 5-fluorouracil. **(C, D)**. The IPS assessment of anti-PD-1, anti-CTLA-4, and their combination therapies, analyzing the differences between patients with high and low *CGAS* and *STING1* expression groups. PD-1, programmed cell death protein 1; CTLA-4, cytotoxic T lymphocyte antigen 4. *p<0.05, **p<0.01, ***p<0.001.

TABLE 1 Baseline characteristics of patients treated with neoadjuvant chemo-immunotherapy.

Patient characteristics	N	%
Age		
≤60	23	60.53
>60	15	39.47
Gender		
Male	37	97.37
Female	1	2.63
Alcohol consumption		
No	4	10.53
Yes	34	89.47
Smoking history		
No	8	21.05
Yes	30	78.95
Tumor site		
Nasal Cavity and Sinus	2	5.26
Oropharynx	9	23.68
Hypopharynx	19	50.00
Larynx	8	21.05
Histological classification		
Poorly differentiated	17	44.74
Moderately differentiated	12	31.58
Well differentiated	3	7.89
HPV status		
negative	24	63.16
positive	7	18.42
T stage		
1	3	7.89
2	12	31.58
3	11	28.95
4	12	31.58
N stage		
0	9	23.68
1	10	26.32
2	19	50.00
Clinical stage		
I	4	10.53
II	1	2.63
III	8	21.05
IV	25	65.79
Radiographic response		
Responders	19	50.00
Non-responders	19	50.00
Pathological response		
pCR	13	34.21
MPR	9	23.68
IPR	9	23.68
NA	7	18.42

differentiated (7.89%). A significant majority (86.84%) had advanced disease (stages III and IV).

Tumor samples were collected from the patients before receiving NACI treatment, and expression levels of cGAS and STING in tumor cells were evaluated by performing immunohistochemistry. The protein levels of cGAS and STING were not associated with clinical characteristics including HPV status (Supplementary Table S1). Notably, we found that cGAS and STING expression levels were significantly higher in responders than in non-responders (Figures 2A–C). To better assess the contribution of cGAS and STING to the efficacy of NACI, we evaluated the pathological responses based on the percentage of RVT cells. As anticipated, the expression of cGAS or STING had a higher level in the patients with MPR than in those with IPR (Figures 2A, B). Additionally, clinical characteristics of these patients has no relationship with the response to NACI (Supplementary Table S2). To date, the CPS score has been developed to predict the response to anti-PD-1 therapy in cancer patients (4), while our results demonstrated the expression levels of PD-L1 CPS expression did not significantly correlate (Figure 2D).

To evaluate the correlation between the expression of cGAS and STING and various clinicopathological factors in our cohort, the waterfall plot of radiological responses for individual patients is shown in Figure 3A. cGAS and STING expressions showed no correlation with common clinical characteristics, including age, gender, alcohol consumption, and smoking history (Supplementary Table S1). Our results indicated that 68.42% (13/19) of responders exhibited high cGAS expression, compared to 31.58% (6/19) of non-responders, suggesting that elevated cGAS expression is associated with a positive therapeutic response. Similarly, 68.18% (15/22) of patients in the MPR group had high cGAS expression, whereas only 22.22% (2/9) of patients in the IPR group displayed high expression, further supporting its correlation with favorable treatment outcomes. Likewise, 68.42% (13/19) of responders displayed high STING expression, compared to 31.58%

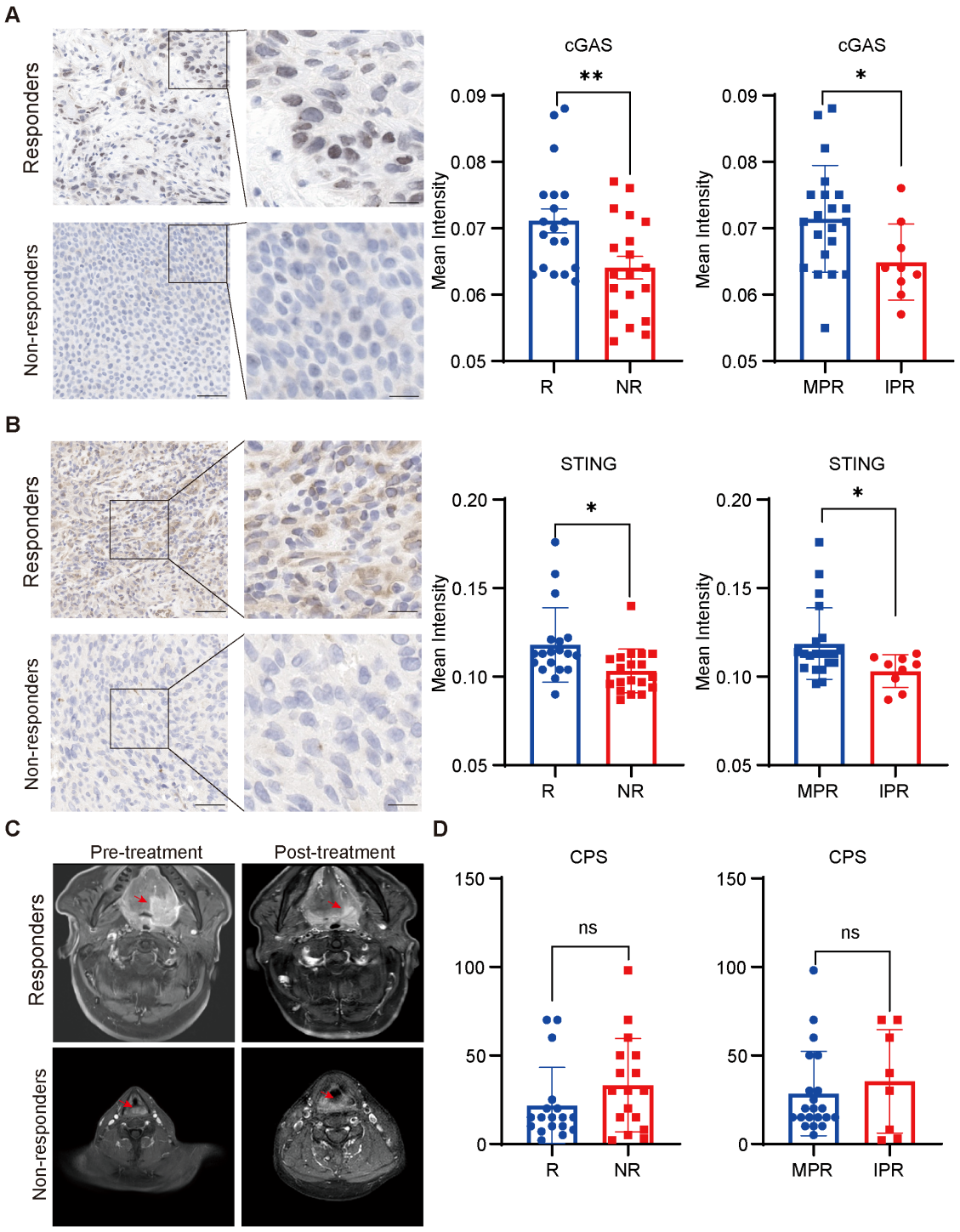

FIGURE 2
Correlation between cGAS-STING pathway levels and the response to NACI **(A, B)**. Immunohistochemical staining for cGAS and STING in the responders (R; n=19) and non-responders (NR; n=19) patients to NACI. expression of cGAS and STING in tumors was assessed in the MPR group (n = 22) and IPR group (n = 9). Scale bar: left panel, 50um; right panel, 25um. (C). Representative images showing the tumor size in responders and non-responders before and after NACI treatment, respectively. (D). CPS scores were assessed in the responders (R; n = 19) and non-responders (NR; n = 19) with NACI. CPS was assessed in the MPR group (n = 22) and IPR group (n = 9). MPR: major pathologic response; IPR: incomplete pathologic response. *p<0.05, **p<0.01.

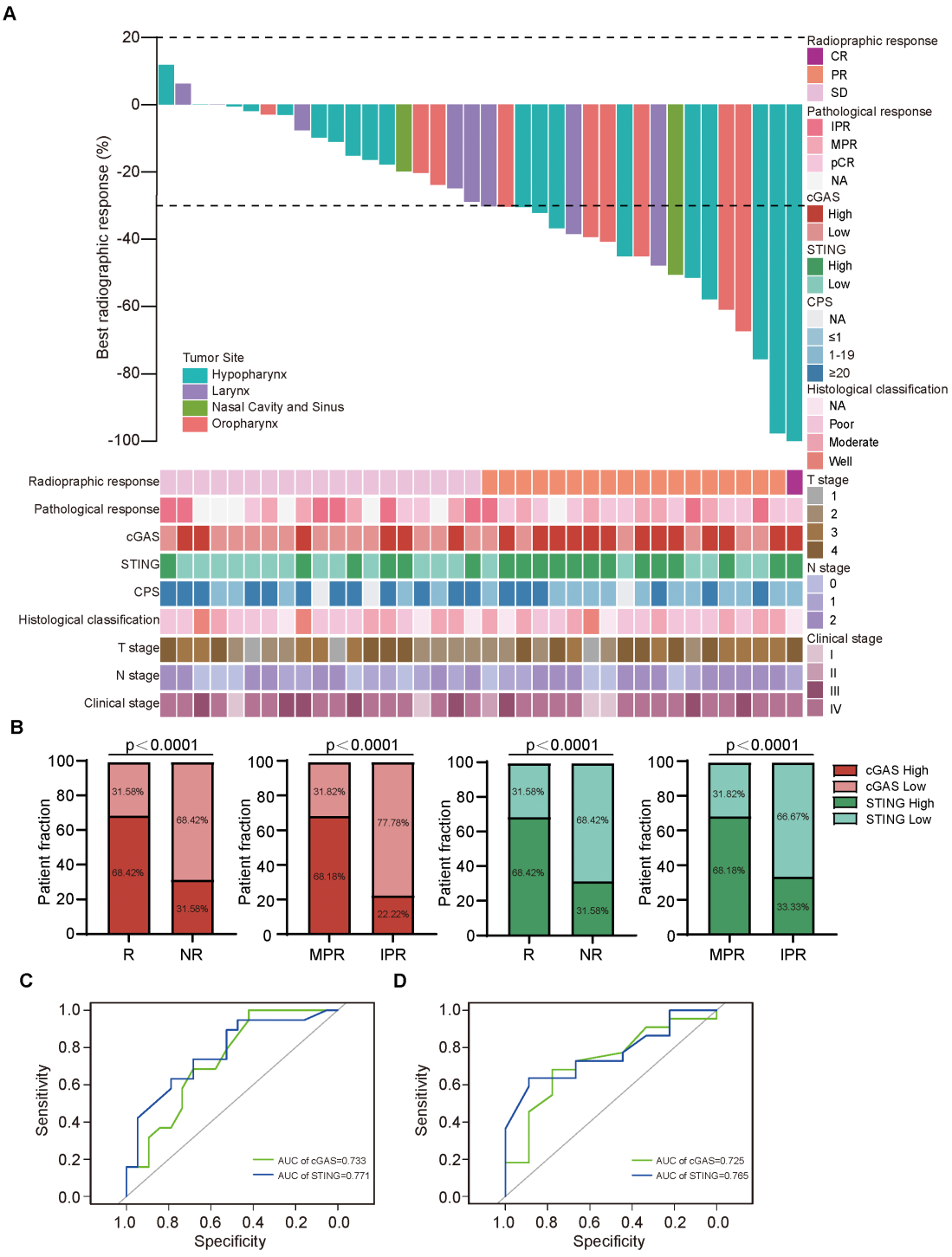

FIGURE 3
cGAS and STING expressions were positively related to responses to NACI in HNSCC patients **(A)**. Waterfall plots depicting the maximum percentage change in target lesion size during neoadjuvant chemo-immunotherapy of HNSCC patients (n = 38). **(B)** Distribution of cGAS and STING expression between responders (R; n=19) and non-responders (NR; n=19), patients with MPR (n = 22) and IPR (n = 9). **(C)** Predictive value of cGAS and STING in discriminating responders and non-responders via ROC analysis. **(D)** Predictive value of cGAS and STING in discriminating MPR and IPR groups via ROC analysis. MPR, major pathologic response; IPR, incomplete pathologic response.

(6/19) of non-responders, indicating that higher STING expression correlates with a better response to treatment. A similar trend was observed in the MPR group, where 68.18% (15/22) exhibited high STING expression, compared to 33.33% (3/9) in the IPR group (Figure 3B). Next, we assessed the predictive value of cGAS and STING in distinguishing responders from non-responders and MPR from IPR groups. Notably, both cGAS and STING expression levels could effectively differentiate potential NACI responders from non-responders (AUC = 0.733 for cGAS and AUC = 0.771 for STING) (Figure 3C), as well as MPR from IPR groups (AUC = 0.725 for cGAS and AUC = 0.765 for STING) (Figure 3D).

3.3 Tumor cells with higher cGAS and STING expression exhibited stronger receptor-ligand interactions with T cells

To further investigate the functional characterization of cGAS and STING in the tumor microenvironment, we utilized the TISIDB database to explore the correlation between *CGAS* and *STING1* expressions and immune cell abundances. Both cGAS and STING1 expressions were positively correlated with Act-CD4 (*CGAS*: rho=0.416, p<2.21e-16; *STING1*: rho=0.26, p=1.82e-09), Act-CD8 (*CGAS*: rho=0.089, p=0.0425; *STING1*: rho=0.303, p=1.98e-12), NKT cell (*CGAS*: rho=0.255, p=0.3.78e-09; *STING1*: rho=0.375, p=2.2e-6) abundance, which are critical for immunotherapy (Figure 4A). Additionally, we performed scRNA-seq data analysis in primary tumor tissues of HNSC-GSE234933. Using uniform manifold approximation and projection (UMAP), we identified 14 cellular clusters, including tumor and T cells (Figures 4B, C). We then a cell-cell interaction analysis was conducted to further investigate the predictive value of cGAS and STING. Based on the expression levels of *CGAS* or *STING1* in tumor cell clusters, the samples were divided into high- and low-expression groups. We found that tumor cell clusters with higher *CGAS* or *STING1* expression exhibited stronger receptor-ligand interactions with T cells (Figure 4D). These findings suggest that cGAS and STING are strongly associated with T cell activity and enhance the response to NACI in HNSCC.

4 Discussion

Immune checkpoint inhibitors have emerged as a promising approach for the treatment of HNSCC. The KEYNOTE-048 trial demonstrated that pembrolizumab, when combined with chemotherapy, improved overall survival (OS) compared to the EXTREME regimen in patients with recurrent or metastatic (R/M) HNSCC, with an OS of 13.0 months versus 10.7 months (HR 0.77 [95% CI 0.63–0.93], p=0.0034) in the overall population (3, 4). Furthermore, several studies have reported that NACI can achieve pCR rates exceeding 50% in HNSCC patients (7, 8). However, patients who exhibit poor responses to NACI may experience treatment-related complications, potentially delaying radical surgery or concurrent chemoradiotherapy, without resulting in any improvement in prognosis (17). Therefore, identifying clinical biomarkers that can accurately predict the therapeutic response to NACI in HNSCC is of significant clinical importance. In this study, HNSCC patients with elevated levels of cGAS and STING demonstrated a higher response rate to NACI, as evidenced by both open-access database and real-world data.

Currently, CPS is the primary biomarker for predicting tumor immunotherapy efficacy, with higher CPS values associated with better responses to PD-1 therapy (4). In the KEYNOTE-012 study, the response rate was 21% in PD-L1+ patients compared to 6% in PD-L1− patients, as assessed by CPS (18). However, clinical trial data on its predictive value are inconsistent, and the long-term analysis of CheckMate-141 indicated that PD-L1− patients may also benefit from immunotherapy treatment (19, 20). Moreover, the CPS score did not correlate with NACI efficacy in the present cohort, with a substantial proportion of non-responders exhibiting CPS ≥20. This undermines the predictive accuracy of PD-L1 expression and highlights the limited predictive value of CPS. Immunotherapy efficacy is largely influenced by tumor antigen levels and inflammation, making these factors essential for optimizing treatment strategies (21, 22). Recent studies demonstrated that activation of the cGAS-STING pathway enhances antigen presentation by dendritic cells and stimulates the secretion of chemokines, such as CXCL9 and CXCL10, which recruit CD8+ T cells and NK cells to the tumor microenvironment, thereby enhancing the efficacy of immunotherapy (23–26). In this study, we assessed the mRNA expression of *cGAS* and *STING1* and found a positive correlation between their expression levels and the efficacy of chemotherapy and immunotherapy. Furthermore, the protein levels of cGAS and STING were significantly higher in responders to NACI treatment compared to non-responders. Additionally, patients with MPR had higher protein levels of cGAS and STING than those with IPR.

The tumor microenvironment plays a pivotal role in malignancy progression and significantly impacts the response to immunotherapy (27). Three primary immune profiles are associated with immunotherapy response: immune-inflamed phenotype, the immune-excluded phenotype and the immune-desert phenotype (28). Notably, the immune-inflamed phenotype, characterized by abundant immune cell infiltration, generally correlates with better responses to immunotherapy in cancer patients (29, 30). In our study, we observed that the mRNA expressions of *CGAS* and *STING1* were positively correlated with the abundance of activated CD4+ T cells, activated CD8+ T cells, and NKT cells. Furthermore, elevated expression levels of CGAS and STING1 in tumor cells promoted their interaction with T cells, which is crucial for enhancing the efficacy of immunotherapy.

In conclusion, we conducted a systematic and comprehensive analysis of the role of cGAS-STING pathway expression in predicting the efficacy of NACI in HNSCC. However, several

10.3389/fonc.2025.1584061

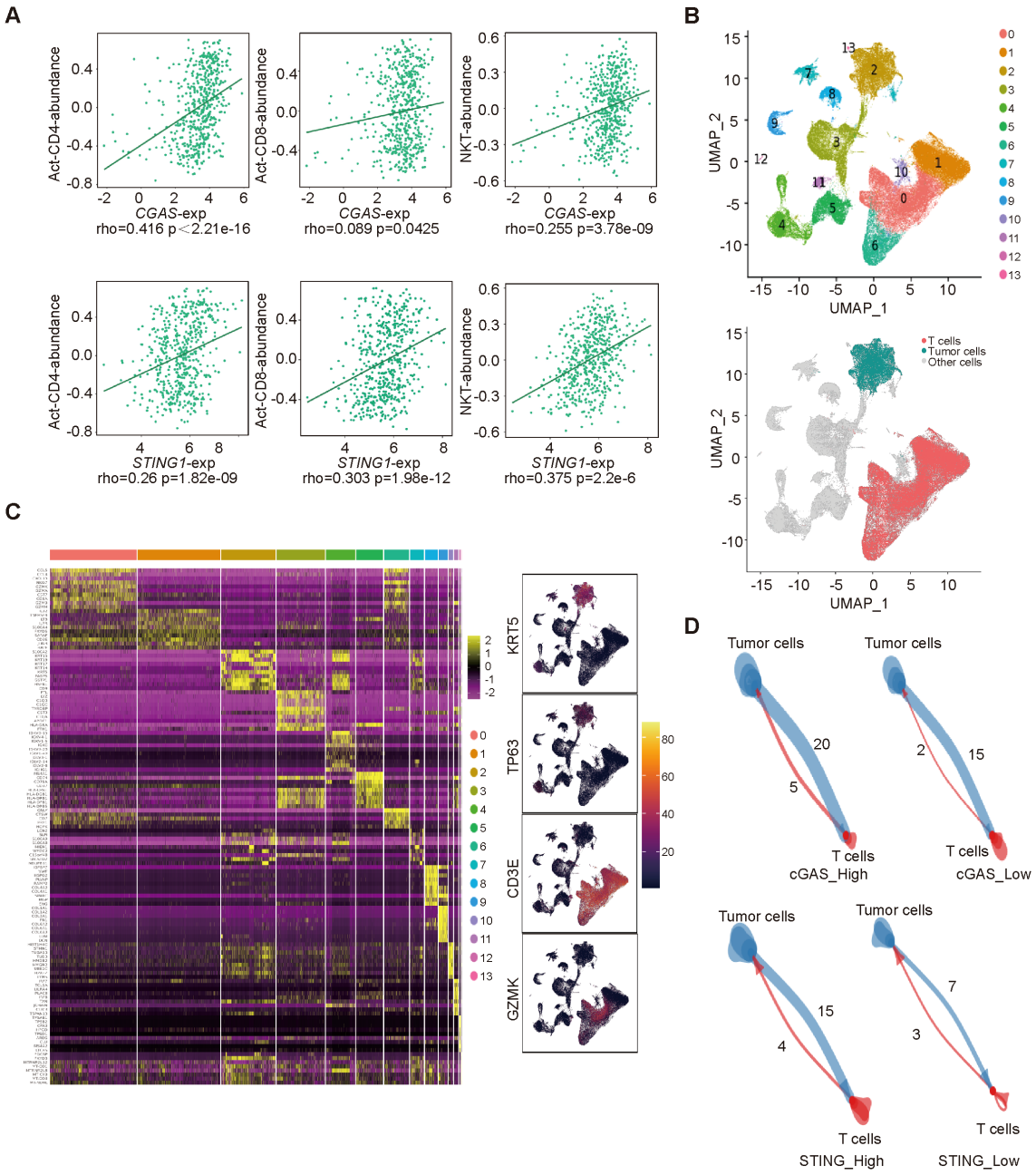

FIGURE 4
The correlation between cGAS/STING expressions and immune cells **(A)**. the relationship between cGAS/STING expressions and Act-CD4, Act-CD8, NKT cell abundance. **(B)** Uniform manifold approximation and projection (UMAP) visualization of single-cell transcriptomic profiles combined from all 24 samples. **(C)** Identification of genes that are dominantly expressed in each major cell type. **(D)** The cell-cell interactions between high- and low- cGAS/STING tumor cells and T cells.

limitations should be noted. First, our study is a single-center retrospective analysis, and the limited sample size may affect the statistical power of subgroup analyses, requiring validation in larger cohorts. Second, although the correlation analysis indicates that the cGAS-STING pathway may enhance therapeutic efficacy through the modulation of T cell infiltration, further studies involving gene knockout or overexpression models are required to establish a causal relationship.

5 Conclusion

In summary, our study demonstrated that cGAS and STING expression levels are positively correlated with the efficacy of NACI in HNSCC, playing crucial roles in immune activation. These findings highlight potential strategies that could guide the development of personalized precision medicine for NACI in HNSCC.

Data availability statement

Publicly available datasets were analyzed in this study. This data can be found here: https://www.ncbi.nlm.nih.gov/geo/query/acc.cgi?acc=GSE229289.

Ethics statement

The studies involving humans were approved by the Medical Ethics Committee of Beijing Tongren Hospital. The studies were conducted in accordance with the local legislation and institutional requirements. The participants provided their written informed consent to participate in this study.

Author contributions

MW: Data curation, Investigation, Methodology, Writing – original draft, Writing – review & editing. MS: Data curation, Methodology, Writing – review & editing. YD: Investigation, Supervision, Writing – review & editing. ZZ: Methodology, Writing – review & editing. YG: Methodology, Writing – review & editing. ZL: Writing – review & editing, Investigation. YJ: Writing – review & editing. HH: Writing – review & editing. XC: Conceptualization, Funding acquisition, Supervision, Writing – review & editing.

Funding

The author(s) declare that financial support was received for the research and/or publication of this article. Talent Cultivation plan of 'Climbing the peak' of Beijing Municipal Hospital Administration (DFL20220201).

Acknowledgments

We would like to express our gratitude to the individuals and institutions that contributed to the development of open databases and shared resources. Additionally, we thank all the authors for their dedication and hard work in completing this article.

Conflict of interest

The authors declare that the research was conducted in the absence of any commercial or financial relationships that could be construed as a potential conflict of interest.

Generative AI statement

The author(s) declare that no Generative AI was used in the creation of this manuscript.

Publisher's note

All claims expressed in this article are solely those of the authors and do not necessarily represent those of their affiliated organizations, or those of the publisher, the editors and the reviewers. Any product that may be evaluated in this article, or claim that may be made by its manufacturer, is not guaranteed or endorsed by the publisher.

Supplementary material

The Supplementary Material for this article can be found online at: https://www.frontiersin.org/articles/10.3389/fonc.2025.1584061/full#supplementary-material

References

1. Bray F, Laversanne M, Sung H, Ferlay J, Siegel RL, Soerjomataram I, et al. Global cancer statistics 2022: Globocan estimates of incidence and mortality worldwide for 36 cancers in 185 countries. *CA Cancer J Clin*. (2024) 74:229–63. doi: 10.3322/caac.21834

2. Smussi D, Mattavelli D, Paderno A, Gurizzan C, Lorini L, Romani C, et al. Revisiting the concept of neoadjuvant and induction therapy in head and neck cancer with the advent of immunotherapy. *Cancer Treat Rev*. (2023) 121:102644. doi: 10.1016/j.ctrv.2023.102644

3. Cohen EEW, Soulières D, Le Tourneau C, Dinis J, Licitra L, Ahn M-J, et al. Pembrolizumab versus methotrexate, docetaxel, or cetuximab for recurrent or metastatic head-and-neck squamous cell carcinoma (keynote-040): A randomised, open-label, phase 3 study. *Lancet*. (2019) 393:156–67. doi: 10.1016/S0140-6736(18)31999-8

4. Burtness B, Harrington KJ, Greil R, Soulières D, Tahara M, de Castro G Jr., et al. Pembrolizumab alone or with chemotherapy versus cetuximab with chemotherapy for recurrent or metastatic squamous cell carcinoma of the head and neck (keynote-048): A randomised, open-label, phase 3 study. *Lancet*. (2019) 394:1915–28. doi: 10.1016/s0140-6736(19)32591-7

5. Ferris RL, Blumenschein G Jr., Fayette J, Guigay J, Colevas AD, Licitra L, et al. Nivolumab for recurrent squamous-cell carcinoma of the head and neck. *N Engl J Med*. (2016) 375:1856–67. doi: 10.1056/NEJMoa1602252

6. Liu J, Blake SJ, Yong MCR, Harjunpää H, Ngiow SF, Takeda K, et al. Improved efficacy of neoadjuvant compared to adjuvant immunotherapy to eradicate metastatic disease. *Cancer Discov*. (2016) 6:1382–99. doi: 10.1158/2159-8290.CD-16-0577

7. Yan S, Liu L, Zhang X, Wei L, Jiang W, Gao X, et al. Neoadjuvant chemoimmunotherapy shows major pathological response and low recurrence in head and neck squamous cell carcinoma. *Clin Transl Oncol*. (2024) 26:1192–202. doi: 10.1007/s12094-023-03342-y

8. Wu D, Li Y, Xu P, Fang Q, Cao F, Lin H, et al. Neoadjuvant chemo-immunotherapy with camrelizumab plus nab-paclitaxel and cisplatin in resectable locally advanced squamous cell carcinoma of the head and neck: A pilot phase ii trial. *Nat Commun*. (2024) 15:2177. doi: 10.1038/s41467-024-46444-z

9. Wu WJ, Liu Q, An PG, Wang L, Zhang JY, Chen Y, et al. Neoadjuvant tislelizumab combined with chemotherapy in locally advanced oral or oropharyngeal squamous cell carcinoma: A real-world retrospective study. *Front Immunol*. (2023) 14:1282629. doi: 10.3389/fimmu.2023.1282629

10. Wang R, Hussain A, Guo Q, Ma M. Cgas-sting at the crossroads in cancer therapy. *Crit Rev Oncol Hematol*. (2024) 193:104194. doi: 10.1016/j.critrevonc.2023.104194

11. Wang K, Gui L, Lu H, He X, Li D, Liu C, et al. Efficacy and safety of pembrolizumab with preoperative neoadjuvant chemotherapy in patients with

resectable locally advanced head and neck squamous cell carcinomas. *Front Immunol*. (2023) 14:1189752. doi: 10.3389/fimmu.2023.1189752

12. Lv J, Wei Y, Yin JH, Chen YP, Zhou GQ, Wei C, et al. The tumor immune microenvironment of nasopharyngeal carcinoma after gemcitabine plus cisplatin treatment. *Nat Med*. (2023) 29:1424–36. doi: 10.1038/s41591-023-02369-6

13. Liu X, Cen X, Wu R, Chen Z, Xie Y, Wang F, et al. Arih1 activates sting-mediated t-cell activation and sensitizes tumors to immune checkpoint blockade. *Nat Commun*. (2023) 14:4066. doi: 10.1038/s41467-023-39920-5

14. Hayman TJ, Baro M, MacNeil T, Phoomak C, Aung TN, Cui W, et al. Sting enhances cell death through regulation of reactive oxygen species and DNA damage. *Nat Commun*. (2021) 12:2327. doi: 10.1038/s41467-021-22572-8

15. Sen T, Rodriguez BL, Chen L, Corte CMD, Morikawa N, Fujimoto J, et al. Targeting DNA damage response promotes antitumor immunity through sting-mediated t-cell activation in small cell lung cancer. *Cancer Discov*. (2019) 9:646–61. doi: 10.1158/2159-8290.CD-18-1020

16. Eisenhauer EA, Therasse P, Bogaerts J, Schwartz LH, Sargent D, Ford R, et al. New response evaluation criteria in solid tumours: Revised recist guideline (version 1.1). *Eur J Cancer (Oxford England: 1990)*. (2009) 45:228–47. doi: 10.1016/j.ejca.2008.10.026

17. Tang AL, O'Neil T, McDermott S, Tripathi S, Tikhtman R, Mark JR, et al. Association of neoadjuvant pembrolizumab for oral cavity squamous cell carcinoma with adverse events after surgery in treatment-naive patients. *JAMA Otolaryngology–Head Neck Surg*. (2022) 148:935–9. doi: 10.1001/jamaoto.2022.2291

18. Seiwert TY, Burtness B, Mehra R, Weiss J, Berger R, Eder JP, et al. Safety and clinical activity of pembrolizumab for treatment of recurrent or metastatic squamous cell carcinoma of the head and neck (keynote-012): An open-label, multicentre, phase 1b trial. *Lancet Oncol*. (2016) 17:956–65. doi: 10.1016/S1470-2045(16)30066-3

19. Bauml J, Seiwert TY, Pfister DG, Worden F, Liu SV, Gilbert J, et al. Pembrolizumab for platinum- and cetuximab-refractory head and neck cancer: Results from a single-arm, phase ii study. *J Clin Oncol*. (2017) 35:1542–9. doi: 10.1200/JCO.2016.70.1524

20. Ferris RL, Blumenschein G, Fayette J, Guigay J, Colevas AD, Licitra L, et al. Nivolumab vs investigator's choice in recurrent or metastatic squamous cell carcinoma of the head and neck: 2-year long-term survival update of checkmate 141 with analyses by tumor pd-l1 expression. *Oral Oncol*. (2018) 81:45–51. doi: 10.1016/j.oraloncology.2018.04.008

21. Karasarides M, Cogdill AP, Robbins PB, Bowden M, Burton EM, Butterfield LH, et al. Hallmarks of resistance to immune-checkpoint inhibitors. *Cancer Immunol Res*. (2022) 10:372–83. doi: 10.1158/2326-6066.Cir-20-0586

22. Dall'Olio FG, Marabelle A, Caramella C, Garcia C, Aldea M, Chaput N, et al. Tumour burden and efficacy of immune-checkpoint inhibitors. *Nat Rev Clin Oncol*. (2022) 19:75–90. doi: 10.1038/s41571-021-00564-3

23. Della Corte CM, Sen T, Gay CM, Ramkumar K, Diao L, Cardnell RJ, et al. Sting pathway expression identifies nsclc with an immune-responsive phenotype. *J Thorac Oncol*. (2020) 15:777–91. doi: 10.1016/j.jtho.2020.01.009

24. Deng L, Liang H, Xu M, Yang X, Burnette B, Arina A, et al. Sting-dependent cytosolic DNA sensing promotes radiation-induced type i interferon-dependent antitumor immunity in immunogenic tumors. *Immunity*. (2014) 41:843–52. doi: 10.1016/j.immuni.2014.10.019

25. Cousin C, Oberkampf M, Felix T, Rosenbaum P, Weil R, Fabrega S, et al. Persistence of integrase-deficient lentiviral vectors correlates with the induction of sting-independent cd8+ t cell responses. *Cell Rep*. (2019) 26:1242–57.e7. doi: 10.1016/j.celrep.2019.01.025

26. Liu Y, Pagacz J, Wolfgeher DJ, Bromerg KD, Gorman JV, Kron SJ. Senescent cancer cell vaccines induce cytotoxic t cell responses targeting primary tumors and disseminated tumor cells. *J Immunother Cancer*. (2023) 11(2):e005862. doi: 10.1136/jitc-2022-005862

27. Adegoke NA, Gide TN, Mao Y, Quek C, Patrick E, Carlino MS, et al. Classification of the tumor immune microenvironment and associations with outcomes in patients with metastatic melanoma treated with immunotherapies. *J Immunother Cancer*. (2023) 11(10):e007144. doi: 10.1136/jitc-2023-007144

28. Kandalaft LE, Dangaj Laniti D, Coukos G. Immunobiology of high-grade serous ovarian cancer: Lessons for clinical translation. *Nat Rev Cancer*. (2022) 22:640–56. doi: 10.1038/s41568-022-00503-z

29. Salmon H, Remark R, Gnjatic S, Merad M. Host tissue determinants of tumour immunity. *Nat Rev Cancer*. (2019) 19:215–27. doi: 10.1038/s41568-019-0125-9

30. Chen DS, Mellman I. Elements of cancer immunity and the cancer-immune set point. *Nature*. (2017) 541:321–30. doi: 10.1038/nature21349

frontiers | Frontiers in Pharmacology

TYPE Original Research
PUBLISHED 18 July 2025
DOI 10.3389/fphar.2025.1573408

OPEN ACCESS

EDITED BY
Fujun Han,
The First Hospital of Jilin University, China

REVIEWED BY
Qiansheng Huang,
Institute of Urban Environment (CAS), China
Elena Niculet,
Dunarea de Jos University, Romania
Eskouhie Tchaparian,
Independent Researcher, Taipei, Taiwan
Qin Wang,
Xiamen University, China

*CORRESPONDENCE
Jianhong Tang,
tjh@glmc.edu.cn

†These authors have contributed equally to this work and share first authorship

RECEIVED 09 February 2025
ACCEPTED 23 June 2025
PUBLISHED 18 July 2025

CITATION
He M, Xie L, Huang J, Su H, Hu J, Xie L, Li M, Zeng X and Tang J (2025) Aloe-emodin mediates the inhibitory effect of LncRNA D63785 on the PI3K/Akt/mTOR pathway in nasopharyngeal carcinoma.
Front. Pharmacol. 16:1573408.
doi: 10.3389/fphar.2025.1573408

Aloe-emodin mediates the inhibitory effect of LncRNA D63785 on the PI3K/Akt/mTOR pathway in nasopharyngeal carcinoma

Min He[1†], Lei Xie[2,3†], Jiayi Huang[4], Han Su[5], Jiahua Hu[6], Liuping Xie[2,3], Mengqin Li[2,3], Xin Zeng[2,3] and Jianhong Tang[1,7,8*]

[1]Department of Pharmacy, The Second Affiliated Hospital of Guilin Medical University, Guilin, China, [2]College of Pharmacy, Guilin Medical University, Guilin, China, [3]Guangxi Key Laboratory of Diabetic Systems Medicine, Guilin Medical University, Guilin, China, [4]Department of Traditional Chinese Medicine, The Second Affiliated Hospital of Guilin Medical University, Guilin, China, [5]Department of Neurology, The Affiliated Hospital of Guilin Medical University, Guilin, China, [6]Central Laboratory, Guangxi Health Commission Key Laboratory of Glucose and Lipid Metabolism Disorders, The Second Affiliated Hospital of Guilin Medical University, Guilin, China, [7]Guangxi Health Commission Key Laboratory of Glucose and Lipid Metabolism Disorders, The Second Affiliated Hospital of Guilin Medical University, Guilin, China, [8]School of General Medical, Guilin Medical University, Guilin, China

Background: Long non-coding RNAs (lncRNAs) are dysregulated in nasopharyngeal carcinoma (NPC), yet their interplay with pharmacological agents like aloe-emodin (AE) remains unclear. This study explores AE's anti-NPC mechanisms via lncRNA D63785 and the PI3K/Akt/mTOR pathway.

Methods: NPC cells (CNE1, C666-1) were treated with AE, followed by qRT-PCR and Western blotting to assess lncRNA D63785 and PI3K/Akt/mTOR pathway proteins. siRNA-mediated lncRNA D63785 knockdown combined with functional assays (CCK-8, EdU, colony/wound-healing) evaluated AE's effects on proliferation, migration, and pathway activity. *In vivo* validation used nude mouse xenografts.

Results: LncRNA D63785 was overexpressed in NPC cells ($p < 0.01$). AE suppressed lncRNA D63785 expression, concurrently reducing PI3K/Akt/mTOR phosphorylation ($p < 0.05$). siRNA knockdown partially reversed AE's inhibition of NPC cell viability, proliferation, and migration. *In vivo*, AE attenuated tumor growth ($p < 0.05$), correlating with lncRNA D63785 downregulation and PI3K/Akt/mTOR dephosphorylation.

Conclusion: AE exerts anti-NPC effects by targeting the lncRNA D63785-PI3K/Akt/mTOR axis, offering a novel therapeutic strategy. These findings bridge AE's pharmacological activity with lncRNA regulatory networks in NPC pathogenesis.

KEYWORDS

AE, NPC, LncRNA D63785, PI3K/Akt/mTOR signaling pathway, proliferation and migration

1 Introduction

Nasopharyngeal carcinoma (NPC), a malignancy with distinct geographical prevalence in East and Southeast Asia, ranks as the third most common cancer in Southern China (Liu et al., 2021; Su et al., 2022). Its multifactorial etiology involves genetic susceptibility, Epstein-Barr virus (EBV) infection, and lifestyle factors such as nitrosamine-rich diets, smoking, and alcohol consumption (Chang et al., 2021; Jicman Stan et al., 2022). Despite advances in radiotherapy and chemoradiotherapy, clinical outcomes remain suboptimal, with a 5-year survival rate below 80% due to frequent late-stage diagnoses and treatment limitations like therapeutic resistance and adverse effects (Wu et al., 2016; Tang et al., 2021). These challenges underscore the urgent need for novel therapeutic strategies targeting NPC pathogenesis.

Natural compounds have emerged as promising candidates for anticancer drug development. Paclitaxel, evodiamine, and curcumin exemplify plant-derived agents with validated efficacy in oncology (Şeker Karatoprak et al., 2022; Abu Samaan et al., 2019; Luo et al., 2021; Shafei et al., 2021; Termini et al., 2020). Among these, aloe-emodin (AE), an anthraquinone isolated from Aloe vera, exhibits multifaceted pharmacological properties, including anti-inflammatory, immunomodulatory, and antitumor activities (Sanders et al., 2018). Preclinical studies highlight AE's ability to suppress proliferation, migration, and invasion across diverse malignancies, such as cervical cancer (via suppression of HPV E6/E7 oncoproteins and GLUT1-mediated glucose metabolism (Gao et al., 2019), melanoma (through Wnt/β-catenin inhibition (Du et al., 2021)), colon cancer (via mitochondrial-mediated apoptotic pathways) (Jiang et al., 2021)), and breast cancer (by inhibiting telomerase activity (Wang S. et al., 2020)). Notably, AE's antitumor effects in NPC remain underexplored, warranting mechanistic investigation.

The PI3K/Akt/mTOR pathway, a central regulator of cell survival, metabolism, and therapy resistance, is frequently dysregulated in NPC, driving tumor progression and chemoradiotherapy failure (Teng et al., 2021; Qin et al., 2020; Li et al., 2022; Chen et al., 2020). Hyperactivation of this pathway enhances NPC cell proliferation, invasion, and metastatic potential while conferring resistance to apoptosis (Xie et al., 2022; Zhang et al., 2020; Feng et al., 2019; Feng et al., 2023). Recent evidence implicates long non-coding RNAs (LncRNAs) as critical modulators of PI3K/Akt/mTOR signaling. For instance, LncRNA PTCSS1 promotes Akt phosphorylation to accelerate tumor growth in hepatocellular carcinoma (Sharma et al., 2022), whereas LncRNA MEG3 suppresses PI3K/Akt signaling in glioma (Jia and Yan, 2022). In NPC, aberrant LncRNA expression profiles correlate with malignant phenotypes, yet the functional roles of specific LncRNAs remain poorly characterized (Yao et al., 2022; Wang Y. et al., 2020; He et al., 2022).

Of particular interest is LncRNA D63785, a highly upregulated transcript in NPC tissues (Zheng et al., 2019). While its oncogenic role in gastric cancer involves miR-422a sequestration to induce chemotherapy resistance (Zhou et al., 2018), the mechanistic interplay between D63785 and PI3K/Akt/mTOR signaling in NPC remains uncharted. Building on AE's documented PI3K/Akt inhibitory effects in other cancers (Peng et al., 2022; Zhu et al., 2023), we hypothesize that AE suppresses NPC progression by targeting LncRNA D63785 to attenuate PI3K/Akt/mTOR pathway activation.

Summary statement: In this study, we aim to explore the hypothesis that aloe-emodin inhibits NPC progression by targeting lncRNA D63785, thereby modulating the PI3K/Akt/mTOR signaling pathway. The results of this study may provide new insights into the therapeutic potential of aloe-emodin in NPC treatment.

2 Materials and methods

2.1 Materials

Human nasal mucosal epithelial cells (HNEpC, non-cancerous controls) were purchased from Guangzhou Suyan Biotechnology Co., Ltd. Nasopharyngeal carcinoma (NPC) cell lines CNE1, 5-8F, HONE1, and C666-1 were obtained from Xiangya Medical College of Central South University and Shanghai Yuchi Biotechnology Co., Ltd. Aloe emodin was purchased from Shanghai Yuanye Biotechnology. RPMI 1640 medium and EMEM medium were sourced from GIBCO and Guangzhou Suyan Biotechnology, respectively. Fetal bovine serum (FBS), penicillin-streptomycin (Cat# SV30010), TRIzol reagent (Cat# DP424), SYBR Green Master Mix, RIPA lysis buffer, BCA Protein Assay Kit, and Laemmli buffer were purchased from Sigma-Aldrich, Tiangen Biotech, Vazyme Biotech, and Beyotime Biotechnology. qPCR primers for LncRNA D63785 and GAPDH (internal control) were synthesized by Sangon Biotech (Shanghai, China). Opti-MEM, Lipofectamine 3000, and EdU reagent were obtained from Thermo Fisher Scientific. Primary antibodies against AKT, p-AKT, PI3K, p-PI3K, mTOR, p-mTOR, and β-actin were purchased from Affinity Biosciences, ABclonal Biotechnology, and Servicebio Biotechnology. HRP-conjugated goat anti-rabbit IgG secondary antibody and ECL Prime Western blotting Substrate were sourced from Beyotime Biotechnology. D63785-targeting siRNA (sense: 5′-GGCAGUUCCACAGAA UUUTT-3′, antisense: 5′-AAAUCUGUGGAAUCTCTT-3′; Cat# 338888) and negative control siRNA were synthesized by GenePharma. BALB/c nude mice (SPF-grade, Cat# SCXK 2019-0004) were purchased from SLAC Jingda Experimental Animal Co., Ltd. Isoflurane was obtained from Sigma-Aldrich. DMSO was purchased from Beijing Solarbio Science & Technology Co., Ltd. All reagents and antibodies were used in accordance with the manufacturers protocols.

2.2 Cell culture

NPC cells (CNE1, 5-8F, HONE1, C666-1) were cultured in RPMI 1640 medium supplemented with 10% FBS and 1% penicillin-streptomycin. HNEpC cells were maintained in EMEM medium with identical supplements. All cells were incubated at 37°C in 5% CO_2.

Our previous studies have shown that AE inhibits the activity of CNE1 and C666-1 cells (Chen et al., 2023). A concentration of

20 μM was selected based on ~70% cell viability after 48 h of treatment. For dose-response studies, concentrations were adjusted in 10 μM increments or decrements relative to 40 μM, which exhibited significant cytotoxicity.

2.3 Real time quantitative PCR

Total RNA was extracted from samples using TRIZOL reagent according to the manufacturer's instructions. RNA concentration and purity were determined using the NanoDrop 2000 spectrophotometer. Reverse transcription was performed with 1 μg of RNA in a 20 μL reaction volume following the PrimeScript™ RT Master Mix protocol. Quantitative PCR amplification was carried out in triplicate using SYBR Green Master Mix under optimized cycling conditions: initial denaturation at 95°C for 30 s, followed by 40 cycles of 95°C for 10 s and 60°C for 30 s. Melt curve analysis confirmed amplification specificity. Relative gene expression was calculated using the $2^{-\Delta\Delta CT}$ method with GAPDH normalization. The assay was performed three times independently.

2.4 Cell Western blot

Total protein was extracted from cells or tumor tissues using RIPA lysis buffer and denatured at 100°C for 10 min in Laemmli buffer. Protein concentrations were quantified via BCA assay, with 100 μg of total protein loaded per lane for separation on 10% SDS-PAGE gels. Electrophoresed proteins were transferred to PVDF membranes at 250 mA constant current for 90 min. Membranes were blocked with 5% non-fat milk (for non-phosphorylated targets) or 5% BSA (for phosphorylated proteins) for 2 h at room temperature. Primary antibodies diluted in TBST containing 5% BSA were incubated with membranes overnight at 4°C, followed by three 10-min TBST washes. Membranes were subsequently incubated with HRP-conjugated secondary antibody for 1 h at room temperature. Protein bands were visualized using ECL substrate and quantified through densitometric analysis. All the Western blot experiments were repeated at least three times.

2.5 Transfection

For siRNA transfection, 125 μL of Opti-MEM was mixed with 100 pmol siRNA in a 1.5 mL tube, followed by the addition of 4 μL LipoRNAi™ Transfection Reagent. The mixture was vortexed briefly and incubated at room temperature for 20 min to form siRNA-lipid complexes. NPC cells in logarithmic growth phase were seeded into 6-well plates at a density of 2 × 105 cells/well and cultured until 70%–80% confluency. The siRNA-lipid complexes were then added to cells and incubated for 48 h under standard culture conditions. Transfection efficiency was verified through quantitative PCR analysis prior to functional experiments. All procedures were performed in triplicate to ensure experimental consistency.

2.6 CCK-8

CNE1 and C666-1 cells were seeded into 96-well plates at a density of 1×10^4 cells/mL (100 μL/well) and allowed to adhere for 24 h. Five experimental groups were established: (1) untreated control, (2) negative control (NC) with empty plasmid transfection, (3) D63785-targeting siRNA transfection, (4) 20μMAE treatment, and (5) combination therapy (siRNA+20μMAE). Following 48 h of treatment, 10 μL of CCK-8 reagent was added to each well and incubated in darkness at 37°C for 1.5 h. Optical density values were measured at 450 nm wavelength, with five technical replicates per group and three independent biological replicates. Data normalization and statistical analysis were performed relative to untreated controls.

2.7 Colony formation experiment

The colony formation assay was performed to evaluate proliferative capacity across experimental groups: (1) untreated control, (2) negative control (empty plasmid transfection), (3) D63785-targeting siRNA transfection, (4) 20μMAE treatment, and (5) combination therapy (siRNA+20μMAE). CNE1 and C666-1 cells in logarithmic growth phase were seeded at 200 cells/well in 6-well plates (three wells per group) and allowed to adhere for 24 h. After 48 h of treatment, the medium was replaced with fresh complete medium, and cells were cultured for 10 days under standard conditions (37°C, 5% CO_2). Colonies were fixed with 4% paraformaldehyde (4°C, 1 h), stained with 0.1% crystal violet for 15 min, and gently rinsed with distilled water. Colonies containing ≥50 cells were counted using ImageJ software. Three independent biological replicates were performed. Colony formation rate = number of colonies/number of inoculated cells ×100%.

2.8 EdU doping experiment

The EdU incorporation assay was conducted to assess cell proliferation across five experimental groups: (1) untreated control, (2) negative control (empty plasmid transfection), (3) D63785-targeting siRNA transfection, (4) 20 μM AE treatment, and (5) combination therapy (siRNA+20μMAE). CNE1 and C666-1 cells in logarithmic growth phase were seeded into 24-well plates at 1×10^4 cells/well (three technical replicates per group) and allowed to adhere for 24 h. After 48 h of treatment, cells were incubated with 10 μM EdU working solution for 2 h at 37°C. Subsequent fixation with 4% paraformaldehyde (15 min, room temperature) and permeabilization with 0.3% Triton X-100 (15 min) preceded the Click reaction (100 μL/well, 30 min, darkness). Nuclei were counterstained with Hoechst 33,342 (1: 1,000 in PBS) for 5 min. Fluorescence images were acquired using standardized exposure parameters across all groups. EdU-positive cells (red fluorescence) and total nuclei (blue fluorescence) were quantified using ImageJ 1.53t across five random fields per well. Three independent biological replicates were analyzed.

2.9 Scratch healing experiment

The wound healing assay was conducted to assess cell migration across five experimental groups: (1) untreated control, (2) negative control (empty plasmid transfection), (3) D63785-targeting siRNA transfection, (4) 20μMAE treatment, and (5) combination therapy (siRNA+20μMAE) NPC cells in logarithmic growth phase were seeded into 6-well plates at 2 × 105 cells/well (three technical replicates per group) and cultured until reaching 80% confluence. A sterile 200 μL pipette tip was used to create a uniform linear scratch in the cell monolayer. After washing three times with PBS to remove cellular debris, the control group received serum-free medium containing 1×10^{-3} μM DMSO (vehicle control),while the experimental group was added with serum-free medium containing different concentrations of AE. Scratch widths were recorded at 0 h (baseline) and 48 h using an Olympus IX83 inverted microscope (×10 objective) under phase-contrast mode. Five random fields per well were imaged with consistent illumination settings. Migration rates were quantified using ImageJ with the MRI Wound Healing Tool plugin by calculating:Scratch closure rate=(scratch width from 0 h to 48 h)/scratch width from 0 h multiplied by 100%.Three independent biological replicates were performed. All procedures were conducted under standard culture conditions (37°C, 5% CO_2).

2.10 Cultivate nude mouse NPC subcutaneous transplant tumor model

Sixteen 4-week-old nude mice (18–20 g) were housed under standardized conditions (22°C–24°C, 12-h light/dark cycle) with autoclaved water and irradiated feed. Following a 7-day acclimatization period, NPC cells (1×10^7 cells/200 μL PBS) were subcutaneously injected into the right upper lumbar region. Tumor volumes were calculated daily using the formula (V = ab2/2), where (a) and (b) represent the longest and shortest diameters, respectively. Mice were randomized into two groups (n = 8/group) upon reaching tumor volumes of ~80 mm^3. The treatment group received daily intraperitoneal injections of 20 mg/kg (Dou et al., 2019) aloe emodin in 5% DMSO/saline (200 μL/mouse), while controls received vehicle alone. Humane endpoints included tumor burden >2,000 mm^3, >20% body weight loss, or impaired mobility. On day 10, mice were anesthetized with isoflurane, euthanized via cervical dislocation, and tumors were excised, weighed, and snap-frozen for molecular analysis. All animal experiments were conducted in accordance with the animal ethics of the Animal Research Center of Guilin Medical College (approval number: GLMC-IACUC-2022015).

2.11 Statistical analysis

All experiments were independently repeated three times (biological replicates) with three technical replicates each. Data were expressed as mean ± standard deviation (SD). For comparisons between two groups, Student's t-test was performed. One-way ANOVA with Tukey's post hoc test was applied for multiple group comparisons. Statistical analyses were conducted using GraphPad Prism 8.0 (GraphPad Software). A probability value of $P < 0.05$ was considered statistically significant.

3 Results

3.1 AE reduced the expression of LncRNA D63785 and inhibited phosphorylation of PI3K/Akt/mTOR pathway in CNE1 and C666-1 NPC cells in a concentration-dependent manner

Real-time quantitative PCR analysis of LncRNA D63785 expression in normal nasal mucosal epithelial HNEpC cells and NPC cell lines (CNE1, 5-8F, C666-1, HONE1) revealed elevated LncRNA D63785 levels in CNE1, C666-1, and HONE1 cells compared to HNEpC controls (Figure 1A). The 5-8F cell line showed comparable expression to HNEpC cells. CNE1 and C666-1 cells, which exhibited the highest LncRNA D63785 expression, were further analyzed.

Treatment of CNE1 and C666-1 cells with AE (10, 20, 30 μM) for 48 h resulted in progressive reductions in LncRNA D63785 expression levels, as quantified by qPCR (Figures 1B,C).

Western blot analysis demonstrated that AE treatment (10, 20, 30 μM) did not alter total PI3K, Akt, or mTOR protein levels in either cell line (Figures 1D–F). However, phosphorylated forms of these proteins (p-PI3K, p-Akt, p-mTOR) showed concentration-dependent decreases in both C666-1 (Figures 1D,E) and CNE1 cells (Figures 1D,F).

3.2 LncRNA D63785 may mediate AE-inhibited NPC cell viability

LncRNA D63785 knockdown models were established in CNE1 and C666-1 cells through siRNA transfection. qRT-PCR confirmed reduced LncRNA D63785 expression in siRNA-transfected cells compared to siNC controls (Figure 2A).

CCK-8 assays revealed decreased cell viability in AE-treated groups relative to untreated controls. This reduction was attenuated in cells co-treated with siRNA D63785 and AE (Figures 2B,C).

Colony formation assays demonstrated fewer colonies in AE-treated cells compared to controls. Co-treatment with siRNA D63785 and AE resulted in increased colony formation relative to AE treatment alone (Figures 2D–G).

EdU incorporation assays showed reduced proliferation rates in AE-treated groups. Co-treatment with siRNA D63785 and AE led to higher proliferation rates compared to AE-only groups (Figures 2H–J).

3.3 AE reduced the migration ability of NPC cells partly by affecting LncRNA

Wound-healing assays were performed to assess NPC cell migration following treatments. Compared to untreated controls,

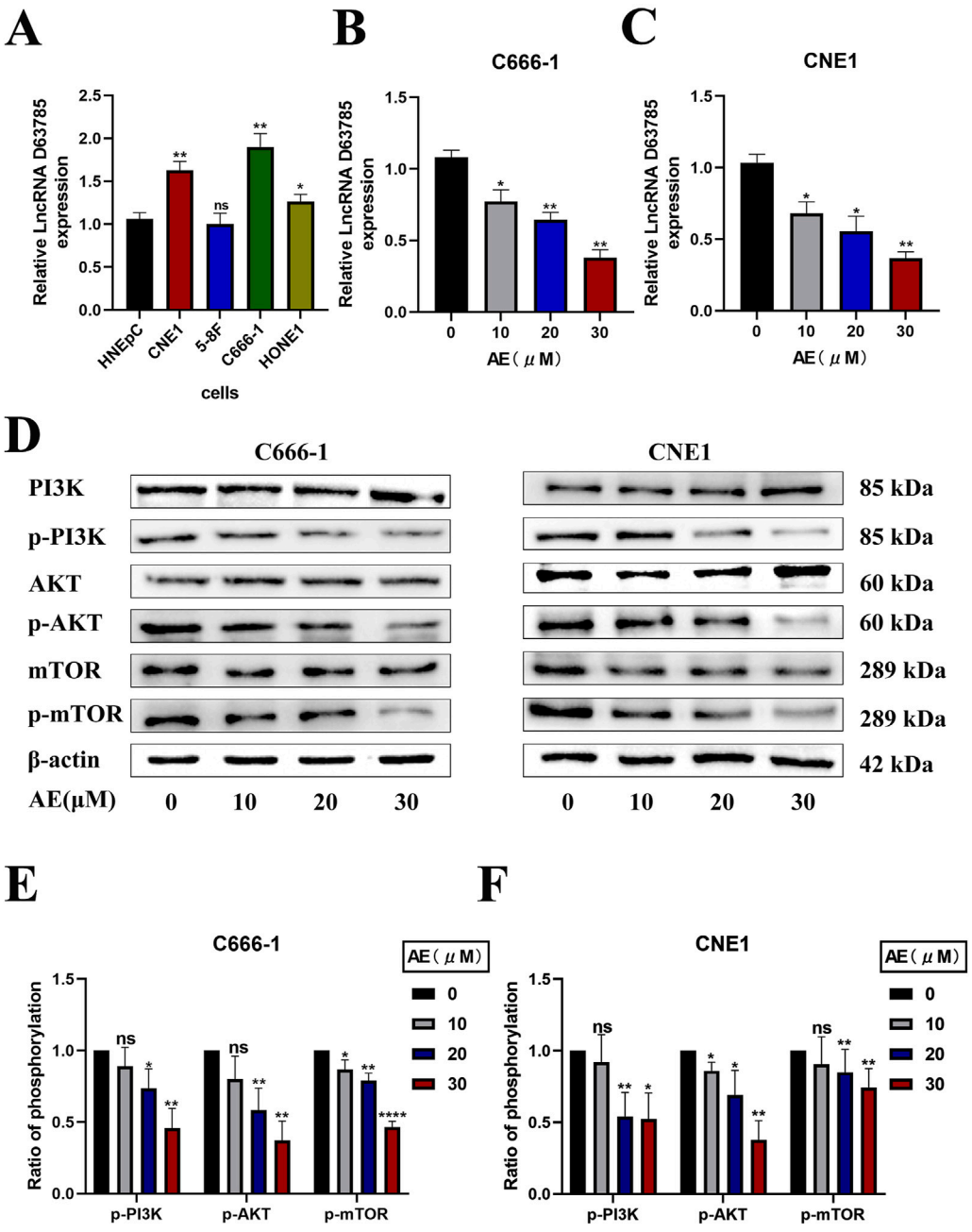

FIGURE 1
AE downregulated lncRNA D63785 and inhibited the PI3K/Akt/mTOR pathway in CNE1 and C666-1 NPC cells in a concentration-dependent manner. AE significantly inhibits the expression of lncRNA D63785 in NPC cells, and this effect is enhanced with increasing concentrations. **(A)** Expression of LncRNA D63785 in normal nasal mucosal epithelial cells and multiple nasopharyngeal carcinoma cells. Comparison of LncRNA D63785 self-expression between normal human nasal mucosal epithelial cells HNEpC and nasopharyngeal carcinoma CNE1, 5-8F, C666-1, HONE1 cells. The data shown is mean ± standard deviation, n = 3. ^{ns}P>0.05,*P < 0.05, **P < 0.01, compared to the HNEpC group. **(B,C)** Changes in LncRNA D63785 under the action of aloe-emodin. The control group and different concentration gradients of aloe-emodin were treated on C666-1 cells for 48 h, and the expression of LncRNA D63785 was detected by real-time quantitative PCR **(B)**. The expression of LncRNA D63785 was detected by real-time quantitative PCR in CNE1 cells treated with control group and different concentration gradients of aloe-emodin for 48 h **(C)**. The data shown is mean ± standard deviation, n = 3. *P < 0.05, **P < 0.01, compared to the control (0) group. **(D–F)** The effect of aloe-emodin on the PI3K/Akt/mTOR signaling pathway in nasopharyngeal carcinoma cells. **(D)** The expression of pathway proteins in C666-1 and CNE1 cells was detected by Western blot after 48 h of treatment with control group and different concentration gradients of aloe-emodin. **(E,F)** Bar chart of phosphorylation protein expression of C666-1 and CNE1 cells under the action of control group and different concentration gradients of aloe-emodin. The data shown is mean ± standard deviation, n = 3. ^{ns}P>0.05,*P < 0.05, **P < 0.01, compared to the control (0) group.

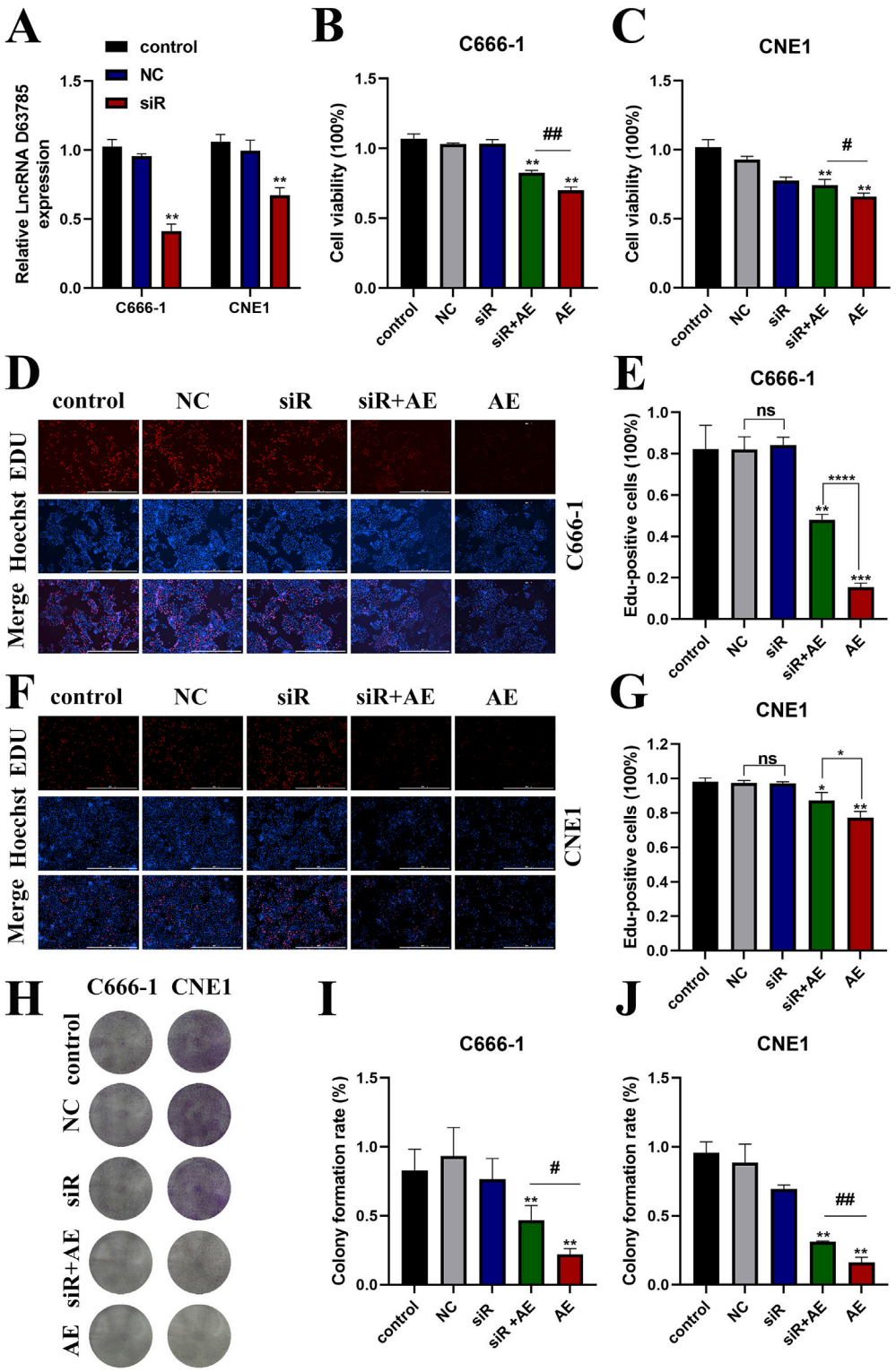

FIGURE 2
AE inhibited NPC cell vibility may be mediated by LncRNA D63785. **(A)** Expression of LncRNA D63785 in nasopharyngeal carcinoma cells transfected with siRNA. The control group, transfected empty plasmid group, and transfected siRNA group were treated with nasopharyngeal carcinoma C666-1 and CNE1 cells for 48 h, and the expression of LncRNA D63785 was detected by real-time quantitative PCR. The data shown is mean ± standard deviation, n = 3. *P < 0.05, **P < 0.01, compared to the control group. **(B,C)** Knockdown of LncRNA D63785 in NPC cells inhibits cell activity. The control group, empty group (NC) siRNA group, AE group, and siRNA + AE group were treated for 48 h, and the viability of C666-1 **(B)** and CNE1 **(C)** was detected by CCK-8. The data shown is mean ± standard deviation, n = 3. *P < 0.05, **P < 0.01, compared to the control group; $^{\#}$P < 0.05,$^{\#\#}$P < 0.01, compared to the siRNA + AE group. **(D–G)** The control group, empty group (NC), siRNA group, AE group, and siRNA + AE group were treated for 48 h, and the proliferation rate of
(*Continued*)

FIGURE 2 (Continued)
nasopharyngeal carcinoma cells was detected by EdU incorporation experiment. **(H–J)** The control group, empty group (NC), siRNA group, AE group, and siRNA + AE group were treated for 48 h, and the proliferation rate of nasopharyngeal carcinoma cells was detected through colony formation assay. Bar = 100 μm. The data shown is mean ± standard deviation, n = 3. *P < 0.05, **P < 0.01, compared to the control group; #P < 0.05, ##P < 0.01, compared to the siRNA + AE group.

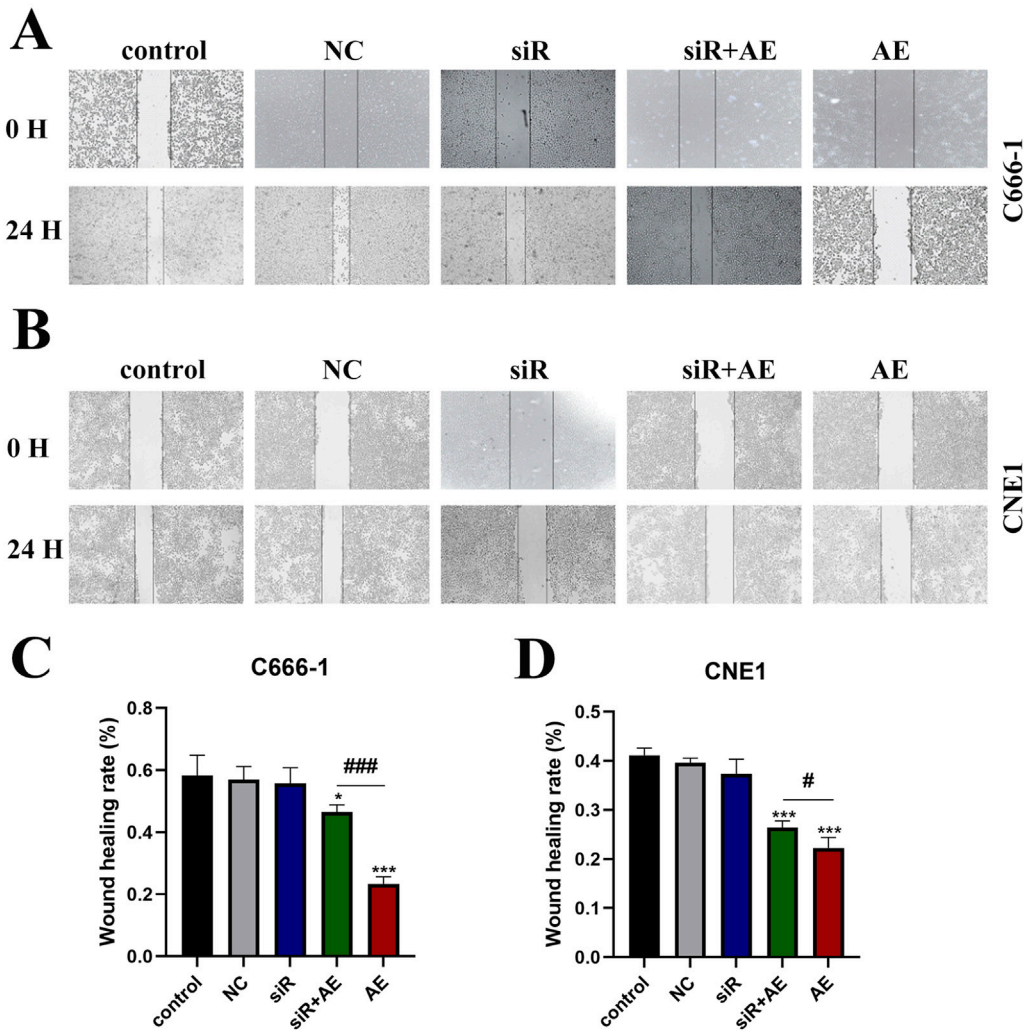

FIGURE 3
AE exerted its inhibitory effect on NPC cell migration ability through LncRNA D63785. **(A,B)** The control group, empty group (NC) siRNA group, AE group, and siRNA + AE group were treated for 48 h, and the scratch healing experiment was used to detect the migration ability of nasopharyngeal carcinoma cells C666-1 **(A)** and CNE1 **(B)**. Bar = 100 μm. **(C,D)** Histogram of migration ability of C666-1 **(C)** and CNE1 **(D)** cells. The data shown is mean ± standard deviation, n = 3. *P < 0.05, *P < 0.01, compared to the control group; #P < 0.05, ##P < 0.01, compared to the siRNA + AE group.

AE-treated groups exhibited reduced scratch closure rates in both C666-1 (Figures 3A–C) and CNE1 (Figures 3B,D) cell lines. Transfection with empty vector (NC) or siRNA D63785 alone showed no measurable impact on migration compared to controls. In AE-treated cells, concurrent siRNA D63785 transfection attenuated the migration-inhibitory effects observed in AE-only groups.

3.4 The effect of knocking down LncRNA D63785 on PI3K/Akt/mTOR pathway proteins

Western blot analysis evaluated PI3K/Akt/mTOR pathway protein expression in C666-1 and CNE1 cells under five experimental conditions: control, empty vector (NC), siRNA

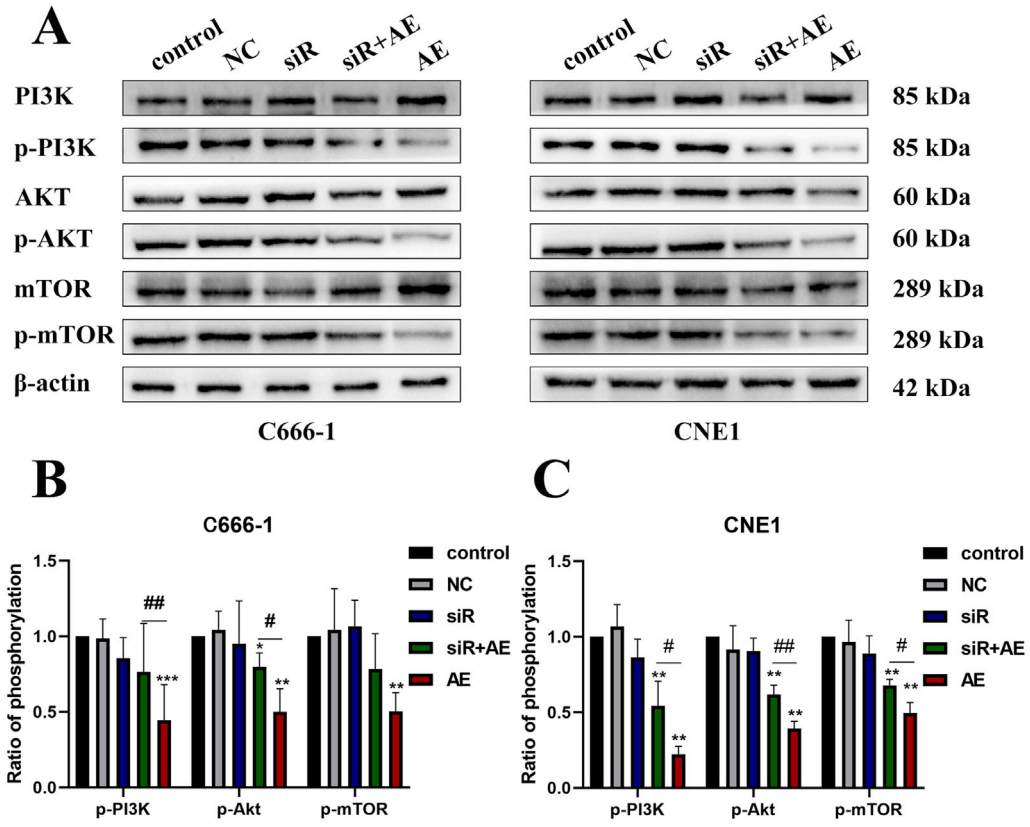

FIGURE 4
The effects of aloe-emodin and knocking down LncRNA D63785 on the PI3K/Akt/mTOR signaling pathway in nasopharyngeal carcinoma cells. **(A)** The control group, empty group (NC) siRNA group, AE group, and siRNA + AE group were treated for 48 h, and the expression of pathway proteins was detected by Western blot. Histogram of C666-1 **(B)** and CNE1 **(C)** cells phosphorylated proteins p-PI3K, p-Akt, and p-mTOR expression. The data shown is mean ± standard deviation, n = 3. ^{ns}P>0.05, *P < 0.05, **P < 0.01, compared to the control group; $^{\#}$P < 0.05, $^{\#\#}$P < 0.01, compared to the siRNA + AE group.

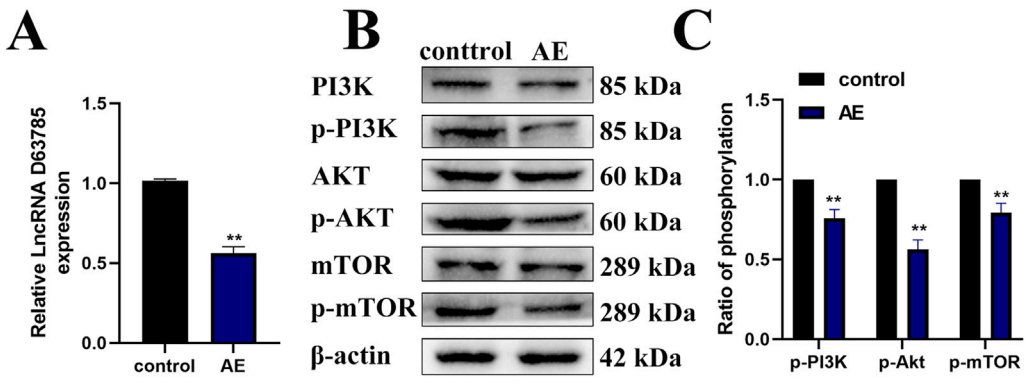

FIGURE 5
AE inhibits the expression of LncRNA D63785 and phosphorylation of PI3K/Akt/mTOR pathway proteins in subcutaneous transplanted tumors of NPC in nude mice. **(A)** Expression of LncRNA D63785 in the control group and aloe-emodin group. The data shown is mean ± standard deviation, n = 3, **P < 0.01, compared to the control group. **(B,C)** Expression of PI3K/Akt/mTOR signaling pathway proteins in the control group and aloe-emodin group. The data shown is mean ± standard deviation, n = 3, **P < 0.01, compared to the control group.

D63785, AE (20 μM), and siRNA + AE co-treatment (Figure 4A). β-actin served as the loading control for protein normalization.

Compared to control groups, AE treatment reduced phosphorylated PI3K (p-PI3K), Akt (p-Akt), and mTOR (p-mTOR) levels in both cell lines. siRNA D63785 transfection

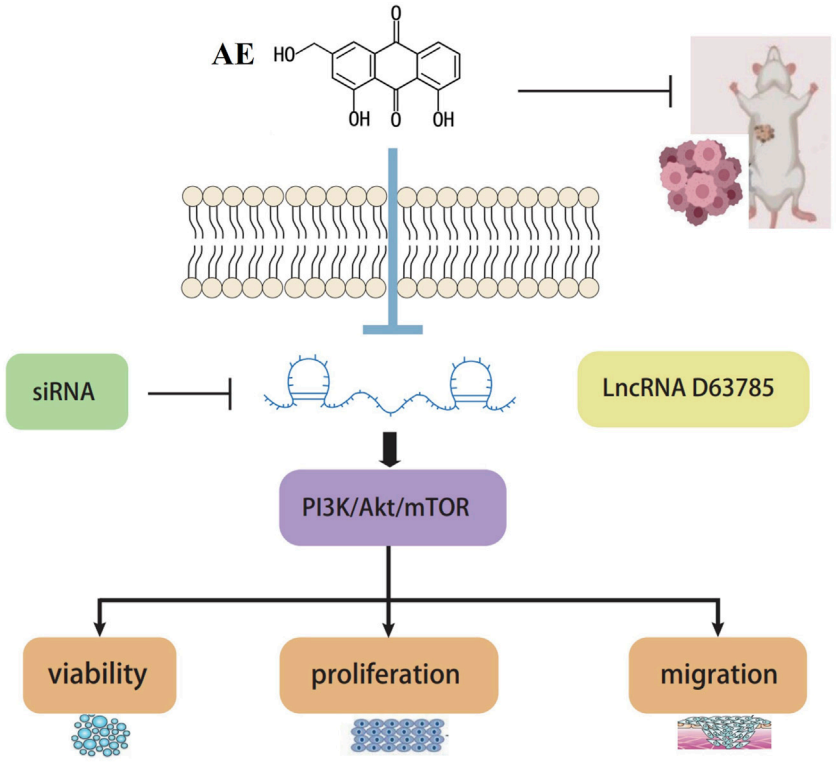

FIGURE 6
Graphical abstract.

alone did not alter baseline phosphorylation status relative to NC groups. In AE-treated cells, concurrent siRNA D63785 transfection attenuated AE-induced reductions in p-PI3K, p-Akt, and p-mTOR expression (Figures 4A–C).

3.5 AE inhibited the expression of LncRNA D63785 and the phosphorylation of PI3K/Akt/mTOR pathway proteins in an NPC tumor mouse model

Our previous studies have shown that AE can inhibit tumor growth in NPC cells xenograft mouse models (Chen et al., 2023). Real-time quantitative PCR analysis of subcutaneous xenograft tissues revealed reduced LncRNA D63785 expression in the AE-treated group compared to controls (Figure 5A). Western blot analysis of the same tissues demonstrated decreased phosphorylation levels of PI3K/Akt/mTOR pathway proteins (p-PI3K, p-Akt, p-mTOR) in the AE-treated group relative to controls (Figures 5B,C). β-actin served as the loading control for protein normalization.

4 Discussion

As a head and neck cancer, distant metastasis and local recurrence are still the two main failure modes for NPC patients (Liu et al., 2021). After recurrence or metastasis, the treatment effect is poor, the prognosis is poor, and the survival rate is significantly reduced. Therefore, it is crucial to study the pathogenesis of NPC, search for new therapeutic targets, and find effective and low-toxicity anti-tumor drugs.

Aloe vera is a perennial herbaceous plant in the lily family, and it has many types, but Curacao aloe vera has been studied the most extensively. It is considered a "healing" plant with medicinal value and has been used for over 3,000 years in different cultures of many countries. AE has anti-tumor and anti-proliferative effects on various types of cancer and cell lines, like HeLa Cells (Gao et al., 2019). However, the molecular mechanism of NPC pathogenesis is still not fully understood, and research on how AE affects NPC is limited. This study, based on our research group's previous research foundation, aims to elucidate the inhibitory effect of aloe-emodin on NPC.

LncRNA has excellent potential in cancer treatment and deserves more attention (Huang et al., 2025; Hsu et al., 2025). Previous reports lncRNAs play important roles in the occurrence and development of NPC, such as HOXA-AS2, HOTAIR, FOXD1-AS1, LINC00669, and so on (Wang et al., 2022). Moreover, LncRNA D63785 is highly expressed in NPC patient tissues (Zheng et al., 2019). Our result showed that LncRNA D63785 is highly expressed in multiple NPC cells as CNE1, C666-1, and HONE1 cell lines, but, interestingly, aloe emodin lacks inhibition of D63785 in 5–8F cells, indicating that cell environment dependence deserves further investigation. Moreover, we found that AE dose-dependently reduced the expression of D63785 in CNE1 and C666-1 cells, which is

related to the decreased phosphorylation of PI3K/Akt/mTOR pathway proteins. Importantly, knocking down LncRNA D63785 alone does not significantly affect NPC cells. However, siRNA-mediated knockout of D63785 partially reversed the anti-tumor effects of aloe-emodin on cell survival, proliferation, migration, and PI3K/Akt/mTOR signaling, strongly indicating that D63785 downregulation mediates at least partial pharmacological activity of aloe-emodin in these models. Suggested LncRNA D63785 mediated AE-inhibited NPC cell viability, etc. The consistency of these findings *in vivo* that aloe-emodin reduces the expression of D63785 and the activation of PI3K/Akt/mTOR while inhibiting tumor growth-further supports this relationship. Moreover, the PI3K/Akt/mTOR signaling pathway is involved in the occurrence and development of tumors and is closely related to the clinical and pathological characteristics of NPC (Li et al., 2022), and its transmission is also of great significance for treating NPC (Zhang et al., 2019). Therefore, AE inhibits the proliferation of CNE1 and C666-1 cells by downregulating LncRNA D63785, and the PI3K/Akt/mTOR pathway may be involved. Although current evidence suggests that D63785 is a key downstream effector of aloe-emodin activity in NPC models with high D63785 expression, It has not yet been confirmed whether aloe emodin directly binds to D63785 RNA to make it unstable or indirectly acts through epigenetic modification factors/transcription factors that control D63785 transcription.

Previous studies have shown, upregulation of lncRNA HAGLROS enhances nasopharyngeal carcinoma development by modulating PI3K/AKT/mTOR signaling mediated by miR-100/ATG14 axis (Zhang et al., 2019). But our current research results indicate that D63785 knockout reduces the phosphorylation levels of PI3K, Akt, and mTOR without significantly altering their total protein expression, suggesting that its regulatory role lies in pathway activation rather than transcriptional control of core components. We hypothesize two possible mechanisms based on observed signal dynamics: 1) D63785 can stabilize pathway activation by interacting with phosphatases or kinases that regulate phosphorylation status, or 2) it can serve as a scaffold to facilitate signal complex assembly. The partial reversal of the knockout effect of aloe-emodin on LncRNA D63785 further supports its upstream regulatory position. It is necessary to study the interaction group of LncRNA D63785, and in the future, we will evaluate its impact on post-translational modifications.

In clinical practice, we discussed the potential use of D63785 as a biomarker for predicting sensitivity to aloe emodin, particularly in tumors with high baseline expression of D63785. We explored strategies for combining aloe emodin with PI3K inhibitors or conventional therapies to overcome drug resistance. In addition, the lack of patient-sourced data is a limitation, and we are collaborating with clinical institutions to validate our findings in patient tumor samples and correlate them with clinical outcomes in ongoing studies.

In summary, this study found a novel target lncRNA D63785 with therapeutic potential, which regulates target proteins and affects NPC cell viability, elucidating an axis of AE targeting NPC and preliminarily elucidating the molecular mechanism of AE inhibition of NPC (Figure 6). It concludes that AE may mediate the PI3K/Akt/mTOR pathway regulation by LncRNA D63785, inhibiting the cell viability, proliferation, migration, and other malignant biological behaviors of NPC cells CNE1 and C666-1. AE may inhibit the growth of subcutaneous transplanted tumors in nude mice NPC through lncRNA D63785 and PI3K/Akt/mTOR pathway. This study starts with the search for long noncoding RNAs, regulates downstream proteins to affect NPC cell phenotype changes and tumor growth, elucidates a signaling pathway through which natural drugs act on tumors, and organically combines natural drug components, molecular mechanisms, cells, and tumor growth to provide ideas for the progress of NPC treatment. It is expected to explain the effects of natural drug components further and lay a solid foundation for later drug research and clinical applications.

Data availability statement

The original contributions presented in the study are included in the article/supplementary material, further inquiries can be directed to the corresponding author.

Ethics statement

The animal studies were approved by IACUC of Guilin Medical University. The studies were conducted in accordance with the local legislation and institutional requirements. Written informed consent was obtained from the owners for the participation of their animals in this study.

Author contributions

MH: Conceptualization, Formal Analysis, Funding acquisition, Project administration, Writing – review and editing. LX: Data curation, Investigation, Project administration, Validation, Visualization, Writing – original draft. JyH: Resources, Supervision, Writing – original draft. HS: Conceptualization, Investigation, Methodology, Writing – original draft. JhH: Software, Supervision, Visualization, Writing – review and editing. LX: Methodology, Resources, Validation, Writing – original draft. ML: Investigation, Resources, Writing – review and editing. XZ: Resources, Supervision, Writing – original draft. JT: Conceptualization, Funding acquisition, Supervision, Writing – review and editing.

Funding

The author(s) declare that financial support was received for the research and/or publication of this article. Natural Science Foundation of Guangxi Province of China (Grant Nos. 2022GXNSFAA103002). Guilin Science and Technology Plan

Project (No. 20210227-8-7). The project of improving the basic scientific research ability of young and middle-aged teachers in Guangxi universities (No. 2022KY0502). Guangxi Zhuang Autonomous Region Traditional Chinese Medicine Administration self-funded scientific research project (No. GXZYC20220317).

Conflict of interest

The authors declare that the research was conducted in the absence of any commercial or financial relationships that could be construed as a potential conflict of interest.

Generative AI statement

The author(s) declare that no Generative AI was used in the creation of this manuscript.

Publisher's note

All claims expressed in this article are solely those of the authors and do not necessarily represent those of their affiliated organizations, or those of the publisher, the editors and the reviewers. Any product that may be evaluated in this article, or claim that may be made by its manufacturer, is not guaranteed or endorsed by the publisher.

References

Abu Samaan, T. M., Samec, M., Liskova, A., Kubatka, P., and Büsselberg, D. (2019). Paclitaxel's mechanistic and clinical effects on breast cancer. *Biomolecules* 9 (12), 789. doi:10.3390/biom9120789

Chang, E. T., Ye, W., Zeng, Y. X., and Adami, H. O. (2021). The evolving epidemiology of nasopharyngeal carcinoma, cancer epidemiology, biomarkers & prevention: a publication of the American association for cancer research, cosponsored by the. *Am. Soc. Prev. Oncol.* 30 (6), 1035–1047. doi:10.1158/1055-9965.EPI-20-1702

Chen, Q., Zheng, W., Zhu, L., Yao, D., Wang, C., Song, Y., et al. (2020). ANXA6 contributes to radioresistance by promoting autophagy via inhibiting the PI3K/AKT/mTOR signaling pathway in nasopharyngeal carcinoma. *Front. Cell Dev. Biol.* 8, 232. doi:10.3389/fcell.2020.00232

Chen, S., Guan, X., Xie, L., Liu, C., Li, C., He, M., et al. (2023). Aloe-emodin targets multiple signaling pathways by blocking ubiquitin-mediated degradation of DUSP1 in nasopharyngeal carcinoma cells. *Phytotherapy Res. PTR* 37 (7), 2979–2994. doi:10.1002/ptr.7793

Dou, F., Liu, Y., Liu, L., Wang, J., Sun, T., Mu, F., et al. (2019). Aloe-emodin ameliorates renal fibrosis Via inhibiting PI3K/Akt/mTOR signaling pathway *in vivo* and *in vitro*. *Rejuvenation Res.* 22 (3), 218–229. doi:10.1089/rej.2018.2104

Du, M., Shen, P., Tan, R., Wu, D., and Tu, S. (2021). Aloe-emodin inhibits the proliferation, migration, and invasion of melanoma cells via inactivation of the wnt/beta-Catenin signaling pathway. *Ann. Transl. Med.* 9 (23), 1722. doi:10.21037/atm-21-5437

Feng, G., Arima, Y., Midorikawa, K., Kobayashi, H., Oikawa, S., Zhao, W., et al. (2023). Knockdown of TFRC suppressed the progression of nasopharyngeal carcinoma by downregulating the PI3K/Akt/mTOR pathway. *Cancer Cell Int.* 23 (1), 185. doi:10.1186/s12935-023-02995-7

Feng, X., Shi, H., Chao, X., Zhao, F., Song, L., Wei, M., et al. (2019). Deciphering the pharmacological mechanism of the herb Radix ophiopogonis in the treatment of nasopharyngeal carcinoma by integrating iTRAQ-Coupled 2-D LC-MS/MS analysis and network investigation. *Front. Pharmacol.* 10, 253. doi:10.3389/fphar.2019.00253

Gao, R., Wu, X., Huang, Z., Wang, B., Li, F., Xu, H., et al. (2019). Anti-tumor effect of aloe-emodin on cervical cancer cells was associated with human papillomavirus E6/E7 and glucose metabolism. *OncoTargets Ther.* 12, 3713–3721. doi:10.2147/OTT.S182405

He, B., Pan, H., Zheng, F., Chen, S., Bie, Q., Cao, J., et al. (2022). Long noncoding RNA LINC00930 promotes PFKFB3-mediated tumor glycolysis and cell proliferation in nasopharyngeal carcinoma. *J. Exp. Clin. Cancer Res. CR* 41 (1), 77. doi:10.1186/s13046-022-02282-9

Hsu, C. Y., Jasim, S. A., Bansal, P., Kaur, H., Ahmad, I., Saud, A., et al. (2025). Delving into lncRNA-Mediated regulation of autophagy-associated signaling pathways in the context of breast cancer. *Cell Biol. Int.* 49, 221–234. doi:10.1002/cbin.12277

Huang, S., Li, B., Chen, H., Rong, C., Yang, Z., and Zhang, X. (2025). Clinical significance and pathogenic mechanisms of long non-coding RNA TRPM2-AS in cancers. *Technol. Cancer Res. Treat.* 24, 15330338251315625. doi:10.1177/15330338251315625

Jia, H., and Yan, X. (2022). lncRNA MEG3 inhibits the proliferation and growth of glioma cells by downregulating Bcl-xL in the PI3K/Akt/NF-κB signal pathway. *Biomed. Res. Int.* 2022, 3729069. doi:10.1155/2022/3729069

Jiang, D., Ding, S., Mao, Z., You, L., and Ruan, Y. (2021). Integrated analysis of potential pathways by which aloe-emodin induces the apoptosis of colon cancer cells. *Cancer Cell Int.* 21 (1), 238. doi:10.1186/s12935-021-01942-8

Jicman Stan, D., Niculet, E., Lungu, M., Onisor, C., Rebegea, L., Vesa, D., et al. (2022). Nasopharyngeal carcinoma: a new synthesis of literature data (Review). *Exp. Ther. Med.* 23 (2), 136. doi:10.3892/etm.2021.11059

Li, H. L., Deng, N. H., He, X. S., and Li, Y. H. (2022). Small biomarkers with massive impacts: PI3K/AKT/mTOR signalling and microRNA crosstalk regulate nasopharyngeal carcinoma. *Biomark. Res.* 10 (1), 52. doi:10.1186/s40364-022-00397-x

Liu, Z., Chen, Y., Su, Y., Hu, X., and Peng, X. (2021). Nasopharyngeal carcinoma: clinical achievements and considerations among treatment options. *Front. Oncol.* 11, 635737. doi:10.3389/fonc.2021.635737

Luo, C., Ai, J., Ren, E., Li, J., Feng, C., Li, X., et al. (2021). Research progress on evodiamine, a bioactive alkaloid of *Evodiae fructus*: focus on its anti-cancer activity and bioavailability (Review). *Exp. Ther. Med.* 22 (5), 1327. doi:10.3892/etm.2021.10762

Peng, M., Zheng, Z., Chen, S., Fang, L., Feng, R., Zhang, L., et al. (2022). Sensitization of non-small cell lung cancer cells to gefitinib and reversal of epithelial-mesenchymal transition by aloe-emodin Via PI3K/Akt/TWIS1 signal blockage. *Front. Oncol.* 12, 908031. doi:10.3389/fonc.2022.908031

Qin, Z. Q., Li, Q. G., Yi, H., Lu, S. S., Huang, W., Rong, Z. X., et al. (2020). Heterozygous p53-R280T mutation enhances the oncogenicity of NPC cells through activating PI3K-Akt signaling pathway. *Front. Oncol.* 10, 104. doi:10.3389/fonc.2020.00104

Sanders, B., Ray, A. M., Goldberg, S., Clark, T., McDaniel, H. R., Atlas, S. E., et al. (2018). Anti-cancer effects of aloe-emodin: a systematic review. *J. Clin. Transl. Res.* 3 (3), 283–296. doi:10.18053/jctres.03.201703.001

Şeker Karatoprak, G., Küpeli Akkol, E., Yücel, Ç., Bahadır Acıkara, Ö., and Sobarzo-Sánchez, E. (2022). Advances in understanding the role of aloe emodin and targeted drug delivery systems in cancer, oxidative medicine and cellular longevity. *Oxid. Med. Cell Longev.* 2022, 7928200. doi:10.1155/2022/7928200

Shafei, L., Mohamed Ibrahim, M. I., and Billa, N. (2021). Is curcumin at the threshold of therapeutic effectiveness on patients with Colon Cancer? A systematic review. *Front. Pharmacol.* 12, 707231. doi:10.3389/fphar.2021.707231

Sharma, U., Murmu, M., Barwal, T. S., Tuli, H. S., Jain, M., Prakash, H., et al. (2022). A pleiotropic role of long non-coding RNAs in the modulation of Wnt/β-Catenin and PI3K/Akt/mTOR signaling pathways in esophageal squamous cell carcinoma: implication in chemotherapeutic drug response. *Curr. Oncol. Tor. Ont.* 29 (4), 2326–2349. doi:10.3390/curroncol29040189

Su, Z. Y., Siak, P. Y., Leong, C. O., and Cheah, S. C. (2022). Nasopharyngeal carcinoma and its microenvironment: past, current, and future perspectives. *Front. Oncol.* 12, 840467. doi:10.3389/fonc.2022.840467

Tang, L. L., Chen, Y. P., Chen, C. B., Chen, M. Y., Chen, N. Y., Chen, X. Z., et al. (2021). The Chinese society of clinical oncology (CSCO) clinical guidelines for the diagnosis and treatment of nasopharyngeal carcinoma. *Cancer Commun. Lond. Engl.* 41 (11), 1195–1227. doi:10.1002/cac2.12218

Teng, Y., Fan, Y., Ma, J., Lu, W., Liu, N., Chen, Y., et al. (2021). The PI3K/Akt pathway: emerging roles in skin homeostasis and a group of non-malignant skin disorders. *Cells* 10 (5), 1219. doi:10.3390/cells10051219

Termini, D., Den Hartogh, D. J., Jaglanian, A., and Tsiani, E. (2020). Curcumin against prostate cancer: current evidence. *Biomolecules* 10 (11), 1536. doi:10.3390/biom10111536

Wang, H., Wang, W., and Fan, S. (2022). Emerging roles of lncRNA in nasopharyngeal carcinoma and therapeutic opportunities. *Int. J. Biol. Sci.* 18 (7), 2714–2728. doi:10.7150/ijbs.70292

Wang, S., Yan, W. W., He, M., Wei, D., Long, Z. J., and Tao, Y. M. (2020a). Aloe emodin inhibits telomerase activity in breast cancer cells: transcriptional and enzymological mechanism. *Pharmacol. Rep.* 72 (5), 1383–1396. doi:10.1007/s43440-020-00062-w

Wang, Y., Wu, N., Luo, X., Zhang, X., Liao, Q., and Wang, J. (2020b). SOX2OT, a novel tumor-related long non-coding RNA. *Biomed. Pharmacother.* 123, 109725. doi:10.1016/j.biopha.2019.109725

Wu, Z.-X., Xiang, L., Rong, J.-F., He, H.-L., and Li, D. J. (2016). Nasopharyngeal carcinoma with headaches as the main symptom: a potential diagnostic pitfall. *J. Cancer Res. Ther.* 12 (1), 209–214. doi:10.4103/0973-1482.157334

Xie, Z., Li, W., Ai, J., Xie, J., and Zhang, X. (2022). C2orf40 inhibits metastasis and regulates chemo-resistance and radio-resistance of nasopharyngeal carcinoma cells by influencing cell cycle and activating the PI3K/AKT/mTOR signaling pathway. *J. Transl. Med.* 20 (1), 264. doi:10.1186/s12967-022-03446-z

Yao, H., Tian, L., Yan, B., Yang, L., and Li, Y. (2022). LncRNA TP73-AS1 promotes nasopharyngeal carcinoma progression through targeting miR-342-3p and M2 polarization via exosomes. *Cancer cell Int.* 22 (1), 16. doi:10.1186/s12935-021-02418-5

Zhang, J., Zhou, J., and Xiao, S. (2020). Shikonin inhibits growth, invasion and glycolysis of nasopharyngeal carcinoma cells through inactivating the phosphatidylinositol 3 kinase/AKT signal pathway. *Anti-cancer drugs* 31 (9), 932–941. doi:10.1097/CAD.0000000000000920

Zhang, W., Zhang, Y., and Xi, S. (2019). Upregulation of lncRNA HAGLROS enhances the development of nasopharyngeal carcinoma via modulating miR-100/ATG14 axis-mediated PI3K/AKT/mTOR signals. *Nanomedicine, Biotechnol.* 47 (1), 3043–3052. doi:10.1080/21691401.2019.1640233

Zheng, Z. Q., Li, Z. X., Zhou, G. Q., Lin, L., Zhang, L. L., Lv, J. W., et al. (2019). Long noncoding RNA FAM225A promotes nasopharyngeal carcinoma tumorigenesis and metastasis by acting as ceRNA to sponge miR-590-3p/miR-1275 and upregulate ITGB3. *Cancer Res.* 79 (18), 4612–4626. doi:10.1158/0008-5472.CAN-19-0799

Zhou, Z., Lin, Z., He, Y., Pang, X., Wang, Y., Ponnusamy, M., et al. (2018). The long noncoding RNA D63785 regulates chemotherapy sensitivity in human gastric cancer by targeting miR-422a. *Nucleic acids.* 12, 405–419. doi:10.1016/j.omtn.2018.05.024

Zhu, M., He, Q., Wang, Y., Duan, L., Rong, K., Wu, Y., et al. (2023). Exploring the mechanism of aloe-emodin in the treatment of liver cancer through network pharmacology and cell experiments. *Front. Pharmacol.* 14, 1238841. doi:10.3389/fphar.2023.1238841

Frontiers in Pharmacology

Explores the interactions between chemicals and living beings

The most cited journal in its field, which advances access to pharmacological discoveries to prevent and treat human disease.

Discover the latest Research Topics

See more →

Frontiers

Avenue du Tribunal-Fédéral 34
1005 Lausanne, Switzerland
frontiersin.org

Contact us

+41 (0)21 510 17 00
frontiersin.org/about/contact